Understanding the Role of TGF-β1 in Interstitial Lung Disease Using A Multi-Scale Systems Biology Approach

by

Hayley Catherine Warsinske

A dissertation submitted in partial fulfillment of the requirements for the degree of Doctor of Philosophy (Microbiology and Immunology) in the University of Michigan 2017

Doctoral Committee:

Professor Denise E. Kirschner , Chair
Professor Krishnakumar R. Garikipati
Assistant Professor Yasmina Laouar
Associate Professor Gary D. Luker
Professor Bethany B. Moore

Acknowledgements

First and foremost I must acknowledge Dr. Denise Kirschner for being an exceptional mentor to me other the past five and a half years. Denise has been an inspiration and support in all of my scientific endeavors. She has taught me to me a bold and enthusiastic scientist, an active member of the community, and an encouragement to my colleagues. Denise has also set a great example of balance and perspective when it comes to science and life outside of science. I aspire to have her drive and sense of purpose as I continue throughout my career.

I would also like to thank my committee members Dr. Bethany Moore, Dr. Gary Luker, Dr. Yasmina Laouar , and Dr. Krishna Garikipati. Beth has been not only a member of my committee but my co-mentor and advisor. She has supported me in all of my studies and even opened her lab up to me to perform experiments outside my expertise. The kindness and friendship that Beth has offered me throughout my career goes above and beyond mentorship. Gary has always been a wonderful committee member providing me with productive feedback and impartial perspective when I need it most. Yasmina always challenges me in a thoughtful way and has certainly contributed to my stringency and rigor as a scientist. She has also been positive and supportive, opening her door to me at any time for question of piece of advice. Krishna has been an excellent committee member, always willing to fully engage my work and provide both topical and technical suggestions and support. I must give a special thanks to Dr. Jennifer Linderman who has been a constant support and collaborator. Jennifer's scientific prowess and levelheaded nature has been invaluable to me throughout my graduate career. She has spent countless hours sitting with me, going through my work, and talking through

challenges. I would also like to thank Drs. Alice Telesnitsky, Nicole Kropotkin, Mary O'Riordan, Joel Swanson, and Michelle Swanson for their personal, professional, and scientific support during my graduate training.

I am extremely grateful to all of my past and present lab partners and colleagues: Paul Wolberg, Joe Waliga, Dr. Elsje Pienaar, Dr. Cordelia Ziraldo, Dr. Nick Cilfone, Dr. Laura Chang, Dr. Fred Gong, Joey Chicchese, Amy Oberlin, Stephanie Thiede and Louis Joslyn. Without your efforts, company, and support none of this work would be possible. I also have many friends to thank past and present without whom I would never have been able to accomplish this goal. Thank you to all the following: Kyle Roell, Jana Florian, Michaela Fraser, Emily Eric, Dr. Almas Chughtai, Courtney Luterbach, Matt Foley, Ada Hagan, Danelle Weakland, Dr. Natalie Maricic, Dr. Tori Holden, Jhansi Leslie, Dr. Kaitlin Flynn, Dr. Aaron Stein, Dr. Ian Beil.

I must also thank my family for their continued love and support. Thank you to my mom Andra Warsinske, my dad Tom Warsinske, my stepmom Aman Warsinske, and my sister Kelsey Warsinske. Finally I would like to thank Dr. Zack Abbott for all of his patience, love, and support.

Table of Contents

List of Figures

List of Tables

List of Appendices

Abstract

Pulmonary diseases are a major global health burden affecting approximately one billion people every year. They result from many types of insults including but not limited to infections, such as tuberculosis (TB), and dysregulations of the lung physiology, such as idiopathic pulmonary fibrosis. (IPF) The key to producing better therapeutics to treat pulmonary diseases is in understanding the role of immune mediators in these diseases. Transforming growth factor-β1 (TGF-β1) is an immune mediator that has been implicated in the exacerbation of both TB and IPF. TGF-β1 is traditionally described as and anti-inflammatory cytokine, thought to restrict the immune response. TGF-β1 affects a variety of cellular processes including proliferation, cytokine secretion, and even apoptosis. These effects are very cell type specific and often concentration dependent. Effective modulation of the immune response through TGF-β1 requires understanding which cells are being regulated, what are the specific results of TGF-β1 regulation, and through what mechanisms TGF-β1 is acting on the cells. To answer these questions it is necessary to look across biological scales at TGF-β1 signaling on a molecular scale, a cellular scale, and a tissue scale.

The role of TGF-β1 across multiple biologic scales has not been well characterized in the context of pulmonary disease. In this work I took a multi-scale systems biology approach to understanding the mechanistic role of TGF-β1 in pulmonary disease across molecular, cellular, and tissue scales. I constructed a novel ordinary differential equation (ODE) model of TGF-β1 receptor ligand signaling in a single fibroblast and from that model, identified the necessity for

simultaneous TGF-β1 and prostaglandin E2 signaling to maintain homeostatic fibroblast response during injury. I then combined this ODE model with a novel *in silico* agent based model (ABM) of fibroblasts and epithelial cells in co-culture in order to evaluate the effects of molecular scale signaling dynamics of cellular scale outputs such as cell proliferation, differentiation, and survival. With this model I identified a need for differential therapeutic treatment of fibroblasts and epithelial cells in order to prevent exacerbation of fibrotic disease. I then introduced TGF-β1 signaling into the existing *in silico* ABM model of TB induced granuloma formation in the lung (*GranSim*). Using this updated version of *GranSim* in combination with studies performed in non-human primates, I demonstrate the inhibition of TGF-β1 in the granuloma increases bacterial killing and promotes lesion sterilization by enabling increased effector functions from cytotoxic T cells. I also show that macrophages and cytotoxic T cells are differentially regulated in the granuloma by interleukin-10 and TGF-β1 respectively. Finally, I combine work on fibrosis and granuloma formation by introducing fibroblasts with an ODE model defining TGF-β1 receptor-ligand signaling dynamics into *GranSim* in order to characterize the formation of fibrotic granulomas. In this work I have advanced the understanding of TGF-β1 regulation in pulmonary disease and opened doors for further examination of potential therapeutic targets to treat these diseases.

Chapter 1

Introduction

1.1 Motivation

Pulmonary diseases are a major health concern affecting an estimated one billion people every year (1). A 2013 report from the Forum of International Respiratory Societies (FIRS) titled "*Respiratory Disease in the World: Realities of Today—Opportunities for Tomorrow"* highlights the global burden of this class of diseases (2). According to the FIRS report 4 million adults die prematurely ever year from chronic respiratory infections (2). The burden of these diseases does not only fall on adults (2). In children under the age of 5, pulmonary diseases are the most common cause of death and are responsible for 9 million deaths annually (3). In the United States, lung diseases account for 8.9% of all deaths (4) and an estimated 15% of adults ages 40–79 live with chronic lung diseases (5). Not only do lung diseases restrict survival and quality of life for millions of people, they also incur tremendous financial burden to health care systems (2). Respiratory infections cost the United States between 71 and 167 billion dollars annually in medical bills and lost wages (6), with asthma costing 50.1 billion dollars in medical expenses alone (7). In addition to the previously mentioned diseases, interstitial lung diseases (ILDs) are a rising health burden in the United States (8). Advancements in prevention, diagnosis, and treatment of pulmonary diseases have the potential to improve hundreds of millions of lives and reduce global health costs immensely. In this work I will focus on the study of two

prototypical interstitial lung diseases, non-infectious pulmonary fibrosis and infectious tuberculosis (TB).

1.1.1 Pulmonary Fibrosis

Pulmonary fibrosis is defined by the thickening, stiffening and scarring of the lung tissue (9-13). Symptoms of pulmonary fibrosis include coughing, shortness of breath, fatigue, chest pain, loss of appetite and weight loss (9, 14, 15). Approximately 50,000 new cases of pulmonary fibrosis are diagnosed every year in the United States (15). The United States also sees approximately 40,000 deaths annually due to pulmonary fibrosis (15). It can be caused by a variety of triggers including infection, antibiotic treatment, occupational and environmental exposure, and smoking (9, 16-23). Pulmonary fibrosis can also be described as idiopathic, meaning it has no known cause.

There are few treatments and no curative therapies available for pulmonary fibrosis (24-26). The FDA recently approved two drugs, Pirfenidone and Nintedinab, for the treatment of pulmonary fibrosis. These drugs slow the progression of the disease, but do not halt or reverse it (27-33). According to a 2014 article by The Bloomberg Report, the cost of treatment with either of these drugs is between $94,000 and $96,000 per year (34). Idiopathic pulmonary fibrosis (IPF) is a particularly devastating diagnosis, with a prognosis for patients between 2 to 5 years from time of diagnosis (14, 35). Understanding the complex immunological regulation that occurs in the lung, and specifically that which contributes to the formation of pulmonary fibrosis enables me to predict new and improved therapies for pulmonary diseases.

1.1.2 Tuberculosis

In contrast to IPF, which although devastating, affects a relatively small number of people, Tuberculosis (TB) is among the pulmonary diseases that have the greatest impact globally. Approximately one third of the world's population is infected with the bacterium *Mycobacterium tuberculosis* (Mtb), the causative agent of TB (36). TB infection is transmitted when an infected individual exhibiting disease symptoms coughs and bacteria are released into the air in sputum droplets. An uninfected individual then inhales these droplets, resulting in a new exposure that likely will lead to infection, particularly upon repeated exposure (36). Of the over 2 billion people that are infected with Mtb, about 10 percent show clinical symptoms of the disease (called primary, active TB). There are 9 million new cases and 1.4 million deaths annually from TB (36). Although the majority of people infected with Mtb have controlled the infection and do not show clinical symptoms (latent TB), there is a 10% chance that these people will experience reactivation (progression from latent to active disease) in their lifetimes (37).

The most common form of TB is pulmonary TB (38). Inhalation of Mtb stimulates the formation of complex immune structures called granulomas, which serve to contain the infection and protect surrounding tissue (39, 40). However not all granulomas successfully contain or clear the bacteria, which can lead to dissemination of the infection to different sites in the lung (41-44). Even for granulomas that do contain the infection, their structure and density can present challenges for treatment and clearance of the bacteria (45). Granulomas are found in infected individuals who show symptoms of TB, as well as those that do not. They are found primarily in the lungs, but can also be seen in lymph nodes and other tissues (40, 41, 46-48). An individual with active TB has on average 42 granulomas (43), each with a unique composition and trajectory. A single person can have granulomas that fall into different categories. Understanding

the complex mechanisms that drive granuloma formation and function provides much needed insight into the dynamics surrounding Mtb infection, and enables me to predict potential therapeutic targets to better treat TB.

Pulmonary fibrosis is a dysregulation of the wound healing process in the lungs, which can be induced by many different insults. It is often seen in association with Mtb infection. Fibrosis can be found surrounding granulomas both in patients that have received antibiotic treatment and those that have not (49). Understanding the coordination between these ILDs can highlight key mechanisms relevant across pulmonary disease.

At the foundation of developing new treatments for pulmonary disease is identifying both the role of the immune system in disease progression and the unique actions of the immune system specific to the lung environment (50-55). The immune system is comprised of cells and cytokines (molecules that drive the immune response) that serve a wide variety of functions in fighting infection and repairing tissue damage. Cytokines and chemokines (a subclass of cytokines specifically involved in cellular recruitment) are key to the recruitment and regulation of immune cells, driving granuloma formation (41, 42, 44, 46, 56-60), and pulmonary fibrosis (61-84). Transforming growth factor-β1 (TGF-β1) is one such cytokine that has been demonstrated to have great importance in lung immunology (61, 62, 64, 66-68, 74, 77, 78, 84-91). While the importance of TGF-β1 has been identified in many pulmonary diseases, the mechanisms of TGF-β1 regulation often remain a mystery. For other diseases the role of TGF-β1 has yet to be identified.

TGF-β1 has been shown to play a central role in the development of pulmonary fibrosis, an interstitial lung disease. Exploring the role of TGF-β1 in these two distinct but overlapping ILD diseases has enabled me to advance the field of pulmonary immunology, to predict potential

therapeutic targets, and to establish a focused trajectory of research to more efficiently explore future questions.

1.2 Fundamentals of transforming growth factor-β1

TGF-β1 is a member of the transforming growth factor-β superfamily of cytokines (62, 89, 92). This is a large family consisting primarily of TGF-βs and bone morphogenic proteins (BMPs) (93, 94). TGF-β1 is secreted as homodimer of the bioactive TGF-β1 ligand molecule (25kDa) covalently bound to a homodimer of a latency-associated peptide (LAP) (95, 96). This complex is called the small latent TGF-β1 complex (42 kDa) (95). Following secretion, TGF-β1 can be stored in the ECM as a large latent TGF-β1 complex (290 kDa) which contains the small complex and an additional protein known as the latent TGF-β1 binding protein (LTBP1) (97). Activation of TGF-β1 occurs through removal of the LAP from the bioactive ligand by proteolytic cleavage, mechanical extraction, or changes in pH of the surrounding environment (95). Once dissociated from the LAP, the bioactive TGF-β1 molecule (active TGF-β1) is free to bind its respective member of the TGF-β1 superfamily of receptors.

1.2.1 TGF-β1 signaling

The TGF-β1 superfamily of receptors is made up of two subpopulations (Type I and Type II) of transmembrane serine/threonine kinase receptors (93). Active TGF-β1 binds first to the TGFβRII (a member of the Type II receptors), which is constitutively active (93). This complex then recruits the activin-like kinase 5 (ALK5) receptor (a member of the Type I receptors) (98, 99). ALK5 is transphosphorylated by TGFβRII, inducing downstream signaling through the canonical SMAD2/3, and non-canonical rho/ROCK signaling cascades (100).

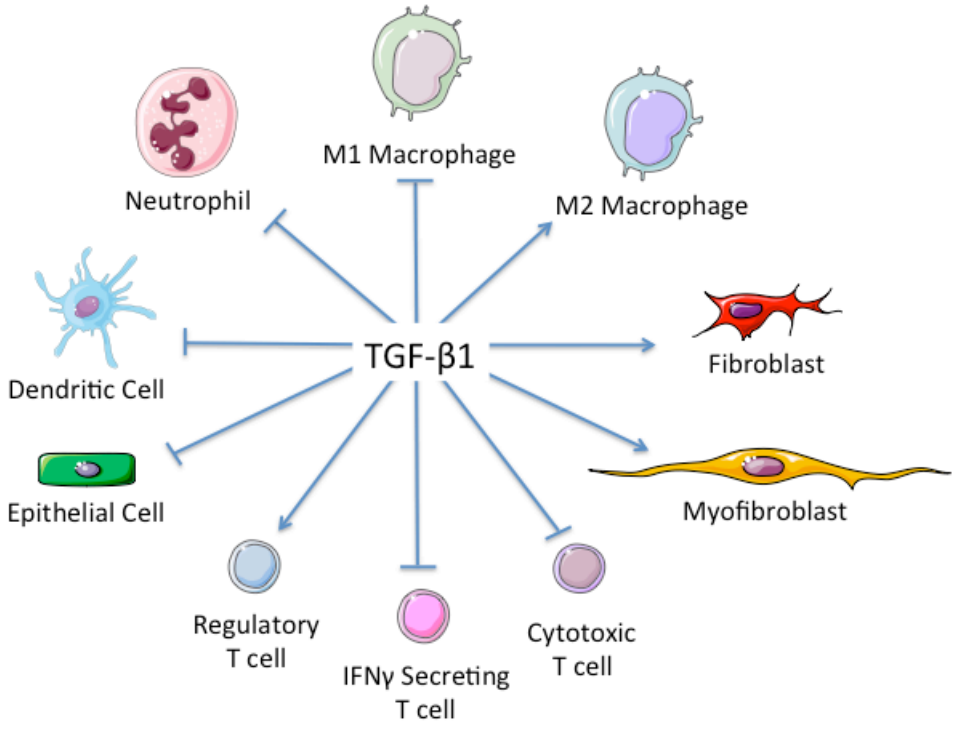

Figure 1.1. General actions of TGF-β1 on various cell types. In clockwise order TGF-β1 inhibits M1 differentiation, promotes M2 differentiation, promotes fibroblast proliferation, promotes fibroblast to myofibroblast differentiation and collagen secretion, inhibits cytotoxic T cell effector functions, promotes regulatory T cell down regulation of other cells, induces epithelial cell apoptosis, inhibits dendritic cell antigen presentation, and inhibits neutrophil degranulation.

TGF-β1 ligand is an autocrine and paracrine signal that is secreted by most cell types (101). Similarly, TGF-β1 receptors are expressed on most cells (102) rendering them sensitive to the signal. Despite the universality of TGF-β1, it plays very specific and different roles for different cell types (Figure 1.1). It is known to induce fibroblast proliferation at low concentrations (70, 103, 104), but drive differentiation and secretion of ECM proteins at higher concentrations (62, 89, 92, 100, 105). Epithelial cells undergo apoptosis in high concentrations of TGF-β1 (67, 106, 107). TGF-β1 has been shown to cause cell cycle inhibition in keratinocytes

(108, 109), inhibits secretion of TNF-α by macrophages (110), and plays a variety of roles in T-cell differentiation and maturation (111-117). The diversity of functions preformed by TGF-β1 is enabled in part by its co-regulation with other cytokines.

1.2.2 Pro- and anti-inflammatory cytokine interactions

Table 1.1 General action of cytokines and mediators of inflammatory processes

Cytokine	Abbreviation	Affect on Inflammation
Transforming growth factor-β1	TGF-β1	↓
Interleukin 10	IL10	↓
Tumor necrosis factor-α	TNFα	↑
Interferon-γ	IFNγ	↑
Prostaglandin E2	PGE_2	↑

↓ Denotes anti-inflammatory, ↑ Denotes pro-inflammatory

Expression of and signaling by TGF-β1 occurs in the context of a complicated cytokine and eicosanoid milieu and, depending on the specific tissue, other cytokines influence cellular response and sensitivity to TGF-β1 (85, 118-124). Cytokines are often descried as generally pro- or anti-inflammatory though there are many exceptions to these categorizations (Table 1.1). TGF-β1 is typically described as anti-inflammatory because the majority of it's known functions in immunity involve suppressing cell activity, regulating effector functions, and inducing apoptosis (63, 85, 92, 108, 110, 113, 119-121, 124-142). Outside of immune-related function, TGF-β1 has been shown to play an important role in embryonic development, tissue genesis, and wound healing (98, 105, 143-156). Other cytokines directly and indirectly affect the role of TGF-

β1 in these processes. A subset of these cytokines specifically relevant to this work includes anti-inflammatory cytokine interleukin 10 (IL10) (157, 158), and pro-inflammatory cytokines tumor necrosis factor-α (TNFα) (158-165), and interferon-γ (IFNγ). In addition to cytokines, lipid mediators can have a strong effect on the functionality of TGF-β1. One particular pro-inflammatory lipid mediator relevant to this work is prostaglandin E2 (PGE_2) (66, 83, 166-169).

Pro-inflammatory cytokines promote cell activation and effector function in order to mount an immune response during infection. TNFα is a 17.4kDa pro-inflammatory cytokine secreted by activated and infected macrophages, as well as CD4+ and CD8+ T cells during infection (170, 171). TNFα secreted by macrophages stimulates the secretion of chemokines such as CCL2, CCL5 and CXCL9 at the site of infection. These chemokines signal for the recruitment of other immune cells to the site of infection. TNFα can also induce cellular apoptosis, a critical component of sterilizing infection and wound healing. Co-regulation between pro-inflammatory TNFα and anti-inflammatory TGF-β1 maintains balance during infection. TNFα promotes macrophage expression of TGF-β1 and MMP9. TGF-β1 inhibits macrophage expression of TNFα. IFNγ is another pro-inflammatory cytokine that plays an important role during pulmonary disease. IFNγ is primarily secreted by Th1 T cells, and works to promote macrophage activation in granulomas.

IL10 is an 18kDa regulator of inflammation during infection (172). It can be secreted by a wide variety of cell types, including T cells and macrophages (41, 173-176). IL10 inhibits pro-inflammatory cytokine secretion, prevents apoptosis and necrosis, and restricts macrophage activation (172, 174-180). These functions serve to control the magnitude of the inflammatory response and prevent excessive tissue damage in the context of infection. The anti-inflammatory effects of IL10 have been correlated with pathogen virulence in Mtb infection because they

restrict the hosts ability to induce inflammatory responses (41). IL10 correlates with a decrease in scar formation during wound healing (181). Scar formation is increased during wound healing in IL10 KO mice (182). IL10 and TGF-β1 have been shown to have regulator effects on each other. TGF-β1 can promote IL10 production by macrophages (183) and T cells (184) in some cases, but can also inhibit IL10 production by peripheral blood monocytes in other cases (185). In the inverse IL10 has been shown to inhibit TGF-β1 synthesis by bone marrow cells (186). IL10 and TGF-β1 are both anti-inflammatory cytokines, however their respective roles may differ depending on the specific tissue context, and in some cases are not known.

Prostaglandin E_2 (PGE_2) is a lipid mediator that induces diverse cell type specific responses including homeostasis, inflammation, and sometimes anti-inflammatory responses. Many different cell types including epithelial cells, neutrophils, macrophages, and fibroblasts secrete PGE_2. PGE_2 is influenced by common non-steroidal anti-inflammatory medications (NSAIDs). In the context of pulmonary disease relevant to this work, PGE_2 induces fibroblast quiescence to prevent excessive fibroblast proliferation, collagen secretion and tissue remodeling (187, 188). TGF-β1 and PGE_2 have inverse regulatory effects on fibroblasts. The combinatorial effects of TGF-β1 and these cytokines and mediators on immune cells are likely the key to understanding the role of TGF-β1 in pulmonary disease.

1.3 Computational modeling of pulmonary diseases

The regulation that occurs between cells, cytokines and the host immune response is extremely complex. Because different aspects of the immune response are so intertwined, performing reductionist experiments *in vitro* and *in vivo* can be challenging and has limitations. These types of studies provide pieces of information about the system, but are not conducive to

comprehensive systems analysis. Systems biology combines *in vitro* and *in vivo* studies with computational methods to predict the mechanisms behind experimental results and clinical outcomes (Figure 1.2).

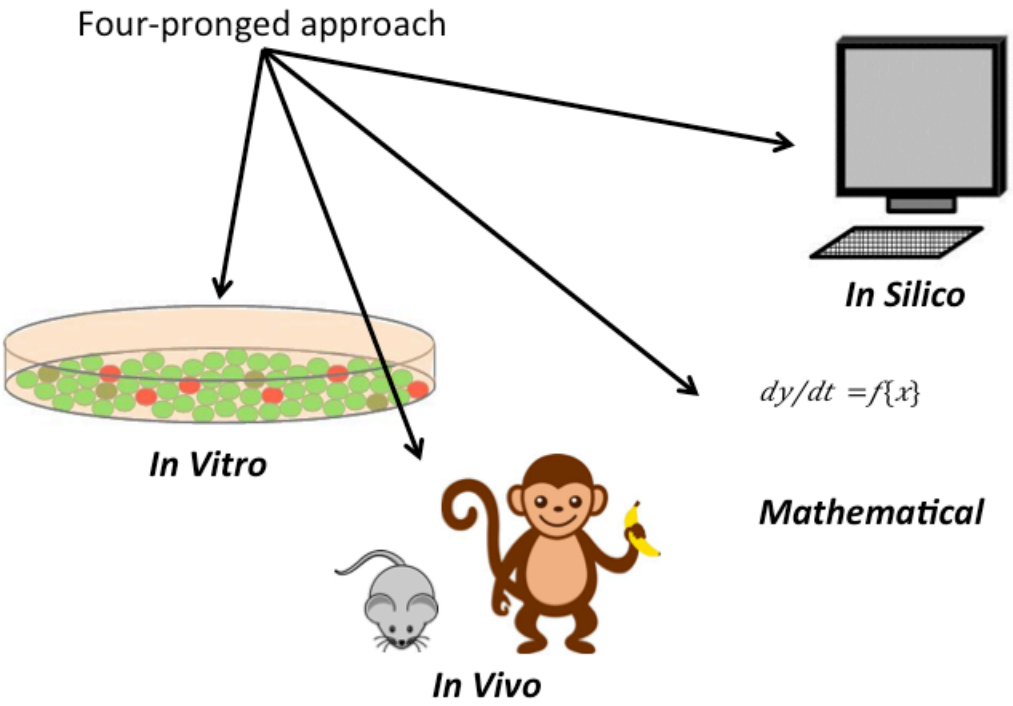

Figure 1.2. Systems biology combines many different scientific approaches including *in vitro*, *in vivo*, *in silico*, and mathematical models. *In silico* is a term used to reference models generated using computer systems rather than biological systems. *In silico* alludes to the use of silicon in computer chips.

Computational models can be constructed using either math and/or computer programming to address different kinds of biological questions (63, 83, 157, 158, 189-198). *In silico* models are similar to *in vitro* models in that they take a reductionist approach focusing on first order interactions including the most important aspects of a system and reducing other noise. *In silico* models can also resemble *in vivo* models that are able to capture complex

dynamics over extended time and space. *In silico* models are calibrated and validated using biological data, which can be derived either *in vitro* or *in vivo*. The origin of the data used for calibration determines which system the model best reflects.

An important feature of mathematical and computational models is that they can be manipulated in ways that biological models cannot. Data can be collected from *in silico* models more easily and more often than either *in vitro* or *in vivo* models. They can be used in high volume to perform thousands of simulated experiments in less time, and requiring less labor than biological models. The outputs collected from mathematical and computational models can be statistically analyzed to indicate specific mechanisms driving different model outcomes. Model outputs that do not reflect biological observations can indicate a key component of the system that is erroneous or absent, further informing both models and experiments.

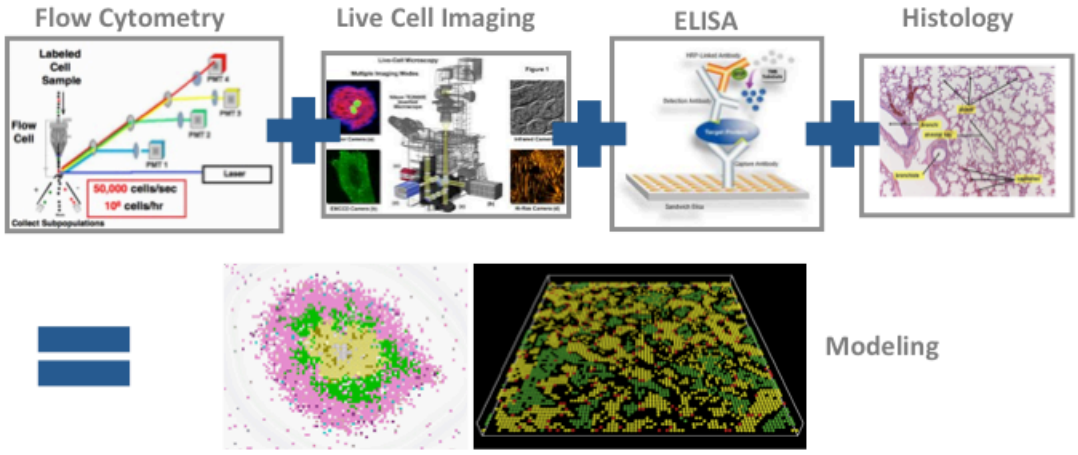

Figure 1.3. Computational models provide outputs at many different biological scales. These outputs can be compared to results provided by different experimental methods including but not limited to flow cytometry, live cell imaging, ELISA assays, and histology.

Ordinary differential equation (ODE) models are mathematical models that track changes in concentration over time. ODE models are continuous, deterministic, and do not account for space or spatial heterogeneity (199). ODE models are relatively quick to run and work well for

processes that occur on short time steps and in homogeneous environments, such as receptor ligand signaling events. ODE models can also be useful for studying long processes that occur over years, like epidemiological models. Because they are continuous, non-spatial, and deterministic, ODEs are not an optimal tool for studying discrete or stochastic events (Figure 1.4).

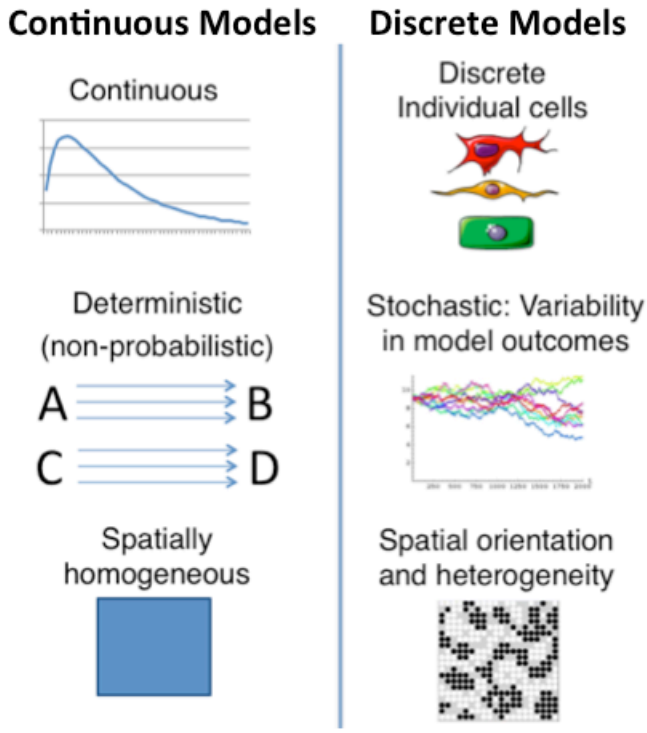

Figure 1.4. Diagram outlining differences between continuous and discrete models. Ordinary differential equation models are classified as continuous. Agent based models are classified as discrete.

For this work, I also use agent-based models (ABMs) to capture discrete, stochastic, and spatial events occurring at the cellular scale. ABMs are a class of *in silico* models that capture system level dynamics as a result of the adaptive behavior of individual agents. These models assign probabilistic actions and traits to individual agents within a system using rules rather than

equations and track these actions over time and space (200). Agents within the model are tracked in a discrete manner and outputs of ABMs can be temporal as well as spatial (Figure 1.4). The behaviors of discrete agents can be probabilistic, and therefore agent-based models are stochastic in nature.

In silico models can capture the dynamics of biological events at different scales including molecular, cellular, tissue, and organismal (Figure 1.3). In this work molecular scale dynamics, such as receptor/ligand binding of TGF-β1, are modeled using ordinary differential equations (ODEs) (83, 157, 158, 169, 201, 202). There are many ODE models of pulmonary disease including those studying IPF (169, 203-207), cystic fibrosis (208), and tuberculosis (160, 165, 209-214). These models focus on specific aspects of pulmonary disease at a single biological scale. In addition to the *in silico* studies of pulmonary disease that utilize ODE models, there are a wealth of studies using ABMs. These models examine the development of such diseases as chronic obstructive pulmonary disease (63, 215), acute inflammation (216), fungal infection (217), and tuberculosis (158, 160, 164, 165, 218-220). These ABMs focus primarily on cellular behavior and intercellular signaling. Still other ABMs study the transmission of pulmonary diseases within populations (221-224). In this work I build off prior studies that examine the behavior of immune cells in the lung following Mtb infection (157-162, 164, 165, 190, 192, 193, 201, 209, 210, 212, 220, 225-228).

In addition to capturing events at individual scales, models can also capture events at multiple biological scales simultaneously. Multi-scale modeling takes a systems approach to studying biological questions. In this work, I use multi-scale hybrid modeling, (i.e. combining molecular scale ODEs and cellular scale ABMs), to capture complex tissue scale dynamics. Output from the ODE model at the molecular scale is a feed forward input into the ABM at the

cellular and tissue scales. Cytokines secreted from cells in the ABM determine concentrations that feed into the ODE models. Therefore, extracellular cytokine levels and intracellular cytokine signaling events link the cellular and molecular scale models creating hybrid multi-scale models for the study of pulmonary disease. Analyses of these complex multi-scale models is approachable and we have developed techniques to explore them including USA (229) and tuneable resolution (230).

1.4 Fundamentals of pulmonary fibrosis studies

Pulmonary fibrosis is thought to be the result of dysregulation of the wound healing process (22, 143, 148, 231). Normal wound healing occurs in four stages: (I) coagulation and hemostasis, (II) inflammation, (III) proliferation, and (IV) remodeling (148). The first and second stages of wound healing are characterized by platelet aggregation at the site of exposed ECM, secretion of large amounts of cytokines, and recruitment of cells to the site of the injury (232, 233). During the third stage of the wound healing process, fibroblasts proliferate into the wound gap (152). Fibroblasts are an essential part of tissue regeneration and wound healing (150, 156). In healthy tissue fibroblasts persist in a quiescent state (105) under continual PGE_2 signaling from epithelial cells (66, 122, 188, 234). Upon injury, the architecture of the tissue is disrupted stimulating the wound healing process to begin and eventually inducing the proliferation of fibroblasts (105) (Figure 1.5).

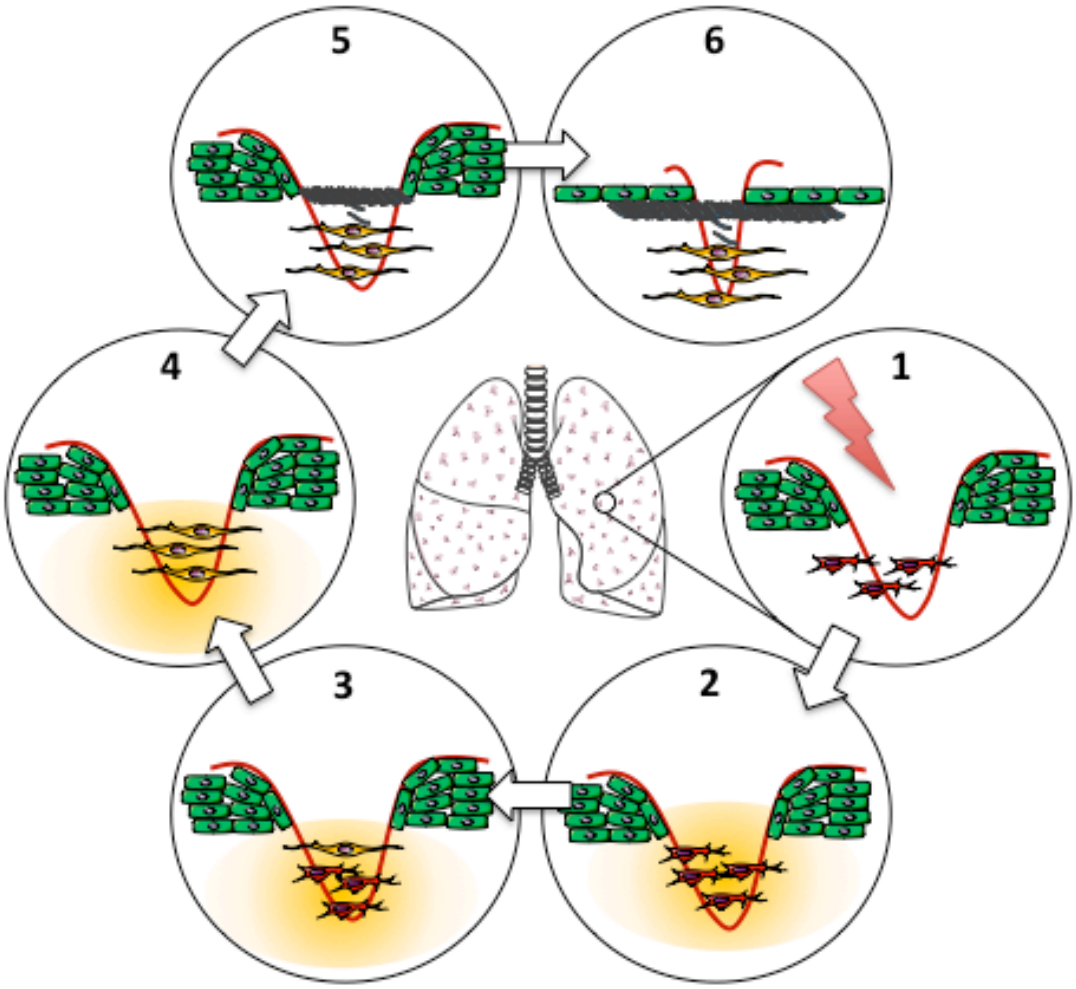

Figure 1.5. Mechanism of wound healing in the lungs. During proliferative phase of the wound healing response, (1) fibroblasts proliferate into the site of the wound. (2) They secrete cytokines including TGF-β1, (3) which induces their own differentiation. (4) Fibroblasts differentiate into myofibroblasts , which preform two key functions during the remodeling phase of the wound healing response. (5) Myofibroblasts secreted ECM proteins, which produce a substrate for re epithelialization. (6) They also synthesize αSMA, which enables them to contract and remodel injured tissue (148, 156).

Fibroblasts secrete TGF-β1 and other growth factors leading to fibroblast-to-myofibroblast differentiation (235-237), and the fourth stage of wound healing (66, 100, 105, 234). During this stage fibroblasts differentiate into myofibroblasts (105). Myofibroblast differentiation is characterized by secretion of ECM proteins (143, 152, 156) and synthesis of α-smooth muscle actin (αSMA). ECM proteins are cross-linked to provide a substrate for re-

epithelialization of the wounded area (152). αSMA is a cytoskeletal protein that gives myofibroblasts a contractile phenotype (105, 189, 238), enabling them to remodel tissue and close the wound gap (148-150, 156, 239, 240).

In conjunction with fibroblasts and myofibroblasts, epithelial cells play an important role in normal pulmonary wound healing (241). Epithelial cells are a substantial component of lung tissue, covering the bronchi, airways, and alveoli. They provide a surface for gas exchange and create a barrier against infection (242-244). Wounds break the epithelial layer causing damage to the cells (18, 66, 245). Regeneration of the epithelium is needed to restore proper function of the lung tissue. During normal wound healing epithelial cells proliferate onto the ECM secreted by myofibroblasts, restoring the integrity of the epithelial barrier (152).

Fibrosis occurs when the normal wound healing processes become dysregulated, specifically during the third and fourth stages. Excessive proliferation and differentiation of fibroblasts destroys the tissue architecture resulting in inhibited inspiration and expiration. This tissue is characterized as being stiff and scarred, and is not suitable for gas exchange (12, 246). Excessive remodeling leads to even further degradation of the tissue by destroying the alveoli. Although the specific cause of dysregulation is often unknown, TGF-β1 is implicated in driving excessive fibroblast proliferation and differentiation. TGF-β1 is also toxic to epithelial cells in high concentrations (84, 88). Epithelial cell damage is associated with the induction of pulmonary fibrosis (187, 241, 245, 247, 248). Stimulation of myofibroblast driven tissue remodeling by TGF-β1 may further exacerbate epithelial damage by reducing the available surface area for re epithelialization (231, 249). The loss of epithelial cells in the tissue further relieves inhibition of fibroblasts and myofibroblasts by PGE_2, and contributes to a snowball effect of tissue remodeling and fibrosis.

Previous studies of wound healing and fibrosis have been preformed *in vitro*, *in vivo*, and *in silico*. Scratch assays are one *in vitro* model used to study wound healing, specifically cell migration during wound healing (250). In a scratch assay, cells (usually epithelial cells and/or fibroblasts) are plated onto a petri dish and a scratch is made through the cells, destroying cells in the middle of the plate. Photos of the plate are taken to track migration of cells and they fill the gap (251-253). Another assay used for studying wound healing *in vitro* is the transwell assay. Transwell assays place cells on one side of a membrane and chemokines on the other (66). Migration of cells though the membrane can be measured.

There are two common *in vivo* models of pulmonary fibrosis in mice. Bleomycin is used to induce pulmonary fibrosis (16, 18, 167, 248, 254-256) and is typically administered either intratracheally or intravenously (254). Bleomycin induces pulmonary injury, which is visible within one week and treatment, and features of fibrosis, which are visible two weeks after treatment (254). Another *in vivo* model of pulmonary fibrosis is the fluorescein isothiocyanate (FITC) induced model. FITC is introduced inratracheally into the lung and has a green fluorescence color that can be visualized to see the initiation of injury (257, 258).

Previous studies by other groups include computational models of wound healing of the epidermis (145, 146, 259-270), cornea (271-274), pressure ulcers (275, 276), and other systems. There are also a number of *in silico* models of extracellular matrix formation, and organization (273, 277, 278). There are also a wide array of models of fibrosis including ODE models, agent based models, and biomechanical models (63, 83, 169, 203, 279-283). However models that focus specifically on pulmonary fibrosis are fewer (63, 203). Current computational models of pulmonary fibrosis focus on cellular scale interactions (63, 203). These models include representations of cytokines but do not focus on molecular scale interactions (63, 203). These

models also do not focus on epithelial cell survival (241, 284). In this work we construct a multi-scale model combining molecular and cellular scale events to study the effects of fibroblasts directly on epithelial cells.

1.5 Fundamentals of tuberculosis studies

Pulmonary TB is the result of infection by inhalation of *Mtb*. Once in the lung, *Mtb* is phagocytosed by an alveolar macrophage at the initial site of infection. The bacteria are able to avoid phago-lysosomal fusion, and can survive within the macrophage (41, 44, 46, 60, 285, 286). Bacterial replication can ultimately lead to rupture of the infected macrophage, releasing bacteria into the surrounding tissue. These, now extracellular, bacteria are available for phagocytosis by other nearby macrophages leading to propagation of the infection in the local area. Infected macrophages secrete cytokines, which recruit monocytes and neutrophils from the blood to the site of infection (41). As cells accumulate at the site of infection they contribute to the early stages of granuloma formation. Two to three weeks following the initial infection, dendritic cells will carry antigen from the site of infection to nearby draining lymph nodes to initiate the adaptive immune response (60, 286). Once primed, T cells are recruited to the site of infection where they perform a variety of effector functions including cytotoxic killing of infected cells and macrophage activation (41, 287). Together, the cells at the site of infection contribute to the formation of granulomas.

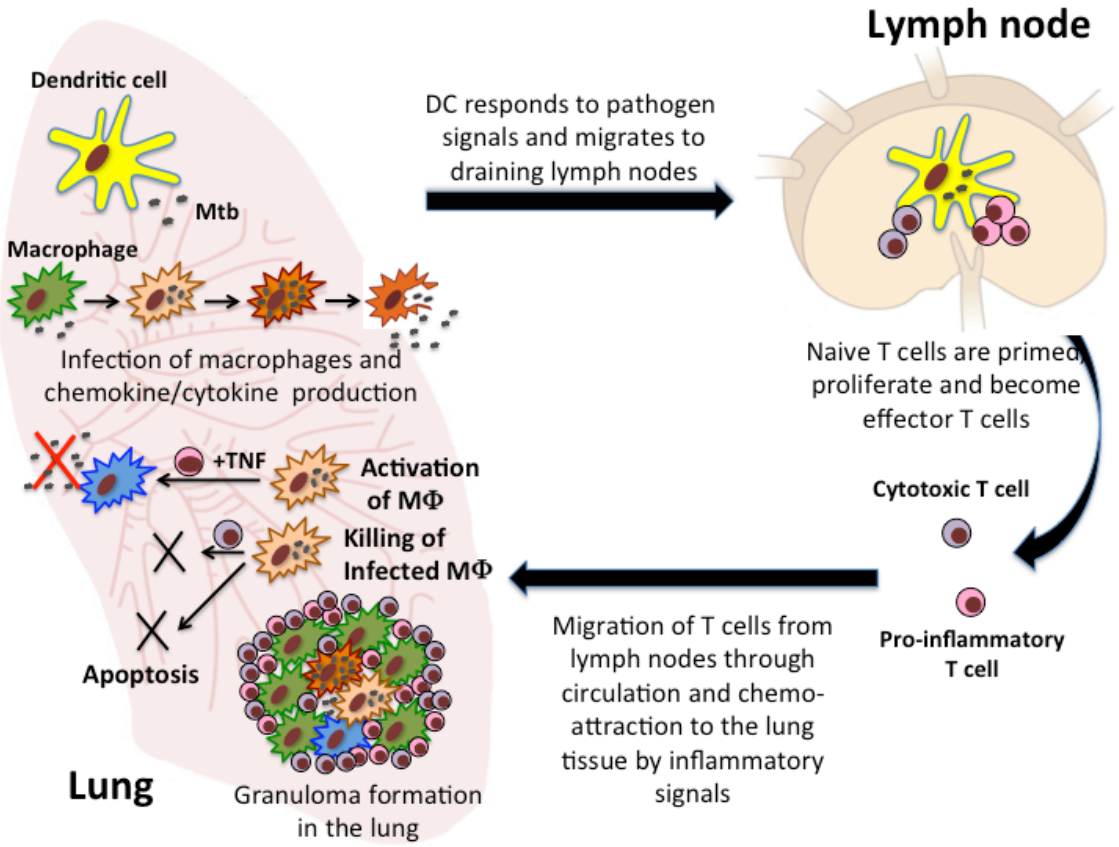

Figure 1.6 Schematic of TB progression and relevant immune response. The process begins in the top left corner where Mtb are inhaled into the lungs and phagocytosed by macrophages resulting in intracellular infection. As a result macrophages secrete cytokines, which recruit dendritic cells to the site of infection. Dendritic cells acquire antigen and travel from the lung to the lymph node where they present antigen to naïve T cells. Stimulated T cells then travel back to the site of infection in the lung and contribute to granuloma formation. Macrophages at the site of infection are activated to kill bacteria by effector T cells. Some macrophages become infected and if they cannot kill the infecting bacteria, will rupture releasing the bacteria and contributing to the spread of infection.

Granulomas are highly organized cellular structures that function in coordination with the immune system to isolate bacteria and infected cells from the surrounding tissue and provide an environment for clearance of the infection. The structure of granulomas also works to the advantage of the pathogen, making it challenging for uninfected cells and drugs to access and effectively kill bacteria (192, 288). The spatial organization of granulomas can vary but generally follows the following pattern from inside out: a caseous center of bacteria, dead cells,

and infected cells; a ring of resting and infected macrophages; a ring of lymphocytes and resting macrophages (57). Due to their complexity, granulomas can be classified based on cellular composition, number of bacteria present, and overall size and shape. Cellular classifications of granulomas include but are not limited to caseus (having a necrotic center of bacteria and dead cells) (Figure 1.7 A), suppurative (made up primarily of neutrophils) (Figure 1.7 B), solid cellular (having no caseum in the center) (Figure 1.7 C), and fibrotic (having collagen and ECM proteins throughout the granuloma and especially on the periphery) (Figure 1.7, D) (46, 57, 285). Granulomas classified by number of live bacteria present (CFU) are referred to as contained (having a CFU that is stable, i.e. neither increasing nor decreasing over time), disseminating (having an increasing CFU) and *sterilized* (having achieved a CFU of zero).

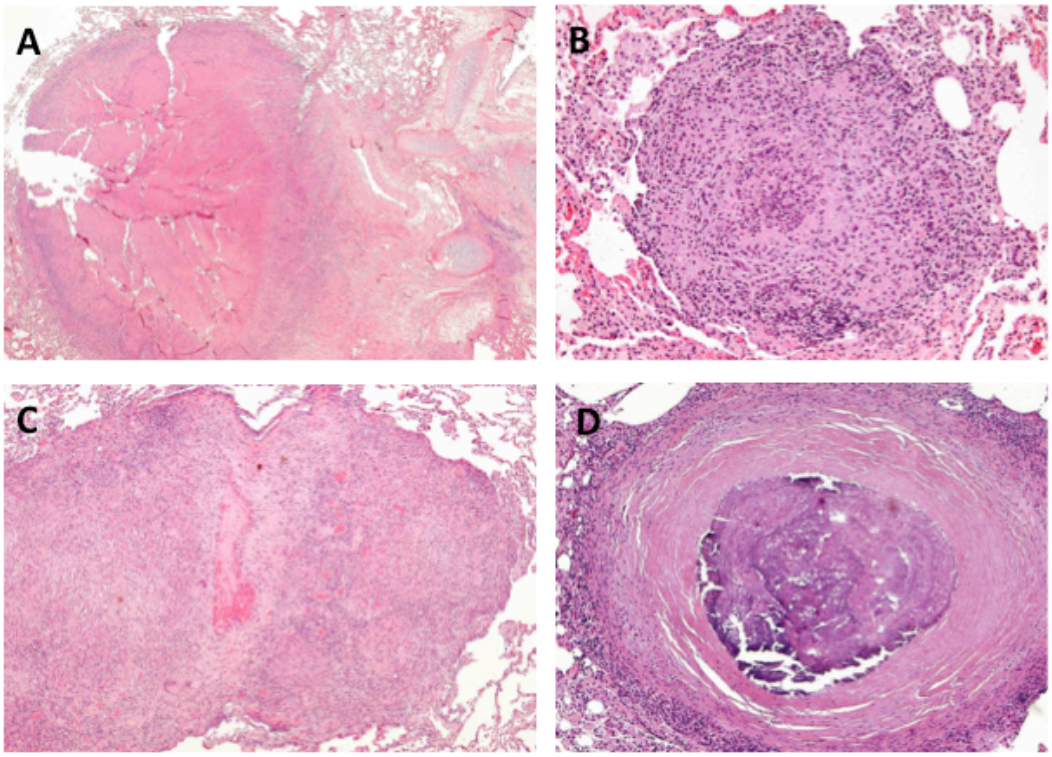

Figure 1.7 Histology of Mtb induced pulmonary granulomas from NHPs. A) Caseus necrotic granuloma. B) Suppurative necrotic granuloma. C) Solid cellular granuloma. D) Fibrotic/calcified granuloma.

Granuloma CFU's are determined largely by the immune response to infection. The host immune system has several mechanisms for killing bacteria utilizing macrophage and T cells specific mechanisms (289). Macrophages phagocytose extracellular bacteria and perform phagolysosomal fusion to kill the bacteria (46), or target them with reactive oxygen species (46). These processes are typically unsuccessful resulting in infection of the macrophage itself (289). Macrophages that have been activated by the second signal IFNγ (through the STAT1 pathway, the signal being bacteria through the NFkB pathway) are better killers of intracellular bacteria. Another first signal can be TNF which also signals through NFkB. Infected macrophages can be killed by T cells through Fas/Fas-ligand mediated apoptosis (290). Infected macrophages are also killed by cytotoxic T cell induced apoptosis through the secretion of perforin, granzymes, and granulysin (289). Collectively, these mechanisms contribute to killing of bacteria within granulomas.

Due to the complex nature of granuloma formation, the best models for studying pulmonary tuberculosis are NHPs (37, 42, 43, 46, 49, 56, 57, 59, 60, 163, 170, 285, 291-295). NHP studies are very expensive because large animals must be housed in a biological safety level three facility and experiments take weeks, months, or years to preform. Limited biological samples and reagents can make some experiments very difficult to do *in vivo*. Rabbits are also used to study the formation of granulomas (192, 193, 285, 296-304). Rabbits face similar reagent limitations to NHPs. In some cases mice are also used to study pulmonary tuberculosis infection despite being a poor model of granuloma formation (170, 305).

Computational models of tuberculosis infection include ordinary differential equation, partial differential equation, and agent-based models. Differential equation models of TB have been used to study the role of cytokines in granuloma formation and function (162, 164, 212,

219). They have also been used to study the pharmacokinetics of drugs during TB treatment (297, 306-309). Agent based models of tuberculosis infection have been used to study the immune response to TB and granuloma formation (220, 227). Agent based models and differential equation models have been combined to form hybrid multi-scale models, which are used to examine the cross-regulation between events at the cellular, molecular, and tissue scales (158-161). In this work we combine a cellular scale agent based model of TB granuloma formation with molecular signaling dynamics of TGF-β1 to study the role of TGF-β1 in granuloma formation and function (83, 169).

1.6 Dissertation overview

The goal of this work is to answer questions regarding the role of TGF-β1 in ILDs such as fibrosis and TB. To address these questions I have developed computational models describing the role of TGF-β1 in fibrotic responses and infection. Using a multi-scale systems biology approach I have predicted mechanisms responsible for dysregulated fibroblast behavior and proposed potential therapeutic targets. In particular my thesis is designed to determine what molecular scale mechanisms are responsible for driving cellular and tissue scale fibrotic phenotypes. I focused on the role of TGF-β1 dynamics in fibroblast activation as well as the interaction between fibroblasts and epithelial cells.

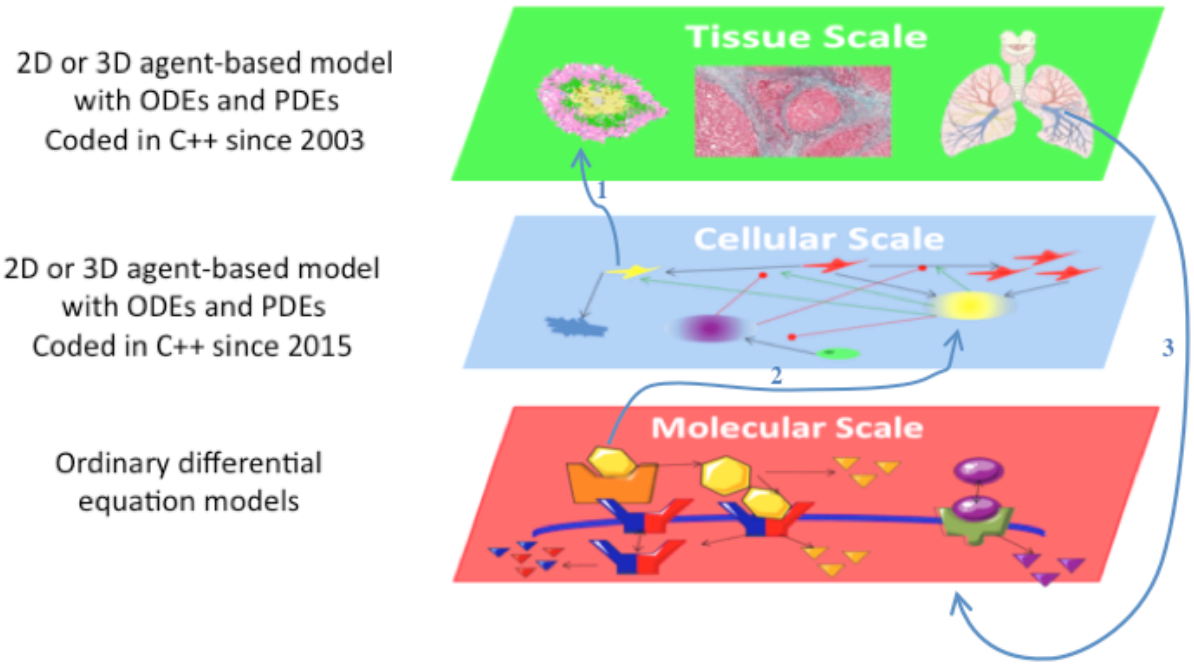

Figure 1.8. Hybrid multi-scale modeling. This is a conceptual illustration of how different types of models are combined to create a single hybrid multi-scale model of granuloma formation in the lungs. At the molecular scale is an ODE model of TGF-β1 receptor ligand signaling dynamics within a single fibroblast (169). Cytokine secretion by cells and diffusion within the environment also occurs at the molecular scale. At the cellular scale is an agent-based model of the immune response in in the lung (158, 160, 220). This model is made up of individual cellular agents including macrophages, T cells, and fibroblasts, which respond based on probabilistic rules to stimuli and cytokines within their local environment. At the tissue scale is emergent behavior determined but the collective behaviors of individual agents within the model. This emergent behavior can be characterized and compared to biological phenomena. Each model scale is linked to the other scales through cytokine concentrations and/or agent behaviors. Molecules secreted and diffused at the molecular scale dictate the behavior of cells at the cellular scale (arrow 1). The actions of cells at the cellular scale dictate the emergent behavior at the tissue scale (arrow 2). The emergent behavior of the tissue scale defines local environments, which in turn influence cytokine concentrations at the molecular scale (arrow 3).

In my thesis I created a hybrid multi-scale model with a focus at the molecular level on the role of TGF-β1 receptor ligand signaling dynamics and downstream signaling events in fibroblast activation, and at the cellular level on fibroblast and epithelial cell co-regulation, as well as the role of TGF-β1 in the context of lung tissue and TB infection with readouts at the tissue scale. This model combines molecular scale, cellular scale, and tissue scale dynamics from

existing and novel models (Figure 1.8). I used this model to evaluate real-time molecular events and derive mechanisms driving pathogenic fibroblast behavior across the tissue, cellular and molecular scales. I am conducting my research according to the following specific aims paralleling *in silico* and *in vitro* approaches:

1.6.1 Aim 1: Predict host factors that regulate fibroblast activation and αSMA synthesis at the molecular scale.

Many previous studies identify an important role for TGF-β1 in fibroblast activation (70, 189, 310, 311), however there are still many question regarding the dynamics of fibroblast regulation that remain unanswered. The temporal dynamics of TGF-β1 and PGE_2 regulation of fibroblast activation have not been characterized. In this work we utilize relevant *in vitro* experiments and ODEs to identify specific characteristics of fibroblast activation and examine the behavior fibroblasts in the context of TGF-β1 and PGE_2 signaling. I develop a molecular scale mathematical model of specific TGF-β1 receptor ligand signaling dynamics to capture molecular scale events of TGF-β1 regulation of a single fibroblast (169). *In vitro* experiments measure fibroblast production of collagen and αSMA in response to TGF-β1 stimulation at different doses and over time. With these combined techniques I identify the time course dynamics of fibroblast response to TGF-β1 signaling and predict cellular conditions that result in healthy wound healing, fibrosis, and anti-fibrotic lack of wound healing. I also preform time course simulations of fibroblast response to different dosing regiments of TGF-β1 and PGE_2 and use uncertainty and sensitivity analysis to predict the mechanisms driving model outcomes.

1.6.2 Aim 2: Identify mechanisms driving fibroblast behavior and epithelial cell survival in a co-culture environment.

TGF-β1 and PGE_2 co-regulation of a single fibroblast alludes to mechanisms that may be relevant in a more complex tissue environment. The development of fibrosis involves both the dysregulation of fibroblasts and the disruption of epithelial cells. Therefore in order to identify key mechanisms driving fibroblast dysregulation during fibrosis, it is necessary to evaluate fibroblast behavior in a complex co-culture environment. In this work we capture the interactions between fibroblasts and epithelial cells in co-culture at a cellular level, integrate molecular scale dynamics, and validate against *in vitro* experimental results (83). In addition, we also perform co-culture experiments with fibroblasts and epithelial cells in different treatment conditions and measure collagen 1 and αSMA synthesis, as well as fibroblast proliferation and epithelial cell death. I construct a cellular scale *in silico* agent-based model of fibroblast and epithelial cell agents in co-culture, and integrate the molecular scale ordinary differential equation model in the fibroblast agents.

I perform time course simulations of the co-culture model under different initial conditions and apply uncertainty and sensitivity analysis to predict the mechanism driving model outcomes. With this model I can characterize the time course dynamics of fibrotic dysregulation in co-culture and predict the outcome of different initial tissue on fibroblast activation and epithelial cell survival, and predict potential therapeutic targets.

1.6.3 Aim 3: Identify a key role for TGF-β1 in regulating granuloma formation and function during pulmonary Mtb infection.

The action of TGF-β1 is relevant to many pulmonary pathologies, in addition to fibrosis. It has been predicted to play a role in TB, although the details and magnitude of this role in a complex immunological environment such as a granuloma have not yet been characterized. Previous work has examined the roles of both pro- and anti-inflammatory cytokines in the context of a granuloma using our hybrid multi-scale model of immune responses in the lung *GranSim* (157-159, 164, 209). In order to identify a mechanistic role of TGF-β1 in the progression of TB granuloma development and in granuloma sterilization, I introduce TGF-β1 dynamics into *GranSim*. I use uncertainty and sensitivity analysis to predict key mechanisms in driving outcome. We pair these *in silico* studies with *in vitro* studies from NHPs infected with Mtb and compare cytokine receptors present on different cell types in the granuloma to validate or refute predicted roles of TGF-β1 in the granuloma.

1.6.4 Aim 4: Predict mechanisms driving regulation and development of fibrosis across biological scales in the complex tissue environment of the lung and predict potential therapeutic targets for different types of pulmonary fibrosis.

In some cases, the development of pulmonary fibrosis is associated with pulmonary TB. Collaborators have characterized the development of fibrosis in association with TB (49). They have identified the occurrence of fibrosis in NHPs that have been treated with antibiotics and those that have not. The appearance of fibrosis differs somewhat between these groups. External fibrosis surrounds the granuloma and is associated with untreated granulomas, while central fibro calcific granulomas are associated with anti-biotic treatment. Because TGF-β1 plays an

important role in the development of both of these pathologies, we suspect that it may be central to the fibrosis developed during infection. To examine mechanisms of fibrosis formation in the context of TB, we combine cellular agents maintaining their molecular dynamics from the co-culture model into the granuloma lung model, *GranSim*. Uncertainty and sensitivity analysis can predict key mechanisms driving different fibrotic outcomes in granulomas. With this model we can identify regulators of fibrotic development in the context of a TB granuloma and compare these regulators to those identified in previous models and experimental studies.

Chapter 2

Identifying Mechanisms of Homeostatic Signaling in Fibroblast Differentiation

2.1 Introduction

Fibroblasts are necessary for tissue regeneration and wound healing (150, 156). Fibroblasts exist in tissue in a quiescent state (105) until disruption of the tissue structure triggers differentiation into myofibroblasts (105). This differentiation is characterized by secretion of extracellular matrix (ECM) proteins and production of α-smooth muscle actin (αSMA), a cytoskeletal protein that enables contraction and tissue remodeling (150, 156). Previous work has identified several critical functions performed by myofibroblasts including ECM protein secretion (148, 149, 239) and remodeling of damaged tissue. Dysregulation of fibroblast to myofibroblast differentiation can result in severe pathology that can compromise function of affected tissue; however, excessive ECM secretion can lead to detrimental tissue remodeling and fibrosis (22). Fibrosis, the stiffening and scarring of tissue, can result in poor clinical outcomes depending on the extent of the affected tissue, and patients with fibrosis often have poor prognoses (312). Idiopathic pulmonary fibrosis (IPF), for example, results in decreased inspiration and expiration capacity and has an average prognosis of 2-4 years (30, 33, 35, 313, 314). There are currently two treatments available for pulmonary fibrosis in the United States, both of which provide only a moderate extension of prognosis (about 6 months) (30, 33, 35, 313, 314). There are no available treatments that halt or reverse fibrosis. We aim to understand why

fibroblast differentiation becomes dysregulated and which signaling mechanisms drive this outcome in order to develop new therapeutics for this and other fibrotic diseases.

The cytokine transforming growth factor-β1 (TGF-β1) has been shown to play a critical role in fibrosis-associated pathologies. TGF-β1 is a major contributing factor to pulmonary complications and fibrosis following bone marrow transplant (20, 87). TGF-β1 sustains myofibroblast function and can exacerbate IPF (78, 241). It has been clearly established that TGF-β1 is key in driving development of fibrosis; however, there are still open questions as to the mechanisms involved in TGF-β1-induced dysregulation of fibroblast differentiation and myofibroblast function. To identify which factors contribute to fibrotic dysregulation and predict how best to inhibit this process, we construct a mathematical model describing the contribution of molecular mechanisms driving fibroblast to myofibroblast differentiation.

TGF-β1 is a growth factor and member of the transforming growth factor-β superfamily of cytokines known to drive differentiation of fibroblasts as well as secretion of ECM proteins (62, 89, 92). TGF-β1 is secreted in a latent form as a homodimer of TGF-β1 bound to a homodimer of the latency associated peptide (LAP) referred to as the small latent TGF-β1 complex (42 kDa) (95). It is stored in the ECM as a large latent TGF-β1 complex (290 kDa) which includes the small complex and an additional protein referred to as the latent TGF-β1 binding protein (LTBP1) (97). Release of TGF-β1 from the LAP produces an active TGF-β1 molecule. Latent TGF-β1 can be activated by proteolytic cleavage, mechanical extraction, and changes in pH of the surrounding environment (95). TGF-β1 is bound in its active form by a specific membrane receptor complex of ALK5 (TGF-β1 receptor 1) and TGFβ1RII (TGF-β1 receptor II) (98, 99). The effect of TGF-β1 on cells is tissue-and-cell specific. For example, TGF-β1 can induce differentiation of fibroblasts through downstream canonical SMAD2/3, and

non-canonical rho/ROCK signaling cascades (100). In keratinocytes TGF-β1 causes cell cycle inhibition (108, 109) and it has been shown to play several opposing roles in T-cell differentiation and maturation (111-117). Because of the cell specificity associated with TGF-β1 signaling, we focus on identifying fibroblast-specific mechanisms of action.

Several mathematical models have been developed to complement experimental approaches in exploring TGF-β1 receptor-ligand signaling dynamics in other cell types (206, 207, 315). Vilar et al. showed that the ratio of constitutive degradation of TGF-β1 receptors to degradation induced by ligand binding dictates whether cellular responses to TGF-β1 are transient or permanently elevated for keratinocytes and pancreatic cancer cell lines (207). Zi et al. identified that the duration of a cellular response to TGF-β1 is dependent on whether the receptor-ligand complex is internalized into a clatherin-coated or clatherin-independent endosomal compartment. In keratinocytes, if the predominant form of endocytosis is clatherin-independent, the response will be transient. However, if the predominate form of endocytosis is clatherin-dependent, the response will be prolonged (205). Recently, Vizan et al. demonstrated that keratinocytes experience a refractory state following a TGF-β1 signaling event, where cells are temporarily insensitive to further TGF-β1 stimulation. They showed that the duration of this refractory period is dependent on the rate of receptor turnover and the ratio of ligand-induced to constitutive receptor degradation for keratinocyte s (315). Together, these models emphasize the importance of endocytosis and constitutive vs. ligand-induced receptor degradation in determining the cellular response to TGF-β1 signaling.

Fibroblast responses to TGF-β1 differ from keratinocyte and pancreatic cell responses. As a result there are mechanisms specific to fibroblasts that were not considered in these prior mathematical models. Fibroblast responses to TGF-β1 are highly dependent on the simultaneous

presence of adhesion signaling (100). Adhesion signaling through integrin binding is necessary for TGF-β1 induced fibroblast to myofibroblast differentiation to occur (100). Previous work has demonstrated that fibroblasts plated onto plastic surfaces, such as a tissue culture plate, respond to TGF-β1 to induce differentiation (measured by synthesis of a-SMA). In contrast, when fibroblasts are suspended in liquid culture they show no response to treatment with TGF-β1 (100). These data indicate that fibroblasts require adhesion in order to respond to TGF-β1 stimulation (100). The stiffness of the substrate adhered to is influential in the strength of the fibroblast response to TGF-β1; the stiffer the substrate the greater the adhesion signaling, and stronger the response (238, 316-321). Another important factor in the regulation of TGF-β1 signaling in fibroblasts is a negative regulator present in the system, namely prostaglandin E_2 (PGE_2). PGE_2 indirectly inhibits TGF-β1 signaling by inhibition of FAK in the adhesion signaling cascade (168) rather than acting directly on TGF-β1 by limiting SMAD phosphorylation (168). No other forms of cross talk between PGE_2 and the canonical TGF -β1 signaling cascade have been demonstrated. PGE_2 has been shown to inhibit adhesion signaling, and in turn inhibit fibroblast responses to TGF-β1 (122, 168, 234, 322). Fibroblasts are exposed *in vivo* to PGE_2 secreted by epithelial cells, and it has been proposed that this constitutive signaling induces fibroblast quiescence, maintaining homeostasis of the tissue environment (187, 188). High levels of PGE_2 have been linked to increased fibroblast apoptosis (323). Previous work has shown that fibroblasts can lose sensitivity to PGE_2 *in vitro* by down-regulating EP2 receptor synthesis (324). This is a phenomenon that is also seen during fibrotic responses in the lung (167). PGE_2 can mediate functions of multiple cells via binding to four unique receptors (325). Because it is a strong inhibitor of adhesion signaling, however, understanding the mechanistic relationships between TGF-β1, adhesion signaling, and PGE_2 allows us to identify

environmental conditions favorable to healthy wound resolution as well as signaling mechanisms that are key to establishing those conditions.

Thus, to gain further insight into the role of TGF-β1 in regulation of fibroblast differentiation into a myofibroblast, we take a systems biology approach to identify the influence of molecular-scale mechanisms of TGFβ signaling on regulation of this transition. We use a combination of *in vitro* experimentation, mathematical modeling, and statistical analyses to identify key mechanisms driving fibroblast differentiation and dysregulation. We developed a nonlinear ordinary differential equation model that tracks the temporal concentrations of key species (Table 2.1) in receptor/ligand binding, trafficking and signaling cascades to evaluate how these events drive αSMA synthesis (Figure. 2.1).

Table 2.1 Model variables

Symbol	Definition	Units
TGF-β1 Receptor Ligand Variables		
$\boldsymbol{TGF\beta1_{lat}}$	Latent TGF-β1	$\frac{moles}{volume}$
$\boldsymbol{TGF\beta1_{act}}$	Activated TGF-β1	$\frac{moles}{volume}$
$\boldsymbol{R_{surf}}$	Free receptor on the cell surface	$\frac{\#}{cell}$
$\boldsymbol{R_{int}}$	Internalized free receptors in the cytoplasm	$\frac{\#}{cell}$
$\boldsymbol{TRC_{surf}}$	Receptor ligand complexes on the surface of the cell	$\frac{\#}{cell}$
$\boldsymbol{TRC_{int}}$	Internalized receptor ligand complexes in the cytoplasm	$\frac{\#}{cell}$
PGE_2 Input Variables		
$\boldsymbol{PGE2_{Sol}}$	Soluble Prostaglandin E2	$\frac{moles}{volume}$
$\boldsymbol{PGE2_{int}}$	Internalized Prostaglandin E2	$\frac{\#}{cell}$
α-Smooth Muscle Actin Output Variables		
$\boldsymbol{PRDS}$	Post-receptor simplified downstream signaling events	$\frac{\#}{cell}$
$\boldsymbol{aSMA}$	α-Smooth Muscle Actin	$\frac{\#}{cell}$

We build and test the model with data derived from fibroblast differentiation experimental studies performed herein, and we analyze the model to predict which mechanisms are affecting fibroblast regulation. These factors are potential therapeutic targets for fibrosis.

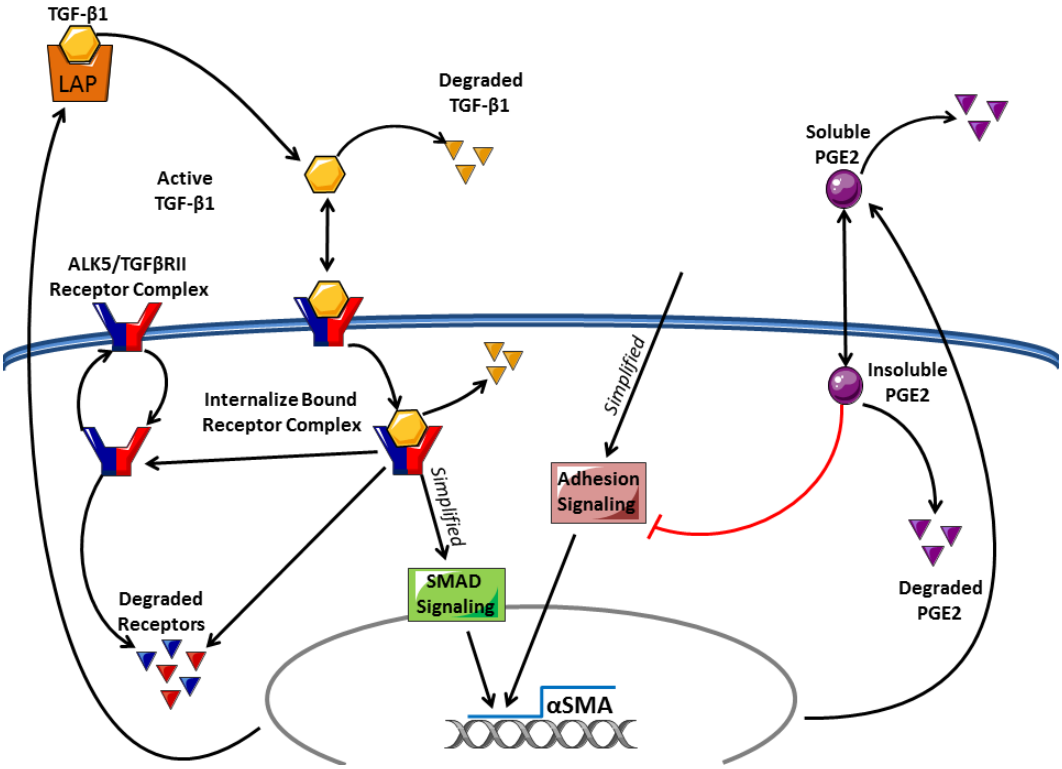

Figure. 2.1. Processes relevant to fibroblast differentiation. Latent TGF-β1 can be activated and then is able to bind surface receptors. Receptor/ligand complexes are internalized, initiating a downstream signaling cascade which, in combination with adhesion signaling, induces the synthesis of α-smooth muscle actin. PGE_2 can inhibit the adhesion signaling, preventing completion of the signal cascade and protein synthesis. Our model tracks latent TGF-β1, active TGF-β1, free surface receptors, free cytoplasmic receptors, bound surface receptors, bound cytoplasmic receptors, the number of bound receptor internalization events, extracellular PGE_2, intracellular PGE_2, and α-smooth muscle actin synthesis. We have simplified the adhesion, SMAD, and PGE_2 signaling pathways.

2.2 Results

2.2.1 PGE_2 is necessary to Explain *In Vitro* Data of αSMA Synthesis

We first evaluated the level of αSMA synthesized in the presence of TGF-β1. We compared fold changes in concentration of αSMA at 4, 12, 24, or 48 hours in the presence of an initial concentration of 1ng/ml of TGF-β1 to 4 hours untreated. Data show no increase at 4 hours post treatment over the untreated and an approximately 2.5 fold increase in αSMA at 12 hours post treatment that is maintained at 48 hours post treatment (Figure 2.2A).

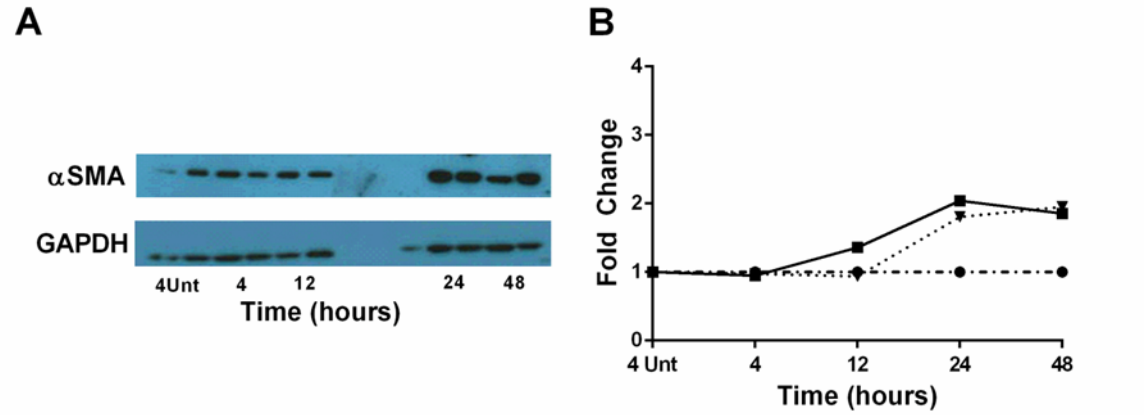

Figure. 2.2 αSMA time course studies and simulations. (A) αSMA measured in 3T12 fibroblasts at either 4 hours untreated or 4, 12, 24, or 48 hours treated with 1ng/ml of activated TGF-β1 using Western blot and densitometry analysis. N=2/condition. (B) Simulation of αSMA production. Solid line with filled squares representing the experimental data described in part a) and gray triangle representing 4 hour untreated sample using 3T12 fibroblast cell line and 1ng/ml of activated exogenous TGF-β1, dotted curve representing simulation results following treatment with 1ng/ml of activated exogenous TGF-β1, and PGE_2 inhibition, and dot-dashed line representing simulation control with no TGF-β1 treatment. We have previously published similar kinetics using 2 ng/ml TGFβ suggesting that TGF-β1 is in excess in this system (168).

These results mirror our earlier findings when stimulating fibroblasts with 2 ng/ml TGFβ, indicating that TGFβ is not limiting. We also simulated fibroblasts with our mathematical model under the same experimental conditions (untreated or 1ng/ml of TGF-β1) and measured the αSMA concentration at 4, 12, 24, 48 hours. We parameterized the model using values derived from previously published data or estimated using uncertainty analysis (Table 2.2), and then validated the model against experimental data generated in our lab (Figure 2.3).

Table 2.2 Model Parameters

Symbol	Parameter	Value	Range	Unit	Source
General Parameters					
$\boldsymbol{vol}$	Volume of media	2	N/A	mL	N/A
$\boldsymbol{cells}$	Total number of cells	5.0e5	N/A	#	N/A
TGF-β1 Receptor Ligand Parameters					
$k_{syn}^{TGF\beta 1_{lat}}$	Latent TGF-β1 Synthesis	5e-15	1.0e-17 – 1.0e-10	moles/min*volume	est.
$k_{deg}^{TGF\beta 1_{lat}}$	Latent TGF-β1 Degradation	0.075	N/A	1/min	(326)
$k_{act}^{TGF\beta 1_{lat}}$	Latent TGF-β1 Activation	0.01	1.0e-4 – 1.0e3	1/min	est.
$k_{indsyn}^{TGF\beta 1_{lat}}$	Latent TGF-β1 Induced Synthesis	0.001	1.0e-4 – 1.0e3	1/min	est.
$k_{on}^{TGF\beta 1}$	Active TGF-β1 Receptor Ligand Binding	4.35e-14	N/A	1/ min	(72)
k_{diss}^{TRC}	Active TGF-β1 Receptor Ligand Dissociation	4.35e14	N/A	1/min	(72)
$k_{deg}^{TGF\beta 1_{act}}$	Active TGF-β1 Degradation	0.577	N/A	1/min	(326)
k_{syn}^{R}	TGF-β1 Receptor Synthesis	4.0	N/A	#/(min)*cell	(327)
k_{int}^{R}	TGF-β1 Receptor Internalization	0.333	N/A	1/(min)	(207)
k_{rec}^{R}	TGF-β1 Receptor Recycling	0.333	N/A	1/(min)	(207)
k_{int}^{TRC}	TGF-β1 Receptor Ligand Complex Internalization	0.333	N/A	1/(min)	(207)
k_{deg}^{R}	TGF-β1 Receptor Degradation	0.003	N/A	1/(min)	(207)
k_{lid}^{R}	TGF-β1 Receptor Ligand Induced Degradation	4.0	N/A	1/(min)	(207)

Table 2.2 Model Parameters cont.

PGE_2 Parameters					
k_{synth}^{PGE2}	PGE_2 Synthesis	$2.1*10^4$	N/A	#/min * cell	(328)
k_{int}^{PGE2}	PGE_2 Receptor Ligand Binding Rate	0.0096	1.0e-3 – 1.0e2	1/min	est.
k_{deg}^{PGE2}	PGE_2 Degradation	0.001	N/A	1/min	(329)
α-Smooth Muscle Actin Parameters					
k_{deg}^{PRDS}	PRDS Degradation Rate	0.004	3e-3 – 1e-1	1/min	est.
$c_{act}^{Adhesion}$	Adhesion Signal Strength	1	0 or 1	N/A	est.
c_{Stiff}^{Matrix}	Matrix Stiffness Effect	100	0 - 1000	N/A	est.
$k_{Inhibit}^{PGE2}$	Strength of PGE_2 Inhibition	1.0e-5	1e-7 – 1e-3	1/min	est.
α_1	Non-zero so denominator ≠0	1	0<n≤1	#/cell	est.
$k_{deg}^{\alpha SMA}$	αSMA Degradation	0.0001	1e-5 – 1e0	1/min	est.

Our simulations show an approximately 2 fold increase in αSMA by 4 hours post treatment and a 6-fold increase by 12 hours post treatment which was maintained at 48 hours (Data not shown). These levels are much higher than the experimental data, indicating a lack of negative regulation in the system. We predicted that the absence of negative regulation is responsible for the discrepancy in experimental and simulation results. We introduced negative regulation by PGE_2 into our model and simulated fibroblasts (untreated or 2ng/ml of TGF-β1) and measured the αSMA concentration at 4, 12, 24, 48 hours in the presence of of 100μM PGE_2 and found no increase in αSMA at 4 hours post treatment over the untreated and an approximately 2.5 fold increase at 12 hours post treatment which is maintained at 48 hours post treatment. Simulation results closely match the experimental data consistent with the idea that a negative regulator is necessary to explain *in vitro* data regarding fibroblast differentiation (Figure. 2.2B).

In order to test our hypothesis that PGE_2 signaling was needed for our model to recapitulate experimental data, we performed the experiment described above with fibroblasts in the absence of PGE_2 signaling by treating them simultaneously with 2ng/ml of TGF-β1 and indomethacin (an inhibitor of PGE_2) (Figure 2.3A). We found that in the absence of PGE_2 signaling the concentration of αSMA in fibroblasts was significantly increased (p-value < 0.05).

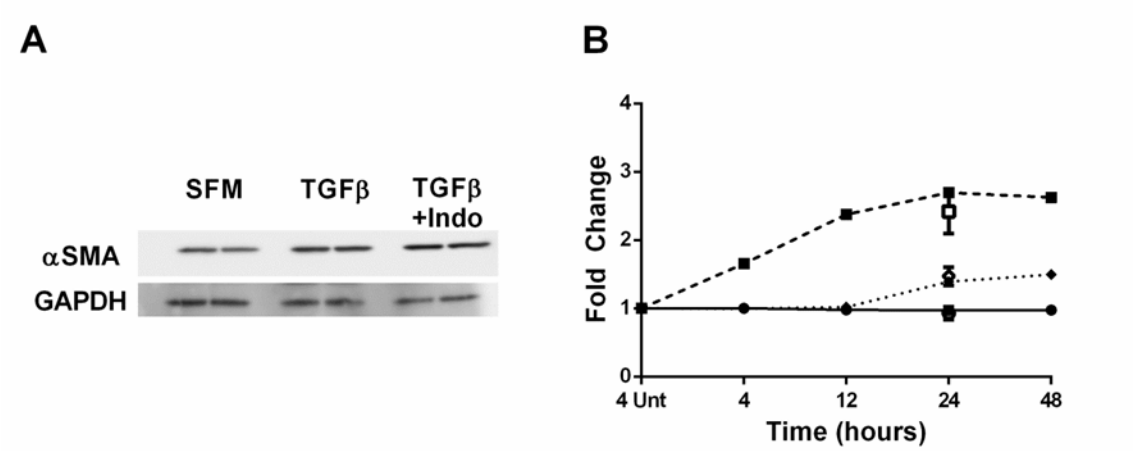

Figure. 2.3 αSMA studies and simulations with and without PGE_2 signaling. (A) αSMA measured in 3T12 fibroblasts at 24 hours untreated, treated with 2ng/ml of TGF-β1, or treated with 2ng/ml of TGF-β1 and 10μM of indomethacin using Western blot and densitometry analysis. N=2/condition. (B) Simulation of αSMA production. Dashed curve represents simulation results in the absence of PGE_2 inhibition. Dotted curve represents simulation results in the presence of PGE_2 inhibition, and solid line represents simulation control with no TGF-β1 treatment. Experimental data for αSMA at 24 hours following treatment with 2ng/ml of TGF-β1 and 10μM of indomethacin, 2ng/ml of TGF-β1, or serum free media (SFM) are represented by open square open diamond and open circle respectively. N=2

2.2.2 Transient TGF-β1 Signaling in the Presence of PGE_2

Previously published work identifies PGE_2 as an important regulator of TGF-β1 signaling (168) and we show above that including PGE_2 gives simulation that are consistent with experimental data of TGF-β1 induced αSMA synthesis. In order to better understand the dynamics of PGE_2 inhibition of fibroblast differentiation, we characterized the fibroblast response to TGF-β1 in the presence of a fixed concentration of PGE_2 using our *in silico* model.

During this simulation we identified two phenomena that we refer to as *response* and *refraction*. Response describes periods of increasing αSMA concentrations in the fibroblast. Refraction refers to periods of declining concentrations of αSMA indicating that fibroblasts are not able to respond to TGF-β1 and that αSMA is degrading in the cell. We define the magnitude and duration of a response as the maximal concentration of αSMA achieved following treatment and the time it takes for this concentration to return to pre-stimulatory levels, respectively. In the transient TGF-β1 signaling simulations we fixed the concentration of PGE_2 and simulated periodic dosing with exogenous active TGF-β1 (Figure. 2.4).

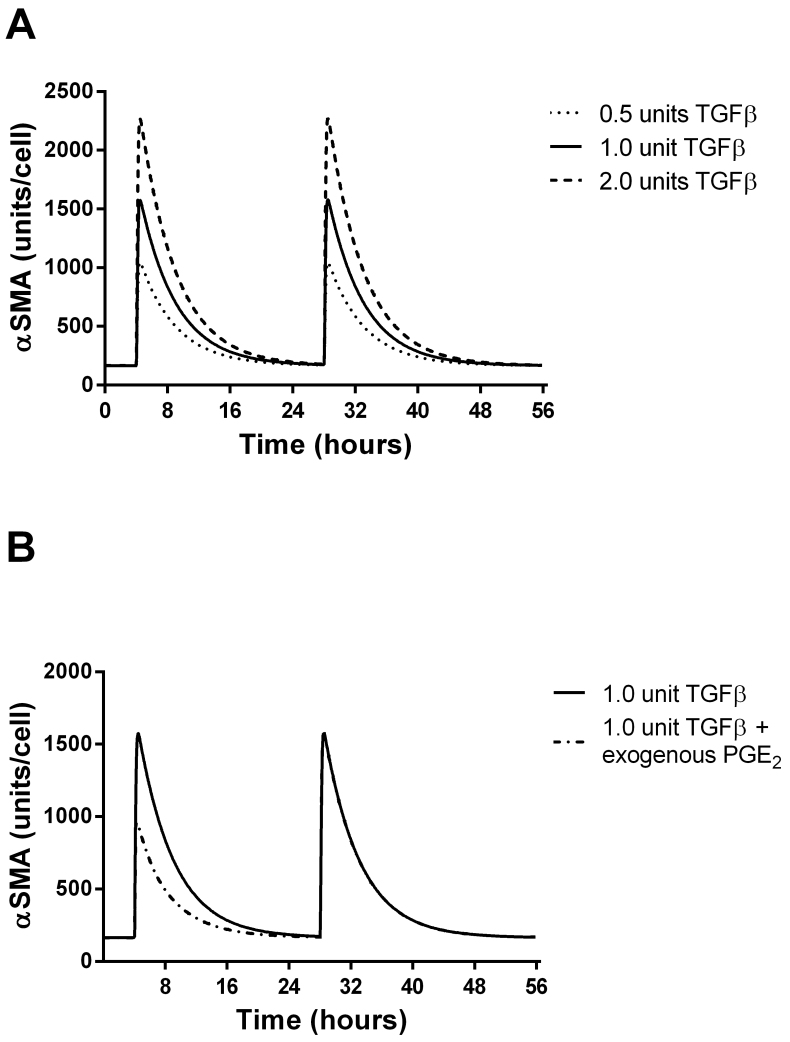

Figure. 2.4 *In silico* TGF-β1-induced α SMA synthesis in the presence of constant concentration of PGE_2. The *x*-axis represents time in hours, and the *y*-axis represents the concentration of α SMA in units/cell. a α SMA synthesis in a constant concentration (1 nmol) of PGE_2 and dosing with 0.5 ng/ml TGF-β1 (*dotted*) 1 ng/ml TGF-β1 (*solid*), and 2 ng/ml (*dashed*) at 4 and 28 h. b α SMA synthesis in a constant concentration (1 nmol) of PGE_2 and dosing with 1 ng/ml TGF-β1 at 4 and 28 h. *Dashed line* simulation receives an additional dose of PGE_2 at 440 min

Prior to TGF-β1 treatment the cells are in a refractory state with no change in concentration of αSMA (Figure. 2.4A). Following treatment with TGF-β1, an induction of αSMA synthesis occurs but is transient and αSMA levels eventually return to a refractory state

indicating that the signal has dissipated. We observed that the magnitude of a signal response increases as the TGF-β1 dose is increased; however, the duration of this response does not change. Having observed a dose dependent signal response to TGF-β1 in the presence of a constant concentration of PGE_2 we wanted to see if this response could be abrogated. We next repeated the simulation but in addition to periodic doses of TGF-β1 we added an additional dose of exogenous PGE_2 during the response phase (Figure. 2.4B). We observe that the addition of exogenous PGE_2 following TGF-β1 treatment does reduce the magnitude of the signal. However, this reduction is transient and restricted to the current dose response. It does not affect the ability of the cell to respond fully to a later dose of TGF-β1. This suggests that intermittent treatment of differentiated cells with negative regulators is only temporarily effective at suppressing αSMA synthesis.

2.2.3 PGE_2 Induced TGF-β1 Signaling Refractory State

We showed above that PGE_2 can reduce the magnitude of response to a single dose of TGF-β1. We tested how PGE_2 affects fibroblast responses to a constant concentration of TGF-β1 in order to evaluate effects of PGE_2 dosing on fibroblasts in the context of excessive TGF-β1 synthesis. We examined αSMA concentration in conjunction with constant TGF-β1 concentrations and periodic PGE_2 dosing. We predicted that dosing with PGE_2 induces a refractory period where a cell is unresponsive to TGF-β1 (Figure. 2.5A). This refractory period is transient and eventually the cellular response to TGF-β1 is restored.

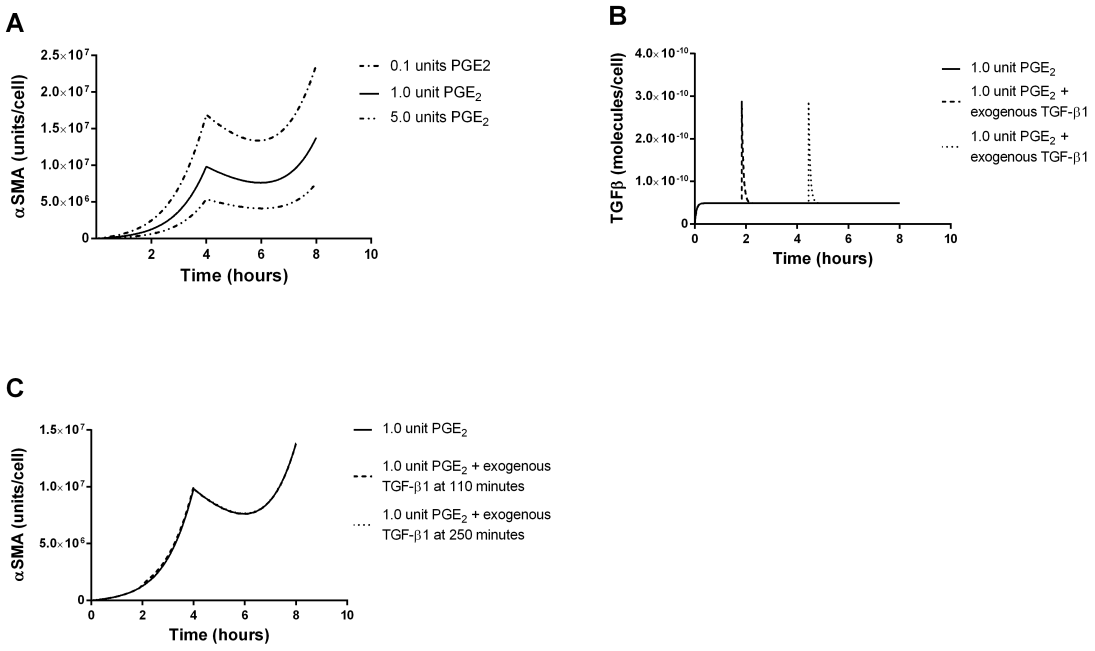

Figure. 2.5 *In silico* PGE_2 -induced refraction in TGF-β1-induced α SMA synthesis. The *x*-axis represents time in hours (A–C). The *y*-axis represents the concentration of α SMA for panels (A) and (C). The *y*-axis represents the concentration of active TGF-β1 for panel (B). A α SMA synthesis in the presence of a constant dose (1ng/ml) of TGF-β1. *Dashed curve* represents dosing with 10nmol PGE_2, *solid curve* represents dosing with 100 nmol PGE_2 , and *dotted curve* represents dosing with 5 μmol of PGE_2 . B Concentration of TGF-β1 over time corresponding to output in panel (C). C All were dosed with 100 nmol of PGE_2 at 0 and 4 h. *Filled curve* simulation was also treated with and additional dose of 1ng/ml of TGF-β1 at 100min during the refractory period. *Dotted curve* simulation was treated with an additional dose of 1ng/ml of TGF-β1 at 220 min during the response period

We varied the size of the dose of PGE_2 and examined how that affects the dynamics of the TGF-β1 signal response. We found that higher doses of PGE_2 induced a longer refractory period and a decreased magnitude of signal response following the refractory period (Figure. 2.5A). As we observed (Figure. 2.5), additional treatment with exogenous PGE_2 during the response phase could reduce the magnitude of the fibroblast response to TGF-β1. We tested the inverse of the phenomenon to see whether a fibroblast could be rescued from refraction by adding exogenous TGF-β1 during the refractory period. We simulated treatment of our *in silico*

cells with PGE_2 and gave an additional dose of exogenous TGF-β1 (Figure. 2.5B) during the refractory period. We observed that additional TGF-β1 could not rescue cells from refraction (Figure. 2.5B). We also treated cells with additional exogenous TGF-β1 during the response phase to test whether we could induce a stronger signal response, however we predict that treatment does not alter the magnitude or duration of the signal response in these cells (Figure. 2.5C). This suggests that consistent exposure to negative regulators such as PGE_2 reduces the cells' sensitivity to fluctuations in concentration of positive differentiation signals such as TGF-β1.

2.2.4 Identifying States of Controlled Myofibroblast Function

We predicted that constitutive levels of PGE_2 result in predominantly quiescent fibroblasts (decreasing concentration of αSMA) with transient responsiveness to periodic dosing with TGF-β1, and that constitutive levels of TGF-β1 result in increasing fibroblast differentiation (based on increasing concentrations of αSMA) with transient refraction following periodic PGE_2 dosing (Figures. 2.3 and 2.4). Based on these studies, we know that PGE_2 and TGF-β1 influence the state of fibroblast differentiation. The question remains as to whether fibroblasts can achieve a steady state in terms of the concentration of αSMA. We simulated treating cells with constant concentrations of both PGE_2 and TGF-β1 and observed that under these conditions, αSMA concentration achieved a steady state that was maintained (Figure. 2.6). The magnitude of this steady state is determined by the ratio of TGF-β1 to PGE_2 (Figure. 2.7).

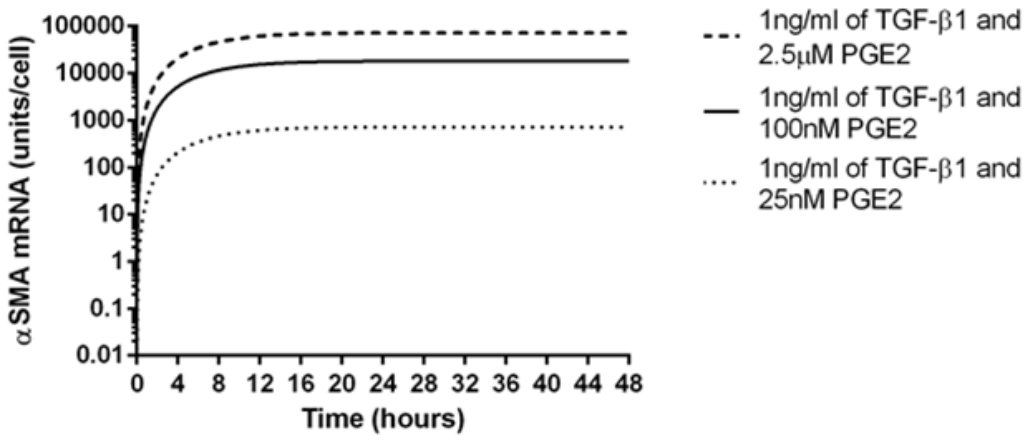

Figure. 2.6. Three Examples of PGE_2 and TGF-β1 induced steady state fibroblast αSMA levels in the model. X-axis represents time in hours, Y-axis represents concentration of αSMA .

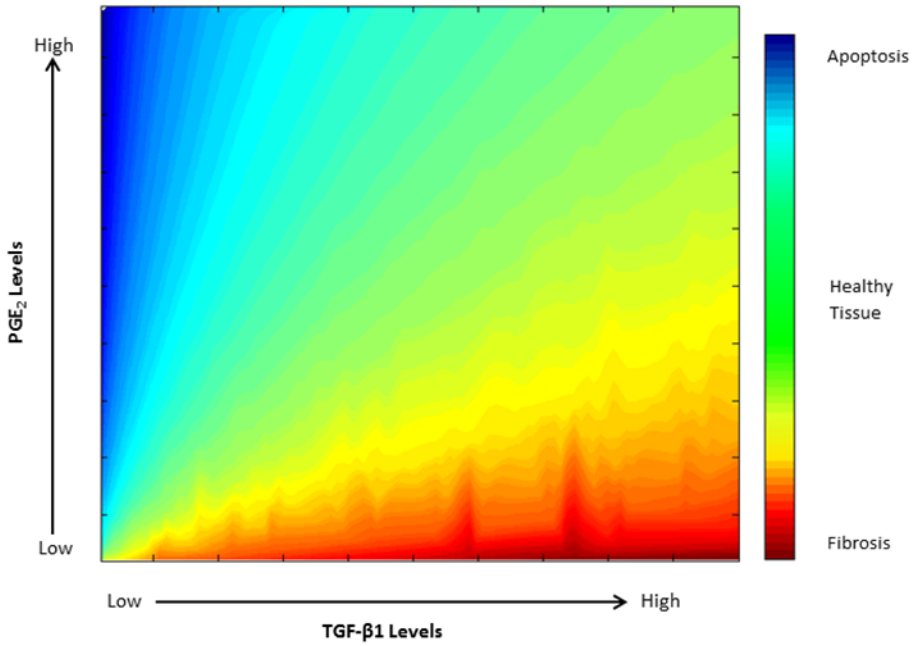

Figure. 2.7. Predicted response outcomes across different TGF-β1 to PGE_2 ratios. We compare αSMA concentrations of a fibroblast under different ratios of TGF-β1 to PGE_2 for 24 hours in the model (1)-(10). The x-axis represents the concentration of TGF-β1, the y-axis represents the concentration of PGE_2. The color gradient represents the level of αSMA produced in response to these levels of TGF-β1 to PGE_2. Blue corresponds to low concentrations of αSMA likely leading to fibrosis and red corresponds to high concentration of αSMA likely leading to apoptosis (22, 323). Plotted are the steady state concentrations of αSMA at 24 hours for these TGF-β1 to PGE_2 levels. A balance of these mediators leads to the best outcome: moderate levels of αSMA produced (green).

2.2.5 Identifying Key Molecular Mechanisms Regulating Fibroblast Differentiation

To identify molecular mechanisms critical to the dynamics of fibroblast differentiation, we performed uncertainty and sensitivity analyses (see Methods). When all model parameters are varied over wide ranges (Table 2.3) and PRCCs are calculated, we can identify mechanisms that are significantly correlated with α-smooth muscle actin concentration over time (Table 2.3). Because ECM stiffness ($\boldsymbol{k_{Stiff}^{Matrix}}$) strongly influences αSMA synthesis (316, 317), we also performed our analysis holding this parameter constant to reflect the biological scenario where we are not able to vary the stiffness of the ECM. In this scenario we can examine the roles of other mechanisms/parameters not influenced by the effects of stiffness (Table 2.4). Several key mechanisms identified by the model analysis to be driving fibroblast activation are: PGE_2 induced inhibition, TGF-β1 receptor recycling rate, and active TGF-β1 degradation rate, indicating the importance of both positive and negative regulators of fibroblast differentiation. Further study of PGE_2 induced inhibition is necessary to characterize specific therapeutic strategies that take advantage of existing negative regulatory pathways. Therapeutic treatments that inhibit receptor recycling or restrict the availability of active TGF-β1 could aid in inducing a shift in the environment by down-regulating positive feedback in the TGF-β1 signaling cascade.

Table 2.3: PRCC Values Varying ECM Stiffness

Time Hours	α1	αSMA Degradation Rate	Active TGF-β1 Degradation Rate	Signal Recovery Rate	Receptor Recycling Rate	PGE_2 Induced Inhibition	Adhesion Dependent Signaling	ECM Stiffness
4	-0.63	-0.23	-0.17	-0.10	0.20	0.65	0.98	0.99
12	-0.63	-0.49	-0.28	-0.16	0.18	0.65	0.98	0.99
24	-0.63	-0.61	-0.53	-0.15	0.18	0.64	0.98	0.99
48	-0.79	-0.64	-0.60	-0.13	0.17	0.63	0.97	0.99

*Parameters with positive values are positively correlated to αSMA synthesis and negative values are negatively correlated to synthesis.

Table 2.4: PRCC Values with Fixed Matrix Stiffness

Time Hours	α1	αSMA Degradation Rate	Active TGF-β1 Degradation Rate	Signal Recovery Rate	Receptor Recycling Rate	PGE_2 Induced Inhibition
4	-0.95	-0.61	-0.54	-0.21	0.50	0.95
12	-0.93	-0.86	-0.62	-0.49	0.44	0.93
24	-0.91	-0.90	-0.85	-0.43	0.39	0.91
48	-0.95	-0.88	-0.87	-0.37	0.33	0.87

2.3 Discussion

Fibroblasts and myofibroblasts play a key role in promoting wound healing. They restore critical extracellular matrix and remodel architecture of damaged tissue (148-150, 156, 239). Their actions are tightly regulated to prevent disruption of healthy tissues but dysregulation can occur resulting in fibrotic diseases that are detrimental to functionality of surrounding tissues. One such disease, IPF, leads to poor prognosis for patients with very limited treatment options and lung transplant is currently the only long term solution. Identifying key mechanisms driving fibroblast to myofibroblast differentiation and dysregulation enables us to predict targets for therapeutic treatment of fibrotic diseases.

We developed a mathematical model that captures the dynamics of TGF-β1 induced fibroblast differentiation under isolated conditions and characterized by the synthesis of αSMA. We utilized previously published (72, 327, 329) and our own *in vitro* data generated herein together with uncertainty and sensitivity analyses to build and test our model. The model details receptor/ligand binding and trafficking of TGF-β1, PGE inhibition, and αSMA synthesis. Our model includes a simple representation of adhesion dependent signaling, which has been shown to be necessary for TGF-β1 induced fibroblast differentiation, and for PGE_2 signaling, a major inhibitor of TGF-β1 induced fibroblast differentiation.

Prior models of TGF-β1 receptor ligand signaling have been developed based on keratinocytes and pancreatic cancer cell lines (206, 207, 315). In these cell types TGF-β1 is a negative regulator of cell growth, and proliferation. These models are able to describe how temporal loss of sensitivity to TGF-β1 plays a key role in keratinocyte and pancreatic cancer cell regulation (330). They demonstrate that desensitization is highly dependent on the ratio of constitutive and ligand induced receptor degradation rates. In our model we examine the regulatory mechanisms of fibroblast differentiation with TGF-β1 as our focus. TGF-β1 has been shown to induce fibroblast differentiation in the presence of adhesion signaling. As a result we see a completely opposite cellular response to TGF-β1 signaling in fibroblasts compared to previously modeled cell types. Dysregulation of fibroblasts during wound healing is characterized by excessive differentiation, characteristic of a positive response to TGF-β1. For this reason, a new model of TGF-β1 signaling specifically for fibroblasts is necessary to identify key molecular factors that result in dysregulation.

Our results suggest that experimental outputs were only able to be recapitulated in the presence of PGE_2 inhibition emphasizing that inhibition of TGF-β1 signaling is important for regulation of fibroblast behavior, and in the absence of inhibition factors like PGE_2 we observe excessive production of αSMA, a marker for myofibroblast function.

We characterized fibroblast responses to different environmental conditions in order to isolate conditions that are favorable for controlled wound healing. These conditions may be artificially created in instances of fibroblast dysregulation in order to limit damaging effects of fibrosis. We predicted conditions resulting in quiescence (no αSMA), increasing differentiation (increasing concentrations of αSMA), and steady state differentiation (constant concentrations of αSMA). We simulated how fibroblasts respond to periodic dosing of TGFβ1 in the presence of a

constant concentration of PGE_2, in order to understand the ability of cells to perform wound healing activities in the presence of continual negative regulation. We found that under these conditions, fibroblasts were able to respond modestly to dosing with TGF-β1 but quickly returned to a quiescent state when the signal was resolved. Cells are not able to maintain a constant concentration of αSMA, with only periodic stimulation from TGF-β1. The magnitude of the response, but not the duration, is dependent on the magnitude of the dose of TGF-β1 administered. We found that while the magnitude of the response in the presence of constant PGE_2 was dependent on the TGF-β1 dose, the concentration of PGE_2 dictated the duration of that response. Higher levels of negative regulators such as PGE_2 present at the site of a wound may inversely correlate with the extent of damage present and thus inversely correlate with the amount of time required for repair mechanisms to take place. It is also possible that rather than shortening the duration of the repair, PGE_2 and other potential negative regulators of TGF-β1 may decrease the amount of time each individual fibroblast responds to TGF-β1 signaling reducing the overall amount of fibroblast differentiation occurring during a repair event. Additional treatment with PGE_2 during the response phase of fibroblasts to TGF-β1 was able to induce a short refractory period and temporarily decrease the strength of the signal response to TGF-β1 following the additional PGE_2 treatment. This finding suggests that the cells are not refractory to PGE_2 signaling in the presence of TGF-β1, and that PGE_2 plays an important role in regulating TGF-β1 signaling. These results imply that fibroblasts are able to produce a limited amount of αSMA in response to TGF-β1 and potentially perform modest wound healing activities in the presence of constant negative regulators, but they are not able to maintain a prolonged state of continuous αSMA synthesis. An environment with sustained concentrations of negative regulatory signals like PGE_2 could be permissive to wound healing but also preventative

of fibroblast dysregulation. It is also possible that under these conditions TGF-β1 levels are insufficient for wound healing. Steady state secretion of PGE_2 by alveolar epithelial cells has been demonstrated, and is suspected of keeping fibroblasts quiescent in the absence of injury (187, 188).

We also tested how fibroblasts respond to periodic dosing with PGE_2 in constant concentrations of TGF-β1 (Figure. 2.5), to evaluate the efficacy of inhibitory factors in the presence of substantial stimulation. We found that in the absence of PGE_2 the fibroblasts were continuously responsive to the presence of TGF-β1, presenting steadily increasing concentrations of αSMA. Following treatment with PGE_2 the cells were refractory to further stimulation of TGF-β1 for a limited period of time and the duration of the refractory state was dependent on the dose of PGE_2 administered. We tested whether cells could be relieved of refraction early if dosed with additional TGF-β1 during that time in order to determine if treatment with PGE_2 could sustain inhibition of the cellular differentiation in the presence of rapidly changing levels of TGF-β1. We found that treatment with additional TGF-β1 could not rescue fibroblasts from the refractory period suggesting that PGE_2 can block TGF-β1 signaling even during a flux in TGF-β1 concentration. These findings illustrate the ability of negative regulators such as PGE_2 to inhibit fibroblast differentiation during response phase and in the presence of constant TGF-β1. This regulation, however, is transient resolving as soon as the inhibitor is degraded. Periodic dosing with PGE_2 cannot sustain a long term steady state of αSMA production. These results suggest that if PGE_2 levels are insufficient or inconsistent during a wound healing response, myofibroblasts may not maintain a steady state level of αSMA production, but rather experience constant stimulation to TGF-β1 except for short transient periods of time when PGE_2 levels are high enough to induce temporary quiescence. Our model

therefore predicts that therapeutic treatments with fluctuating concentrations of negative regulators may be insufficient to restrict fibroblast differentiation for extended periods of time. It calls instead for treatment strategies that provide prolonged alterations to the environmental concentrations of positive and negative regulators. Our predictions remain to be tested experimentally, not only *in vitro* but *in vivo* as well.

Having identified environmental conditions that result in constant induction and quiescence of fibroblasts, we predict that constitutive concentration of both TGF-β1 and PGE_2 will result in steady state levels of fibroblast differentiation. Our model allows us to compare the contribution of each of these molecular factors to the overall outcome of fibroblast differentiation characterized by αSMA synthesis, and predict patterns of signal availability that are currently untestable *in vitro*. We tested how fibroblasts respond to simultaneous constant levels of PGE_2 and TGF-β1 (Figure. 2.6), and found that in the presence of both molecules fibroblasts maintained a steady concentration of αSMA. This result indicates that a continuous presence of both molecules is necessary for sustained and controlled fibroblast response. This suggests that periodic inhibition of TGF-β1 is insufficient to prevent fibroblast dysregulation. Periodic dosing with TGF-β1 may or may not induce levels of fibroblast αSMA sufficient for successful wound healing, depending on the size and severity of the wound as well as the number of fibroblasts available to respond. Further characterization of the functionality of these environmental conditions in restricting and reversing the effects of fibroblast dysregulation will require a multi-cellular scale model capturing events at molecular, cellular and tissue scale, which we are currently building.

Sensitivity analysis indicates that the parameters responsible for controlling strength of PGE_2 induced inhibition ($\boldsymbol{k_{Inhibit}^{PGE2}}$, $\boldsymbol{\alpha 1}$) are the most significant factors for regulating fibroblast

differentiation. In addition to the strength of PGE_2 induced inhibition, rates of active TGF-β1 degradation and receptor recycling were also found to be very important. These parameters contribute to either the actual concentration of TGF-β1 and PGE_2 in the media or to the level of concentration at which the receptor ligand interaction becomes saturated. These findings indicate that PGE_2 and TGF-β1 receptor ligand signaling dynamics simultaneously contribute to fibroblast regulation and together dictate the differentiation of the cell. Because PGE_2 inhibition was found to be one of the most important parameters in regulating fibroblast differentiation, but fibroblasts lose sensitivity to PGE_2 over time (167), our findings call for therapeutics that mimic the effects of PGE_2 through inhibition of adhesion signaling. Therapeutics that provide constant inhibition of adhesion signaling are needed to establish favorable environmental conditions for regulated wound healing. Inhibition of TGF-β1 receptor recycling ($\boldsymbol{k_{rec}^{R}}$) and decreased availability of active TGF-β1 ($\boldsymbol{TGF\beta 1_{act}}$) may increase the efficacy of PGE_2 mimics in establishing favorable environmental conditions.

The findings of our model indicate that restricting positive differentiation signals like TGF-β1, alone cannot account for the regulation of fibroblast differentiation. We identify a need for balanced environmental conditions for fibroblasts with consistent levels of positive and negative regulators (Figure. 2.7). Extremely high ratios of TGF-β1 to PGE_2 produce outcomes of excessive αSMA synthesis which we hypothesize correlate to fibrosis. Extremely low ratios of TGF-β1 to PGE_2 result in very minimal fibroblast differentiation which may be insufficient for effective wound healing. In order to better understand this system and identify specific targets for therapeutic treatment, there is great need to explore more detailed dynamics of PGE_2 inhibition of adhesion signaling in conjunction with TGF-β1 receptor ligand signaling dynamics.

2.4 Methods

2.4.1 In Vitro Studies of TGF-β1 induced αSMA Synthesis

3T12 mouse fibroblast cell line obtained from American Type Culture Collection (ATCC; CCL-164). Approximately $7.5x10^5$cells/400k cells/ well are plated onto 6 well plates and either left untreated, treated with 1-2ng/ml of activated TGF-β1, or treated simultaneously with 2ng/ml of activated TGF-β1 and 10 μM indomethacin. Untreated cells were harvested at 4 hours post treatment. Treated cells were harvested at 4, 12, 24 or 48 hours post treatment. Cells were lysed in radioimmunoprecipitation assay buffer with protease inhibitor cocktail (Sigma) for 15 min at 4°C and centrifuged. Total protein concentrations in the supernatants were determined by the Bicinchoninic acid assay (Pierce). Equal amounts of protein from each sample were separated on a 4–20% gradient SDS-polyacrylamide gel and transferred to a PVDF membrane (Amersham/GE Healthcare, Pittsburgh, PA). PVDF membrane was then probed with a monoclonal anti-body (Clone 1A4; Dako, Carpinteria, CA) for 1 hour to detect αSMA protein. This process was repeated to detect GAPDH (Santa Cruz).

2.4.2 Mathematical model

2.4.2.1 TGF-β1 Receptor Ligand Dynamics

To construct a model of fibroblast differentiation that captures molecular mechanisms necessary to fibroblast dysregulation, we first describe TGF-β1 receptor/ligand binding and trafficking kinetics using mass action kinetics (331), building on studies in a variety of human and mouse cell lines and primary cells(206, 207, 315). We account for the TGF-β1 receptors ALK5 and TGF-β1RII as a single receptor complex. Because we are exclusively studying TGF-β1 and no other members of the TGF-β family, we disregard competition for subunits in

establishing receptor complexes and assume that all stable receptor complexes include the ALK5 and TGF-β1RII. Modeling these receptors together as a single receptor unit is relevant because both receptors are required for induction of downstream signaling cascades. Because receptor subunits have different parameter values, we use the rate limiting value for each parameter to describe the dynamics of the receptor complex. About 10% of the TGF-β1 receptors are present on cell surfaces in the absence of stimulation; the remaining 90% are sequestered intracellularly (327).

Equations 1-6 track rates of change over time for concentrations of six TGF-β1 signal cascade species. These species include the following: latent TGF-β1 $[TGF\beta1_{lat}]$, active unbound TGF-β1 $[TGF\beta1_{act}]$, unbound receptors on the fibroblast surface $[R_{surf}]$, unbound receptors in cytoplasm $[R_{int}]$, bound receptor/TGF-β1 complexes on the fibroblast surface $[TRC_{surf}]$, and bound receptor/TGF-β1 complexes in cytoplasm $[TRC_{int}]$ (Table 2.1, Figure. 2.1). The rates of change in concentration of these species are dictated by parameter values (see Table 2.2 and below).

The rate of change in concentration of latent TGF-β1 is captured by:

$$\frac{d}{dt}[TGF\beta1_{lat}] = k_{syn}^{TGF\beta1_{lat}} - \left(k_{deg}^{TGF\beta1_{lat}} + k_{act}^{TGF\beta1_{lat}}\right) * [TGF\beta1_{lat}] + \frac{k_{indsyn}^{TGF\beta1_{lat}} * [TRC_{int}]}{Nav * Vol} * Cells \quad (1)$$

The first term on the right hand side (RHS) of the equation is $k_{syn}^{TGF\beta1_{lat}}$, the constitutive TGF-β1 synthesis by fibroblasts, and is estimated by uncertainty analysis (described below) (229). The next term in the RHS of the equation represents the loss of latent TGF-β1 to degradation ($k_{deg}^{TGF\beta1_{lat}}$) and activation ($k_{act}^{TGF\beta1_{lat}}$).The final term on the RHS of the equation is a positive

feedback term for additional latent TGF-β1 synthesis in the presence of TGF-β1 signaling. The rate constant $k_{indsyn}^{TGF\beta 1_{lat}}$is also estimated by uncertainty analysis. Nav represents Avogadro's number and Vol represents the volume of the experimental environment. $Cells$ represents the number of fibroblasts in a given simulation.

The rate of change in concentration of active TGF-β1 is described by:

$$\frac{d}{dt}[TGF\beta 1_{act}] = k_{act}^{TGF\beta 1_{lat}} * [TGF\beta 1_{lat}] - k_{on}^{TGF\beta 1} * [TGF\beta 1_{act}] * [R_{surf}] * cells + \frac{1}{Nav * vol} * k_{diss}^{TRC} * [TRC_{surf}] * cells - k_{deg}^{TGF\beta 1_{act}} * [TGF\beta 1_{act}] \quad (2)$$

The first term on the RHS of the equation represents the rate of activation of latent TGF-β1 (from Equation 1). The second term in the equation is the rate of active TGF-β1 binding to the receptor. The next term in the equation is the dissociation rate of active TGF-β1 from cell surface receptors. The final term in this equation represents the rate of degradation of active TGF-β1.

Equation 3 represents the rate of change over time of the concentration of unbound surface receptor complexes.

$$\frac{d}{dt}[R_{surf}] = k_{syn}^{R} - Nav * vol * k_{on}^{TGF\beta 1} * [TGF\beta 1_{act}] * [R_{surf}] + k_{diss}^{TRC} * [TRC_{s\square rf}] - k_{int}^{R} * [R_{surf}] + k_{rec}^{R} * ([R_{int}] + [TRC_{int}]) \quad (3)$$

(k_{syn}^{R}) represents the constitutive rate of receptor synthesis. The second and third terms on the RHS of the equation represent the rates of active TGF-β1 binding to and dissociation from

receptors on the surface of the cell (from Equation 2). The fourth term is the rate of internalization of unbound receptors into the cytoplasm and is proportional to the concentration of unbound surface receptors ($[R_{surf}]$). The last term in the equation is the rate of receptor recycling from the cytoplasm to the surface of the cell (327).

Equation 4 represents the rate of change over time in the concentration of internalized unbound receptors.

$$\frac{d}{dt}[R_{int}] = k_{int}^{R} * [R_{surf}] - (k_{rec}^{R} + k_{deg}^{R}) * [R_{int}] \quad (4)$$

The first term on the RHS of the equation represents the rate of receptor internalization as described for Equation 3. The second term in the equation is the loss of internal unbound receptors to recycling and degradation. The rate constant k_{deg}^{R}represents receptor degradation and is defined to satisfy the experimental data as described for k_{syn}^{R} above.

Equation 5 represents the rate of change over time in concentration of bound surface receptors.

$$\frac{d}{dt}[TRC_{surf}] = Nav * vol * k_{on}^{TGF\beta1} * [TGF\beta1_{act}] * [R_{surf}] - k_{diss}^{TRC} * [TRC_{surf}] - (k_{int}^{TRC} * [TRC_{surf}]) \quad (5)$$

The first and second terms on the RHS of the equation represent the rate of TGF-β1 binding to unbound surface receptors and the dissociation of active TGF-β1 from surface receptor ligand complexes (from Equation 2). The last term in the equation represents the rate of internalization of bound receptor ligand complexes.

Equation 6 represents the rate of change over time in the number of internalized bound receptor ligand complexes per cell.

$$\frac{d}{dt}[TRC_{int}] = \left(k_{int}^{TRC} * \left[TRC_{surf}\right]\right) - (k_{rec}^{R} + k_{deg}^{R} + k_{lid}^{R}) * [TRC_{int}] \quad (6)$$

The first term on the RHS of the equation represents the rate of internalization of surface receptor ligand complexes (from Equation 5). The second term in the equation represents the loss of internalized receptor ligand complexes to recycling, ligand independent degradation, and ligand induced degradation and is proportional to the number of internalized receptor ligand complexes ($[TRC_{int}]$).

2.4.2.2 PGE_2 Dynamics

Equations 7 and 8 track the concentration of extracellular PGE_2 as well as the intracellular concentration of PGE_2 (Table 2.1, Figure. 2.1). Recent studies have shown that PGE_2 is an effective inhibitor of TGF-β1 induced fibroblast differentiation (168). PGE_2 can be synthesized and bound by fibroblasts making it a component of fibroblast autocrine signaling. Thus, to fully understand factors involved in fibroblast regulation and differentiation we include equations for soluble and internalized PGE_2 that allow for tracking of inhibition of TGF-β1 induced differentiation.

$$\frac{d}{dt}[PGE2_{Sol}] = k_{synth}^{PGE2} - \left(k_{int}^{PGE2} * [PGE2_{Sol}]\right) - (k_{deg}^{PGE2} * [PGE2_{Sol}]) \quad (7)$$

$[PGE2_{Sol}]$ represents the concentration of soluble PGE_2. The first term on the RHS of the equation represents the constitutive rate of PGE_2 synthesis by the fibroblast. The second term in the equation represents the rate of PGE_2 being internalized in to the cell. The final term in the equation is the rate of degradation of extracellular PGE_2.

.

$$\frac{d}{dt}[PGE2_{int}] = \left(k_{int}^{PGE2} * [PGE2_{Sol}] * Nav * vol * \frac{1}{cells}\right) - k_{degint}^{PGE2} * [PGE2_{int}] \quad (8)$$

$[PGE2_{int}]$ represents the concentration of internalized PGE_2. The first term on the RHS of the equation represents the rate of PGE_2 being internalized in to the cell (from Equation 7). The second term in the equation is the rate of degradation of internalized PGE_2.

2.4.2.3 αSMA Synthesis

We track αSMA concentration, a known indicator of fibroblast differentiation (105). αSMA serves to increase the contractile strength of fibroblasts a phenotype that is associated with their differentiated state (189). This phenotype is important for wound contraction and tissue remodeling. TGF-β1 receptor binding and internalization induces a signaling cascade through either the canonical SMAD2/3 pathway or the non-canonical Rho/ROCK pathway (332). Because experimental data detailing the rates of SMAD2/3 and Rho/ROCK signaling cascades are limited in fibroblasts, we focused on the receptor/ligand dynamics of the TGF-β1 signaling cascade and simplified, i.e. we replaced the entire signaling cascade with a term that tracks the effect of the kinase signaling cascade (see more below), the downstream phosphorylation cascades into a single event. We can still learn much about the system using this approach, and our analyses point to which elements can be elaborated later for further study.

We have two equations in our model that enable us to track the synthesis of αSMA. Equation 9 tracks the number of receptor ligand internalization events over time[$\boldsymbol{PRDS}$]. Because we do not explicitly measure all the kinase signaling cascades down stream of receptor

ligand complex internalization, we use this equation as a surrogate for those events. This equation contains a loss term which is the degradation of signaling complexes. These complexes serve as a simplification of the complex biological signal cascade far downstream of the initial internalization event. We use this equation to bridge the temporal gap between receptor ligand events which occur very fast (on a timescale of minutes) and the protein synthesis events that occur much slower (on a timescale of hours), without the need to explicitly model every signal in the cascade. It is one way to coarse grain (simplify) these intracellular signaling events. Course graining the kinase signaling cascades, for which many parameter values are not known, allows us to reduce ambiguity from many unknown parameter values and processes. However, as key factors are identified, our model can point to features that can be fine-grained in future studies to further elucidate key signaling mechanisms driving fibroblast differentiation.

$$\frac{d}{dt}[PRDS] = (k_{int}^{TRC} * [TRC_{surf}] - (k_{deg}^{PRDS} * [PRDS]) \quad (9)$$

The first term on the RHS of the equation represents the rate of internalization of receptor complexes (from Equation 5). The second term represents the rate of degradation of the signal. Equation 10 captures the rate of change over time for the concentration of αSMA per cell $[aSMA]$.

$$\frac{d}{dt}[aSMA] = [PRDS] * \left(c_{act}^{Adhesion} * c_{Stiff}^{Matrix}\right) * \frac{k_{Inhibit}^{PGE2}}{cells * ([PGE2_{int}] + \alpha_1)} - k_{deg}^{\alpha SMA} * [aSMA] \quad (10)$$

The first term on the RHS of the equation represents the rate of αSMA synthesis and is proportional to the number of receptor ligand complex internalization events ($[PRDS]$) which promote αSMA synthesis and inversely proportional to the concentration of internalized PGE_2 ($[PGE2_{int}]$) which antagonizes αSMA synthesis. The rate constant c_{Stiff}^{Matrix} represents the stiffness of the matrix to which the cell is adhering which positively correlates to adhesion signaling (238, 317, 333, 334). $k_{inhibit}^{PGE2}$ represents the rate of PGE_2 inhibition of adhesion signaling. This term dictates how well PGE_2 is able to antagonize the induction of αSMA synthesis by TGF-β1. α_1 represents a small, non-zero number, to bound the denominator away from zero. The final term in the equation represents the rate of degradation of αSMA.

2.4.3 Parameter Derivation and Estimation

We use uncertainty analysis (below) to estimate parameters in our model. When a parameter value is available from the literature, it is used directly, and others are obtained during model calibration (Figure. 2.2, also see ranges in Table 2.2). For the parameters that were available in literature, we computed their values as follows. The rate constants for latent TGF-β1 degradation ($k_{deg}^{TGF\beta 1_{lat}}$) and active TGF-β1 degradation($k_{deg}^{TGF\beta 1_{act}}$) are derived from the half-life of latent and active TGF-β1 in rat plasma (9.2 ± 1.4 min and 2.7 ± 0.4 min respectively) and published by Wakefield et al.(326) assuming first order kinetics. The rate constants for TGF-β1 binding and dissociation from the receptor $k_{on}^{TGF\beta 1}$ and k_{diss}^{TRC} are estimated based on the equilibrium dissociation constant of TGF-β1 ($K_d = 23pm$) published by Kalter et al. (72). The rate k_{syn}^{R} is fit to satisfy the experimental data suggesting that approximately 90 of the total TGF-β1 receptors reside in the cytoplasm of the cell with the remaining 10% localizing to the surface under steady conditions (335), given that there are approximately 10,550 ± 1400

receptors per cell (72). Rate constants for receptor recycling (k_{rec}^{R}), constitutive receptor degradation (k_{deg}^{R}), and ligand induced receptor degradation (k_{lid}^{R}) are derived from Vilar et al. (207). The rate k_{synth}^{PGE2} is derived from Lin et al. (328).(329) assuming first order kinetics.

The parameter $k_{act}^{Adhesion}$ represents a switch for the presence or absence of adhesion signaling and has a value of either 0 or 1. $k_{inhibit}^{PGE2}$ represents the magnitude of PGE_2 inhibition of adhesion signaling and is estimated by uncertainty analysis. α_1 represents a small non-zero number. In the absence of PGE_2, α_1 is given the same numerical value as $k_{inhibit}^{PGE2}$, these terms reduce to 1 resulting in no inhibition by PGE_2 and avoid dividing by zero.

For the remaining parameters, quantitative values for these rate constants were not available in literature and would be difficult to measure *in vitro* ($k_{act}^{TGF\beta 1_{lat}}$, k_{int}^{PGE2}, k_{degint}^{PGE2}, $k_{deg}^{TGFBint}$, and $k_{deg}^{\alpha SMA}$) so we estimate their values using uncertainty analysis and model calibration techniques.

2.4.4 Uncertainty Analysis

We use uncertainty analysis to quantify how variations in parameter values leads to variations in model outputs. Uncertainty analysis allows us to examine outcomes based on a wide value range for each unknown parameter value individually and simultaneously. We vary numerous parameters in the model over a wide range (Table 2) and compare how these variations affect model outputs. Latin hypercube sampling (LHS) is a method for varying multiple parameters simultaneously and then sampling the parameter space (229). When used for parameter estimation, uncertainty analysis allows model calibration to available data and identification of values for unknown parameters that allow for this when varied simultaneously.

.

2.4.5 Sensitivity Analysis

We use sensitivity analyses to identify which model parameters have a significant effect on model output and the extent of this effect. Sensitivity analysis identifies which parameters have a significant effect and the extent of the effect. Partial rank correlation coefficients (PRCCs) are used to quantify the effects of varying each parameter on the model output and therefore discerning which parameters have the strongest influence on a given output, or in other words the sensitivity of an output to a given parameter. PRCC values range from -1 to +1. A value of -1 signifies a perfect negative correlation between the parameter and the output whereas a value of +1 signifies a perfect positive correlation between the parameter and the output. The closer a PRCC value is to 0 the weaker the correlation, whether positive or negative. PRCC values are differentiated with a student t-test of significance. However since PRCC quantifies non-linear correlations, even small PRCC values can be significant. In this work we use the LHS algorithm to generate 1000 unique parameter sets. This number of simulations gives high accuracy when identifying PRCC values (229). PRCC values are considered significant and with a p-value of 0.01.

2.4.6 Model Solution, Calibration and Validation

We solve Equations (1)-(10) with parameters as listed in Tables 1 and 2 using MATLAB ODE15s solver. While the equations are given in units/time, we simulate both calibration and validation studies using quantities in terms of fold change. This is how experimental data for these studies are measured and it allows us to compare directly with data. We also compare the relative outputs in responses to treatment as fold change compared to untreated simulations.

Initial conditions are chosen to calibrate the model based on previously identified values specific for fibroblasts to achieve a steady state (327), or selected to replicate experimental conditions (Figure. 2.2). Kalter et al. observed that fibroblasts have approximately 10,550 ± 1400 TGF-β1 receptors per cell, and approximately 90% of those receptors are in the cytoplasm at steady state (72). Based on this observation and rates derived in Vilar et al. for receptor recycling and synthesis we select parameter values using uncertainty analysis that allow us to achieve these steady states. Variables for which the steady state is unknown are given initial values of 0 (Table 2). Using our model and the set of identified baseline parameter values that reflect differentiation of fibroblasts (Table 2), we validate our model by comparing output to additional experimental data derived in our lab and not used in the calibration of the model (Figure. 2.3). First, we simulate exposing our model fibroblasts to an initial concentration of 0.6nM of TGF-β1 and compare the concentration of αSMA at 4, 12, 24 and 48 hours as well as a 4 hour untreated control to *in vitro* experimental data described below (Figure. 2.2). Second, we simulate how output from different model constructions compares to experimental data published previously by our group. For example, we introduce into the model PGE_2 inhibition of adhesion signaling and compare to simulation experimental results in the presence and absence of PGE_2 (Figure. 2.2) (168). Time course *in vitro* experiments were performed on mouse 3T12 transformed fibroblasts Additional *in vitro* experiments were performed using primary mouse lung fibroblasts to effectively capture the sensitivity of lung fibroblasts to PGE2. Comparative simulations were done using different initial concentrations of TGF-β1 to reflect differences in effective concentration of and sensitivity to TGF-β1 between these two cell types. The difference in magnitude of αSMA synthesis in response to TGF-β1 treatment between in vitro experiments (Figure. 2.2) is likely due to differences between transformed cells and primary cells.

2.4.7 Calculating the Balance between TGF-β1 and PGE_2 levels

We use LHS sampling as described above to generate 1000 simulations of our model with different TGF-β1 and PGE_2 concentrations and then compare the concentration of αSMA at 48 hours. From this simulated data we generated a heat map of the concentration of αSMA with respect to TGF-β1 and PGE_2 using the meshgrid, TriSCatteredInterp, and contour functions in MATLAB (Figure. 2.7). The outcomes vary from severe fibrosis to healthy tissue to apoptosis (323).

Chapter 3

Computational Modeling Predicts Simultaneous Targeting of Fibroblasts and Epithelial Cells is Necessary for Treatment of Pulmonary Fibrosis

3.1 Introduction

Pulmonary fibrosis is a pathologic feature associated with many interstitial lung diseases (24). A wide range of lung insults can result in development of fibrosis, including antibiotic treatment, infection, and environmental exposures (16, 23, 336, 337). In cases described as idiopathic pulmonary fibrosis (IPF), no explicit cause of fibrosis can be identified (8). Disease presentation includes stiffening and scarring of lungs, decreased flexibility of tissues, and diminished gas exchange (12, 13, 17, 312, 313, 338). Patients suffering from pulmonary fibrosis have difficulty breathing, reduced quality of life, and ultimately a poor prognosis (10, 13, 246, 312, 330, 338-341).

Although mechanisms leading to pulmonary fibrosis are not well-characterized, it is believed that pulmonary fibrosis occurs as the result of dysregulation during the wound healing process (22, 143, 148, 231). Wound healing occurs in four stages: (I) coagulation and hemostasis, (II) inflammation, (III) proliferation, and (IV) remodeling (12). During the third stage of wound healing, fibroblasts proliferate into the wound gap (152). They secrete cytokines, including transforming growth factor-β (TGF-β), which act in both an autocrine and paracrine manner to induce further proliferation and/or eventual differentiation of fibroblasts into myofibroblasts (66, 100, 105, 234). Myofibroblasts play an important role in the fourth stage of

the wound healing process, the remodeling stage. They secrete extracellular matrix (ECM) proteins including collagen and fibronectin (143, 152, 156) that are cross-linked to provide a substrate for re-epithelialization of wounded tissue (152). Myofibroblasts also express α-smooth muscle actin (α-SMA), a protein that integrates into actin filaments giving cells a contractile phenotype (105, 189, 238). Through integrin binding, myofibroblasts are able to adhere to surrounding tissue and contract, collapsing the wound gap (100, 240). Dysregulation of this process, through unknown mechanisms, results in excessive ECM protein secretion and tissue remodeling. These actions result in the formation of stiff, scarred tissue that is inflexible and unproductive for gas exchange (12, 246).

In addition to fibroblasts and myofibroblasts, epithelial cells are a critical component of effective pulmonary wound healing (241). Epithelial cell damage is congruent with pulmonary fibrosis (187, 241, 245, 247, 248). Epithelial cells are an essential component of properly functioning lung tissue. They line the bronchi, airways, and alveoli of the lungs providing a surface for gas exchange and a barrier for infectious agents (242-244). During pulmonary injury, epithelial cells are damaged and repair is needed in order to restore functionality to the wounded tissue (18, 66, 245). During fibrosis, excessive secretion of pro-fibrotic cytokines such as TGF-β (associated with deregulation of the third stage of wound healing) produces an environment that is toxic to epithelial cells (84, 88). Furthermore, excessive tissue remodeling (deregulation occurring during the fourth stage of wound healing) can induce further epithelial cell damage, loss of epithelial protective factors and tissue contraction reducing the surface area available for re-epithelialization (231, 249).

At the apex of cell-cell interactions during pulmonary wound healing are two key classes of cytokines: pro-fibrotic mediators and anti-fibrotic mediators. TGF-β1, the most well

characterized pro-fibrotic mediator in pulmonary fibrosis, is a cytokine secreted by a wide range of cell types including fibroblasts, with effects that are cell type and tissue specific (100, 108, 109, 111-114, 116, 117). TGF-β1 is an autocrine and paracrine signal that can induce fibroblast proliferation and/or differentiation into myofibroblasts (Figure 3.1) (235-237). Growth factors are necessary for fibroblast proliferation and TGF-β1 is representative of these growth factors. Fibroblasts cultured *in vitro* in serum free media are unable to proliferate well. In some studies, TGF-β1 is sufficient to stimulate proliferation *in vitro* (70, 103, 104). TGF-β1 is also able to induce fibroblast to myofibroblast differentiation, which can be measured by the presence of αSMA in cultured cells (Figure 3.1) (89, 100, 105). Once differentiated into myofibroblasts, these αSMA positive cells have not been found to proliferate (342). High concentrations of TGF-β1 have been shown to induce alveolar epithelial cell apoptosis (Figure 3.1) (67, 106, 107) and are therefore detrimental to epithelial cell survival during wound healing. In contrast, TGF-β1 may prevent apoptosis of fibroblasts and this differential response of these cell types to TGF-β1 has been called the "apoptosis paradox" (343). In opposition to TGF-β1, PGE_2 is a well characterized anti-fibrotic lipid mediator with a wide range of influence that is cell and tissue type specific. In pulmonary tissues, PGE_2 is predominantly secreted by epithelial cells as an inducer of fibroblast quiescence (187, 188). It also serves as a negative regulator of TGF-β1, inhibiting fibroblast proliferation and differentiation, myofibroblast ECM secretion, and TGF-β1 induced epithelial cell apoptosis (Figure 3.1) (66, 122, 188, 234, 322). PGE_2 inhibits FAK mediated adhesion signaling, indirectly inhibiting TGF-β1 signaling cascades (168). We consider PGE_2 is representative of mediators that inhibit fibroblast activation. It is well established that epithelial cells, fibroblasts, and myofibroblasts all play important roles in lung function and pulmonary wound healing (22, 88, 148, 150, 241). Their interactions and co-regulation are

paramount to understanding the mechanisms underlying dysregulation of the wound healing process and the development of fibrosis (Figure 3.1). Recent work published by the Sime laboratory at the University of Rochester shows that alveolar epithelial cells from healthy lungs are able to inhibit TGF-β1-induced fibroblast differentiation and secretion of ECM proteins in a PGE_2 dependent manner *in vitro* (66). Recent systems biology and modeling approaches by our group further demonstrate the importance of PGE_2 in regulating the activation of fibroblasts (344). Using computational analyses, we predicted that modulation of fibroblast differentiation by targeting pro-fibrotic signaling cascades alone is insufficient for prolonged regulation of the fibroblast (344). As observed in other systems, it is likely that a balance of both positive and negative regulators (e.g. TGF-β1 and PGE_2 respectively) is necessary for achieving homeostasis and avoiding excessive fibroblast activation (158, 344). PGE_2 is also shown to protect epithelial cells from toxicity of pro-fibrotic mediators like TGF-β1 (345). Together TGF-β1 and PGE_2 serve as examples of positive and negative regulators to preserve balance in the responses of epithelial cells, fibroblasts, and myofibroblasts to tissue damage (Figure 3.1).

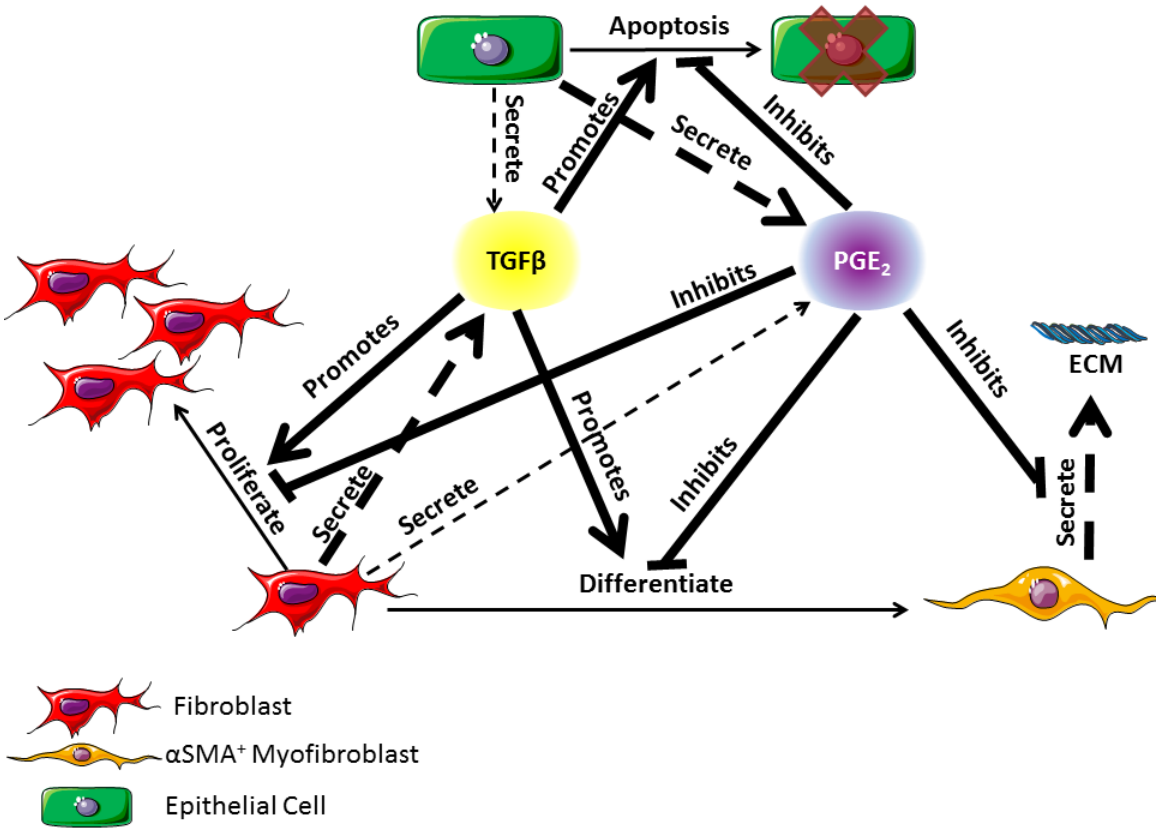

Figure 3.1: Diagram of the co-regulatory relationship between fibroblasts, myofibroblasts, and epithelial cells through TGF-β1 and PGE_2 signaling occurring in lung tissue. Dashed arrows indicate secretion of a molecule. The thickness of the arrow indicates relative contribution of the cell type to the mediator concentration. Solid lines indicate an action of the cytokine on a given cell type. Arrows indicate a positive effect on the cell while dashed lines indicate a negative effect. ECM is the extracellular matrix.

Treatments for pulmonary fibrosis are limited. Until recently the only therapeutic treatments available for pulmonary fibrosis were treatments for the causative agents themselves. Cases of fibrosis with unknown cause could not be treated. Lung transplantation was considered the only available intervention. In October of 2015, two drugs were approved by the United States Food and Drug Administration (FDA) for the treatment of IPF (25). One of the drugs is nintedanib, a tyrosine kinase inhibitor that blocks ATP binding to the receptors of several pro-fibrotic growth factors including, but not limited to, vascular endothelial growth factor (VEGF), fibroblast growth factor (FGF), and platelet derived growth factor (PDGF) (27, 28, 32, 314, 346).

The second drug is pirfenidone, which is reported to have anti-inflammatory, anti-fibrotic, and anti-oxidant properties (25). While the specific mechanisms of action of pirfenidone are unknown, pirfenidone can reduce TGF-β1 signaling and inhibit fibroblast differentiation *in vitro* and *in vivo* in a rat model (30, 33, 346). Regardless, neither of these available therapies is curative. Both treatments slowed but did not halt or reverse the progress of IPF marked by a reduction in the decline of patients forced vital capacity (FVC) (28, 30, 31, 267, 347).

The current therapeutic strategies for treating pulmonary fibrosis can reduce the rate of decline in patient lung function. Both therapies approved for use by the FDA target the dynamics of fibroblasts, namely inhibiting proliferation, differentiation, and TGF-β1 production. However, neither nintedanib nor pirfenidone have been demonstrated to promote the survival or regeneration of epithelial cells in a fibrotic lung. There is evidence that pirfenidone may even inhibit retinal epithelial cells (250).

Here we construct an *in silico* model that captures the co-regulation of fibroblasts and epithelial cells *in vitro*. There is substantial support for constructing agent-based models *of in vitro* co-culture systems in the literature. These models are used to study a wide range of processes including but not limited to wound healing (191, 195, 196, 273), tissue patterning (348), and tumor progression (198, 349, 350). The construction of this model is based on previous work in our lab building a 3D model of granuloma formation in the lung.

With this model we seek to identify which mechanisms of co-regulation determine fibroblast and epithelial cell outcomes during wound healing. By capturing a wide range of possible outcomes we are able to predict which mechanisms would be good potential therapeutic targets for preventing and reversing fibrosis. We hypothesize that a two-hit approach targeting specific mechanisms to both inhibit fibroblast dysregulation and simultaneously promote

epithelial cell survival is necessary to halt or reverse damage associated with pulmonary fibrosis. In order to construct the model and test this hypothesis, we take a systems biology approach that combines *in vitro* experiments with *in silico* simulations of a co-culture system. We use a multi-scale, hybrid agent-based model to identify mechanisms that simultaneously and independently drive fibroblast dysregulation and epithelial cell death. We take a reductionist approach to fibrosis, looking solely at the cells that are experiencing damage (epithelial cells) or inflicting damage (fibroblasts and myofibroblasts) and model representative pro- and anti-fibrotic mediators rather than a more complex tissue environment. This co-culture environment enables us to focus our search for mechanisms driving outcomes for these cells while limiting potentially confounding factors in our system. It also allows us to look specifically at co-regulation of fibroblasts and epithelial cells and concurrently compare the effects of intervention strategies. Our model enables us to predict whether a two-hit synergistic therapeutic strategy for pulmonary fibrosis addressing multiple aspects of the disease will be the most successful at improving cellular outcomes.

3.2 Results

3.2.1 TGF-β1 and PGE_2 Modulate Fibroblast Proliferation *In Vitro* in a Dose Dependent Manner

Previous work has demonstrated the roles of TGF-β1 and PGE_2 in fibroblast to myofibroblast differentiation (66, 100, 234, 344). We sought to determine the capacity for TGF-β1 and PGE_2 to influence IMR-90 fibroblast proliferation *in vitro*. We first compared levels of radioactive thymidine incorporation after 48 hours in IMR-90 cultures with complete media (CM) or CM and the addition of 0.1 – 4.0 ng/ml acid activated TGF-β1 (Figure 3.2A). Data

show no increase in proliferation and no decrease in proliferation in fibroblasts treated with 0.1ng, 0.5ng, or 1.0ng of acid activated TGF-β1. A significant decrease in proliferation in 2.0ng or 4.0ng of TGF-β1 indicates decreased proliferation under these conditions (Figure 3.2A). We next compared levels of radioactive thymidine incorporation after 48 hours of culture in CM media alone, or CM and 0.1 - 100nM of exogenous PGE_2 (Figure 3.2B). Data show increased proliferation of fibroblasts in 0.1nM PGE_2. Fibroblasts cultured in CM with 1.0nM PGE_2 showed no change in proliferation. Data also show that 10nM or 100nM concentrations of PGE_2 induced a significant decrease in proliferation (Figure 3.2B).

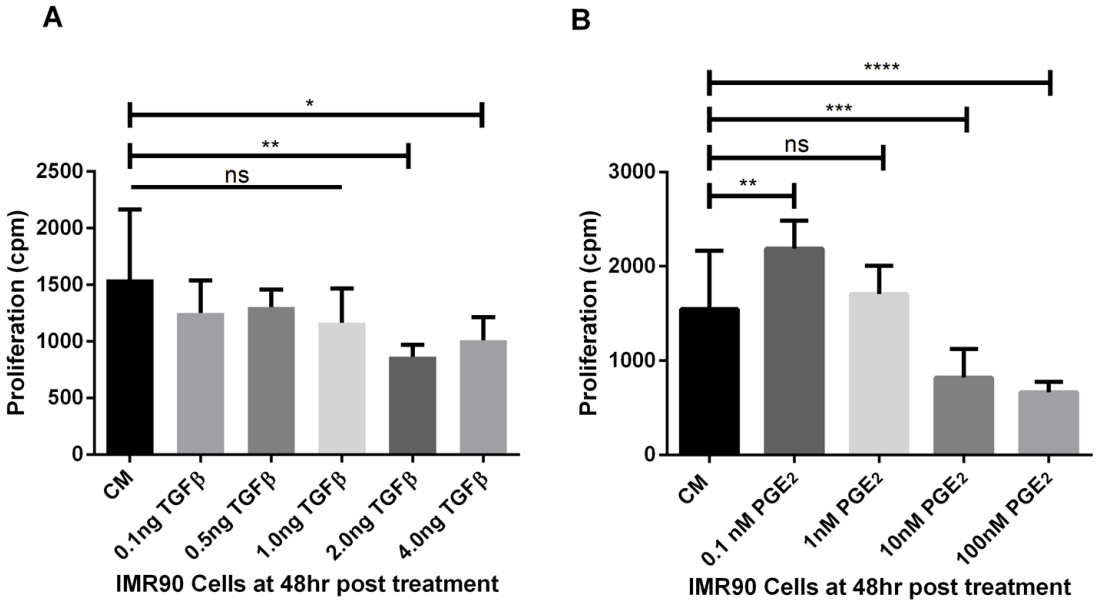

Figure 3.2: Estimating fibroblast proliferation thresholds modulated by TGFβ and PGE_2. A) IMR90 fibroblasts were cultured in complete media (CM) and treated with different concentrations of TGFβ1 for 48 hours in the presence of radioactive thymidine. Proliferation was measured in counts per minute (cpm). Sidak's multiple comparison test was used to determine significance(351). B) IMR90 fibroblasts were culture in CM and treated with different concentrations of PGE_2 for 48 hours in the presence of radioactive thymidine. Proliferation was measured in cpm. Sidak's multiple comparison test was used to determine significance(351). The significance line without the end irons indicates $p>0.05$ for all comparisons under the line. *$p<0.05$ **$p<0.01$ ***$p<0.001$ ****$p<0.0001$

3.2.2 TGF-β1 Mediates Fibroblast Differentiation and Epithelial Cell Death *In Vitro* in a Dose Dependent Manner that is Captured by the Multi-scale Model

TGF-β1 has been demonstrated to induce fibroblast differentiation (66, 100, 105, 168, 234). αSMA expression is a marker of fibroblast differentiation (352). We sought to determine the ability of TGF-β1 to induce fibroblast differentiation by determining how an initial dose of TGF-β1 affects the proportion of differentiated fibroblasts at 24 hours. We cultured fibroblasts in serum free media (SFM) alone, or SFM plus initial concentration of 0.1ng/ml, 0.5ng/ml, 1.0ng/ml, 2.0ng/ml, and 4.0 ng/ml exogenous acid-activated TGF-β1 for 24 hours and counted the number of αSMA positive cells compared to the total number of cells present in high powered microscope fields (Figure 3.3A, 3B). Data show a positive dose response between the concentration of initial active TGF-β1 and the proportion of activated fibroblasts at 24 hours.

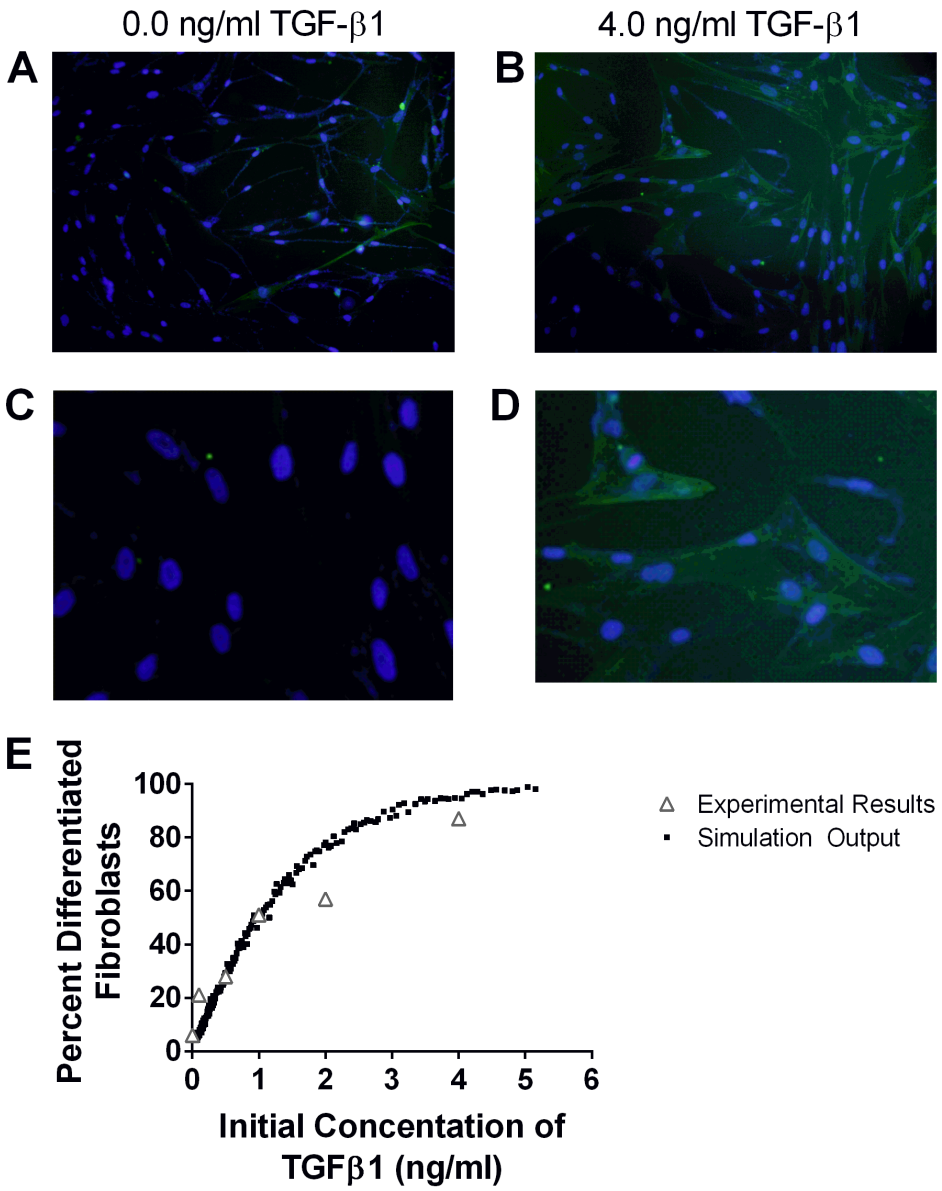

Figure 3.3 Comparison between data and computational model fit for fibroblast differentiation at 24 h in response to TGF-β1 treatment. IMR90 fibroblasts were cultured in serum free media (SFM) alone or with an additional 0.1, 0.5, 1.0, 2.0, 4.0 ng/ml acid activated TGF-β1. The proportion of differentiated cells at 24 h was determined by staining with anti-αSMA and DAPI. A) Representative image of fibroblasts cultured in SFM alone at 100x magnification. (B) Representative image of fibroblasts cultured in 4.0 ng/ml TGF-β1 at 100x magnification. (C) Representative images of fibroblasts cultured in SFM alone at 400x magnification. (D) Representative images of fibroblasts cultured in 4.0 ng/ml TGF-β1 at 400x magnification. (E) Open gray triangles indicate experimental results. Solid black squares indicate simulation output. The proportion of either experimental or simulated fibroblasts having undergone differentiation at 24 h is compared to the initial concentration of active TGF-β1 in the tissue culture or simulation. The simulation data closely matches the experimental data.

To capture this fibroblast dynamic in our computational model, we used Eqn. 1 to express the relationship between αSMA synthesis and fibroblast differentiation. We performed 1500 simulations each with 5000 fibroblasts and an initial concentration of 0.0-5.0 ng/ml exogenous acid-activated TGF-β1. After a simulated time of 24 hours, we calculated the percent of αSMA positive cells in the total cell population (Figure 3.3C). Our model captures the biology of fibroblast differentiation by recapitulating the dose response observed in the experimental dataset.

We sought to identify the correlation between TGF-β1 and epithelial cell death by determining how an initial dose of TGF-β1 affects the percentage of caspase positive epithelial cells at 24 hours. TGF-β1 has been demonstrated to induce epithelial cell apoptosis (353, 354)and caspase activation is a marker of apoptosis (355). We cultured type II alveolar epithelial cells in SFM or SFM plus an initial concentration of 0.5ng/ml, 1.0ng/ml, 2.0ng/ml, and 4.0 ng/ml exogenous acid-activated TGF-β1. At 24 hours, we calculated the percentage of caspase positive cells in high-powered microscope fields (Figure 3.4A). Data show a positive dose response between the concentration of initial active TGF-β1 and the proportion of apoptotic epithelial cells at 24 hours.

To capture epithelial cell dynamics in our computational model, we used Eqn. 2 to express the relationship between TGF-β1 and epithelial cell apoptosis. We performed 1500 simulations each with 5000 epithelial cells and an initial concentration of 0.0-4.0 ng/ml exogenous acid-activated TGF-β1. After a simulated time of 24 hours, we calculated the percent of the total population of dead epithelial cells. Our model captures the biology of epithelial cell apoptosis by recapitulating the dose response observed in the experimental dataset (Figure 3.4B).

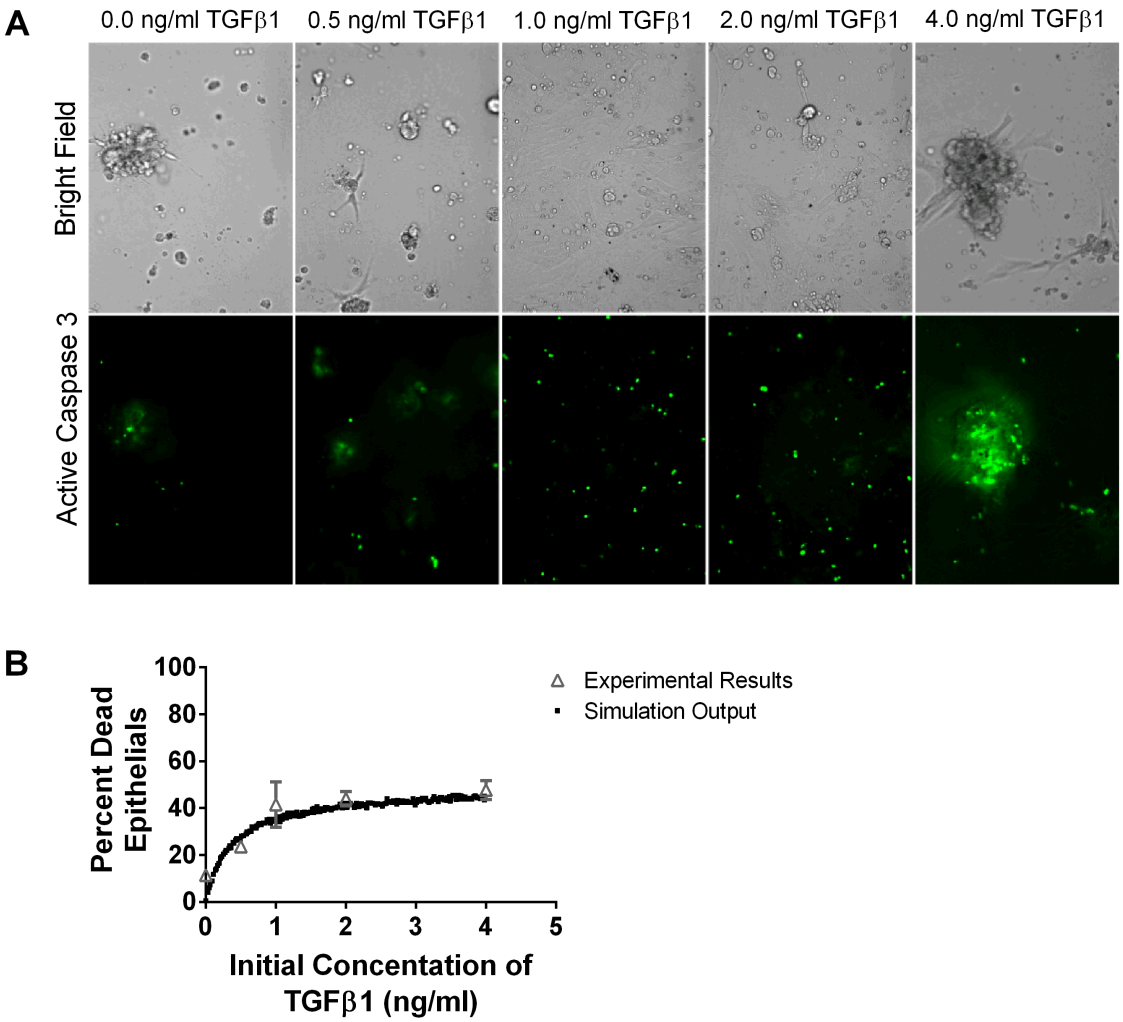

Figure 3.4 Comparison between data and computational model fit for epithelial cell survival at 24 h in response to TGF-β1 treatment. Type II alveolar epithelial cells were cultured in SFM alone or with an additional 0.5, 1.0, 2.0, 4.0 ng/ml acid activated TGF-β1. The number of caspase 3 positive cells was evaluated at 24 h by fluorescent staining. (A) Representative image of cell cultures treated with 0.0, 0.5, 1.0, 2.0, or 4.0 ng/ml of TGF-β1 at 200x magnification. These images show an increase in caspase 3 activation of the epithelial cells in the presence of increasing concentrations of TGF-β1. (B) Open gray triangles indicate experimental results. Solid black squares indicate simulation output. We compare the proportion of experimental or simulated epithelial cells having undergone apoptosis at 24 h to the initial concentration of active TGF-β1 in the cell culture or computer simulated model. The simulation output closely matches the experimental outputs.

3.2.3 Multi-scale Model Captures a Wide Range of Possible Fibroblast, Myofibroblast, and Epithelial Cell Outcomes in a Virtual Co-culture Environment

We next tested whether our computational model can capture the range of possible biological co-culture outcomes observed experimentally. We explored outcomes for a range of physiologically plausible parameter values derived from literature, our work, or estimated using uncertainty analysis (Tables S1-S4); varying parameter values allows us to manipulate the relative importance of particular mechanisms in the model. Multi-scale model outcomes fell primarily into four categories that we classify as: *healthy tissue outcome*, *rapid epithelial cell death with fibroblast proliferation and differentiation*, *gradual epithelial cell death with fibroblast proliferation*, and *early epithelial cell death with excessive fibroblast proliferation and differentiation*. Representative simulations at the end of seven days illustrate model outcomes (Figure 3.4B). We have selected four outcomes that are representative of common trends identified in our LHS. Outcomes falling into each category share some parameter trends. These trends are described in the figure legend with specific values given for the simulation shown (see Appendix Tables S1-4 for full parameter ranges). Our first outcome category, a healthy tissue outcome, shows that under idealized conditions epithelial cells survive and fibroblasts remain quiescent (Figure 3.5A). By the end of seven days fibroblasts had not proliferated and the epithelial cells survived. Our second outcome category, rapid epithelial cell death with fibroblast proliferation and differentiation, shows that under some conditions epithelial cells undergo rapid apoptosis (Figure 3.5B); approximately 50% of the epithelial cells died in the first 24 hours. Fibroblast proliferation occurs during the first 24 hours. Fibroblast to myofibroblast differentiation begins very early in the simulation. By 24 hours all fibroblasts have differentiated restricting proliferation and resulting in fewer cells overall. In the third outcome category,

gradual epithelial cell death with fibroblast proliferation, fibroblasts undergo a large amount of proliferation more than doubling in the first 48 hours of the simulation (Figure 3.5C). In this simulation epithelial cells experience gradual cell death, and by 168 hours nearly half of the epithelial cells have died. Our fourth outcome category, excessive fibroblast proliferation and differentiation, shows nearly complete epithelial cell death by 168 hours (Figure 3.5D). In this simulation fibroblasts proliferate rapidly doubling by 48 hours. At this time some fibroblasts begin to undergo differentiation while others continue to proliferate. After 168 hours all of the fibroblasts have differentiated so that the entire plate is covered with myofibroblasts (Figure 3.5D).

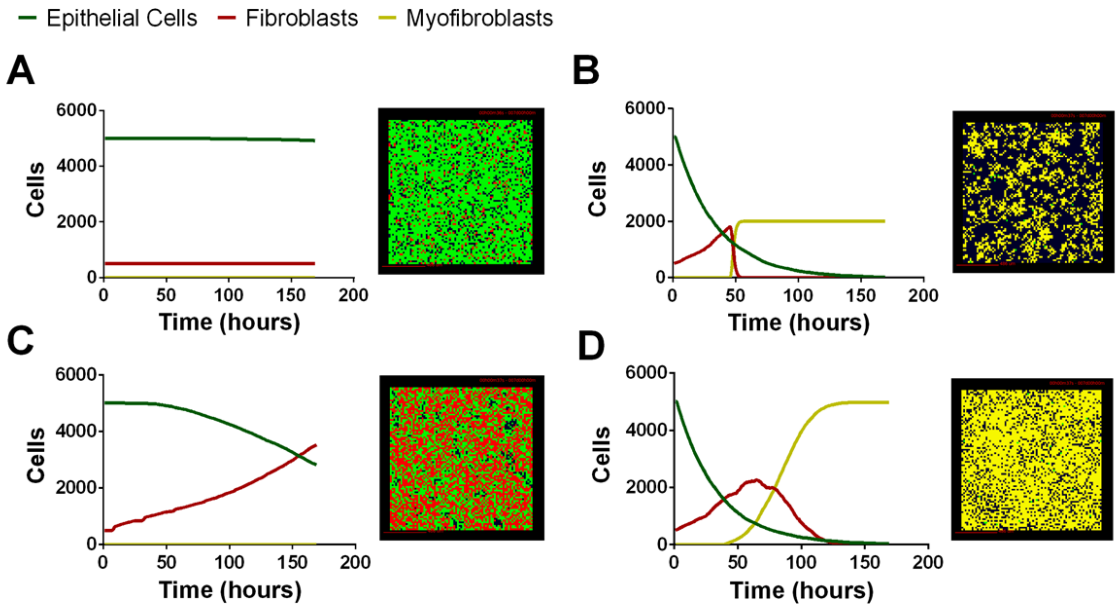

Figure 3.5 Four distinct classes of multi-scale model simulation outcomes varying parameter values. (A) *Healthy tissue outcome*. Complete epithelial cell survival can be achieved by baseline parameter values in the model. (B) *Rapid epithelial cell death with fibroblast proliferation and differentiation*. Parameter combinations leading to rapid epithelial cell death and early fibroblast differentiation include high TGF-β1 synthesis ($k^{TGF\beta 1 lat} = 1.07 \times 10^{-16}$). (C) *Gradual epithelial syn cell death with fibroblast proliferation*. Parameter combinations leading to gradual epithelial cell death include low PGE_2 synthesis ($V_{ePGE2} = 3.16 \times 10^{-27}$) and low TGF-β1 proliferation threshold ($min_{prolifTGF\beta 1} = 1.15 \times 10^{-25}$). (D) *Excessive fibroblast proliferation and differentiation*. Parameter combinations leading to excessive fibroblast proliferation include high TGF-β1 synthesis ($k^{TGF\beta 1 lat} = 9.86 \times 10^{-19}$), high myofibroblast TGF-β1 binding ($k = 0.001$, and decreased PGE synthesis *syn onM* 2 $V_{ePGE2} = 1.69 \times 10^{-29}$). For complete parameter ranges please see Supplementary Material Tables S1–S4. For full length time-lapse simulations please see http:// malthus.micro.med.umich.edu/lab/movies/Co- culture/.

3.2.4 Analysis of the Multi-Scale Model Reveals Key Mechanisms Driving Fibroblast Proliferation, Differentiation, and Epithelial Cell Survival in a Co-culture Environment

A wide range of possible multi-scale model simulation outcomes for fibroblast proliferation, differentiation, and epithelial cell survival can be achieved by manipulating mechanisms of fibroblast and epithelial cell co-regulation (Figure 3.5). To determine which

mechanisms and to what extent they are responsible for driving these different outcomes, we performed sensitivity analysis on the outputs from 1500 simulations of our multi-scale model at day 7 as described in Methods. The analysis predicts mechanisms dictating fibroblast proliferation without differentiation (determined by fibroblast number) (Table 1A). Of the mechanisms found to drive fibroblast proliferation, PGE_2 synthesis had the strongest influence ($p < .01$). The analysis predicts which mechanisms dictate myofibroblast differentiation (determined by number of myofibroblasts) (Table 1B). Of these mechanisms, TGF-β1 synthesis and PGE_2 inhibition of TGF-β1-induced differentiation had the strongest effect on myofibroblast number ($p< .01$). PRCC analysis predicts that the strongest mechanisms driving epithelial cell survival (determined by epithelial cell number) (Table 1C) are predominantly different from mechanisms driving fibroblast proliferation (Table 1A) and differentiation (Table 1B). Of the mechanisms found to drive epithelial cell survival; TGF-β1 synthesis and TGF-β1 activation had the strongest effect on epithelial cell number ($p < .01$). These mechanisms may be strong candidates for therapeutic intervention.

3.2.5 Multi-target Intervention Strategies Promote Healthy Tissue Repair Better than Single Target Strategies

From our sensitivity analysis, we established a list of the primary mechanisms driving fibroblast, myofibroblast, and epithelial cell outcomes (Table 1). Some of these mechanisms reiterate previous understandings about fibrosis, and others provide new insight. Current therapies for pulmonary fibrosis target TGF-β1 signaling in order to prevent fibroblast dysregulation (30, 33, 346). Our analysis identifies that inhibiting TGF-β1 receptor/ligand complex internalization, the first step in TGF-β1 signaling, results in an overall decrease in

myofibroblast number (Table 1B). *In vitro* studies show that high levels of PGE_2 inhibit fibroblast proliferation (Figure 2). Our sensitivity analysis further emphasizes this relationship by highlighting the strong negative correlation between fibroblast number and epithelial cell synthesis of PGE_2 (Table 1A).

Table 3.1: Primary mechanisms driving fibroblast, myofibroblast, and epithelial cell numbers.

(A) Significant PRCC Values for Fibroblast Number at Day 7 (p <0.01)					
TGF-β1 Synthesis	PGE2 Binding Rate	Fibroblast Sensitivity to PGE2	Fibroblast Insensitivity to TGF-β1	TGF-β1 Proliferation Threshold	PGE2 Proliferation Maximum
-0.11	-0.17	-0.12	0.12	-0.11	0.14
Probability of Fibroblast Movement	αSMA Differentiation Maximum	TGF-β1 to PGE2 Differentiation Threshold	PGE2 Synthesis	Epithelial Cell Sensitivity to PGE2	
-0.08	0.07	0.19	-0.40	0.07	
(B) Significant PRCC Values for Myofibroblast Number at Day 7 (p<0.01)					
TGF-β1 Activation	TGF-β1 Synthesis	Fibroblast Insensitivity to TGF-β1	PGE2 Inhibition of TGF-β1 Induced Differentiation	PGE2 Synthesis	Epithelial cell TGF-β1 Binding Rate
0.10	0.54	-0.13	-0.26	-0.14	-0.09
(C) Significant PRCC Values for Epithelial Cell Number at Day 7 (p<.01)					
TGF-β1 Receptor Dissociation	TGF-β1 Synthesis	TGF-β1 Activation	PGE2 Binding Rate	Fibroblast Insensitivity to TGF-β1	αSMA Differentiation Maximum
-0.10	-0.79	-0.47	0.11	-0.14	-0.09

To predict the success of potential therapeutic strategies, we simulated therapeutic interventions by either promoting or inhibiting the mechanisms identified by our sensitivity analysis as the most significant for driving fibroblast proliferation, fibroblast differentiation, and epithelial cell survival. We simulated these therapeutic strategies in the three outcome categories

identified as rapid epithelial cell death with fibroblast differentiation, gradual epithelial cell death with fibroblast proliferation and differentiation, and excessive fibroblast proliferation and differentiation (Figure 3.6). We first tested single intervention strategies intended to either inhibit fibroblast proliferation or differentiation, or to promote epithelial cell survival for each outcome category. We then took a two-hit approach and combined treatment strategies that inhibit fibroblast proliferation or differentiation together with strategies that promote epithelial cell survival. Thus, for each case we tested two interventions independently (Figure 3.6 top) and then in combination (Figure 3.6 bottom).

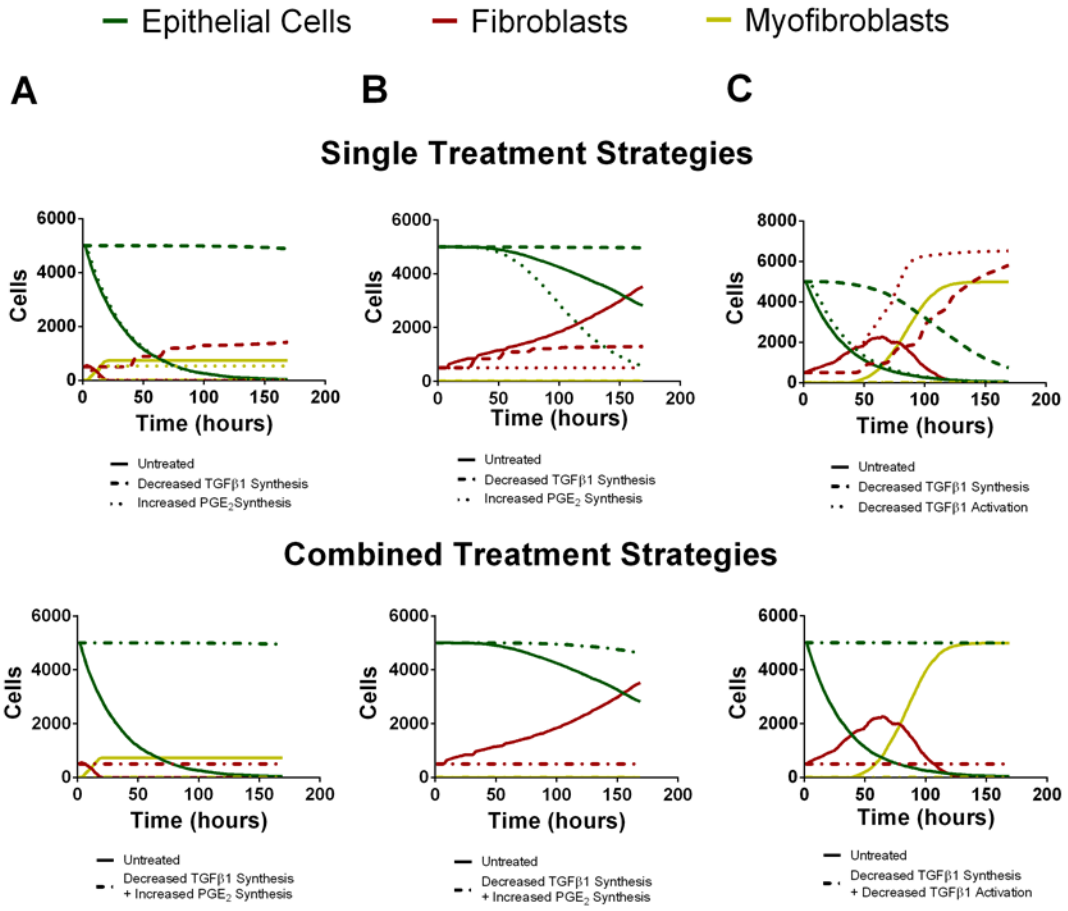

Figure 3.6 Virtual individual and combined treatment outcomes for three case studies (compare to B,C,D from Figure 3.5). Green line represents epithelial cells, red line represents fibroblasts and yellow line represents myofibroblasts. (A) *Rapid epithelial cell death and recovery*. The top panel depicts untreated simulation (solid line) decreased TGF-β1 synthesis

(dashed line) or increased PGE_2 synthesis (dotted line) in isolation. Decreased TGF-β1 synthesis preserves epithelial cell number but does not inhibit fibroblast proliferation. Increased PGE_2 synthesis inhibits excessive fibroblast proliferation but does not rescue epithelial cell number. The bottom panel depicts untreated simulation (solid line) and decreased TGF-β1 synthesis in combination with increased PGE_2 synthesis (dot-dashed line). Combined treatment restricts fibroblast proliferation and preserves epithelial cell survival. (B) *Gradual Epithelial cell death and recovery*. The top panel depicts untreated simulation (solid line) decreased TGF-β1 synthesis (dashed line) or increased PGE_2 synthesis (dotted line) in isolation. Decreased TGF-β1 synthesis preserves epithelial cell number but does not inhibit fibroblast proliferation. Increased PGE_2 synthesis inhibits excessive fibroblast proliferation but results in more rapid decline in epithelial cell number. The bottom panel depicts untreated simulation (solid line) and decreased TGF-β1 synthesis in combination with increased PGE_2 synthesis (dot-dashed line). Combined treatment restricts fibroblast proliferation and preserves epithelial cell survival. (C) *Excessive fibroblast proliferation and recovery*. The top panel depicts untreated simulation (solid line) decreased TGF-β1 synthesis (dashed line) or decreased TGF-β1 activation (dotted line) in isolation. Decreased TGF-β1 synthesis increases but does not preserve epithelial cell number and does not inhibit fibroblast proliferation. Decreased TGF–β1 activation does not inhibit excessive fibroblast proliferation or rescue epithelial cell number The bottom panel depicts untreated simulation (solid line) and decreased TGF-β1 synthesis in combination with or decreased TGF-β1 activation (dot-dashed line). Combined treatment restricts fibroblast proliferation and preserves epithelial cell survival.

For the outcome category rapid epithelial cell death with fibroblast differentiation (Figure 3.6A), we virtually reduced fibroblast synthesis of TGF-β1 or we increased epithelial cell synthesis of PGE_2. Decreasing TGF-β1 synthesis alone inhibits fibroblast to myofibroblast differentiation and rescues the epithelial cells at 168 hours but due to the presence of low levels of TGF-β1 fibroblast proliferation is not inhibited. Increased synthesis of PGE_2 inhibited fibroblast proliferation but did not decrease the rate of epithelial cell death (Figure 3.6A top). Simultaneously decreasing TGF-β1 synthesis together and increasing PGE_2 synthesis inhibited fibroblast to myofibroblast differentiation and also restored epithelial cell survival by day 7 (Figure 3.6A bottom).

For the outcome category, gradual epithelial cell death with fibroblast proliferation (Figure 3.6B), we virtually reduced fibroblast synthesis of TGF-β1 or we increased the rate of

PGE_2 synthesis by epithelial cells. Reducing TGF-β1 synthesis alone rescues the epithelial cells at 168 hours but it does not inhibit fibroblast proliferation. Increasing PGE_2 synthesis inhibited fibroblast to myofibroblast differentiation and fibroblast proliferation. Increased PGE_2 synthesis improved epithelial cell survival by day 7 but not to the same level as decreasing TGF-β1 synthesis (Figure 3.6B top). Combining these effects both inhibited fibroblast proliferation and differentiation while fully restoring epithelial cell survival by day 7 (Figure 3.6B bottom).

Finally, for the outcome category, excessive fibroblast proliferation and differentiation, we virtually reduced TGF-β1 synthesis or reduced TGF-β1 activation. Reducing TGF-β1 synthesis alone inhibited fibroblast to myofibroblast differentiation and made a dramatic improvement in epithelial cell survival at day 7, but did not inhibit fibroblast proliferation. Decreasing TGF-β1 activation had almost no effect on epithelial cell survival, strongly inhibited fibroblast differentiation, but showed no ability to inhibit fibroblast proliferation (Figure 3.6C top). However, combining these effects restored epithelial cell survival by day 7 while inhibiting fibroblast proliferation and differentiation (Figure 3.6C bottom). *A conclusion from the model different mechanisms must be targeted simultaneously to affect outcomes of epithelial cell survival, fibroblast proliferation, and myofibroblast differentiation.*

3.3 Discussion

Pulmonary fibrosis results from dysregulation of the wound healing process in the lungs. Epithelial cells, fibroblasts, and myofibroblasts each play key roles in tissue regeneration after injury. The actions of these different cell types are regulated by pro- and anti-fibrotic cytokines such as TGF-β1 and PGE_2 respectively. During fibrosis, excessive fibroblast proliferation/accumulation and differentiation into myofibroblasts paired with epithelial cell

death results in thick, stiff, and scarred lung tissue that is not suitable for breathing and gas exchange. Our analysis allowed us to Identifying key mechanisms driving fibroblast/myofibroblast dysregulation and epithelial cell death. With this analysis we can predict potential therapeutic targets and strategies for the treatment of pulmonary fibrosis.

The use of *in silico* methods in tandem with experimental approaches allows us to identify relationships between specific mechanisms contributing to fibroblast and epithelial cell co-regulation and their outcomes such as epithelial cell survival and fibroblast proliferation and differentiation during fibrosis. Our multi-scale, hybrid agent-based model is a tool that simulates a computation platform similar to an *in vitro* co-culture system. To ensure that our model accurately reflects biology we used data from the literature or generated it herein to calibrate it. We take a reductionist approach to understanding fibroblast differentiation and epithelial cell regulation and do not capture the full complexity of the lung environment. Nevertheless, like an *in vitro* culture system, our model allows us to test specific mechanisms involved in fibroblast/epithelial cell co-regulation. With this unique tool we can evaluate all parts of the co-regulatory system simultaneously at multiple biological scales over time. Within our multi-scale model simulations we can vary rates and magnitudes of cellular and chemical interactions across a wide range, simulating the effects of thousands of theoretical intervention strategies. The information produced by these simulations includes cell number, local and total chemical concentrations, numbers of proliferation or apoptosis events within a given time frame, and many other details about the simulated cells and environment. Analysis of these simulated outputs allows us to determine which potential interventions or combinations of interventions promote epithelial cell survival and inhibit dysregulation of fibroblasts and myofibroblasts.

Our simulations yield four major categories of outcomes characterized by the number of cells left in each cell class after seven days. We describe these common cases as healthy tissue outcome, rapid epithelial cell death with fibroblast proliferation and differentiation, gradual epithelial cell death with fibroblast proliferation, and excessive fibroblast proliferation and differentiation. It should be clear that there is a wide range of outcomes in between these four classes, as cell behavior in our model and in reality is not discrete but a continuous range of possibilities. Our results hold nonetheless. Through uncertainty and sensitivity analysis, we identify mechanisms driving fibroblast, myofibroblast, and epithelial cell outcomes defined by cell numbers at 7 days. Although several mechanisms have a significant impact on fibroblast cell number, the strongest regulator is PGE_2 synthesis by epithelial cells. For myofibroblasts, TGF-β1 synthesis and the ratio of TGF-β1 to PGE_2 permissive for differentiation are the key mechanisms driving cell number. Epithelial cell outcome is most dependent on TGF-β1 synthesis and TGF-β1 activation. It is important to note that fibroblast, myofibroblast and epithelial cell survival outcomes are largely affected by different mechanisms. This implies that treatment strategies intended to reduce or reverse tissue damage associated with fibrosis need to target multiple mechanisms specific to different cell types.

Further exploration of this "two-hit" therapeutic approach emphasizes the efficacy of combinatorial treatment strategies over single target strategies. We performed rescue experiments on the three previously identified poor model outcome categories. We reduced the synthesis of TGF-β1, increased the synthesis of PGE_2, and or decreased TGF-β1 activation in these cases and found that in each case, a two-hit treatment strategy was more effective than a single target approach. In most cases, one intervention targeted epithelial cells and the other targeted fibroblasts and/or myofibroblasts. In some cases there were overlapping effects on

multiple cell types, but in all cases at minimum **two** strategies were required for a complete rescue effect.

As previously described, there are only two therapeutics available for the treatment of pulmonary fibrosis in the United States; Nintedanib and Pirfenidone. Neither of these drugs has been carefully tested for effects on epithelial cells as well as mesenchymal cells. Nintedanib inhibits fibroblast proliferation by inhibiting the signaling of receptors of multiple pro-fibrotic growth factors (346). This therapeutic is a direct regulator of fibroblast and myofibroblast outcomes but may not affect epithelial cell survival. Pirfenidone inhibits TGF-β1 signaling (29) and fibroblast to myofibroblast differentiation. Because TGF-β1 synthesis is a key mechanism in epithelial cell survival, Pirfenidone may promote epithelial cell survival but may not explicitly address fibroblast proliferation. Independently these drugs each target one aspect of fibrotic dysregulation. Combined they could potentially have a synergistic effect. While it is interesting to speculate on the biologic usefulness of this approach, currently the costs associated specifically with of Pirfenidone and Nintedanib would be prohibitive for most patients. However, our model predicts that therapeutic strategies addressing multiple aspects of fibrotic disease are essential for the effective treatment of pulmonary fibrosis, and previous analyses have suggested that single therapeutic strategies are insufficient (284). We must identify combined therapeutics strategies that are not cost prohibitive to improve the prognosis of pulmonary fibrosis patients.

Other existing therapeutic strategies that could be considered for a more cost effective combined treatments include, but are not limited to, TGF-β1 receptor fusion proteins (356), recombinant human IL-1α and/or TNFα, arachidonic acid (357), and IL-13 receptor inhibitors (358-360) (Table 2). TGF-β1 receptor fusion proteins have been shown to block TGF-β1 signaling in cell types such as mammary tumor cells (356). The use these proteins to inhibit

TGF-β1 signaling in epithelial cells could directly reduce their sensitivity to TGF-β1 in a fibrotic environment. These proteins could potentially limit myofibroblast differentiation, but may be insufficient in protecting tissue integrity if fibroblast proliferation were not also managed, further calling for a two-hit therapeutic approach. In thinking about inhibition of TGF-β1 signaling as a therapeutic, one must be cautious of the fact that TGF-β1 is a potent regulator of autoimmunity (361) and global inhibition of TGF-β1 receptor signaling could result in the development of profound immune activation and systemic autoimmunity. Thus, localized delivery to the lung and perhaps more targeted approaches to block downstream mediators may show better efficacy overall (202).

Table 3.2: Potential therapeutics for key mechanisms of fibrosis

Fibroblasts			
Mechanism	*Influence on cell number*	*Therapeutic*	*Influence on mechanism*
TGF-β1 Synthesis	↑	Pirfenidone	↓
PGE2 Synthesis	↓	IL-1α, TNFα, AA, IL-13 receptor antagonist	↑
PGE2 Binding	↓	CP-533536	↑
PGE2 Sensitivity	↓	Forskolin	↑
Proliferation	↑	Nintedanib, IL-13 receptor antagonist (QAX 576)	↓
Epithelial Cells			
Mechanism	*Influence on cell number*	*Therapeutic*	*Influence on mechanism*
TGF-β1 Synthesis	↓	Pirfenidone	↓
TGF-β1 Activation	↓	anti-αVβ6	↓
TGF-β1 Sensitivity	↓	TGF-β1 receptor fusion, TGF-β1 receptor antagonist (A8301)	↓

↑ indicates promotes cell number, ↓ indicates restricts cell number

Recombinant human IL-1α and recombinant human TNFα have been shown to stimulate PGE_2 synthesis by endometrial cells via the up regulation of the rate-limiting cyclooxygenase-2 (COX-2) enzyme important for conversion of arachindonic acid to PGH_2 (357). The addition of arachidonic acid (AA) with recombinant TNFα and IL-1α further increased the synthesis of PGE_2 by endometrial cells by providing substrate for COX-2 actions (357). PGE_2 can bind to 4 different cell surface receptors, but the cyclic adenosine monophosphate (cAMP)-coupled EP2 and EP4 receptors are known to regulate the inhibitory effects of PGE_2 on fibroblasts. EP2 (234) receptor agonists can simulate PGE_2 binding (362). By mimicking PGE_2 binding, a mechanism highlighted by our sensitivity analysis, cAMP analogues could not only limit fibroblast activation, but also promote epithelial cell survival. One of the challenges with PGE_2-based therapeutics are that lipid mediators have short half-lives in vivo, and systemic delivery of PGE_2 could result in hemodynamic complications due to signaling via other EP receptors in multiple cell types (325, 363). For this reason, targeted EP2 agonist approaches may be more selective, but still need to be delivered locally to the lung to limit off-target effects. This process is complicated by the loss of EP2 receptor expression and sensitivity in IPF (167, 364). Thus, better therapeutics may come in targeting downstream mediators of PGE_2-EP2 actions.

IL-13 has been show to promote fibroblast proliferation and increase αSMA synthesis, ultimately leading to differentiation (358-360). Reduction of IL-13 signaling in fibroblasts through receptor inhibitors such as QAX 576 (Novartis) (26) could reduce fibroblast cell number, differentiation, and tissue remodeling functions. It has also been hypothesized that IL-13 may reduce PGE_2 production (360). Thus inhibition of IL-13 receptor signaling may have a dual effect of decreasing fibroblast proliferation and increasing PGE_2 synthesis.

In simulated combinations targeting fibroblasts and promoting epithelial cells, these therapeutics and others have the potential to provide synergistic improvement in outcomes over individual treatment strategies (Table 2). Fibroblasts, myofibroblasts, and epithelial cells have distinct regulatory mechanisms during wound healing. The dysregulation of any or all of these processes requires a multifaceted approach for the full restoration of tissue integrity. Addressing epithelial cell survival in conjunction with solving fibroblast dysregulation using either new or already available therapeutics is the necessary next step to providing therapy for pulmonary fibrosis.

3.4 Methods

3.4.1 *In Vitro* Studies of Fibroblast Proliferation

The IMR-90 normal human lung fibroblast cell line was obtained from American Type Culture Collection (ATCC; CCL-186). Approximately 5000 cells/ well are plated onto each well of a 96 well plate and either left untreated, treated with 0.1-4ng/ml of activated TGF-β1, or treated with 0.1-100nM of PGE_2. Cells were treated with 10 μCi of radioactive thymidine (Fisher) at 32 hours and harvested at 48 hours post treatment. Cells were harvested onto glass fiber filters using an automated cell harvester and filters were counted using a beta scintillation counter. Proliferation was compared by counts per minute (cpm) between samples using ANOVA with a post-hoc Sidak multiple comparisons test.

3.4.2 *In Vitro* Studies of Fibroblast Differentiation

Approximately 75,000 IMR-90 cells were plated into 8-well Titer-tek slides and cultured in SFM for 16 hours to synchronize cells and restore basal levels of αSMA. After 16 hours the

cells were left untreated, or treated with 0.1ng/ml, 0.5ng/ml, 1.0ng/ml, 2.0ng/ml, or 4.0ng/ml of TGF-β1 for 24 hours. Cells were then blocked with 1% fetal bovine serum and stained with a 1:500 fold dilution of anti-αSMA (Sigma F3777) fluorescently-conjugated antibody. The cell nuclei were stained with DAPI and coverslips were added using Vectashield (Vector brand) H1200. 3-5 fields per well were counted (at least 300 total cells) and the proportion of total cells expressing αSMA was determined.

3.4.3 *In Vitro* Studies of Epithelial Cell Death

Type II alveolar epithelial cells were isolated from wild type mice per standard protocol (365) and then plated on Matrigel (BD Biosciences) in Small Airways Growth Media (SAGM) (Lonza) with 5% Fetal Bovine Serum (FBS) (Hyclone) and 10ng/ml KGF (PeproTech). 24 hours later cells were trypsinized and replated in serum free SAGM on Matrigel in a 24-well plate. 70,000 cells were plated in each well. 24 hours later, the cells were treated with TGFb added at different concentrations as well as IncuCyte Caspase-3/7 Reagent for Apoptosis (Essen BioScience) at 5 mM, according to the manufacturer's instructions. This reagent is cleaved by activated caspase-3/7 resulting in nuclear fluorescent staining. 24 hours later, cells were analyzed under a fluorescent microscope. The percent of fluorescent cells was manually counted for each dose of TGF-β1. We had four replicate wells and counted 2-4 fields per each replicate a total of 8-16 fields for each dose of TGF-β1.

3.4.4 Multi-scale Model Construction

3.4.4.1 Cellular scale agent-based model. Agent-based models (ABMs) are a class of *in silico* models that demonstrate how system level dynamics can emerge as a result of the adaptive

behavior of individuals. They do this by assigning probabilistic actions and traits to individual agents within a system, and then tracking these actions over time and space. These models have a defined domain where agents can interact with each other and their environment. Agents (cells) are tracked in a discrete fashion (i.e. counted) and therefore some agent-based models can provide spatial outputs as well as numerical outputs. Because the behaviors of agents can be probabilistic, agent-based models are stochastic in nature. Our ABM consists of three cellular agent types: fibroblasts, myofibroblasts, and epithelial cells. The environment of our ABM simulates an *in vitro* cell culture plate representing a cubic area of 1.73mm x 1.73mm x 6.20mm, or about one tenth the volume of a well in a 96 well plate (Figure 3.7). We choose to model one tenth of the well to reduce the computational burden of the three dimensional (3D) model. Our simulated plate is partitioned into a grid with side lengths of 81 compartments (81 x 81) and makes up the first layer of our model. There are 6,561 compartments in each layer of the model and 282 layers in total. The bottom layer represents the surface of the dish. The 281 layers above the dish make up a large media compartment that represents the depth of a plate (approximately6.2mm). There are a total of 1,850,202 compartments in the model with a total volume of approximately 19.7 μL. The construction of this model is based on our previous work with agent-based models, including unpublished work with 3D models (157-159, 227, 366, 367).

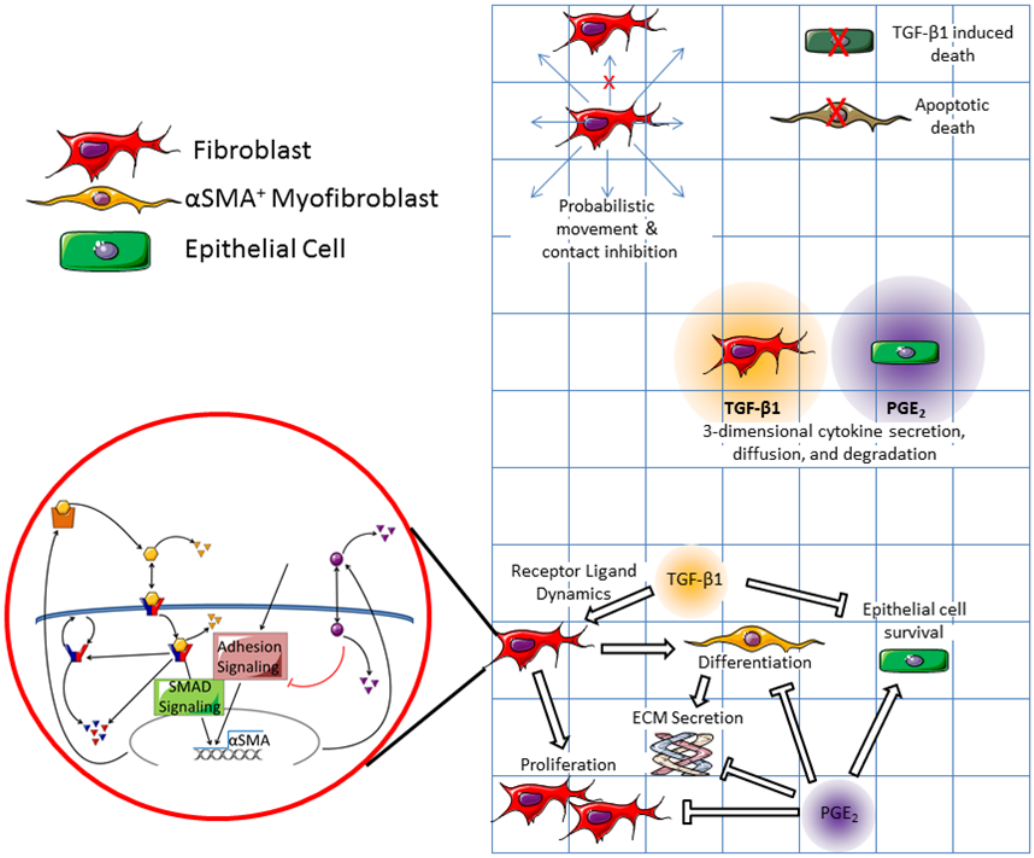

Figure 3.7: Schematic representation of both cellular and molecular scale physiological interactions in the hybrid multi-scale computational co-culture model showing linking of models. Arrows indicate promotional effect while barred lines indicate inhibitory effect. Contents within the red circle depict a previously published molecular scale model of TGFβ signaling (344) that is operational within all fibroblasts.

Within this framework, agents follow cell-type-specific rules capturing physiological interactions tracked at the cellular scale (Figure 3.7). Cellular interactions are guided by rules that include movement of fibroblasts on the surface of the plate, cellular contact inhibition; myofibroblast cell death, TGF-β1 mediated epithelial cell death, TGF-β1- and PGE_2-mediated fibroblast proliferation, fibroblast differentiation into myofibroblasts, and myofibroblast secretion of ECM. For a full list of cellular model rules, see Appendix. Cells in our simulated culture dish, like cells *in vitro*, are adhesion-dependent, meaning that they adhere to the surface of the plate (100). ECM and latent TGF-β1 also adhere to the bottom of the plate (368). The

ECM proteins are assumed to be cross-linked, forming a matrix on the bottom of the plate (368). Latent TGF-β1 adheres to this matrix. When TGF-β1 is activated, the active molecule is released from the matrix and can diffuse through the media.

3.4.4.2 Molecular scale ordinary differential equation model. Figure 3.7 shows a schematic of the molecular scale model. We use our ordinary differential equation (ODE) model of fibroblast receptor-ligand dynamics described previously (344). Briefly, non-linear ODEs capture not only TGF-β1 synthesis, degradation, activation, receptor binding, and dissociation but also receptor dynamics including synthesis, internalization, recycling, and degradation of the TGF-β1 receptor complex. The model provides coarse-grained dynamics for SMAD and Rho/ROCK signaling as well as for adhesion and PGE_2 signaling in fibroblasts. This earlier work identified the need for both a positive and negative regulator to achieve homeostatic fibroblast activation. For example, periodic signaling from either TGF-β1 (an example positive regulator) or PGE_2 (an example negative regulator) was insufficient to produce controlled fibroblast activation.

Active TGF-β1 and PGE_2 are secreted from cells or released from the ECM into the media compartment where they diffuse in 3D (218). Both TGF-β1 and PGE_2 can degrade over time. Extracellular mediator concentrations influence αSMA synthesis by fibroblasts and myofibroblasts, as detailed in the molecular model described below. Similarly, αSMA from the molecular model described below drives fibroblast differentiation (see list of all rules in Appendix).

3.4.4.3 Linking molecular and cellular scale models. We capture both molecular and cellular actions in a multi-scale hybrid model by linking the cellular scale virtual co-culture ABM and molecular scale TGFb dynamics ODE model described above using techniques previously described (157-159, 218). In particular, an output from the molecular level model – αSMA – is a feed forward input into the cellular level model, driving fibroblast to myofibroblast differentiation. The concentration of TGF-β1 and PGE_2, secreted by fibroblasts and epithelial cells, are outputs of the cellular scale model and inputs into the molecular scale model of fibroblast activation. These mediators dictate αSMA synthesis in the molecular scale model completing the connection between the two models and scales. Thus, the cellular and molecular scale models are connected by extracellular levels of TGF-β1 and PGE_2, and intracellular αSMA (Figure 3.7).

3.4.5 Parameter Derivation and Estimation

Parameter values are identified from published experimental work, estimated from experiments herein, and/or predicted using uncertainty analysis. The rate constants for latent and active TGF-β1 degradation were derived from half-lives published by Wakefield et al. (9.2 ± 1.4 min and 2.7 ± 0.4 min respectively) assuming first order kinetics (326). Additional parameters obtained from the literature are as described in Warsinske et al. (344).

The threshold concentrations of TGF-β1 and PGE_2 that allow or inhibit fibroblast proliferation *in vitro* were derived from experiments herein. Fibroblasts proliferate in concentrations of TGF-β1 up to 1ng/ml as compared to fibroblasts cultured in complete media (CM) alone (Figure 3.2A). At 2ng/ml and 4ng/ml fibroblast proliferation is significantly reduced compared to untreated cells, likely due to myofibroblast differentiation. Fibroblasts proliferate

uninhibited in concentrations of PGE_2 up to 1nM (Figure 3.2B). At 0.1nM PGE_2 fibroblasts proliferate significantly more than fibroblasts cultured in CM alone (Figure 3.2B). Fibroblast proliferation is significantly inhibited at 10nM and 100nM concentrations of PGE_2 (Figure 3.2B). Fibroblasts cultured in complete media had a doubling time of approximately 24 hours (data not shown).

Parameters estimated using uncertainty analysis (described below) include soluble PGE_2 degradation rate constant, fibroblast sensitivity to PGE_2, probability of fibroblast movement, αSMA synthesis rate, max αSMA, and level of TGF-β1 lethal to epithelial cells.

3.4.6 Cellular-Scale Model Calibration

The cellular scale ABM is calibrated to reflect *in vitro* experimental data generated by our group (Figures 3.3, 3.4). Fibroblast differentiation is calibrated to fit *in vitro* studies of fibroblast differentiation described above. We assume that the probability that a fibroblast will differentiate in a given simulation time step is linearly related to the amount of αSMA synthesized by the fibroblast:

(EQN 1)

$$Probability\ of\ differentiation = slope * \frac{amount\ of\ \alpha SMA\ synthesized\ by\ the\ cell}{maximum\ amount\ of\ \alpha SMA\ a\ cell\ can\ synthesize}$$

where the slope determines the sensitivity of the system to αSMA. This relationship allows us to calibrate the slope and max αSMA so that the system reasonably fits experimental data of fibroblast differentiation (Figure 3.3). We also assume that the probability that an epithelial cell will apoptose in a given time step is proportional to the amount of TGF-β1 it has bound (Figure 3.4), and that this relationship is captured by a saturation curve:

(EQN 2)

$$Probability\ of\ apoptosis = m * \frac{amount\ of\ TGF\beta 1\ bound\ by\ the\ cell}{amount\ of\ TGF\beta 1\ bound\ by\ the\ cell + (k * amount\ PGE_2 bound\ by\ the\ cell) + C}$$

where m determines the sensitivity of the system to TGF-β1, k determines the sensitivity of the system to inhibition by PGE_2, and C is a non-zero constant. We calibrate m, k, and C so that the system reasonably fits experimental data.

Initial conditions for the cellular scale virtual co-culture ABM are chosen to replicate experimental conditions. 5000 epithelial cells and 500 fibroblasts are seeded on the surface of the model plate at time 0, creating a simulation environment that has approximately 84% cellular confluence. 1500 simulations (virtual experiments) were performed varying all parameter values by approximately 2 orders of magnitude except for the initial conditions and diffusivities of TGF-β1 and PGE_2.

3.4.7 Uncertainty and Sensitivity Analysis

We use uncertainty analysis to quantify how variation in parameter values leads to variation in model output (229). These variations can occur at the molecular and cellular scales in the model and can influence outputs spanning these biological scales. When parameters at one scale influence outcomes at that scale they are considered to have an intra-model influence. Intra-model influences can occur within either the molecular or cellular scale models. When mechanisms at one scale effect outcomes at the other scale these parameters are said to have inter-model influence. Uncertainty analysis allows us to observe model outcomes based on a wide value range for each parameter value. We vary numerous parameters in the model over a wide range (two orders of magnitude) and compare how these variations affect model outputs.

Sensitivity analyses enable us to identify which model parameters have a significant influence and the extent of that influence on a given model output (229, 344). Partial rank correlation coefficients (PRCCs) are used to determine the sensitivity of an output to a given parameter. PRCC values describe the correlation between the parameter value and the output in a range from -1 to +1. PRCC values are differentiated using a student t-test of significance. In this work we use the LHS algorithm to generate 500 unique parameter sets, and run each set in triplicate (229). PRCC values are considered significant and with a p-value less than 0.01. We evaluate our model simulations (defined below) at day 7 because this time-point reflects the full range of possible model outcomes.

3.4.8 Multi-Scale Model Simulation

Our hybrid multi-scale model links both the molecular and cellular scale models, described previously. The combined model, resulting from the linking of the two models (see *Linking molecular and cellular scale models* above) allows us to simulate biological events with molecular and cellular scale details over time. Simulations are defined as an iteration of the multi-scale model that is run on the computer over a defined period of time. Simulations include a set of initial conditions, model rules, equations, and parameter values (see Appendix for complete description of parameters and rules).

Model simulations can be evaluated by comparing individual outputs or the combined overall outcome of the simulation. Initial conditions include the number of each cell type, the concentrations of TGF-β1 and PGE_2 in the environment, and the number of TGF-β1 receptors present on each fibroblast at time 0. In our model we track number of epithelial cells, fibroblasts, and myofibroblasts over time and position in the environment. Model outputs consist of not only

these numbers in space and time but also concentrations of PGE_2 and TGF-β1. A model outcome differs from a model output in that it encompasses multiple outputs and evaluates them over the entire timespan of the simulation. An example of a model outcome would be "*Rapid epithelial cell death with fibroblast proliferation and differentiation"* where outputs for all cell types are considered.

Chapter 4

Deletion of TGF-β1 Increases Bacterial Clearance by Cytotoxic T Cells in a Tuberculosis Granuloma

4.1 Introduction

Mycobacterium tuberculosis is a pathogenic bacterium and causative agent of tuberculosis (TB). Approximately one in three people are infected with *M. tuberculosis*, resulting in 1.4 million deaths in 2015, including 140,000 children (369). The only vaccine for TB is a live, attenuated *M. bovis* strain that confers some protection against severe manifestations of pediatric TB but does not offer lasting protection. With the development and spread of multi-drug resistant TB, there is a need for new therapeutics for TB (169). Current therapeutic strategies require months of multi-drug treatment and treatment failures can lead to reactivation disease, sometimes years after initial infection (37). Developing new therapies to address TB will require an improved understanding of host immune responses to *M. tuberculosis*.

The most common outcome of infection is formation of dense, organized immunological structures called granulomas in lungs (295, 370). Granulomas isolate infected cells from adjacent tissue and prevent bacterial dissemination, but can also make it difficult for the immune system and drugs to kill all bacteria, leading to a stalemate between the immune system and bacteria (192, 288, 371). Granulomas are complex structures that can be classified by their cellular composition, the number of bacteria present, and overall shape (372). Three categories that can be used to describe granulomas include *contained*, indicating the number of live bacteria in a

granuloma has stabilized over time, *disseminating,* indicating the bacterial load in a granuloma is increasing and the infection is not well controlled, and *sterilized*, indicating all the bacteria have been killed (Table 1) (294). Identifying immunological mechanisms that differentiate sterilized, contained, and disseminating granulomas could present therapeutic targets to improve TB treatment.

Table 4.1: Categorization of simulated granulomas by bacterial status

	Description	CFU by day 200	Simulation snapshot
Sterilized	All bacteria have been killed	0	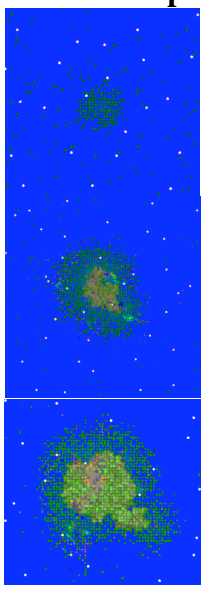
Contained	Number of live bacteria has stabilized over time	Less than or equal to twice CFU at day 100	
Disseminated	Number of live bacteria is increasing, infection is not well controlled	Greater than of equal to twice CFU at day 100	

There is increasing evidence suggesting that cytokine signaling is responsible for establishing granulomas that successfully control *M. tuberculosis* infection. Pro-inflammatory cytokines including TNFα and IFNγ have been investigated for their anti-microbial functions. TNFα has been shown to induce macrophage activation (373), recruit immune cells to the site of infection by promoting chemokine secretion from macrophages (291), and can induce cellular apoptosis (305). Inhibition of TNFα during *M. tuberculosis* infection leads to unstructured granulomas and increased bacterial burden (158, 165, 374). Similarly, IFNγ is also responsible for macrophage activation during infection (59, 60). A balance of pro- and anti- inflammatory

cytokines is required for establishing granulomas that successfully control *M. tuberculosis* infection (41, 46, 158, 164).

Anti-inflammatory cytokines including TGF-β1 and IL10 have come under increasing scrutiny for their association with severe TB (85, 158, 163, 173, 174). TGF-β1 is highly conserved across taxa (375) and can influence many cell types (108, 111, 113, 249) by signaling through the TGFβR1/TGFβR2 receptor complex (93). TGF-β1 has a variety of inhibitory effects including the ability to downregulate macrophage activation and effector function (129, 135, 138, 376, 377), decreasing cytokine secretion by macrophages and cytotoxic T cells (110, 378), and decreasing proliferation of T cells (134). Moreover, TGF-β1 inhibits effector functions in antigen-stimulated cytotoxic T cells in tumors, (125, 379) and TGF-β1-expressing regulatory T cells (Tregs) suppress cytotoxic T cell function (380). TGF-β1 may also exacerbate TB by downregulating *M. tuberculosis*-specific pro-inflammatory cytokine secretion and proliferation by T cells (110, 134, 381). Systemically, *M. tuberculosis* infection upregulates TGF-β1 expression, and peripheral blood monocytes from TB patients display elevated TGF-β1 secretion (90, 132, 382). Granulomas from non-human primates (NHPs) show high levels of TGF-β1 (49). *In vitro* studies have demonstrated that TGF-β1 promotes mycobacterial growth within mononuclear cells, and addition of exogenous TGF-β1 leads to increased *M. tuberculosis* replication (131, 133). Inhibiting TGF-β1 restricts bacterial growth (131, 133). Despite evidence of the effects of TGF-β1, the role of TGF-β1in the granuloma is still unknown.

IL-10 is another anti-inflammatory cytokine expressed by T cells and macrophages in granulomas. It signals through its receptor, IL-10R (175), and can inhibit macrophage antimicrobial activities that are critical for protection against TB (173, 179). These actions play an important role in early granuloma formation and macrophage regulation (157, 164). *In silico*

deletiion of IL-10 between the time of infection and 45 days post-infection increases granuloma sterilization and this effect is attributable to modest increases in macrophage activation (157). However, the benefit of IL-10 deletion decreases at later time points and there is an increase in potentially pathologic inflammation (157). Moreover, virulent *M. tuberculosis* strains are associated with upregulated IL-10 expression, suggesting the effects of IL-10 may have survival benefits for *M. tuberculosis* (41, 383, 384). The trade off between the cause and effect of IL10 and TGF-β1 remains unclear.

The effects of TGF-β1 on overall granuloma development and function, as well as the interplay between IL10 and TGF-β1 in regulating inflammation in granulomas remain unknown (54, 158). Both cytokines are elevated in the bronchoalveolar lavage fluid in patients with pulmonary TB when compared to patients with other lung diseases and healthy patients (85). These findings, and others (69, 85, 90, 120, 131-133, 382, 385-387), emphasize the importance of TGF-β1 and IL10 in pulmonary TB, but their interaction and regulation remain uncharacterized (46). Previous work indicates TGF-β1 and IL10 may differentially regulate lymphoid- and myeloid-derived cells. For example, TGF-β1 regulates lymphoid-derived NK cell involvement in T helper type 1 cell development and NK cell maturation (388), but not myeloid-derived dendritic cell involvement in T helper type 1 cell development (136). In contrast, IL-10 is a major regulator for myeloid-derived cells including dendritic cells and monocytes (177, 178). This dichotomous regulation has not been examined in TB, and could significantly impact development of new vaccines and therapeutics.

With this study, we identify TGF-β1 as an important regulatory factor impacting mycobacterial control in granulomas with effects that are distinct from those of IL10. NHPs and rabbits are the best animal models for TB with human-like granulomas, but these animals have

practical limitations making their study challenging (57). We take a systems biology approach pairing *GranSim* (157, 159, 164, 192, 193, 219, 220, 389), an *in silico* hybrid multi-scale agent-based model that captures tissue, cellular, and molecular scale interactions of cells and cytokines in granulomas, with experimental data from NHPs with TB. This unique combination of computational and experimental methods represents a novel approach to investigating questions that cannot be addressed by traditional experimental systems. We find that TGF-β1 primarily regulates the effector function of cytotoxic T cells, and not macrophages, in granulomas. Deletion of TGF-β1 leads to improved bacterial clearance and lesion sterilization. The role of TGF-β1 in granulomas differs from that of IL10, highlighting a novel differential regulation of cytotoxic T cells and macrophages. Understanding regulatory roles of cytokines can further our ability to predict therapeutic targets.

4.2 Results

4.2.1 Deleting anti-inflammatory mediators decreases colony-forming units (CFU) and improves granuloma sterilization.

We simulated a set of 1337 granulomas using our *baseline parameters* (see Methods and Table S1) to serve as our *wild-type (WT) containment set* of granulomas. For direct comparison, we simulated the same 1337 granulomas three additional times in the absence of IL10, TGF-β1, or both IL10 and TGF-β1 to create virtual *IL10 knockout (KO)*, *TGF-β1 KO*, and *double KO* sets, respectively. Simulation results show that removal of the anti-inflammatory cytokines decreases CFU per granuloma over time (Figure. 4.1A) with greatest decreases in the double KO set compared to WT followed by TGF-β1 KO and IL10 KO sets, respectively. The effects of cytokine removal are visible in the double KO set as early as day 20 post infection (PI), and

remain present in all simulation sets from day 30 through day 200 PI. Lesion sterilization increased in the absence of one or both anti-inflammatory cytokines (Figure. 4.1B). Consistent with previously published computational studies (157), we observed that 60% of the lesions in IL10 KO sets experienced sterilizing immunity, while TGF-β1 KO resulted in 85% of lesions becoming sterile and knocking out both IL10 and TGF-β1 led to 98% of lesions being sterilized (Figure. 4.1B). These simulation results suggest that TGF-β1 plays a stronger role in inhibiting bacterial clearance than IL10.

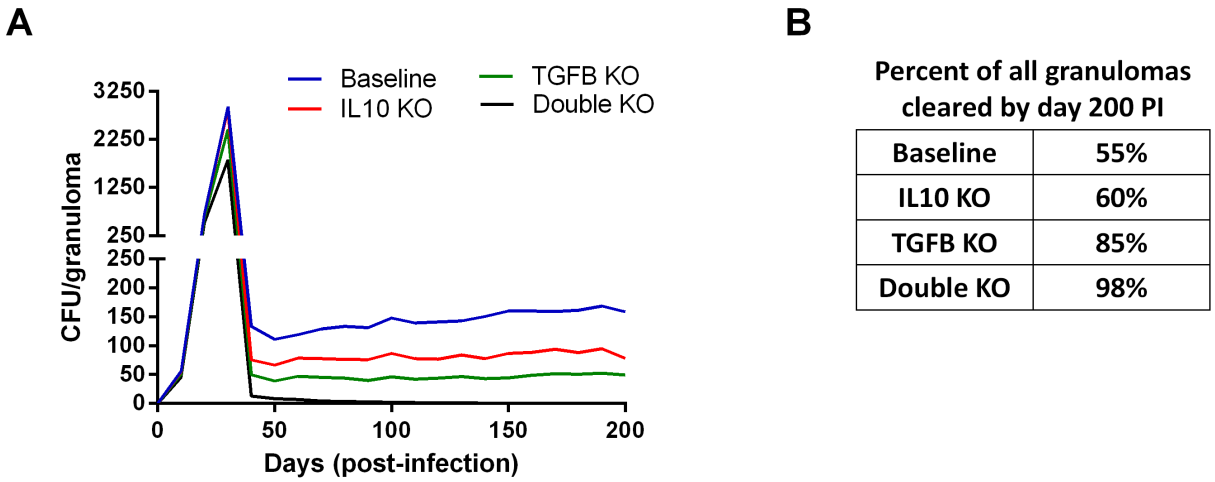

Figure 4.1: Comparison of CFU from simulated granulomas between wild type, IL10 knockout (KO), TGF-β1 KO, and TGF-β1/IL10 double KO days 50 to 200 post-infection. A) Each line represents the mean CFU of all1337 simulated granulomas. B) Table indicates percentage of simulated granulomas when CFU = 0 at day 200 PI under the aforementioned conditions.

4.2.2 Cytotoxic T cells are responsible for decreased bacterial load in TGF-β1 knockout granulomas.

We performed a sensitivity analysis on our simulations (see Methods) and identified that TGF-β1 has a strong influence on cytotoxic T cell effector function (Table A.2-A.3). Using the model, we have the ability to dissect individual activities of cells. Thus, we compared the number of bacteria killed by cytotoxic T-cell activity in our knockout containment sets by day

200 post infection (PI) (Figure. 4.2A). Granulomas without TGF-β1 killed significantly more bacteria by cytotoxic T-cell activity than any other KO set (Figure. 4.2A). The double KO set shows significantly better bacterial killing by cytotoxic T cells than the baseline set, while the IL10 KO sets kill significantly fewer bacteria by cytotoxic T cells (Figure. 4.2A). We also compare sets for the total percent of bacteria killed per granuloma due to activity attributable to cytotoxic T-cells by day 200 PI (Figure. 4.2B). The percent in the TGF-β1 KO and double KO sets was significantly greater than in the baseline set. There was no significant difference between the TGF-β1 KO and double KO sets. The IL10 KO showed no significant increase in percent bacterial killing by cytotoxic T-cell activity compared to baseline granulomas. These data indicate that in the absence of TGF-β1, cytotoxic T cells kill more bacteria than they do in the presence of TGF-β1.

To confirm that this result could not be attributed to macrophage-directed behaviors, we also examined the percent of bacteria killed by macrophage activity and did not find significant differences between the knockout containment sets (Figure. 4.2C). When we compared bacteria killed by Fas/Fas-ligand activity we found significant reductions in the TGF-β1 KO and double KO sets compared to baseline granulomas (Figure. 4.2D). This decrease is attributable to lower numbers of infected macrophages over the 200 days PI in the TGF-β1 KO and double KO scenarios (Figure. A.1). In addition to killing by macrophages, cytotoxic T cells, and Fas/Fas-ligand interactions, bacteria can also be killed by starvation in the caseum of the granuloma (193). Together these four actions account for all bacterial killing in *GranSim* (Figure. 4.2E) but we found the effect of TGF-β1 on bacterial killing is primarily due to the effects of TGF-β1 on cytotoxic T cells (Figure. 4.2). In the absence of cytotoxic T cells we see increased bacterial killing by Fas/Fas-ligand activity that is more similar to what we see in baseline granulomas

(Figure. 4.2F). In the absence of both TGF-β1 and cytotoxic T cells we also observed slight increases in bacterial killing by macrophages reflecting the baseline scenario (Figure. 4.2F).

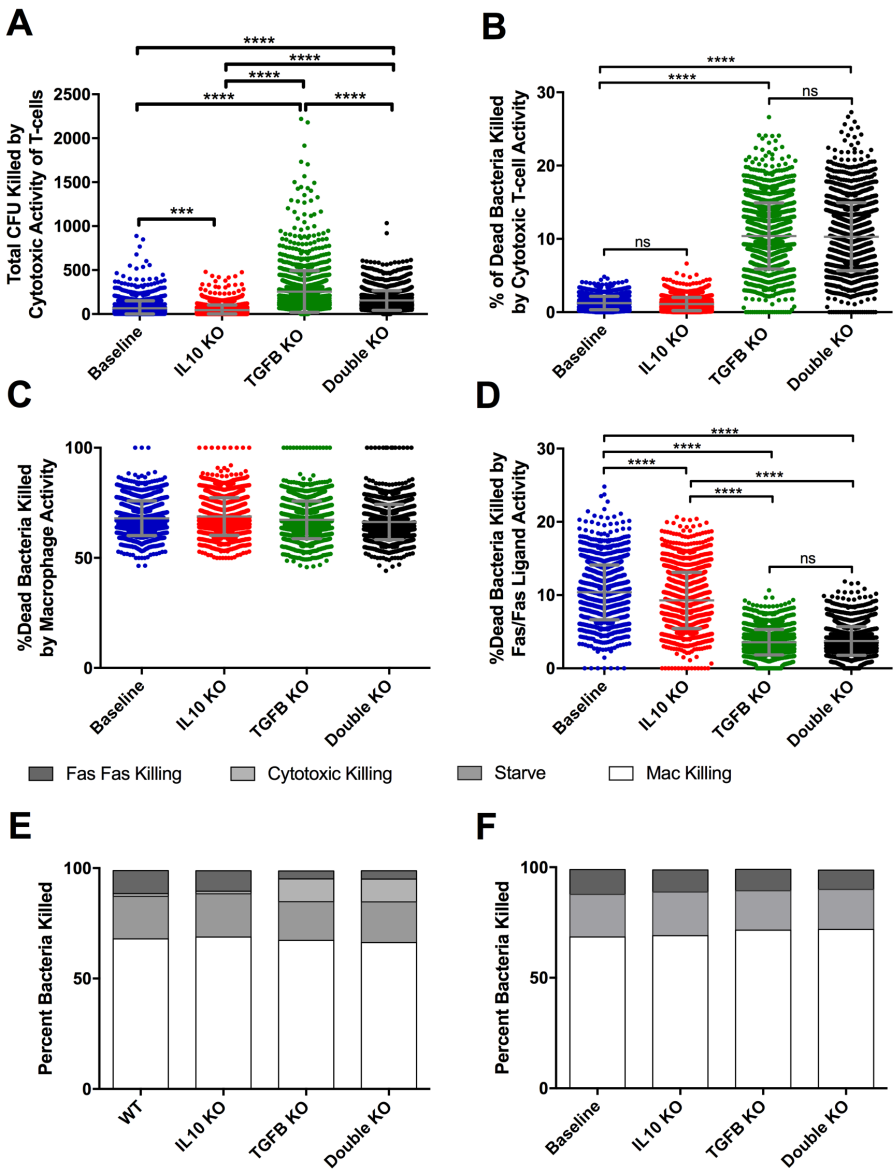

Figure 4.2: Comparison of cumulative bacterial killing by cytotoxic T-cells and macrophages between *simulated* wild type, IL-10 knockout (KO), TGF-β1 knockout, and TGF-β1/IL-10 double knockout granulomas over 200 days post-infection. A) CFU per granuloma killed by cytotoxic T-cells in 1337 simulated granulomas. B) Percent of dead bacteria in simulated granulomas killed by cytotoxic T-cells. C) Percent of dead bacteria killed by macrophages in simulated granulomas. D) Percent of dead bacteria killed by Fas/Fas-ligand in simulated granulomas. E) Percent of bacterial killing caused by Fas/Fas-ligand signaling, cytotoxic effector functions, starvation, and macrophages in the four cytokine-knockout (KO) sets. F) Percent of bacterial killing caused by Fas/Fas-ligand signaling, cytotoxic effector functions, starvation, and macrophages in the four cytokine KO sets with the additional KO of cytotoxic T-cells. **** = p<0.0001, *** = p<0.001, ** = p<0.01, * = p<0.05, ns = p >0.05

The increased bactericidal activity by cytotoxic T cells seen in the absence of TGF-β1 (Figure. 4.2A) could be due to an increased number of cytotoxic T cells or to increased cytotoxic T cell effector functions. As shown in Figure 4.3A, at day 40 PI we see fewer total cytotoxic T cells (both effector and those primed but not effector) in TGF-β1 KO and double KO granulomas than baseline and IL10 KO granulomas (Figure. 4.3A). Of the total cytotoxic T cells, approximately 6% of those in the baseline and IL10 KO cases are effector, and approximately 98% of those in the TGF-β1 KO and double KO cases are effector (Figure. 4.3A). The same trend occurs at day 200 PI with a mean of approximately 10% effector cytotoxic T cells in the baseline and IL10 KO cases and a mean of approximately 98% effector cells in the TGF-β1 KO and double KO cases (Figure. 4.3A). These results suggest that increased bacterial killing by cytotoxic T cells in the absence of TGF-β1 is due to increased cytotoxic T cell effector functions, and not an increase in number of cytotoxic T cells in the granuloma. These results cannot be attributed to an overall increase in inflammation. We observed no increase in numbers of activated macrophages (Figure. 4.3B) or total TNFα (Figure. 4.3C) in the absence of TGF-β1 that would indicate increased levels of inflammation.

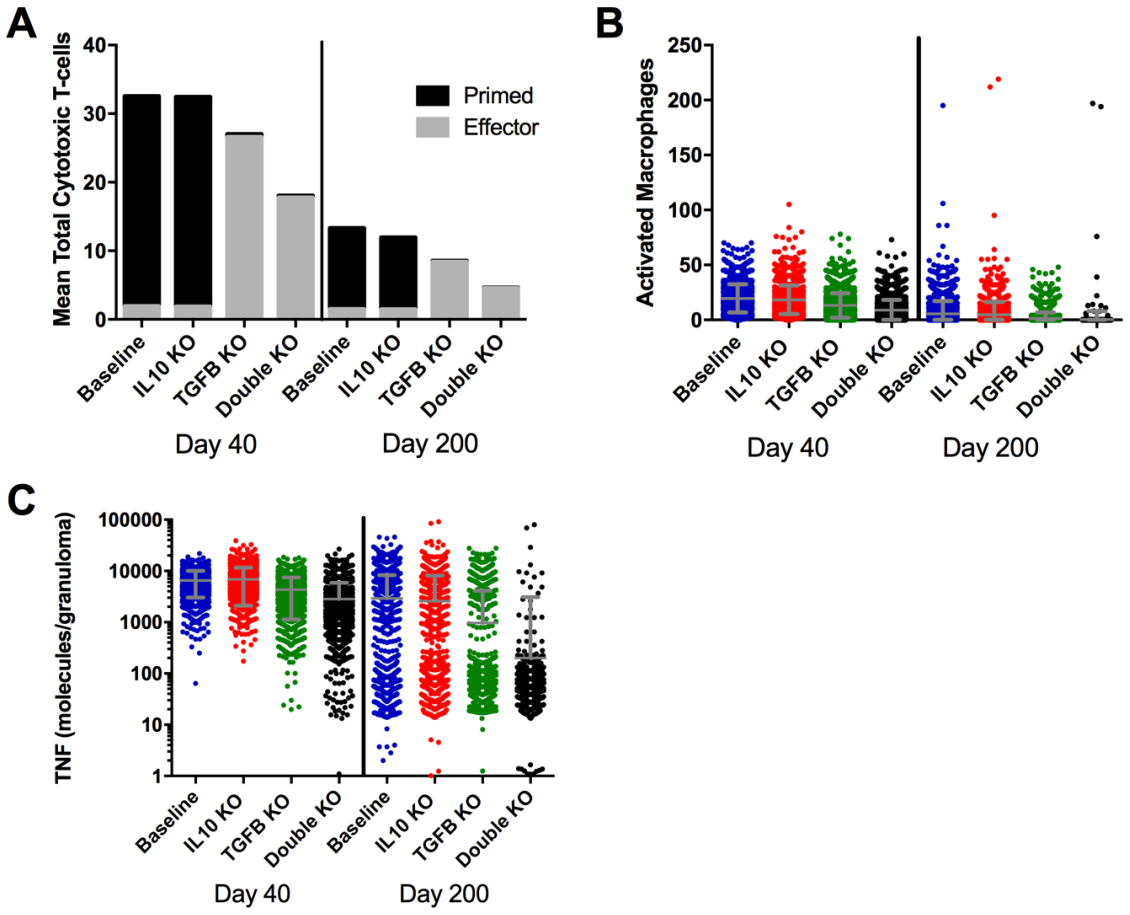

Figure 4.3: Comparison at two time-points post-infection between effector and non-effector cytotoxic T-cells, activated macrophages, and total TNFα in wild type, IL10 knockout (KO), TGF-β1 knockout, and TGF-β1/IL10 double knockout *simulated* granulomas. A) Black fill indicates mean cytotoxic T-cells in 1337 simulated granulomas. Grey fill indicates mean effector cytotoxic T-cells in 1337 simulated granulomas. B) Total number of activated macrophages per granuloma. C) Total number of TNFα molecules per granuloma.

4.2.3 Macrophages and cytotoxic T cells differentially express anti-inflammatory cytokine receptors.

We next sought to determine if TGF-β1 regulation of cytotoxic T cells as observed in simulations is consistent with cells from the NHP granuloma and to compare TGF-β1 and IL10 receptor expression between macrophages and cytotoxic T cells (Figure. 4.4). Flow cytometry shows increased expression of IL10 receptors on macrophages compared to granzyme B positive (cytotoxic) and negative (not cytotoxic) T cells. Expression of TGF-β1 receptor on the surface of

granzyme B positive T cells is increased compared to granzyme B negative T cells and macrophages (Figure. 4.4A). Due to small sample size these trends are not statistically significant but support other data (137, 388) suggesting that there is differential regulation of TGF-β1 and IL10, and strengthen our prediction that TGF-β1 and IL10 differentially regulate T cells and macrophages in granulomas. We also examined localization of IL10R and TGFβR1 in serial sections of a formalin-fixed paraffin-embedded NHP granuloma (Figure. 4.4B). We found IL10R localization corresponded with macrophage-rich regions of the granuloma and the TGFβR2 corresponded with lymphocyte-rich and neutrophil-rich regions (Figure. 4.4B).

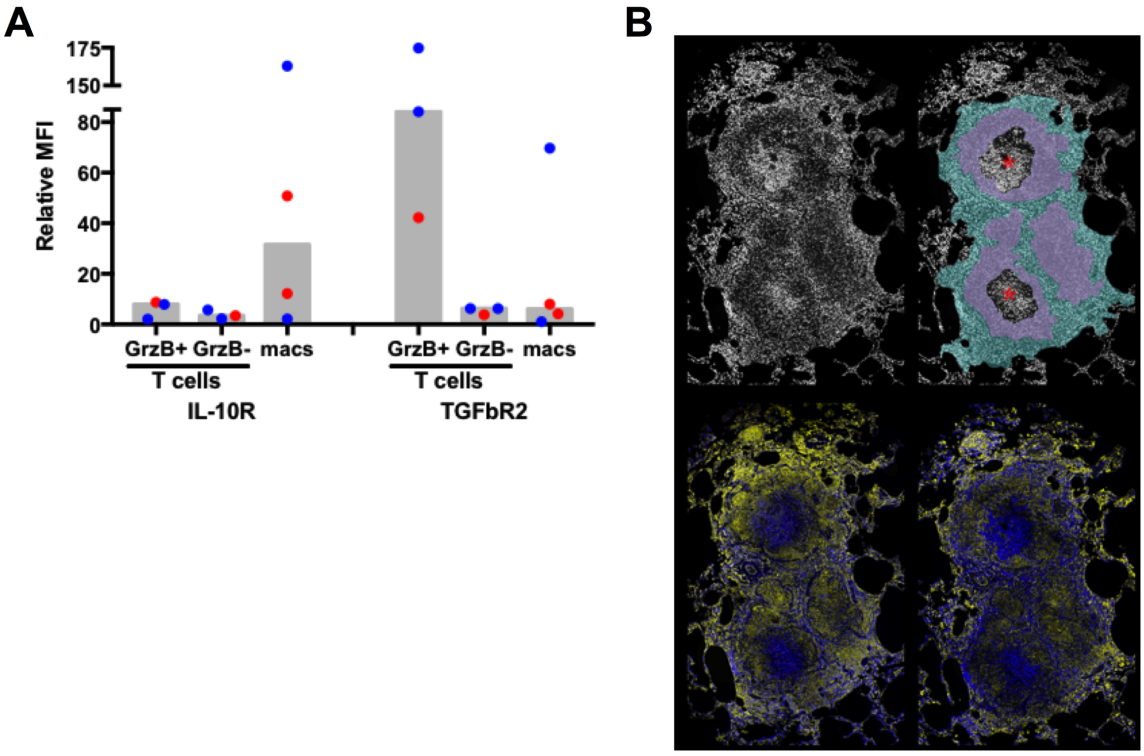

Figure 4.4: Flow cytometry and immunohistochemistry examining expression of TGF-β1 and IL10 receptor for macrophages, granzyme B (GrzB) positive (cytotoxic) T cells, and GrzB- (not cytotoxic) T cells. Dots indicate an individual granuloma. Blue dots come from a single NHP, red dots come from another NHP.A) Flow cytometry was performed comparing the expression of IL10 and TGF-β1 receptor on three cell types. B) Top left: Serial sections of a NHP granuloma. Top right: colored for lymphocyte-rich regions in cyan, epithelioid macrophage regions in magenta and neutrophil-rich caseous regions are indicated with asterisks. Bottom left: Stained for IL-10R (yellow) and DAPI (Blue). Bottom right: stained for TGF-βR1 (yellow) and DAPI (blue).

4.2.4 Virtual depletion of TGF-β1 at day 200 post-infection decreases CFU and increases bacterial clearance.

In the simulations examined above, we focused on the early period of granuloma formation and function (0-200 days PI). In order to determine if TGF-β1 regulates fully formed granulomas, we simulated the granulomas from our baseline containment set for 400 days (Figure. 4.5A), and then simulated the same 1337 granulomas depleting IL10, TGF-β1, or both IL10 and TGF-β1 at day 200 PI. These simulations make up a new group of containment sets: IL10 depletion, TGF-β1 depletion, and double depletion sets. We observed that depleting IL10, TGF-β1, and both IL10 and TGF-β1 decreases the mean CFU per granuloma (Figure. 4.5A). In addition to decreased mean CFU per granuloma we observe an increased percent of granulomas that are cleared between day 200 and day 400 PI. Simulations predicted that 70% of granulomas in our baseline containment set, and 71% in IL10 depletion set would have sterilizing immunity by 400 days PI (Figure. 4.5B). These results indicate that IL10 is not playing an important role in bacterial clearance late in infection. Removing IL10 from a fully formed contained granuloma will not increase the likelihood of bacterial clearance (157). We also predict that 88% of granulomas would clear bacteria by day 400 PI after TGF-β1 depletion (Figure. 4.5B). This result suggests that removing TGF-β1 improves bacterial clearance in fully formed granulomas as effectively as knocking out TGF-β1 at the time of infection (Figure. 4.1B). There was no significant difference in the effect on bacterial clearance between TGF-β1 depleted and double depleted granulomas, further demonstrating that IL10 is not playing an important role in bacterial clearance between day 200 and day 400 PI (Figure. 4.5B).

Taken together, these results suggest that depletion of TGF-β1 in contained granulomas decreases CFU per granuloma and increases lesion sterilization. To determine if these results are consistent in disseminating granulomas, we simulated a 1500 granuloma baseline *dissemination set*. We also simulated the same 1500 granulomas with IL10, TGF-β1, or both IL-10 and TGF-β1 depleted at 200 days PI. The mean CFU per granuloma of the baseline dissemination set increases continuously from day 50 PI (Figure. 4.5C). Anti-inflammatory cytokine depletion decreases the mean CFU per granuloma (Figure. 4.5C). The TGF-β1 and IL10/TGF-β1 depletions show the greatest decrease in CFU compared to baseline dissemination set (Figure. 4.5C). In both cases, the mean CFU per granuloma stabilizes indicating that these granulomas are no longer disseminating. The IL10 depletion has a decreased mean CFU per granuloma relative to baseline, but continues to increase over time (Figure. 4.5C). We also looked at the ability of disseminating granulomas to achieve sterilization under these conditions and found at 400 days PI the baseline dissemination granulomas become sterile 3% of the time, IL10 depletion leads to sterilization in 5% of granulomas, and the TGF-β1 depletion leads to sterilizing immunity in 29% of granulomas, while the double depletion leads to sterilization in 24% of granulomas (Figure. 4.5D). These results corroborate results seen in the simulated knockout containment granulomas (Figure. 4.1) and further emphasize that TGF-β1 signaling inhibits granuloma sterilization.

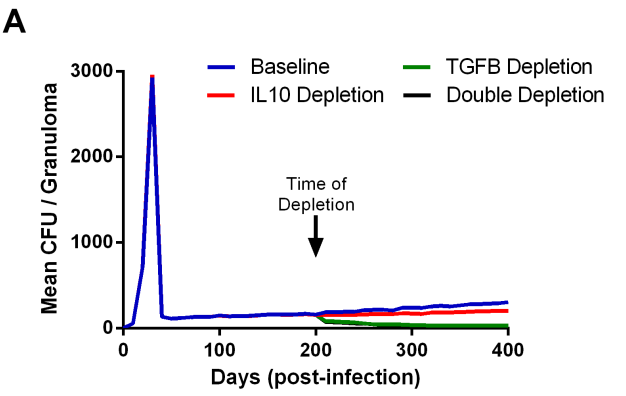

B

Percent of all granulomas cleared by day 400 PI

Baseline	70%
IL10 Depletion	71%
TGFB Depletion	88%
Double Depletion	90%

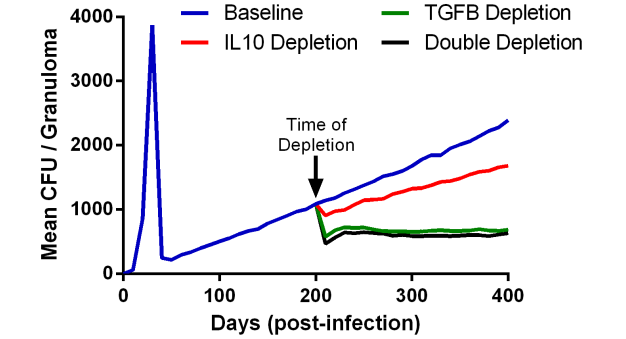

D

Percent of all granulomas cleared by day 400 PI

Baseline	3%
IL10 Depletion	5%
TGFB Depletion	29%
Double Depletion	24%

Figure 4.5: Mean CFU for cytokine depleted *simulated* granulomas at day 200 post-infection. A) Mean CFU of 1337 simulated granulomas from a containment scenario over time. B) Table indicates percentage of simulated granulomas in panel A with CFU = 0 at day 400 PI. C) Mean CFU of 1337 simulated granulomas from a disseminating scenario over time with cytokine depletions at day 200. D) Table indicates percentage of simulated granulomas in panel C with CFU = 0 at day 400 PI.

4.3 Discussion

Vast numbers of people remain infected with *M. tuberculosis* despite efforts to improve diagnosis and treatment of TB. With increases in antibiotic resistance rates, and no broadly effective vaccine, novel therapeutic approaches are desperately needed to curb this pandemic. Many of the challenges in TB treatment stem from factors associated with the complex environment of granulomas where immune mechanisms may work against the host and favor the bacterium. It is becoming increasingly clear that a balance of pro- and anti-inflammatory

mechanisms are required for protection, and this may present opportunities for host-directed therapies for TB (295). While this strategy of manipulating the granuloma environment could improve bacterial clearance, too much of a change, changing the wrong factor, or a poorly timed perturbation in either a pro- or anti-inflammatory direction could be detrimental to the host.

Combining *GranSim*-based *in silico* analyses with experimental macaque-based studies enabled us to identify previously unknown relationships between regulatory mechanisms contributing to granuloma formation and infection outcomes in TB. This exclusive platform allows us to evaluate regulation in granulomas at multiple biological scales simultaneously over time. Because of the expedited rate of computational studies, we can simulate thousands of independent and stochastic granulomas and examine them in ways that cannot be accomplished *in vivo*. In this study, we identified TGF-β1-regulated mechanisms of granuloma formation, function, and bacterial control, including a key role for TGF-β1 regulated cytotoxic T-cell responses that led to suppression of effector functions in cytotoxic T cells during infection. Our data suggest that depleting TGF-β1 in TB can increase the effector functions of cytotoxic T cells without increasing their numbers and improve bacterial clearance without increasing inflammation. Thus, therapeutic inhibition of TGF-β1 signaling may improve lesion sterilization in TB and represent a new strategy that can be exploited to improve host responses against *M. tuberculosis*. Pirfenidone, a drug that inhibits TGF-β1 signaling, has recently been approved for treating pulmonary fibrosis (33) and our results suggest this compound may have potential to promote bacterial clearance during TB treatment. Inhibiting TGF-β1 presents clinical challenges because of its pleotropic physiologic importance, but our study highlights the importance of cytotoxic T cell effector function in bacterial clearance and suggests stimulating cytotoxic T cells may also have therapeutic value in treating TB.

We also examined whether IL10 and TGF-β1 represent redundant regulatory mechanisms at the site of infection and found that these cytokines differentially regulate TB granuloma macrophage and T cell responses. Inhibitory effects of IL-10 on macrophages have been characterized previously by our group (157, 164) and others (390). Identification of cytotoxic T-cell regulation by TGF-β1 in this context is novel, but it has been suggested by other works that TGF-β1 predominantly regulates lymphoid-derived cells while IL-10 predominantly regulates myeloid-derived cells (388, 391). The dichotomous regulation of myeloid and lymphoid cells by anti-inflammatory cytokines could help us better understand mycobacterial persistence in TB, and has implications that span the spectrum of infectious diseases and immunological disorders. Removing TGF-β1 *in silico* improves bacterial clearance in the granuloma by enabling cytotoxic T cell effector functions without increasing potentially pathologic inflammatory responses. TGF-β1 regulation of cytotoxic T cells differs from IL10, which has been shown to regulate macrophage activation. Identifying specific mechanisms of cytokine regulation in granulomas affords better identification of therapeutic targets for TB.

4.4 Materials and Methods:

4.4.1 Study Design

The goal of our study was to assess the role of TGF-β1 in the formation and function of a *Mycobacterium tuberculosis (Mtb)* induced granuloma. We used *GranSim*, a well-validated agent-based model of granuloma formation and function in the lung, along with *ex vivo* studies from NHPs to identify the primary role of TGF-β1 in pulmonary TB infection. We simulated a total of 16,500 granulomas: 1337 granulomas for each of the following categories: baseline containment, IL10 KO containment, TGF-β1 KO containment, IL10/TGF-β1 double KO

containment, IL10 depletion containment, TGF-β1 depletion containment, IL10/TGF-β1 depletion containment. We simulated 1500 granulomas for each of the following categories: baseline dissemination, IL10 depletion dissemination, TGF-β1 depletion dissemination, and IL10/TGF-β1 double depletion dissemination. We used multiple granulomas from two cynomolgus macaques infected with *M. tuberculosis*.

4.4.2 Non-human Primate Immunohistochemistry and flow cytometry Studies

All samples from cynomolgus macaques (*Macaca fascicularis*) originated from animals in ongoing or completed studies, and procedures and husbandry practices were included in protocols approved by the University of Pittsburgh's Institutional Animal Use and Care Committee. Flow cytometry was performed on granulomas excised from macaque lung tissue at necropsy as previously described (163). Single suspensions were prepared with either a Medimachine and Medicon system (BD Biosciences, San Jose, CA) or enzymatically with a GentleMACS tissue dissociator (Miltenyi Biotec, San Diego, CA) using the human tumor dissociation kit (Miltenyi) with the tubes heated at 37°C for 37 minutes. Cells were stained for CD3 (clone SP34-2; BD Bioscience), CD11c (clone S-HCL-3; BD Bioscience), CD163 (clone GHI/61; BD Bioscience), TGFβR2 (goat polyclonal; R&D Systems, Minneapolis, MN) and IL-10R (clone 3F9; Biolegend, San Diego, CA) under BSL3 conditions, fixed and stained for granzyme B (clone GB11, BD Biosciences) intracellularly using the Fix-Perm reagents (BD Bioscience). Erythrocyte-free whole blood was prepared with PharmLyse RBC lysing buffer (BD Bioscience) and similarly stained as gating controls. Cells were acquired on a LSRFortessa flow cytometer (BD Bioscience) and data were analyzed with FlowJo (TreeStar Inc, Ashland, OR). Cells were gated as indicated in Supplemental Figure A.2 and to be considered for analysis,

granulomas needed to have at least 100 CD3+CD11c- (T cells) or CD11c+CD163- (epithelioid macrophages (295)) events. For analysis of cell surface receptor abundance, a "relative MFI" was calculated by dividing the mean fluorescence intensity (MFI) of the positive population by on the negative population's MFI to account for the differences in each cell population's autofluorescence.

Immunohistochemistry and confocal microscopy was performed on formalin-fixed paraffin-embedded granulomas as previously described (295) Serial 5 mm sections were stained with rabbit anti-human TGF-βR1 (Cell Signaling Technologies, Danvers, MA) or IL-10R (Millepore, Billerica, MA), labeled with AlexaFluor546-conjugated donkey anti-rabbit secondary antibodies (ThermoFisher Scientific, Waltham, MA), and coverslips were mounted with DAPI-containing Prolong Gold Mounting medium (Thermo Fisher). Individual overlapping microscopic fields were assembled into full-granuloma composites with Photoshop CS6 (Adobe, San Jose, CA). For representation in the Figure 4.4, epithelioid macrophage-rich regions were identified by their morphologic characteristics (high cytoplasm:nucleus ratio, large lightly-staining nuclei) and position adjacent to caseum (295)).

4.4.3 *In silico* Studies

4.4.3.1 Agent-Based Model

The simulation studies in this paper are performed using *GranSim*, a 2D hybrid agent-based model of *M. tuberculosis* granuloma formation and function in the lung (157, 159, 162, 164, 201, 220, 227, 228). *GranSim* captures molecular, cellular, and tissue scale dynamics of granuloma formation. This version of the model accounts for chemical diffusion of chemokines and cytokines at the molecular scale (218). At the cellular scale, *GranSim* accounts for individual

cells including four states of macrophages (resting, activated, infected, and chronically infected) and three distinct types of T-cells (cytotoxic, regulatory, and IFNγ producing T-cells). Interactions between cells are also captured at this scale. At the tissue scale, *GranSim* accounts for chemokine-directed cellular movement. Granuloma formation is an emergent behavior of the model. A complete list of model rules can be found at *http://malthus.micro.med.umich.edu/GranSim*. *GranSim* provides us with a large amount of information about TB granulomas. Much of this information is currently impossible to collect *in vivo*. At the molecular scale, *GranSim* provides chemokine and cytokine concentration gradients over the entire simulation space for every time point. At the cellular scale *GranSim* tracks macrophages and T cells along with their respective states and interactions. This information can be quantitative, expressed in numbers and concentrations over time, or it can be qualitative in the form of spatial snapshots that provide a spatial-temporal perspective. These snapshots can be linked to stream a time-lapse movie (*http://malthus.micro.med.umich.edu/lab/movies/TGFB_GranSim/*). A full list of parameters for the model is included in the supplementary material (Table A.1). Prior versions of *GranSim* include rules describing the actions of TNFα, IFNγ, and IL10 on macrophages and T-cells (157, 159, 164, 165, 227-229). In this version of the model, we introduce rules governing the actions of TGF-β1 (Figure. 4.6).

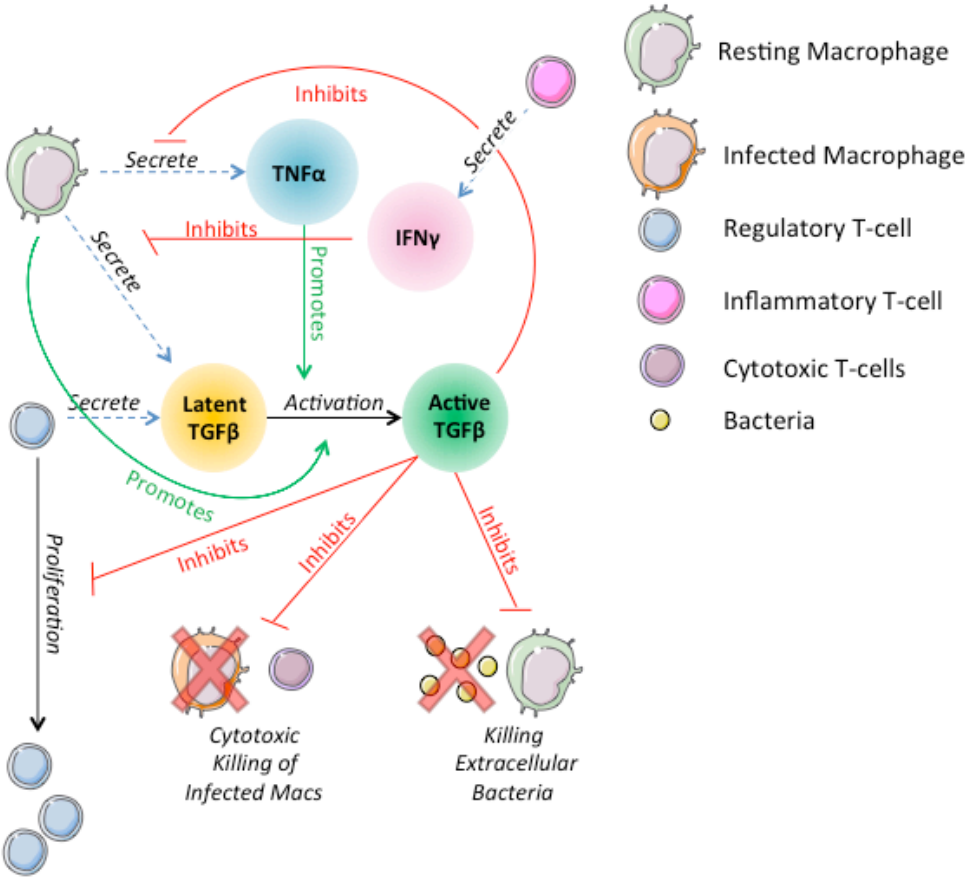

Figure 4.6: Schematic representation of physiological interactions of TGF-β1 in the hybrid multi-scale computational lung model, *GranSim*. TGF-β1 is secreted in latent form by macrophages and regulatory T-cells. Latent TGF-β1 is activated in the presence of macrophages. TNFα promotes activation of latent TGF-β1. Active TGF-β1 inhibits T-cell proliferation, cytotoxic killing of infected macrophages by cytotoxic T-cells, killing of extracellular bacteria by macrophages, and macrophage secretion of TNFα. IFNγ signaling by inflammatory T-cells inhibits macrophage secretion of TGF-β1. These interactions are included as part of the larger ABM *GranSim*. Full rules for *GranSim* are found at http://malthus.micro.med.umich.edu/GranSim.

In the model, TGF-β1 is secreted in latent form by macrophages and regulatory T-cells. Secretion of TGF-β1 occurs on the molecular time-step (Table A.1). Latent TGF-β1 activation is coarse-grained in our model: we consider compartments that contain a macrophage to have MMP9 (392, 393) (394), which activates latent TGF-β1 in that compartment (*Amount TGFβ1 activated*) (Table A.1). The activation of latent TGF-β1 is described by:

(EQN 1)

$$Amount\ TGF\beta1\ activated = \left(Activation_{fraction} + \left(\left(1 - Activation_{fraction}\right) * TNF\alpha_{signaling}\right)\right) * [TGF\beta1]$$

The fraction of TGF-β1 that is activated is a function of TNFα concentration in the compartment where $Activation_{fraction}$ is the fraction of TGF-β1 activated by the macrophage and $\left(\left(1 - Activation_{fraction}\right) * TNF\alpha_{signaling}\right)$ is the additional amount activated in response to TNFα.

T-cell proliferation is inhibited by bound active TGF-β1 ($BoundTGF\beta1$). The probability of proliferation is described by the following equation:

(EQN 2)

$$Probability\ of\ Tcell\ proliferation = \frac{(TGF\beta1max_{Tcell} - BoundTGF\beta1)}{TGF\beta1max_{Tcell}}$$

Where $TGF\beta1max_{Tcell}$ is the amount of bound active TGF-β1 ($BoundTGF\beta1$) that completely inhibits proliferation.

Active TGF-β1 deregulates cytotoxic T cells, inhibiting their ability to kill infected macrophages. The probability of a macrophage killing of extracellular bacteria is reduced up to 50% by active TGF-β1:

(EQN 3)

$$Probability\ macrophage\ kills\ bacteria = MacKill_{baseline} * \frac{(TGF\beta1max_{Mac} - (0.5 * BoundTGF\beta1))}{TGF\beta1max_{Mac}}$$

Where $MacKill_{baseline}$ is the baseline probability a macrophage will kill extracellular bacteria and $TGF\beta1max_{Mac}$ is the amount of bound active TGF-β1 ($BoundTGF\beta1$) that fully inhibits bacterial killing.

Macrophage secretion of TNFα is reduced up to 50% by active TGF-β1:

(EQN 4)

$$TNF\alpha\ secretion = MacTNF\alpha_{synth} * \frac{(TGF\beta1max_{Mac} - (0.5 * BoundTGF\beta1))}{TGF\beta1max_{Mac}}$$

Where $MacTNF\alpha_{synth}$ is the baseline TNFα synthesis rate and $TGF\beta1max_{Mac}$ is the amount of bound active TGF-β1 ($BoundTGF\beta1$) that fully inhibits synthesis.

IFNγ signaling by inflammatory T cells inhibits macrophage secretion of TGF-β1 by 50% until the macrophage is no longer sensitive to the T-cell signal (Table A.1). These interactions are included as part of the larger ABM *GranSim*. Full rules for *GranSim* are found at http://malthus.micro.med.umich.edu/GranSim.

4.4.3.2 Simulated Granulomas

For this study we calibrate parameters in *GranSim,* including TGF-β1 rules, to a NHP dataset of granulomas (Figure. 4.7) (42, 163, 294). CFU per granuloma is scaled from 2D to 3D for our simulated granuloma for direct comparison with NHP data. Scaling is performed as described in prior work (157). This produces our baseline parameters, which satisfy criteria for containment (193). Because of the stochastic nature of *GranSim*, multiple simulations are required. In NHPs the median number of granulomas per infected individual is 46 (42). It has been shown that each NHP granuloma has a unique trajectory (42). To capture this naturally occurring variation, we vary the baseline parameters by 20% and simulate 500 unique granulomas each in triplicate (to account for stochastic as well as parametric uncertainty) (229).

From these we excluded all disseminating granulomas. The remaining 1337 granulomas make up our baseline containment set. At 200 days PI we see about 50% of granulomas sterilize their bacterial load. This is consistent with previous studies (157). The granulomas that do not sterilize, have a CFU below 2500 at day 200, and have fewer than twice as many CFU at day 200 than they did at day 100 PI. An occasional outlier in this set will progress to dissemination. We repeat this same process for a parameter set representing dissemination to generate a baseline dissemination set of granulomas.

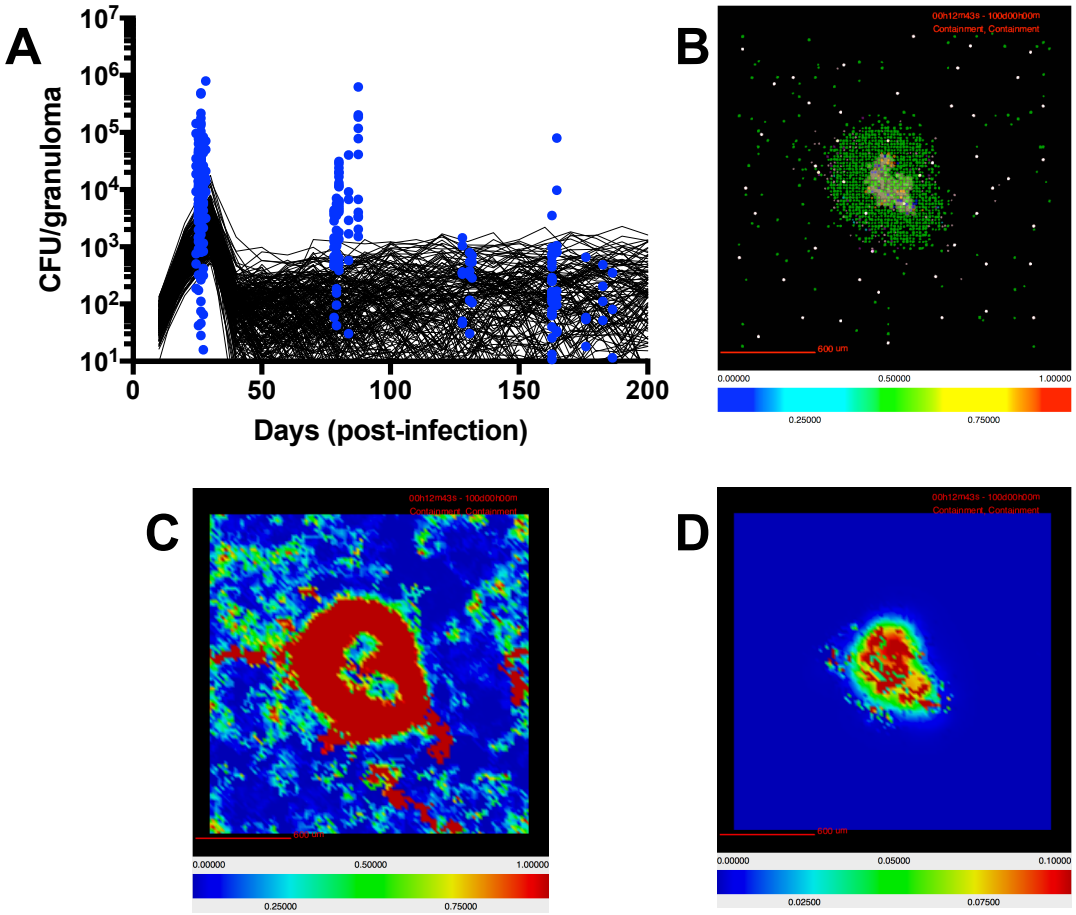

Figure 4.7: Model quantitatively and qualitatively recapitulates non-human primate granuloma dataset. A) CFU per granuloma of simulated granulomas scaled to 3D (see methods) and granulomas extracted from non-human primates at different time points (42, 43, 56, 294). Black lines indicate CFU/granuloma over time for 256 individual representative simulations of 1500 total simulations. Blue dots indicate CFU/granuloma of granulomas extracted from non-human primates at different time points (190). B) Simulated granuloma captures spatial organization of granulomas from non-human primates. Simulated granuloma showing resting macrophages (green), infected macrophages (orange), chronically infected macrophages (red), activated macrophages (blue), Cytotoxic T cells (magenta), IFNγ producing T cells (pink), and regulatory T cells (cyan) at 100 days PI. C) Snapshot of the same simulated granuloma from panel B showing localization of latent TGF-β1. D) Snapshot of the same simulated granuloma from panel B showing localization of active TGF-β1.

4.4.3.3 Virtual Deletion Studies

For our knockout studies we use our baseline containment granuloma set. We re-simulate them in the absence of different cytokines from day 0. We do this by setting the initial values of specified cytokines to be zero as well as preventing any production of these cytokines throughout

the duration of the simulation. These simulations become our virtual IL10 knockout, TGF-β1 knockout, and IL10/TGF-β1 double knockout sets (Figure. 4.1).

4.4.3.4 Virtual Depletion Studies

For our first set of depletion studies we take our virtual baseline containment set and re-simulate each granuloma for 200 days. At day 200 PI we block secretion of a cytokine(s), causing concentrations in a granuloma to (rapidly) approach zero, and continue to simulate for an additional 200 days. These simulations become our IL10 depletion, TGF-β1 depletion, and IL10/TGF-β1 double depletion sets for contained granulomas, respectively (Figure. 4.5A-B). We also preform depletion studies on our virtual knockout dissemination set. We re-simulate the depletion set for 200 days. At day 200 PI we block secretion of different cytokines and continue to simulate for an additional 200 days. These simulations in turn become our IL10 depletion, TGF-β1 depletion, and IL10/TGF-β1 double depletion sets for disseminating granulomas, respectively (Figure. 4.5C-D).

4.4.3.5 Uncertainty and Sensitivity Analysis

Uncertainty analysis allows us to quantify how variation in parameters values drives variation in model output (229). Parameter variation can occur at the molecular and cellular scales and can affect outputs at the molecular, cellular and tissue scales. Often variation in parameter values at one scale can influence model outcomes at another scale a phenomenon referred to as intra-model influence (229). Uncertainty analysis enables us to observe model behavior given a wide value range for each parameter. We vary parameters over two orders of magnitude and compare how these input variations affect model outputs. In this work we use the

Latin hypercube sampling algorithm to sample from the parameter ranges and generate 500 unique parameter sets (229). We describe this analysis as spanning the full parameter space, and simulate each set in triplicate to account for aleatory uncertainty (229). We also preform uncertainty analysis where we vary only certain parameters to see how their influence on model outcomes compares. Sensitivity analyses allow us to identify which parameters have a significant influence on model outcomes and the extent of that influence (229, 344). We use partial rank correlation coefficients (PRCCs) to identify the sensitivity of each output to each parameter (229). PRCC values range from -1 to +1, indicating the non-linear correlation between a parameter and model output. PRCC values are differentiated using Student's T-test of significance. PRCC values are considered significant with a p-value less than 0.01.

4.4.4 Statistical Analysis

Student's T-tests were performed to compare significant difference between means throughout the paper.

Chapter 5

Fibrosis in TB

5.1 Introduction

Granulomas are highly organized immunological structures that form around infectious agents (47, 295, 395). They are the major pathologic feature of pulmonary *Mycobacterium tuberculosis* (Mtb) infection; affecting one in three people worldwide (369). Ten percent of Mtb infections will result in active, contagious tuberculosis disease (TB) (369). There is currently no curative therapy for TB. Antibiotic treatment can induce a state of latency, which is not symptomatic or infectious, but can reactivate if the host immune system becomes weakened (36-38, 46, 57, 225, 285, 288, 292, 396). Patients with latent TB have a one in ten chance of experiencing reactivation in their lifetimes (369), which is even higher if HIV-1 is present [ref]. The dense cellular structure of granulomas can also make therapeutic treatment of Mtb infection difficult by restricting access of drugs to live bacteria (192, 202, 225, 309). Mtb induced granulomas simultaneously isolate the bacteria from the surrounding unaffected tissue and restrict immune clearance of the infection. Understanding the formation and function of Mtb induced granulomas is the key to identifying therapeutic treatments that promote access of drugs and immune cells to persistent bacteria, while maintaining the integrity of surrounding tissue.

Granulomas can be categorized by size, shape, number of colony forming units (CFU), or morphology (40, 45, 56, 69, 219, 295, 397, 398). Granulomas are unique with each having its own trajectory (43), but there are common morphological classifications. These include:

caseous, having a necrotic core of dead tissue surrounded by a cuff of live cells, *dense cellular*, having no distinguishable core but rather cells throughout, *suppurative*, having a large amount of neutrophil infiltration, and *fibrotic*, having a cuff of collagen surrounding the exterior of the granuloma (43, 163) which eventually calcifies, leading to the final stage known as tubercles (Figure 5.1). This last type of granuloma has been poorly studied and the processes of how and when fibrosis occurs, as well as how it is regulated, are not known.

Fibrosis is a dysregulation of the wound healing process and thus fibrotic granulomas are considered to be healing (9, 15, 49, 62, 395, 398, 399). They are typically found during latent TB. Different granuloma classes do not necessarily correlate with a specific host disease state, and can be found simultaneously within a single individual. Because the development of different classes of granuloma cannot be explained on a host level, factors leading to these differences must be the result of environmental differences at the lesion scale. Identifying specific immunological mechanisms that drive the formation of different granulomas is key to understanding granuloma formation and function in a therapeutic context.

Within the classification of fibrotic granulomas exist multiple morphologies that are associated with antibiotic treatment status of the presenting individual (Figure 5.1). Our understanding of fibrotic granuloma morphology is due in large part to work preformed in non-human primates (NHPs) (49). Non-human primates are a good model for studying pulmonary TB because they develop granulomas much like adult humans. NHPs exhibit two primary fibrotic granuloma morphologies (400). The first is peripheral fibrosis found in the form of a fibrotic cuff surrounding the perimeter of lesions (49, 400). This fibrotic cuff is thought to contribute to lesion containment and restrict disease dissemination (49, 400) (Figure 5.1 A, B). The second form of fibrotic lesion has a collagenous structure throughout a lesion, and can be referred to as centrally

fibrotic (49, 400) (Figure 5.1 E). These lesions look more like scars than contained granulomas and are often associated with sterilization of the lesion. Centrally fibrotic lesions occur more frequently following antibiotic treatment than prior to treatment (400). Joanne Flynn's group at the University of Pittsburgh has recently characterized the histology of NHP fibrotic lesions (49) and additional images were provided to us (Figure 5.1).

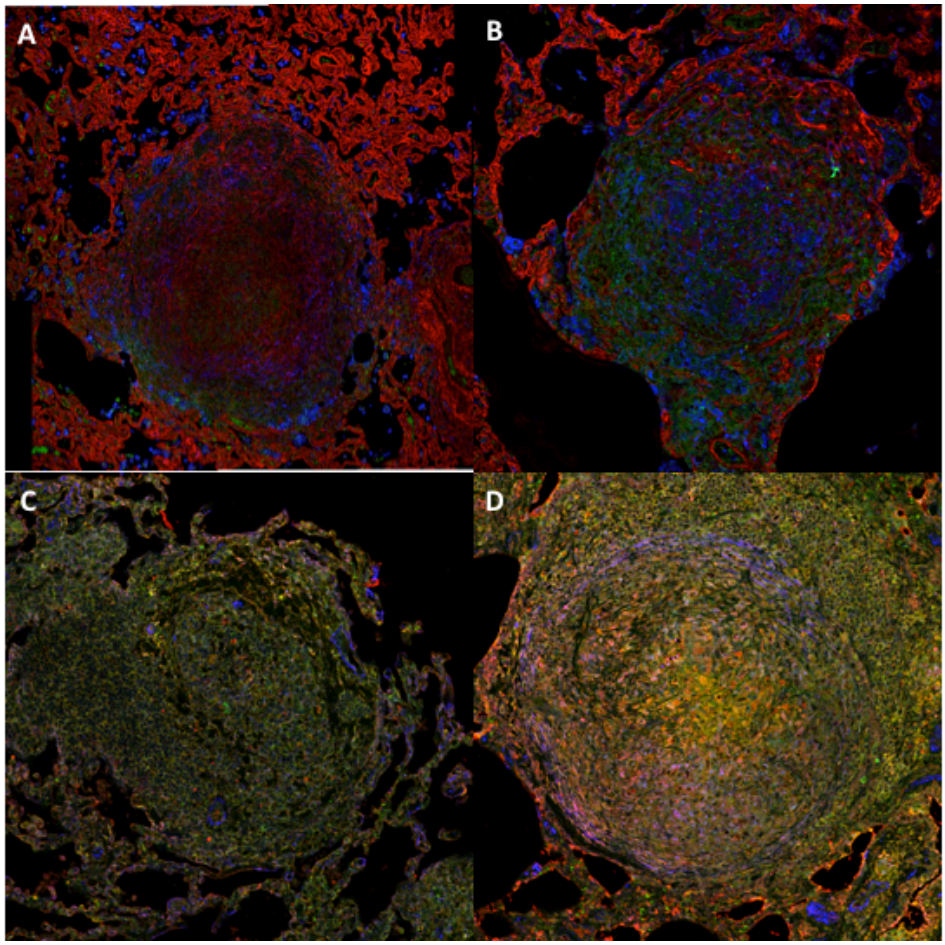

Figure 5.1 Tuberculous granulomas show signs of TGFβ-driven fibrosis. *Top panels* feature granulomas stained for collagen I (*red*), phosphorylated SMAD-2/3 (*green*), and CD163 (*blue*). *Bottom panels* feature granulomas stained for TGFβ (*red*), L-TGFβ (*green*), and αSMA (*blue*). Magnification ×200.A) Granuloma from animal with active disease. B) Granuloma from animals following two months of antibiotic treatment. C, D) Granulomas are from animals with active disease.

Fibroblasts are responsible for proliferating into wounds where they differentiate into myofibroblasts and secrete extra cellular matrix proteins (ECM) during the process of fibrosis (88, 143, 146, 148, 155, 156). The ECM secreted by myofibroblasts provides a substrate for re-epithelialization of the wound. Myofibroblasts also have a contractile phenotype, which enables them to close the wound gap and further restore tissue integrity (100, 231, 240, 317, 352, 401). Granulomas are different than traditional wounds because they involve a highly dense organized structure that serves to wall off an irritant or infection rather than to restore tissue architecture. Granulomas have a unique architecture that differs dramatically from surrounding tissue. Fibroblasts have been identified by histology studies to be present in granulomas but how they arrive there and what purpose they serve is not well understood (49). Certainly the presence of fibrosis is an indication of fibroblast activity, but what stimulates them in the context of the granuloma is still unknown.

High levels of TGF-β1 have been associated with many fibrotic processes (62, 64, 148, 385) and also in fibrotic granulomas (49). TGF-β1 is known to play an important role in driving fibroblast proliferation, differentiation, and the development of fibrotic tissue in other contexts, however its role in granuloma formation and function has not been fully characterized (49, 64, 90, 385, 402, 403). TGF-β1 stimulates fibroblast synthesis of α-smooth muscle actin (αSMA) and collagen secreted. αSMA is an indicator of fibroblast to myofibroblast differentiation (100, 105, 169, 231, 352, 401, 404). Myofibroblasts secrete large amounts of collagen, which are synonymous with fibrosis and can be seen in fibrotic granulomas (49, 83, 169). TGF-β1 is an important and possibly even necessary driver of fibrosis, however, whether it is sufficient for inducing fibrotic granuloma formation has not been determined.

While TGF-β1 signaling has been shown to promote fibrotic outcomes, IL10 has been associated with improved epithelial integrity and inhibition of TGF-β1 synthesis during pulmonary fibrosis (61, 79, 181, 405). IL10 acts on fibroblasts to counteract TGF-β1 signaling by blocking adhesion signaling, a requirement for efficient transmission of the TGF-β1 signal cascade. IL10 is present throughout the granuloma (295). Its role in macrophage activation during TB has been explored (157, 158), but its influence on fibroblasts in this context has not been characterized. The regulation of fibroblasts by TGF-β1 and IL10 may be the key to understanding the formation of fibrotic granulomas.

In this work we develop next-generation *GranSim*, a hybrid multi-scale model of granuloma formation and function, to include fibroblasts and molecular scale TGF-β1 signaling dynamics. We calibrate and validate this model against NHP studies of fibrotic granuloma morphology (49). With this model we can recapitulate the formation of fibrotic granulomas, and identify key mechanisms driving their formation. This model enables us to explore the role of fibroblasts in granulomas and predict mechanisms leading to fibrotic granuloma formation.

5.2 Results

5.2.1 Fibrosis morphology in granuloma simulation

In this section we track simulated morphological changes of developing fibrotic granulomas over time. In these studies we simulate granulomas for 200 days. We take snapshots at 5 time points: day 50 post infection (PI), day 100 PI, day 125 PI, day 150 PI, and day 200 PI in order to capture the progression of fibrosis in a single granuloma. We examine many model outputs including: total cell localization (Figure 5.2), fibroblast and myofibroblast specific localization (Figure 5.3), and collagen localization (Figure 5.4) as granulomas progress. We

compare morphology of simulated granulomas to histology sections of fibrotic granulomas from Mtb infected NHPs (see Figure 5.1). Collagen in the simulated granulomas recapitulates the NHP histology (Figure 5.4). We find that *GranSim* can simulate the formation of fibrotic granulomas that qualitatively match sections from NHP samples (49). Because initial time of granuloma formation cannot be identified in NHPs, it is impossible to compare specific time points between simulation and histology.

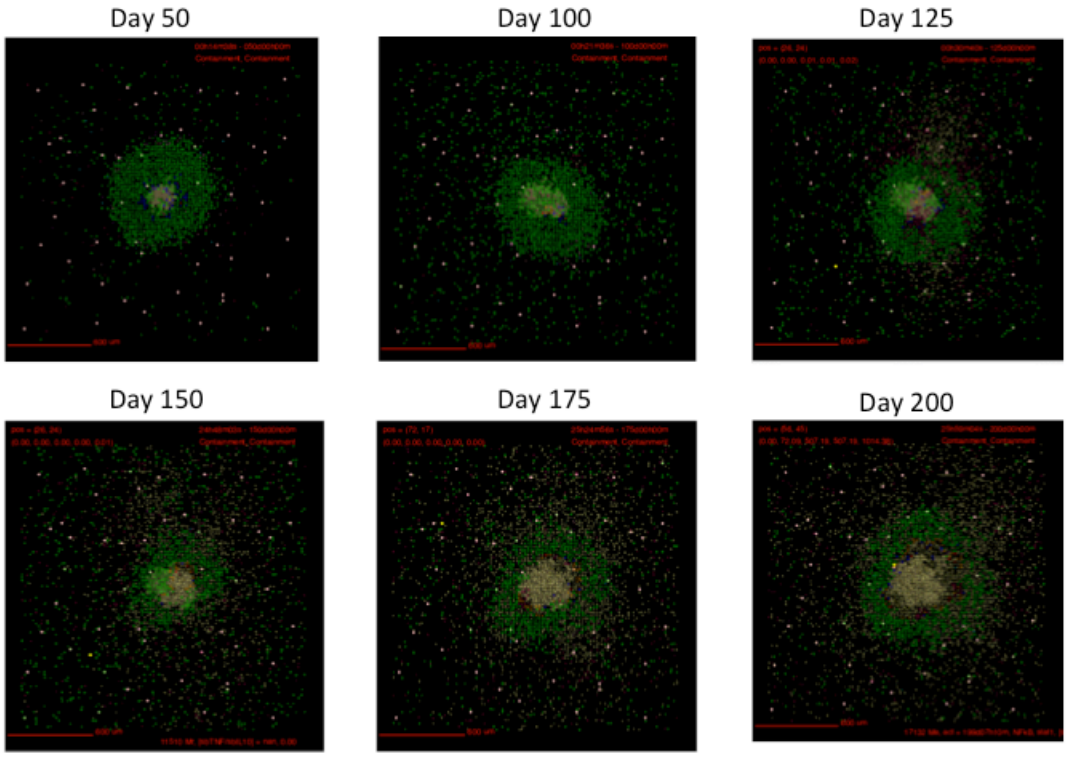

Figure 5.2: Simulations of cellular localization and granuloma morphology over time. Representative images of a single granuloma over time generated with baseline parameter set (Table. 5.1). Cells are represented by different colors as follows: resting macrophages are green, activated macrophages are blue, infected macrophages are orange, chronically infected macrophages are red, IFNγ producing T-cells are pink, cytotoxic T cells are violet, regulatory T cells are cyan, fibroblasts are maroon, and myofibroblasts are gold. Caseum is represented in these images as brown compartments. The entire simulation space shown is representative of 2mm x 2mm section of the lung.

Over the course of time following infection we observe the formation of a caseus necrotic granuloma (Figure 5.2). This granuloma becomes fibrotic which is evidenced by the presence of fibroblasts and myfibroblasts surrounding the lesion. The localization of fibroblasts and myofibroblasts is comparable to NHP granulomas (Figure 5.1 B, D). In this simulation we observe primarily peripheral localization of fibroblasts and myofibroblasts (Figures 5.A B, 5.1, 5.2) with some penetration into the center of the lesion by day 200 PI (Figures 5.A F, 5.1, 5.2).

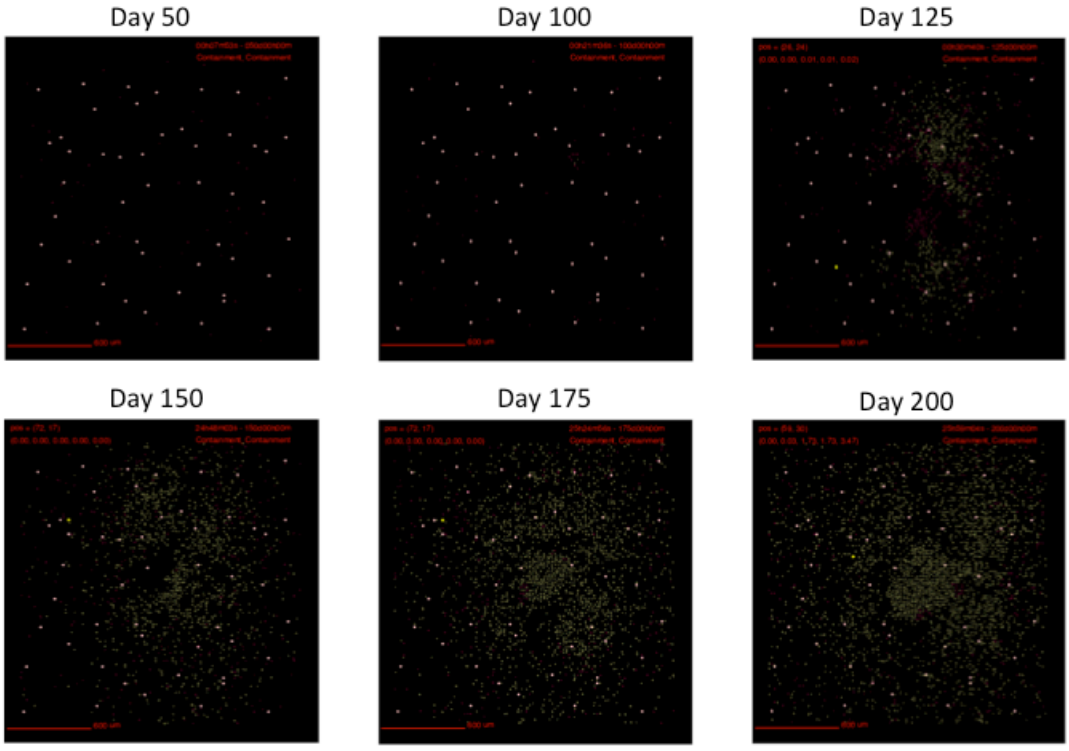

Figure 5.3: Localization of fibroblasts and myofibroblasts from a simulated fibrotic granuloma over time. In this representative simulation (same simulation as Figure 5.2) fibroblasts are represented as maroon, and myofibroblasts are represented as gold. As time progresses the number of both fibroblasts and myofibroblasts increases. They surround and penetrate the granuloma beginning at about 125 day PI.

Similar to the localization of fibroblasts and myofibroblasts, collagen is also initially located on the periphery of the granuloma and is deposited in the center and fibroblast and

myofibroblasts penetrate the lesion (Figure 5.4). The peripheral (5.A C) and central (Figure 5.1 A, E) collagen localization is also reflected in the NHP granulomas.

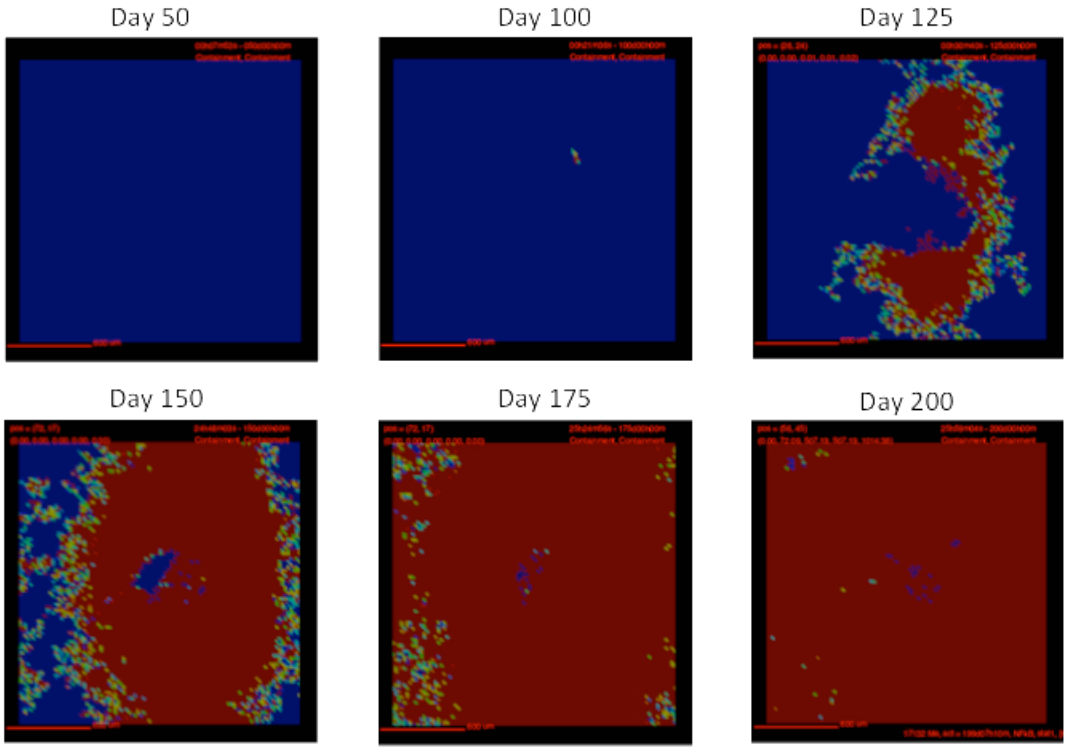

Figure 5.4. Collagen localization in a simulated fibrotic granuloma over time. Collagen concentration is represented in the above images with red representing the highest concentration and blue representing no collagen (same simulation as Figure 5.2). Collagen formation is first visible at day 100 PI and it continues to spread throughout the duration of the simulation, until day 200 PI when it covers the entire simulation space.

5.2.2 Cytokine localization in fibrotic granulomas

We also compared the localization of cytokines between simulated granulomas and NHP histology sections. We examine the localization of TNFα (Figure 5.5), IL10 (Figure 5.6), active TGF-β1 (Figure 5.7), and latent TGF-β1 (Figure 5.8) in the progressing granulomas. The localization of TNFα and IL10 is consistent with previously published simulations of *GranSim*. TNFα stays relatively localized to the granuloma with some pockets that disseminate from the

center of the lesion. These pockets of high TNFα concentration are transient and exist in the same location only for a short amount of time (Figure 5.5). IL10 also stays somewhat concentric to the granuloma. The amount of IL10 in the simulation decreases as the number of fibroblasts and myofibroblasts in the simulation increase. IL10 concentration appears to be inversely correlated with fibrosis.

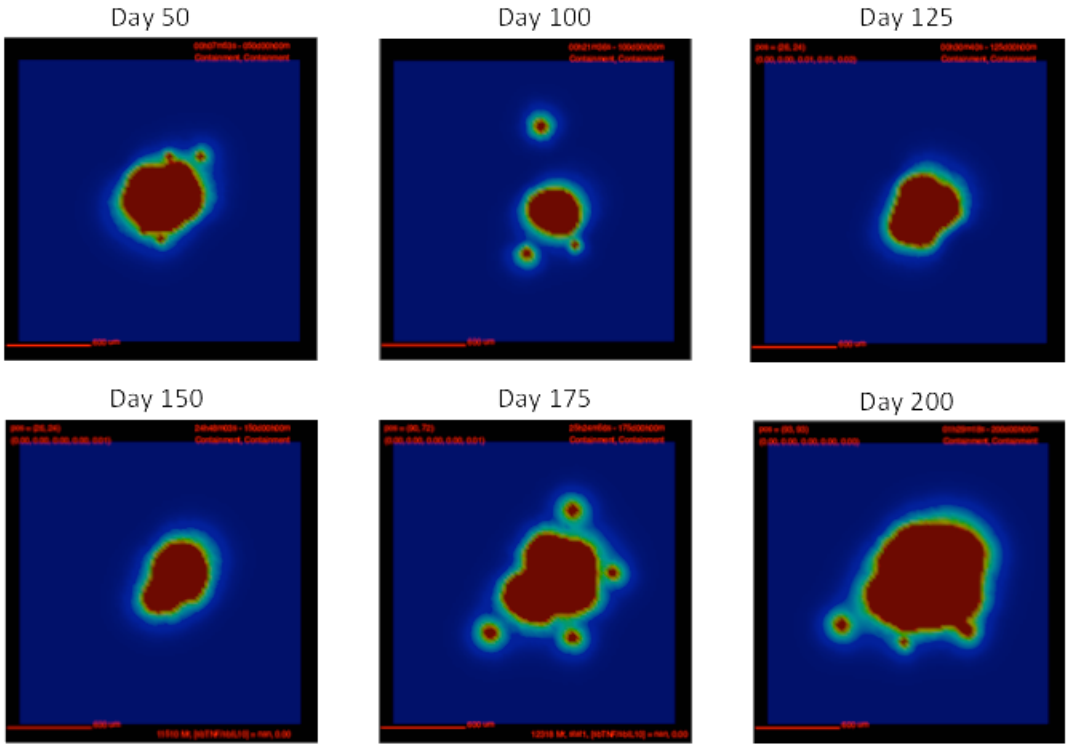

Figure 5.5. TNFα localization in a simulated fibrotic granuloma over time. TNFα concentration is represented in the above images for a single representative granuloma over time with red being the highest concentration and blue being no TNFα (same simulation as Figure 5.2). TNFα is visible from the time of infection. TNFα stays concentric to the granuloma throughout the simulation. The amount of TNFα fluctuates somewhat throughout the simulation.

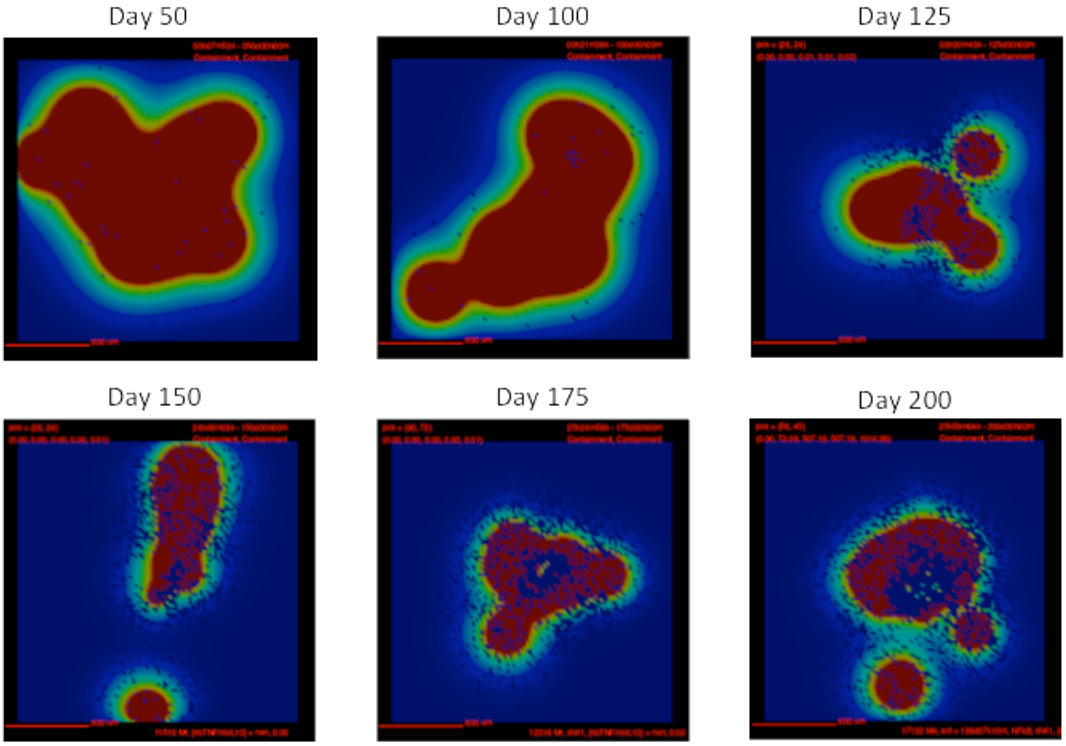

Figure 5.6. IL10 localization in a simulated fibrotic granuloma over time. IL10 concentration is represented in the above images for a single representative granuloma over time with red being the highest concentration and blue being no IL10 (same simulation as Figure 5.2). IL10 is visible early in infection and continues be present throughout the infection.

Localization of active and latent TGF-β1 in simulated granulomas qualitatively matches NHP granulomas (Figure 5.1) (49). Active TGF-β1 is visible early in infection and continues be present throughout the infection (Figure 5.7). Active TGF-β1 is somewhat concentric to the granuloma prior to day 125 PI. As the granuloma becomes more fibrotic active TGF-β1 spreads and becomes more prevalent. The highest concentrations of active TGF-β1 are found on the periphery of the granuloma, consistant with NHP data (Figure 5.1 B, D, F) Late in infection the concentration in the center of the granuloma is depleted. Latent TGF-β1 is visible early in infection and continues be present throughout the course of infection. As is the case for NHP granulomas, latent TGF- β1 is prevalent throughout the granuloma starting at a relatively early

time post infections (Figures 5.A, 5.7). Latent TGF-β1 is somewhat concentric to the granuloma very early in infection but is rapidly distributed throughout the simulation space. Latent TGF-β1 is present throughout the simulation space for the majority of the simulation.

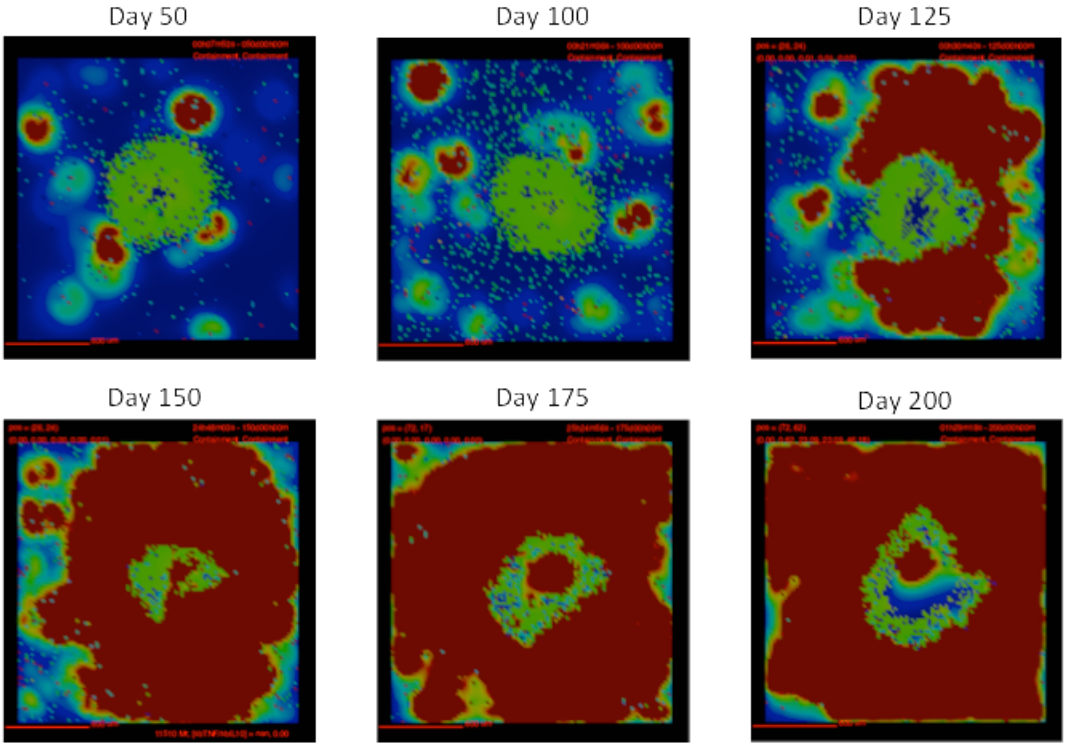

Figure 5.7. Active TGF-β1 localization in a simulated fibrotic granuloma over time. Active TGF-β1 concentration is represented in the above images for a single representative granuloma over time with red being the highest concentration and blue being no active TGF-β1.

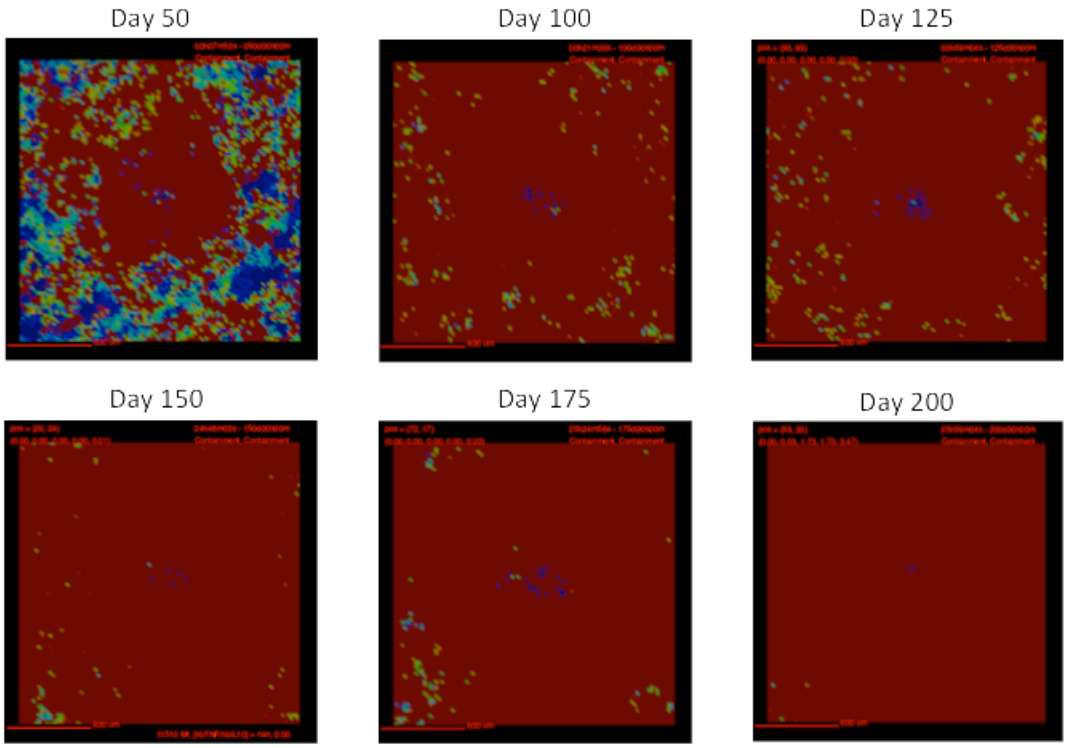

Figure 5.8. Latent TGF-β1 localization in a simulated fibrotic granuloma over time. Latent TGF-β1 concentration is represented in the above images for a single representative granuloma over time with red being the highest concentration and blue being no latent TGF-β1. Latent TGF-β1 is visible early in infection and continues be present throughout the infection.

5.2.3 Relationship between development of fibrotic lesions and high bacterial burden

In addition to qualitative assessment of simulated granulomas, we preformed uncertainty analysis to identify the spectrum of possible fibrotic outcomes in our simulated granulomas. We simulated 500 granulomas 3 times each, our baseline granuloma set, and to examine the full spectrum of possible outcomes. With this model we are able to generate a spectrum of fibrotic granulomas (Figure 5.9) with differing levels of fibrosis based on the numbers of fibroblasts and myofibroblasts present. Interestingly, not only the levels of fibrotic cells present change, but also the timing of onset of fibrosis. We next explore what drives these differences through statistical analysis of the model using US/A.

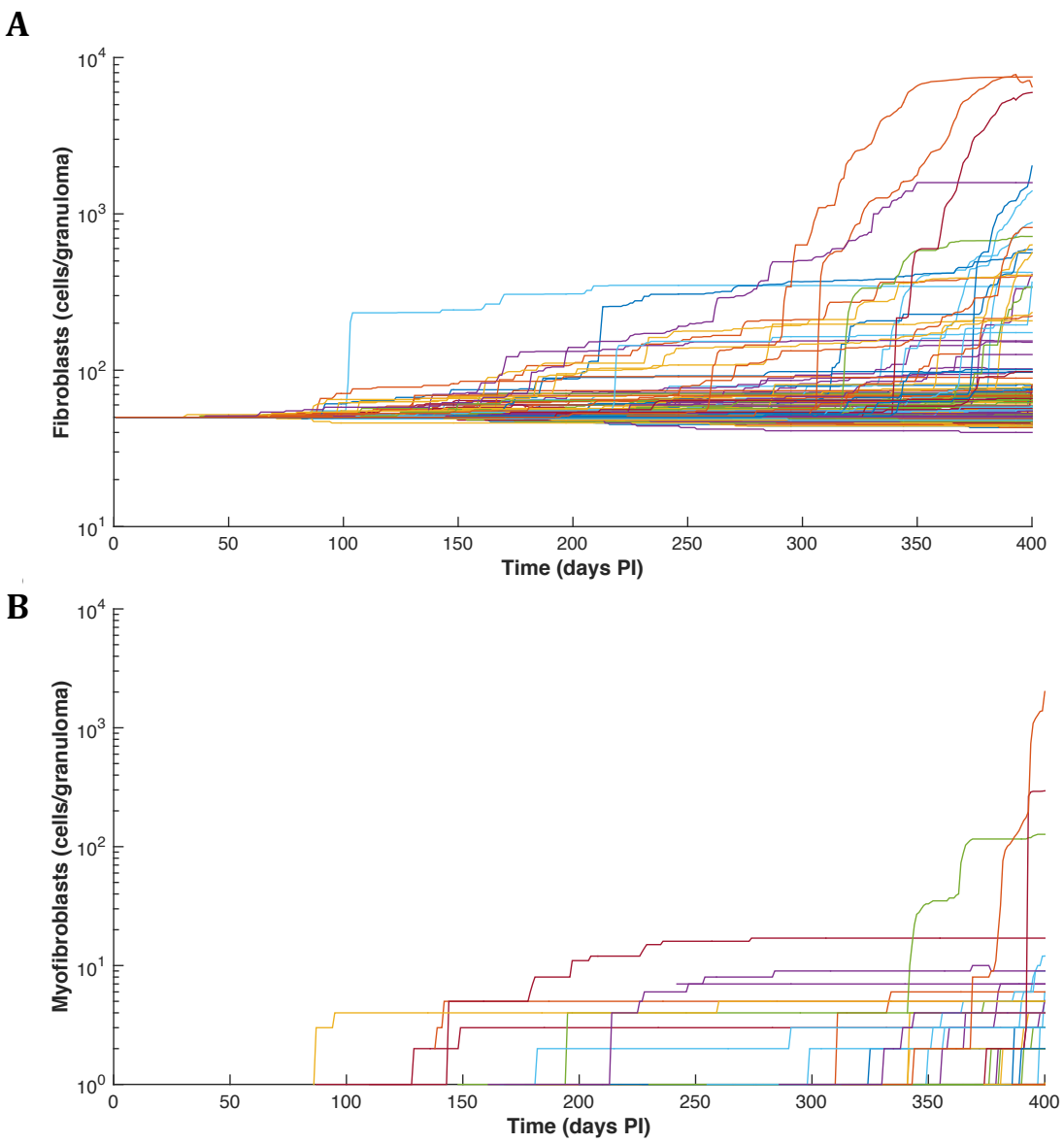

Figure 5.9 Fibroblast and myofibroblast numbers in 1500 simulated granulomas over time. Each line represents and individual granuloma from the baseline set (Table 5.1). A) Fibroblasts per granuloma over 400 days PI. B) Myofibroblasts per granuloma over 400 days PI. Parameter values from Table 5.1.

5.2.4 Mechanisms driving fibrotic granuloma formation *in silico*

We applied PRCC sensitivity analysis to our baseline granuloma set (Figure 5.9) to identify key mechanisms driving fibrotic outcomes. Fibrotic granulomas are characterized by the presence of fibroblasts and myofibroblasts as well as collagen. We found that nine model

parameters significantly influence the number of fibroblasts at day 300 PI (Table 5.1). Among these parameters the probability that a fibroblast will move had the greatest correlation to fibroblast number. This strong correlation suggests that fibroblasts are highly sensitive to local environments and that the more they move the more they are able to find profibrotic environments. We found seven parameters significantly influenced the number of myofibroblasts and collagen in the simulation at day 300 PI. Of these parameters the degradation rate of αSMA and fibroblast sensitivity to IL-10 had the strongest influence on myofibroblast number at day 400 PI ($p<0.001$ for Fisher's z test). Collagen is a product of myofibroblasts. We saw that parameters influencing collagen were the same as those influencing myofibroblast number.

Table 5.1 Significant PRCC values for parameters driving cell number at day 300 PI. $p > 0.001$

Fibroblasts				
Degradation rate of active TGF-β1	Macrophage sensitivity to TGF-β1	T cell sensitivity to TGF-β1	TGF-β1 synthesis by regulatory T cell	Probability of fibroblast movement
0.15	-0.11	0.10	0.09	0.77
Fibroblast IL-10 proliferation threshold	Fibroblast sensitivity to TNFα	Fibroblast synthesis rate of Il10	Fibroblast sensitivity to TGF-β1	
0.13	0.09	-0.10	0.09	
Myofibroblasts				
Degradation rate of active TGF-β1	Probability of fibroblast movement	TGF-β1 fibroblast proliferation threshold	TGF-β1 fibroblast differentiation threshold	
0.10	0.17	-0.16	-0.21	
Fibroblast IL10 binding rate	Fibroblast sensitivity to IL-10	Degradation rate of αSMA		
-0.13	-0.36	-0.42		
Collagen				
Degradation rate of active TGF-β1	Probability of fibroblast movement	TGF-β1 fibroblast proliferation threshold	TGF-β1 fibroblast differentiation threshold	
0.10	0.20	-0.16	-0.22	
Fibroblast IL10 binding rate	Fibroblast sensitivity to IL-10	Degradation rate of αSMA		
-0.14	-0.39	-0.42		

5.2.5 Relationship between fibrotic granulomas and bacterial burden

As previously described in this chapter, fibrotic granulomas come in two primary forms. Some fibrotic granulomas have a cuff of fibrosis surrounding the lesion. Other granulomas have are fibrotic throughout. Solid fibrotic granulomas are more commonly seen following antibiotic treatment and are associated with sterilization. Fibrotic granulomas that were simulated using *GranSim* most commonly exhibit the peripheral fibrosis, and they also typically have higher bacterial numbers (data not shown). In some cases *GranSim* produces fibrotic granulomas that have fibrosis throughout the lesion. These granulomas differ, however, from those seen in non-human primates as they too tend to have very high bacterial numbers (Figure 5.10). As shown in Figure 5.10 B, even granulomas with centrally located fibrotic cells tend to have substantial caseum and bacterial burden.

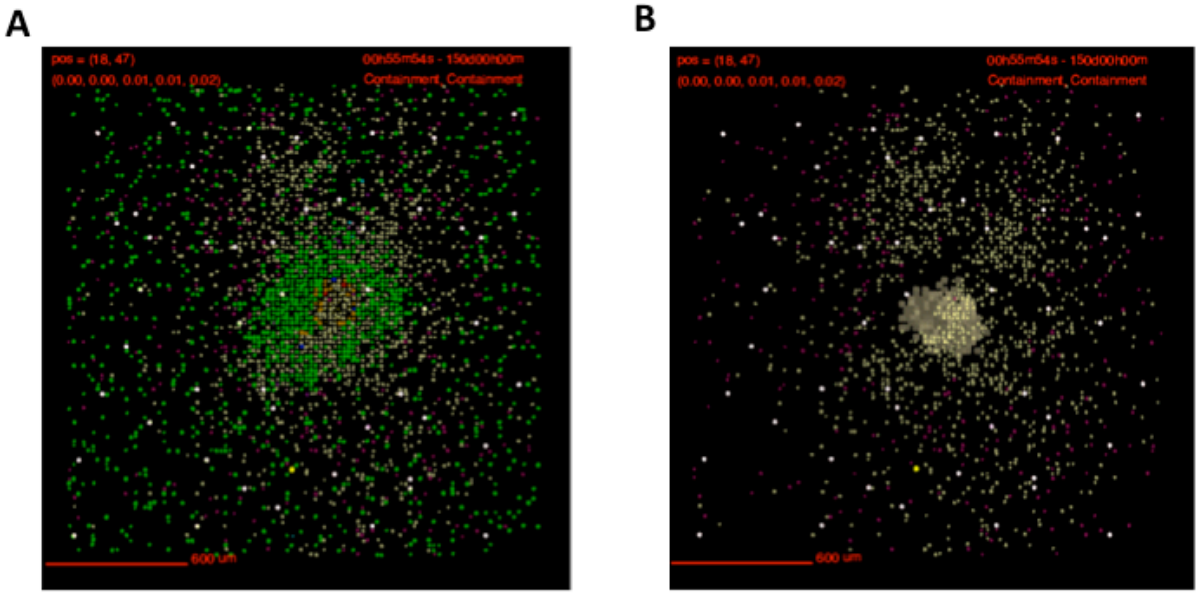

Figure 5.10 Snapshot of a simulated granuloma exhibiting central fibrosis at 150 days post infection. A) Snapshot of simulated granuloma showing the localization of all cell types. Myofibroblasts can be seen in the center of the lesion. Cells are represented by different colors as follows: resting macrophages are green, activated macrophages are blue, infected macrophages are orange, chronically infected macrophages are red, IFNγ producing T-cells are pink, cytotoxic T cells are violet, regulatory T cells are cyan, fibroblasts are maroon, and myofibroblasts are gold. B) Snapshot of simulated granuloma displaying only fibroblasts, myofibroblasts, and caseum. Caseum is represented in these images as brown compartments.

5.3 Discussion

In this work we have examined the simulated morphology of fibrotic granulomas and identified key mechanisms driving these morphologies. We found that both fibroblast and myofibroblast cell numbers at day 400 PI positively correlated with the amount TGF-β1 activated by a macrophage in a given compartment. This result indicates that the prevalence of fibroblasts and myofibroblasts in a granuloma is sensitive to the amount of active TGF-β1 available to them. We saw no significant correlation with the number of fibroblasts or myofibroblasts with the total amount of active TGF-β1 in simulated fibrotic granulomas. This data is consistent with NHP data showing high concentrations of TGF-β1 throughout both fibrotic and non-fibrotic granulomas (49). Together these observations indicated that total TGF-β1 levels in the granuloma is a necessary but not sufficient condition for inducing fibrotic outcomes.

Concentrations of active TGF-β1 in specific areas of a granuloma may be the key to whether or not a cell will proliferate and/or differentiate. The overall availability of active TGF-β1 in the granuloma does not necessarily influence the number of fibrotic cells, nor does it enable us to predict whether a granuloma will become fibrotic, however the concentration of active TGF-β1 in the vicinity of fibroblasts may be a driving factor for why some granulomas become fibrotic. This scale effect is currently under investigation.

In addition to the amount of TGF-β1 activated by a macrophage in a given compartment, the probability that a fibroblast will move has a significant and positive correlation to the number of fibroblasts in a given granuloma. This result suggests that fibroblast movement promotes fibroblast proliferation. One possible explanation for this is that fibroblasts are very sensitive to

local cytokine milieu. Movement enables them to sample many different cytokine environments. The more a fibroblast is able to move the better chance it has of finding a cytokine environment that is permissive to proliferation. TGF-β1 and IL10 concentrations affect the ability of fibroblasts to proliferate and this result further emphasizes that local cytokine concentrations, and not the overall environment of the granuloma, have a major influence on fibroblast behavior. Again, this scale effect is currently being explored.

These results provide challenges in determining what drives fibrotic granuloma formation because they indicate that lesion scale outputs are not ideal for studying the behavior of fibroblasts and myofibroblasts in the context of the granuloma. In order to better evaluate what drives formation of fibrotic granulomas future studies will require quantifiable spatial outputs. It may be the case that heterogeneity of granuloma environments is key to both whether and where fibrosis occurs. One way to better evaluate whether this is occurring would be to quantify the number of compartments within the simulation space that have high, medium or low concentrations of latent TGF-β1, active TGF-β1, IL10 and the ratios between these cytokines. Due to the volatility of localized cytokine concentrations, these outputs will need to be tracked over time and will require the use of a computational model like *GranSim*.

As I have alluded to in this chapter, *GranSim* is more successful at recapitulating the morphology of peripheral fibrotic granulomas than central fibrosis. This may be due in part to a lack of antibiotic treatment simulated in our system as compared to the NHP, where antibiotics were used (224). They found that solid fibrotic granulomas have been found more commonly following antibiotic treatment, which may be necessary for eliminating the surviving bacteria in those granulomas. It is also possible that the architecture of GranSim may make if difficult to differentiate between fibrotic granuloma types. Lack of epithelial cells and additional tissue

mediators may make it difficult to recapitulate all forms of fibrosis, and to differentiate between them.

In future work we would like to preform computational histology, applying quantitative spatial metrics to our two dimensional simulation snapshots. We would like to further explore the influence of specific local cytokine environments on the development of fibrotic granulomas. Additional mechanisms including the structural properties of collagen and enzymes that remodel collagen architecture would improve our ability to characterize fibrotic granulomas.

5.4 Materials and Methods

In this work we take a systems biology approach to understanding the formation of fibrotic granulomas and the role of TGF-β1 in this process. We combine *in silico* studies with *in vitro* and *in vivo* data to calibrate and validate our hypotheses wherever possible.

5.4.1 Agent based model (*GranSim*)

In this work we use *GranSim*, our 2D hybrid agent-based model of *M. tuberculosis* granuloma formation and function in the lung (157, 159, 162, 164, 201, 220, 227, 228). *GranSim* has been continuously updated and validated against experimental data since 2003. It captures the molecular, cellular, and tissue scale dynamics of granuloma formation and function in the lung. *Gransim* includes cellular, molecular, and tissue scale dynamics. At the molecular scale this version of *GranSim* includes diffusion of chemokines and cytokines (218), and fine grained fibroblast specific TGF-β1 receptor/ligand signaling dynamics. These mechanisms are described by partial differential equations (PDEs) and ordinary differential equations (ODEs) respectively. Both the diffusion and TGF-β1 signaling mechanisms have been described previously (83, 169, 218). At the cellular scale, *GranSim* accounts for discrete cellular agents whose actions are

governed by model rules. A full list of *GranSim's* rules can be found at *http://malthus.micro.med.umich.edu/GranSim*. Within this updated version of *GranSim* there are four macrophage states (resting, activated, infected, and chronically infected) and three distinct T-cell types (cytotoxic, regulatory, and IFNγ producing T-cells). This model also include two states of fibroblasts (activated fibroblast and myofibroblast), which were imported from a previously published model (83). The cellular scale captures interaction between these agent groups, and chemokine-directed cellular movement.

Granuloma formation occurs at the tissue scale and is an emergent behavior of the model. This means that granuloma formation is the product of individual agents actions and not a higher-level architecture. The model produces reams of information about TB granulomas, most of which is impossible to acquire from animal studies. Outputs of the model include: chemokine and cytokine concentration gradients over the entire simulation space for every time point, details of the position and state for all agents within the simulation, and overall morphological depictions of the simulation space. This information can be quantitative or qualitative and can be directly compared to data from *in vitro* and *in vivo* studies. Snapshots of the simulation environment can be linked to produce time-lapse movies (*http://malthus.micro.med.umich.edu/lab/movies/TGFB_GranSim/*).

5.4.2 Fibroblast and myofibroblast agents

Fibroblasts from the previously described co-culture model (see Chapter 3) (83) were incorporated into *GranSim* as a unique agent class. This class contains both fibroblasts and the differentiated myofibroblasts. These cells maintain their molecular scale TGF-β1 signaling dynamics (as described in Chapter 3 and below). Additional rules governing fibroblast and

myofibroblast behavior have been incorporated into *GranSim*. Fibroblasts can proliferate in GranSim if they have bound a sufficient amount of TGF-β1 in their lifetime (*amount of TGF-β1 required for fibroblast proliferation*), have not bound more than a maximum amount of IL10 (*molecules of IL10 that inhibits fibroblast proliferation/differentiation*), and are present in a sufficient concentration of TNFα (*molecules of TNFα necessary for fibroblast proliferation/differentiation*). Once a fibroblast has proliferated, it cannot attempt proliferation again for 24 hours. Fibroblasts have a probability of moving randomly into an available grid compartment if one is available in their Moore neighborhood (the eight compartments that share and edge with the compartment they occupy) (*probability a fibroblast will move*). Fibroblasts bind and secrete TGF-β1 according to the equations described previously (see Chapter 2)(169). In this work fibroblasts do not bind PGE_2 because epithelial cells, the primary source of PGE_2 in the lungs, are not included in this version of GranSim. In place of PGE_2, fibroblasts bind and are inhibited by IL10, which works through the same mechanism as PGE_2, to inhibit fibroblast adhesion signaling. Fibroblasts can differentiate into myofibroblasts if: they have not proliferated in the current time step, have bound a sufficient amount of TGF-β1 in their lifetime (*amount of TGF-β1 required for myofibroblast differentiation*), have not bound more than a maximum amount of IL10 (*molecules of IL10 that inhibits fibroblast proliferation/differentiation*), and are present in a sufficient concentration of TNFα (*molecules of TNFα necessary for fibroblast proliferation/differentiation*). Because *GranSim* models granuloma formation and not the surrounding tissue a signal is necessary to inform fibroblasts they have arrived at the site of injury/infection. We use TNFα as a proxy for all the cytokines that signal tissue damage to a fibroblast. Myofibroblasts maintain TGF-β1 binding and receptor ligand signaling but no longer secrete TGF-β1. Myofibroblasts have chemotactic movement

within the simulation space (they are sensitive to the pro inflammatory chemokine milieu). They also secrete collagen according to the parameter collagen secretion (*collagen synthesis rate*), and synthesize αSMA. Myofibroblasts have a probability of undergoing apoptosis (*probability of apoptosis*) at each time step.

5.4.3 Fibroblast TGF-β1 signaling dynamics

Fibroblast TGF-β1 signaling dynamics are described in detail in Chapter 2 (169). Because *GranSim* does not contain PGE_2, IL10 is used as an inhibitor of TGF-β1 signaling in fibroblasts (79, 185, 186, 406). IL10 acts in the same way as PGE_2 by inhibiting the adhesion-signaling cascade necessary for effective TGF-β1 signal transduction (168, 234).

5.4.4 Hybrid multi-scale model

In this work we build upon the existing hybrid- multi-scale model *GranSim*. We introduce a new class of cellular scale agents, and molecular scale TGF-β1 receptor-ligand signaling within those agents. Model linking techniques have been described in detail in previous works (157-159, 218). In this work we link new cellular and molecular scale attributes into the existing model primarily through TGF-β1 and IL10. Fibroblasts secrete latent TGF-β1, which exists in the simulation environment, and is activated by macrophages. Active TGF-β1 is bound by many cell types (see Chapter 4). Fibroblasts themselves bind active TGF-β1 linking them to macrophages and regulatory T cells. Fibroblasts bind IL10, which is also secreted by macrophages and regulatory T cells, and works to inhibit TGF-β1 signaling. Fibroblasts are sensitive to TNFα secreted by activated macrophages. Cellular and molecular scales within the model are linked when cytokines regulated at the molecular scale influence the states and

behaviors of agents at the cellular scale. Thus, the cellular and molecular scale aspects of the model are connected by extracellular cytokine and agent behaviors (Figures 4-7).

5.4.5 Hybrid multi-scale model simulations

In this work we simulated 500 granulomas 3 times each with large parameter value ranges (Table 5.1). These 1500 simulations allowed us explore the full parameter space and explore all possible outcomes model outcomes including biologically infeasible outcomes. From these simulations we identified a baseline parameter set for a fibrotic granuloma with CFU that stabilizes over time. This baseline granuloma set is used for uncertainty and sensitivity analysis studies. We selected a representative granuloma from our baseline set for comparative histology studies. We present simulation snapshot of the representative granuloma at 50, 100, 125, 150, and 200 days PI in order to sufficiently capture the onset and progression of fibrosis. Because development of fibrosis typically occurs weeks, months and even years following infection, we did not show early PI snapshots.

5.4.6 Uncertainty and sensitivity analysis

Uncertainty and sensitivity analysis can be applied to the information provided by *GranSim* in order to quantify how variation in parameter values contributes to variation in model output (229). This analysis can highlight key mechanisms responsible for different model outcomes or predict key components of the biological system that are from the model. Because *GranSim* is multi-scale, parameters that contribute specifically to molecular, cellular, or tissue scale mechanisms, may affect outputs at other scales. When parameter values at one scale can influence model outcomes at another scale it is described as intra-model influence (229). With

uncertainty analysis, we can use the Latin hypercube sampling algorithm to sample from large parameter ranges, and model behavior given a wide value range for each parameter (229). We consider this analysis to span the full parameter space. In this work we simulate each parameter set chosen though LHS three times to account for aleatory uncertainty (229). We also preform sensitivity analyses, which allow us to identify parameters that have a significant influence on individual model outcomes and the extent of their influence on each outcome (229, 344). We use partial rank correlation coefficients (PRCCs) to determine how sensitive a given output is to each parameter (229). PRCC values range from -1 to +1, indicating the non-linear correlation between a parameter and model output. PRCC values are differentiated using Student's T-test of significance. PRCC values are considered significant with a p-value less than 0.01. Fishers Z test is applied to determine if PRCC values are significantly different form each other P-value < 0.001.

Table 5.1. Parameters used for wide parameter sweep

Parameter name	Value or range	Units
Mtb parameters		
Growth rate intracellular Mtb	1.003	cells
Growth rate extracellular Mtb	1.001	cells
Death rate of extracellular Mtb in caseum	1.5	cells
Core model parameters		
Diffusion time step	60	seconds
Molecular time step	6	seconds
Diffusion smoother time step	1.2	seconds
Number of smoother steps	0	n/a
Number of host cells causing caseation	10	n/a
Time to heal caseation	[1642, 2462]	days
Threshold for TNFα induced apoptosis	[1393, 2089]	molecules
Rate of TNFα induced apoptosis	[1.17e-6, 1.76e-6]	1/seconds
Minimum number of molecules allowing chemotaxis	[0.514, 0.77]	molecules

Maximum number of molecules allowing chemotaxis	[374, 562]	molecules
Diffusivity of TNFα	5.2e-8	cm^2/s
Diffusivity of IL10	5.2e-8	cm^2/s
Diffusivity of active TGF-β1	5.2e-8	cm^2/s
Diffusivity of chemokines	5.2e-8	cm^2/s
Degradation rate of TNFα	0.00158	molecules/molecular time step
Degradation rate of IL10	0.00048	molecules/molecular time step
Degradation rate of inactive TGF-β1	[9.28e-6, 1.39e-5]	molecules/molecular time step
Degradation rate of active TGF-β1	[8.0e-4, 0.0012]	molecules/molecular time step
Macrophage parameters		
Fraction of grid compartments with a macrophage	[0.024, 0.036]	n/a
Number of time steps before a resting macrophage can move	2	n/a
Number of time steps before an activated macrophage can move	16	n/a
Number of time steps before an infected macrophage can move	[112, 168]	n/a
Synthesis rate of TNFα ($MacTNF\alpha_{synth}$)	1.5	molecules/diffusion time step
Synthesis rate of CCL2	6	molecules/diffusion time step
Synthesis rate of CCL5	6	molecules/diffusion time step
Synthesis rate of CCL9	12	molecules/diffusion time step
Synthesis rate of IL10 by an activated macrophage	0.3	molecules/diffusion time step
Synthesis rate of IL10 by and infected macrophage	0.02	molecules/diffusion time step
Synthesis rate of Inactive TGF-β1 by macrophages	[0.0001, 0.01]	molecules/diffusion time step
Number of bacteria a resting macrophage can phagocytose	1	n/a
Probability of resting macrophage killing bacteria ($MacKill_{baseline}$)	[0.23, 0.35]	n/a
Threshold for intracellular bacteria causing chronically infected macrophages	[8,12]	bacteria
Threshold for intracellular bacteria causing macrophage to burst	[13, 20]	bacteria

Number of bacteria an activated macrophage can phagocytose	[4, 6]	n/a
Fraction of inactive TGF-β1 activated by a mac ($Activation_{fraction}$)	[1e-6, 1]	n/a
Amount of TGF-β1 that inhibits macrophages ($TGF\beta 1max_{Mac}$)	[1e-6, 1]	molecules
Fraction of active TGF-β1 in a compartment bound by a mac	[1e-6, 1]	n/a
Probability of an activated macrophage healing a caseated compartment in its Moore neighborhood	[0.0128, 0.0129]	n/a
T cell parameters		
Probability of a T cell moving to the same compartment as a macrophage	[0.05, 0.08]	n/a
Probability of a T cell moving to the same compartment as a T cell	0.08	n/a
Synthesis rate of TNFα by IFNγ-producing T-cell	0.15	molecules/diffusion time step
IFNγ-producing T-cell probability of inducing Fas/FasL mediated apoptosis	[0.0152, 0.0228]	n/a
Probability of IFNγ-producing T-cell to secrete TNFα	[0.048, 0.072]	n/a
Probability of IFNγ-producing T-cell to secrete TNFα	[0.288, 0.432]	n/a
Synthesis rate of TNFα by cytotoxic T-cell	0.015	molecules/diffusion time step
Probability of a cytotoxic T-cell killing a macrophage	[0.012, 0.18]	n/a
Probability of a cytotoxic T-cell killing a macrophage and all associated Mtb	[0.61, 0.91]	n/a
Probability of cytotoxic T-cell to secrete TNFα	[0.056, 0.084]	n/a
Synthesis rate of IL10 by regulatory T-cell	0.739	molecules/diffusion time step
Synthesis rate of TGF-β1 by regulatory T cell	[0.0001, 0.01]	molecules/diffusion time step

Probability a regulatory T cell will deactivate an activated macrophage	[0.011, 0.016]	n/a
Amount of TGF-β1 that inhibits T cells ($TGF\beta 1max_{Tcell}$)	[0.04, 0.2]	molecules
Fraction of active TGF-β1 in a compartment bound by a T cell	[1e-4, 0.2]	n/a
Fibroblast Parameters		
Maximum fibroblast age	28800	agent timesteps
Initial number of fibroblasts in a simulation	50	n/a
Probability a fibroblast will move	[0.001, 0.5]	n/a
Synthesis rate of TGF-β1 by a fibroblast	[0.001, 0.1]	molecules/diffusion time step
Units of αSMA synthesized per TGF-β1 binding event	1e-10	n/a
Time until a fibroblast can attempt to proliferate	[24, 48]	hours
Number of molecules of IL10 that inhibits fibroblast proliferation/differentiation	[1e4, 2e4]	molecules
Amount of TGF-β1 required for myofibroblast differentiation	[2.0e-7, 8.0e-7]	molecules
Amount of TGF-β1 required for fibroblast proliferation	[2.0e-7, 8.0e-7]	molecules
Minimum ratio of TGF-β1 to IL10 required for myofibroblast differentiation	[1e-11, 1e-9]	n/a
Molecules of TNFα necessary for fibroblast proliferation/differentiation	[0.025, 0.5]	molecules
Myofibroblast Parameters		
Collagen synthesis rate	[1e-7, 1e-5]	molecules/agent time step
Probability of apoptosis	[0.002, 0.2]	n/a
Recruitment Parameters		
Maximum macrophage recruitment probability	[0.112, 0.168]	n/a
Maximum IFNγ-producing T cell recruitment probability	[0.112, 0.168]	n/a
Maximum cytotoxic T cell recruitment probability	[0.079, 0.12]	n/a

Maximum regulatory T cell recruitment probability	[0.0232, 0.0348]	n/a

Chapter 6

Conclusions and Future Directions

The work described herein focuses on the role of TGF-β1 in interstitial lung diseases. This work takes a theoretical approach to studying how disease pathology forms and evolves within the lung, with a focus on identifying important mechanisms that drive pathology and predicting intervention strategies that could halt and/or reverse pathology. By combining mathematical and computation methods with traditional experimental methods, I identify system level dynamics and expedite the development of new therapeutic treatments for two classes of pulmonary disease (83, 169). TGF-β1 is a pleotropic cytokine that is bound and secreted by many cell types (86, 93, 98, 101, 151, 361, 386, 407-411). The effects of TGF-β1 are cell- and tissue-type specific, however it is primarily thought of as an anti-inflammatory cytokine that inhibits cell cycle activation and effector functions (184). It is known to promote fibrosis (61, 77, 84, 148, 406, 412) over inflammation and inhibit proliferation for many cell types (108, 113, 119, 134, 140, 151). Throughout this work I explore the role of TGF-β1 in two different lung pathologies, idiopathic pulmonary fibrosis and tuberculosis, associated with lung healing and tissue integrity.

6.1 Regulating fibroblast activation

In these studies I first explore the role of TGF-β1 in fibroblast activation (169). Fibroblasts are important during the wound healing response and regulation of their activation is

critical to prevent pathologic fibrotic outcomes (88, 143, 148, 150, 155, 156, 196, 232, 233, 239, 259-261, 264, 413, 414). Because of their critical role in wound healing and fibrosis, many groups have explored what molecules induce fibroblast activation (76, 151, 316, 317, 342, 353, 415-421). Some groups have also looked at what molecules inhibit activation, although this area is less well studied (168, 234, 311, 323, 422). I build upon prior work identifying TGF-β1 as a major driver of fibroblast activation and explore which specific mechanisms within the TGF-β1 receptor/ligand-signaling cascade were most important for inducing fibroblast activation (169).

6.1.1 Abrogation of TGF-β1 alone is not sufficient for controlled fibroblast activation

A key and unexpected finding from this study was that a positive feedback loop generated by TGF-β1 signaling could not be effectively regulated by reducing or removing TGF-β1 alone (169). Instead, an independent negative regulator of fibroblast activation, such as PGE_2, is necessary to restrict the positive feedback cycle and regulate fibroblast activation. Many efforts have been made to generate therapeutic targets that restrict TGF-β1 signaling (12, 25, 27-33, 250, 267, 313, 314, 346, 347) in an attempt to regulate fibroblast activation, but none have been very successful. This finding highlights the need to focus on therapeutic targets of fibroblast activation that do not act through the TGF-β1 signaling cascade but rather target inhibitors that act downstream.

6.1.2 Potential TGF-β1 independent methods of regulating fibroblast activation

Based on the results I generated from the models, I propose that future studies should focus on identifying inhibitors of fibroblast activation that act on signals downstream of the TGF-β1 induced SMAD2/3 signaling cascade, or those that act independently of TGF-β1

signaling altogether. Numerous pathways have been identified that act downstream of SMAD signaling and include but are not limited to $PGE_{2\,(168)}$, *Wnt* family ligands (423), and β-cantenin signaling (424). Increased levels of β-cantenin in the cell nucleus have been associated with increased fibrotic outcomes in fibroblasts (425). Decreasing the cellular concentration of β-cantenin can reduce fibrotic outcomes without fully restricting the ability of fibroblasts to become activated. In other words, decreased levels of β-cantenin in the nucleus of fibroblasts reduce the magnitude of fibroblast activation (426). *Wnt* signaling is highly linked to β-cantenin levels in fibroblasts. Increased expression of some Wnt family receptors, such as SFRP1 and FRBZ, has been correlated with reduced nuclear β-cantenin levels in fibroblasts (426). Other studies have shown that increased Wnt signaling is positively correlated with nuclear β-cantenin levels in fibroblasts (427). Although there is disagreement in the field as to whether increasing or decreasing Wnt signaling reduces β-cantenin levels in fibroblasts, this signaling cascade works downstream of TGF-β1 signaling and provides an avenue for TGF-β1 independent therapeutic targets.

In addition to targeting Wnt signaling and reducing nuclear β-cantenin levels, two methods that inhibit pro-inflammatory signals, another avenue for possible therapeutics could be to promote either prevalence of, or cell sensitivity to, existing inhibitors. For example, inhibition of fibroblast adhesion signaling through PGE_2 is an existing regulator of fibroblast activation that could be exploited as a therapeutic (66, 88, 188, 234, 322, 345, 357, 428). One possible way to exploit this system is by inducing the expression of the EP2 receptor, which is primarily responsible for binding PGE_2, and could promote fibroblast regulation by increasing fibroblast sensitivity to PGE_2 (364). Therapeutic interventions that promote naturally occurring inhibitory mechanisms could be effective TGF-β1 independent targets of fibroblast activation.

6.2 Fibroblast/epithelial cell co-regulation

In the second part of this work, I build upon the previously described studies of fibroblast activation to explore the co-regulation of fibroblasts and epithelial cells (83). One role of epithelial cells in the tissue environment is to secrete cytokines and lipids that inhibit fibroblast activation (187, 188). The absence of these signals following tissue damage or epithelial cell disruption enables fibroblasts to become activated and initiate wound healing mechanisms. Having predicted the need for external negative regulators in order to achieve controlled fibroblast activation, we suspect that the interplay between fibroblasts and epithelial cells is central to the tradeoff between normal wound healing and fibrotic outcomes. Here we explore the mechanisms that regulate fibroblast proliferation, fibroblast to myofibroblast differentiation, and epithelial cell survival. We compare good and bad tissue outcomes to determine what mechanisms drive fibroblast regulation and epithelial cell survival (83).

6.2.1 Independent regulation of fibroblasts and epithelial cells

Through uncertainty and sensitivity analysis (229) we identified key mechanisms driving both fibroblast inhibition and epithelial cell survival. A major discovery within this work was that the mechanisms driving fibroblast proliferation and differentiation differ from the mechanisms driving epithelial cell survival. Attempts to improve fibrotic outcomes by affecting single cell specific mechanisms were unsuccessful. Only combined treatments intended to simultaneously promote epithelial cell survival while inhibiting fibroblast proliferation improved fibrotic outcomes (83). Up to this point all attempted treatments for fibrosis in the clinic have focused on inhibiting fibroblast proliferation (284). Thus, we believe that efforts to both inhibit

fibroblast proliferation and improve epithelial cell survival are necessary for effectively treating fibrosis.

6.2.2 Potential therapeutic strategies to preserve epithelial cell integrity during fibrosis

The most often prescribed treatments for fibrosis have focused on inhibiting fibroblast proliferation and differentiation (as well as the actions of myofibroblasts following differentiation) (26, 284, 346, 419). These treatments focus primarily on inhibiting the actions of pro-fibrotic mediators. I suggested, based on studies described herein, that negative regulators of fibrosis are the key mechanisms in regulating fibroblast activation (see Table 3.1). Inhibiting pro-fibrotic mediators is not sufficient for regulating fibroblast activation. On the other hand, inhibiting pro-fibrotic mediators (primarily growth factors) is important for promoting epithelial cell survival. These strategies alone will not work well in late stage fibrosis when substantial epithelial cell damage has resulted in few to no surviving epithelial cells, but may have some advantageous effects in promoting epithelial cell survival during early pathology. In the previous section I describe several strategies for increasing fibroblast sensitivity to existing negative regulators, and/or targeting fibrotic regulators downstream of growth factor signaling. These methods leading to fibroblast regulation could be combined with existing therapeutics for inhibiting growth factor signaling and promoting epithelial cell survival, to target both cell types necessary for healthy tissue outcomes. I propose that a novel two-hit approach, inhibiting fibroblast proliferation and promoting epithelial cell survival, to treating fibrosis will provide synergistic improvements over single mechanism strategies (83).

6.3 The role of TGF-β1 in granuloma formation and function

In the third section of my work I explore the role of TGF-β1 in granuloma formation and function. TGF-β1 has the capacity to act on many cell types within the granuloma, however in this work I focus on the impact of TGF-β1 signaling on T cells and macrophages. Previous studies have examined the role of another anti-inflammatory cytokine, IL10, in a similar context (85, 158, 163, 164, 173, 174). Recently, *in vivo* histological studies have been performed looking at the localization of TGF-β1 in the granuloma (49), but due to the nature of granulomas, it has been impossible to study mechanistic action of TGF-β1 within a relevant system, like primate granulomas. In this work I identify a role for TGF-β1 in regulating cytotoxic T cells, and not macrophage anti-microbial functions.

6.3.1 Potential host directed therapies for chronic inflammatory diseases utilizing differential regulation of lymphoid and myeloid derived cell types by TGF-β1 and IL10

Previous studies have alluded to a dichotomous regulation of lymphoid and myeloid derived cell types by TGF-β1 and IL10 respectively (136, 137, 388, 391). These studies have focused on NK and dendritic cells. In this work we find the same dichotomous regulation to occur between cytotoxic T cells and macrophages in the context of Mtb induced granuloma. This discovery, if applied to a broader immunological context has implications for host directed treatment of many different diseases.

Diseases that could be improved by cell specific host directed therapies include age-related chronic inflammatory diseases (429, 430). Aging is a co-morbidity for many chronic diseases, in part, because of waning immunity that occurs during aging. People with advanced age are described as having immunoscenescence, and are less effective at fighting off pathogens

and establishing memory responses (430). Despite the presumed non-responsiveness of the advanced immune system, immunoscenescence is also characterized by an overall inflammatory state (430). This increase in overall inflammation may be due to hormonal changes, increased cell death, or dysregulated cytokine signaling. Whatever the source, heightened inflammation is associated with many kidney diseases, dementia, and is a major source of discomfort for the elderly. Understanding the interplay between different anti-inflammatory cytokines could lead to improved treatment of chronic inflammation without putting patients at increased risk of infection.

In the context of TB we find that depleting TGF-β1 has a much greater effect on improving bacterial clearance by stimulating cytotoxic T cell effector functions than depleting IL-10, which is a major suppressor of macrophage activation. In contrast, we find that depleting IL-10 results in a state of increased inflammation compared to depleting TGF-β1. Macrophage secretion of pro-inflammatory cytokines is highly associated with chronic inflammation in the context of advanced age. Macrophages, a myeloid derived cell type, are highly sensitive to suppression by IL-10. On the other hand cytotoxic T cells, a lymphoid derived cell type, are not significantly impaired in the presence of IL10. Increasing IL-10 signaling while suppressing TGF-β1 signaling in elderly patients could reduce chronic myeloid derived inflammation without impairing anti-microbial responses. Further exploration in the dichotomous regulation of immune cells by anti-inflammatory molecules will optimal cytokines profiles and potential therapeutic treatments for people with chronic inflammatory diseases.

6.3.2 Potential host directed cell therapies for TB using cytotoxic T cells

In this work we identified a role for TGF-β1 in suppressing cytotoxic T cell effector function in the context of the TB granuloma. Deletion of TGF-β1 increased bacterial killing by cytotoxic effector functions and improved granuloma sterilization. From this study we can conclude that inhibiting TGF-β1 within the granuloma specifically could improve TB outcome. Several challenges arise with exploiting this strategy for therapy. TGF-β1 has been proposed as a target of therapy to treat numerous diseases but therapeutics intended to inhibit TGF-β1 signaling have been relatively unsuccessful. One reason for their failure is that TGF-β1 plays such a critical role in so many aspects of cellular regulation, and inhibitors frequently have severe side effects. The dense cellular architecture of granulomas and their localization within the lung provides additional challenges for treatment (192).

Because of the difficulty with specifically and effectively inhibiting TGF-β1, I propose that therapeutic strategies should focus on promoting cytotoxic T cell effector functions independent or downstream of TGF-β1 signaling within granulomas. Recent work in cancer treatment has proposed the use of specifically engineered T cells to recognize tumor-associated antigens (431). This therapeutic strategy could be relevant in treating TB as well. Genetically engineered cytotoxic T cells that lack sensitivity to TGF-β1, but have artificial shutoff switches could be introduced to improve bacterial clearance independent of TGF-β1 concentrations in granulomas. These cells would be highly active and antigen specific. If introduced to the lungs, these cells would have access to the site of infection. Small molecules that are sensitive kill switches could reduce the risk of rogue cells and protect patients from aberrant cytotoxicity. Cellular therapy strategies could circumvent some of the challenges associated with Mtb induced immunomodulation.

6.4 Formation of fibrotic granulomas

Fibrosis has been associated with Mtb induced granulomas in humans and NHPs (49, 303, 395, 398, 399). Histological studies of granulomas show the formation of a fibrotic cuff surrounding the densely cellular structure (49). The role of this cuff, although only recently explored in detail, is proposed to be containment and isolation of the infectious structure. Some granulomas present fibrosis throughout the structure and not just on the periphery suggesting an additional role beyond containment for fibrotic mechanisms (49). Granulomas that present continuous fibrotic phenotypes are often sterile; leading to a hypothesis that fibrosis is associated with lesion healing. This is not a far stretch because fibrosis is associated with wound healing in many other tissue contexts. Fibrotic lesions are found in both NHPs that have been treated with antibiotics and those that have not [ref]. The continuous fibrotic phenotype is more closely associated with antibiotic treatment while the peripheral fibrotic phenotype is more closely associated with untreated animals (49). Better characterization and understanding of the formation and function of these fibrotic phenotypes could highlight potential therapeutic strategies to induce lesion containment of clearance in patients with TB.

6.4.1 Mechanisms driving fibrotic granuloma formation and morphology

Fibrotic granulomas have only recently been extensively characterized. In this work we build upon that characterization to explore the progression of fibrosis in the context of Mtb induced granulomas, and to begin to identify mechanisms responsible for driving different fibrotic outcomes. We find that the development of fibrotic granulomas is closely related to local cytokine environments in the vicinity of fibroblasts and that likelihood of fibrosis developing

cannot be easily correlated to the overall environment of the granuloma. Macrophage activation of latent TGF-β1 and the probability of fibroblast movement within the tissue were both positively correlated with the number of fibroblasts present in the simulation at day 400 PI. Myofibroblast numbers were also primarily sensitive to the amount of latent TGF-β1 activated by macrophages in a given compartment. These results emphasize the influence of local cytokine environments and heterogeneity of the lesion on overall tissue outcome. The influence of these mechanisms could not be identified using homogenous methods and further studies will require highly sensitive spatial analysis.

6.4.2 Computational histology studies to further elucidate the significant of fibrosis in the context of TB and beyond

Our studies of fibrotic granuloma formation are in their infancy and there is still a good deal of work to do to fully understand the mechanisms behind fibrotic granuloma formation. To date we have introduced fibroblasts and TGF-β1 receptor ligand signaling into *GranSim* (157-162, 164, 165, 190, 201, 209, 210, 218, 219). These fibroblasts are capable of proliferating and differentiating into myofibroblasts. Myofibroblasts in *GranSim* can secrete collagen and produce αSMA. Collagen secreted in the simulation environment can be directly compared to histology studies from NHP granulomas. At this time however it does not serve any structural purpose in the simulated granulomas. In future work, I propose introducing collagen restricted cell migration where cell movement is slowed and possibly even inhibited by the presence of collagen (432). This additional function would serve two purposes. First, it would allow fibrotic granulomas to be contained not only by the functions of immune cells, but also by the presence of collagen itself, and second, it would prevent migration of resting macrophages from outside

the granuloma into fibrotic granulomas (49, 385). Effects of these changes would be non-linear and cannot be explicitly predicted without running the simulations.

In addition to updating collagen associated cell behavior in the granuloma, I also propose studies that introduce epithelial cells to the simulation environment. The current simulation environment of *GranSim* is a homogenous space where cytokines can diffuse and cells can move about. Epithelial cells are a major component of the lung architecture and are present of the site of granuloma formation (88, 244). Though they are not predicted to play a large role in granuloma formation; previous studies suggest that they do play a role in progression of pulmonary fibrosis. Epithelial cells signaling could be a key factor deciding whether granulomas become fibrotic or not (18, 66, 88, 241, 248, 254). Epithelial cells are also known to secrete many pro-inflammatory mediators, such as PGE_2, which could influence the behavior of fibroblasts and myofibroblasts in this environment (66, 88, 188, 322, 357). The presence of epithelial cells would provide a more dynamics simulation environment, more similar to the actually tissue environment of the lung.

One reason that epithelial cells have not already been introduced into *GranSim* is because the model focuses on granuloma formation, not changes in the overall lung architecture during infection. This focus has been sufficient for studying many elements of the immune response. The mechanical nature of fibrosis, however, beckons for a more complex tissue environment, which can be remodeled as a mark of severe fibrotic disease (401). With the addition of epithelial cells and some elements of tissue structure, *GranSim* can be adapted to study fibrosis in the context of Mtb induced granulomas, and other non-infectious causes of pulmonary fibrosis. The presence of epithelial cells in the simulation space of *GranSim* would provide a

more realistic lung environment that could be used to study a wide variety of pulmonary diseases such as cystic fibrosis.

With this additional architectural aspect of the tissue surrounding granulomas, *GranSim* will be primed for extensive computational histology studies. Simulation snapshots can be processed using CellProfiler and other histology software. What would normally be descriptive and qualitative information could be converted into quantitative data with the high throughput nature of our simulation studies. Histological samples are very limited *in vivo*, but can be generated in mass using tandem simulations. These studies will not only shed light on the role of fibrosis during Mtb infection, but will also contribute to the development of novel computational histology methods.

Appendix A

Supplementary Information for Chapter 3

A.1 Multi-Scale Model Rules

Here we describe the overall structure of our multi-scale hybrid agent-based model of a fibroblast/epithelial cell co-culture system. There are two key models that are linked to create the multi-scale model: *a cellular scale* model and a *molecular scale* model. Here we include a detailed description of the stochastic processes occurring in the cellular scale model that reads out at a tissue scale. The discrete molecular scale processes are described in full detail in a previous study (344). A schematic capturing how these models were derived independently and are linked is included in the main text (Figure 3.2) along with a description of how the model linking is done (see Methods). All values and definitions of parameter that are used in the models are listed in the Supplementary Tables S1, S2, S3, S4.

A.2 Overall Structure of the Cellular Scale ABM

Agent based models are designed focusing on four components as follows: an environment (simulated tissue culture plate), agents (fibroblasts, myofibroblasts, and epithelial cells), rules that govern agent behavior, and a time-step that dictates how frequently events in the model are updated (Δt).

A.2.1 Environment

The three-dimensional environment in this model represents one tenth of a well in a 96 well tissue culture plate. At the bottom of the model environment is a square surface measuring 1.78mm x 1.78mm. This surface represents the plastic at the bottom of a dish. The plate is divided into a 6561 compartment grid (81 compartments by 81 compartments). Each compartment is a 22μm x 22μm x 22μm cube. Cellular agents are adherent to the "plastic" and are therefore restricted to the grid compartments directly above the *in silico* plastic bottom surface in what will be defined as the cellular layer. Because cells are adhesion dependent, cells can only move in two dimensions within the cellular layer. We assume that each grid compartment can contain only one agent at a time based on their size. Their movement is guided by the ABM rules defined below. Above this layer is a three-dimensional layer that represents the volume of the plate (81 compartments by 81 compartments by 281 compartments). The full 3D model contains 282 layers each with 6561 compartments. All layers above the cellular layer represent *in silico* media in the well of a tissue culture plate.

Some mediators are restricted to the two-dimensional (2D) bottom surface layer while others can diffuse throughout the three dimensional compartments. Extra-cellular matrix (ECM) proteins are secreted directly only the surface of the virtual dish where they are cross-linked into a matrix. These proteins accumulate on this layer and do not diffuse. Latent TGF-β1 (as secreted by fibroblasts and myofibroblasts) is secreted into the extracellular matrix where it adheres until the protein is activated. Proteins that do not diffuse are stored as continuous values in the compartment where they are secreted. Activated TGF-β1 and PGE_2 are soluble mediators which can diffuse in three dimensions throughout the entire volume of the model, including the cellular

layer and all media layers above it. These mediators are also stored as continuous values that occupy space anywhere within the model.

We built an 81 x 81 x 282 3D grid. We assume there are no flux boundary conditions for all boundaries of the model grid for all agent movement and molecular diffusion steps. 5000 epithelial cells and 500 fibroblasts are randomly placed on the grid, each within its own compartment in the cellular layer. This is consistent with *in vitro* studies typically plating a 10:1 ratio of epithelial cell to fibroblasts (187).

A.2.2 Agents

There are two distinct types of cellular agents in the model, fibroblasts (representing pulmonary fibroblasts) and epithelial cells (representing alveolar epithelial cells). We assume that fibroblasts can differentiate into myofibroblasts, a process that is driven by αSMA synthesis (see Methods in main text). We also assume they do not de-differentiate back into a fibroblast, but rather remain a myofibroblast for the duration of a simulation. Once differentiated, we assume that myofibroblasts can no longer move or proliferate. Myofibroblasts are also susceptible to undergoing apoptosis in a probabilistic fashion.

A.2.3 Cellular Scale ABM Rules

ABM rules define cellular interactions as well as other processes in the model including cell movement, proliferation, death, and mediator secretion according to known biological behaviors in vitro. Additional rules in the model define molecule diffusion and degradation based on known rates identified in the literature (see Parameters below).

A.2.3.1 Cell Movement

We assume that fibroblasts are the only cellular agents with the ability to move. They can move in 8 possible directions within the cellular layer. Fibroblasts examine their Moore neighborhood (the nine grid compartments surrounding the cell including the compartment occupied by the cell) and determine whether there is an unoccupied compartment. If an unoccupied compartment is found, then the cell has a probability of moving into that compartment (Table A.2). A fibroblast can move no more than once during a single model time step.

A.2.3.2 Cell death, proliferation and differentiation

A.2.3.2.1 Cell death due to age

Two agent types, myofibroblasts and epithelial cells, can die of old age. When a cell reaches its maximum allowable age there is a probability that the cell will die. Dead cells will be removed from the grid (Table A.1, A.3).

A.2.3.2.2 Epithelial cell apoptosis due to TGF-β1 concentration

Epithelial cells are sensitive to high concentrations of TGF-β1. At birth each epithelial cell is assigned a maximum TGF-β1 threshold from a uniform distribution. This threshold captures the idea that that each epithelial cell has a slightly different sensitivity to TGF-β1 (67). At each model time step, epithelial cells checks the cumulative amount of TGF-β1 that it has bound. If the cumulative bound TGF-β1 reaches or exceeds the cells maximum threshold, then the cell dies and is removed from the grid. ***C.*** *Fibroblast proliferation*. Four rules govern when a

fibroblast can proliferate. (1) It must be 24 hours since the cell last divided (433). (2) The cell must have bound enough TGF-β1 to meet the TGF-β1 proliferation threshold (Table A.1). (3) The cell must not have bound more than the maximum amount of PGE_2 permissive of proliferation (Table A.1). (4) There must be an empty compartment in the fibroblast's Moore neighborhood for a daughter cell to enter (434, 435). If these four conditions are met, then the fibroblast has a non-zero probability of proliferating (Table A.1). ***D.*** *Fibroblast to myofibroblast differentiation*. We assume that fibroblast to myofibroblast differentiation is determined by the amount of αSMA synthesized by a fibroblast and is described in detail in the "Multi-scale Model Calibration" section of the main text.

A.2.3.3 Mediator Secretion

We assume that fibroblasts are able to secrete both TGF-β1 and PGE_2 at rates listed in Table A.1, respectively. We also assume that epithelial cells secrete only PGE_2 at rates listed in Table A.4. Finally, we assume that myofibroblasts secrete ECM proteins with rates listed in Table A.3.

A.2.3.4 Diffusion and degradation

Continuous molecular diffusion is calculated in three dimensions using the Fast Fourier Transform method (436). To integrate this numerical method into the framework of an ABM we use the methods described in detail by Cilfone et al. (218). Active TGF-β1 and αSMA model have degradation rate constants (Table A.1). Latent TGF-β1 is stabile throughout the duration of the simulations in this paper.

A.2.3.4.1 Time step

Interactions between agents are updated for each ABM time step (Δt = 1 hour) and are described above. Molecular scale processes, specifically TGF-β1 receptor ligand signaling in fibroblasts and secretion of mediators by all agent types, generally occur more quickly than cellular scale processes. For example, fibroblast proliferation takes about 24 hours (70, 103) where TGF-β1 receptor synthesis is around 4 minutes (207). These molecular processes are therefore updated on a more frequent molecular time step (Δt = 10 seconds), and thus each molecular process is updated 360 times per ABM time step. Diffusion of soluble molecules is updated at the diffusion time step (Δt = 60 seconds).

A.2.3.4.2 Simulation

Our combined model is implemented in C++ and runs on Linux/MacOS/Windows. Documentation and pseudo code are available in the online Supplement. A Runge-Kutta 4 method is used to solve the ODEs. Each time step of the ABM simulation is further divided into 60 pieces (step size of 60s) to reduce error. Fast Fourier Transform and forward Euler methods are used to solve the chemical diffusion equation (218) The molecular sub-model takes less than 0.1 second of real time each iteration of the molecular dynamics model (437). Each simulation describing 7 days of co-culture takes 40 to 50 minutes to run on a 300 core computer cluster.

A.3 Multi-Scale Model Parameters

Table A.1: Extracellular mediator Parameters and model simulation times

Parameter	*Definition*	*Value*	*Source*
Δt_{ABM}	Time over which the ABM is updated	1 h	N/A
$\Delta t_{diffusion}$	Time over which diffusion is solved	60 s	N/A
$\Delta t_{smoother}$	Time over which diffusion smoother is solved	0.1 s	N/A
$N_{smoother}$	Number of times diffusion smoother is solver in one diffusion time step	10	N/A
$\Delta t_{molecular}$	Time over which TGF-β1 receptor ligand molecular model is solved	10 s	N/A
$D_{TGF\beta1}$	Diffusivity of active TGF-β1	$2.7\text{x}10^{-7}$ cm^2/s	DMW
D_{PGE2}	Diffusivity of PGE_2	$5.23\text{x}10^{-6}$ cm^2/s	DMW
$\delta_{TGF\beta1}$	Active TGF-β1 degradation rate constant	[0.001 , 0.1] pM/min	(326)
δ_{PGE2}	PGE_2 degradation rate constant	[0.001 , 0.1] pM/min	Est.

N/A = not applicable DMW = derived from molecular weight Est. = estimated by uncertainty and sensitivity analysis

Table A.2: Fibroblast Parameters

Parameter	*Definition*	*Value*	*Source*
$t_{proliferation}$	Minimum time between proliferation events	24 h	DNS
$max_{prolifPGE2}$	Maximum bound PGE_2 permissive of proliferation	$[5\text{x}10^{-21}, 1\text{x}10^{-9}]$ pM	Est., Fig 3.3B
$min_{prolifTGF\beta1}$	Minimum bound TGF-β1 necessary for proliferation	$[1\text{x}10^{-16}, 1\text{x}10^{-14}]$ pM	Figure. S
$m_{differentiation}$	Slope of the linear regression dictating fibroblast differentiation	0.5	Est.
P_{move}	Probability of fibroblast movement	$[1\text{x}10^{-2}, 1]$	N/A

DNS = data not shown N/A = not applicable Est. = estimated by uncertainty and sensitivity analysis

Table A.3: Myofibroblast Parameters

Parameter	*Definition*	*Value*	*Source*
V_{ECM}	Rate of ECM synthesis	[1, 100] units	Est.
min_{age}	Minimum lifespan of myofibroblasts	1440 h	(438)
P_{death}	Probability of death	[0, 1]	N/A
max_{ECM}	Maximum amount of ECM in a single compartment	100 units	N/A

Est. = estimated by uncertainty and sensitivity analysis N/A = not applicable

Table A.4: Epithelial Cell Parameters

Parameter	*Definition*	*Value*	*Source*
V_{ePGE2}	Rate of PGE2 synthesis by epithelial cells	[$1x10^{-20}$, $1x10^{-18}$] pM/s	
k_{onE}	Rate of TGF-β1 binding by epithelial cells	[0.0009, 0.09] pM/s	Est.
k	Magnitude of PGE2 protection from TGF-β1 induced apoptosis	[0.0001, 100/0]	Est.
C	Non-zero constant	$7x10^{-14}$	Est.

Est. = estimated by uncertainty and sensitivity analysis

Table A.5A: Significant PRCC Values for Cell Number at Day 1 (p<0.01)

	TGF-β1 Activation	*TGF-β1 Receptor Internalization Rate*	*TGF-β1 Receptor Recycling Rate*	*TGF-β1 Synthesis*	*TGF-β1 Receptor Degradation Rate*	*Latent TGF-β1 Degradation Rate*
Fibroblast				0.18		
Myofibroblast	0.10			0.44	-0.09	
Epithelial Cell	-0.65	-0.10	-0.08	-0.87		-0.07

	PGE2 Binding Rate	*Fibroblast Sensitivity to PGE2*	*Fibroblast Insensitivity to TGF-β1*	*TGF-β1 Proliferation Threshold*	*PGE2 Proliferation Maximum*	*αSMA Differentiation Maximum*
Fibroblast	-0.18	0.09	0.12	-0.12	0.17	0.10
Myofibroblast			-0.11		-0.13	
Epithelial Cell	0.11		-0.15		-0.07	

	TGF-β1 to PGE2 Differentiation Threshold	*PGE2 Synthesis*	*Epithelial Cell TGF-β1 Binding Rate*
Fibroblast	0.18	-0.45	-0.07
Myofibroblast	-0.23	-0.09	
Epithelial Cell			

Table A.5B: Significant PRCC Values for Cell Number at Day 2 (p<0.01)

	TGF-β1 Activation	*Active TGF-β1 Degradation Rate*	*TGF-β1 Receptor Dissociation*	*TGF-β1 Receptor Internalization Rate*	*TGF-β1 Receptor Recycling Rate*	*TGF-β1 Synthesis*
Fibroblast						
Myofibroblast		0.07	0.08			0.09
Epithelial Cell	-0.07		-0.08	-0.07	-0.09	

	TGF-β1 Receptor Degradation Rate	*Latent TGF-β1 Degradation Rate*	*PGE2 Binding Rate*	*Fibroblast Sensitivity to PGE2*	*Fibroblast Insensitivity to TGF-β1*	*TGF-β1 Proliferation Threshold*
Fibroblast	0.10			-0.16	0.09	0.11
Myofibroblast	0.48	-0.086				-0.12
Epithelial Cell	-0.86		-0.60	0.10		-0.15

	PGE2 Proliferation Maximum	*TGF-β1 to PGE2 Differentiation Threshold*	*αSMA Differentiation Maximum*	*TGF-β1 to PGE2 Differentiation Threshold*	*PGE2 Inhibition of TGF-β1 Induced Differentiation*	*Myofibroblast TGF-β1 Binding Rate*
Fibroblast	-0.11	0.15		0.09	0.17	0.08
Myofibroblast		-0.07			-0.25	
Epithelial Cell			-0.09	-0.07		

	PGE2 Synthesis	*Epithelial Cell TGF-β1 Binding Rate*	*Epithelial Cell Sensitivity to PGE2*
Fibroblast		-0.46	-0.10
Myofibroblast	-0.07	-0.12	

Table A.5C: Significant PRCC Values for Cell Number at Day 3 (p<0.01)

	TGF-β1 Activation	*TGF-β1 Receptor Dissociation*	*TGF-β1 Receptor Internalization Rate*	*TGF-β1 Receptor Recycling Rate*	*TGF-β1 Synthesis*	*PGE2 Binding Rate*
Fibroblast						-0.16
Myofibroblast	0.09			0.07	0.51	
Epithelial Cell	-0.58	-0.09	-0.08		-0.85	0.11

	PGE2 Binding Rate	*Fibroblast Sensitivity to PGE2*	*Fibroblast Insensitivity to TGF-β1*	*TGF-β1 Proliferation Threshold*	*PGE2 Proliferation Maximum*	*αSMA Synthesis Efficiency*
Fibroblast	-0.16	0.07	0.13	-0.11	0.18	
Myofibroblast			-0.13		-0.08	
Epithelial Cell	0.11		-0.16		-0.08	-0.07

	αSMA Differentiation Maximum	*TGF-β1 to PGE2 Differentiation Threshold*	*Myofibroblast TGF-β1 Binding Rate*	*PGE2 Synthesis*	*Epithelial Cell TGF-β1 Binding Rate*
Fibroblast	0.09	0.17		-0.43	
Myofibroblast		-0.26	-0.08	-0.13	-0.09
Epithelial Cell	-0.07				

Table A.5D: Significant PRCC Values for Cell Number at Day 4 (p<0.01)

	TGF-β1 Activation	*TGF-β1 Receptor Dissociation*	*TGF-β1 Receptor Internalization Rate*	*TGF-β1 Synthesis*	*PGE2 Binding Rate*	*Fibroblast Sensitivity to PGE2*
Fibroblast					-0.16	0.08
Myofibroblast	0.10			0.52		
Epithelial Cell	-0.55	-0.07	-0.07	-0.84	0.12	

	Fibroblast Insensitivity to TGF-β1	*TGF-β1 Proliferation Threshold*	*PGE2 Proliferation Maximum*	*αSMA Synthesis Efficiency*	*αSMA Differentiation Maximum*	*TGF-β1 to PGE2 Differentiation Threshold*
Fibroblast	0.14	-0.09	0.17		0.08	0.19
Myofibroblast	-0.14		-0.07			-0.26
Epithelial Cell	-0.17			-0.07	-0.07	

	Myofibroblast TGF-β1 Binding Rate	*PGE2 Synthesis*	*Epithelial Cell TGF-β1 Binding Rate*	*Epithelial Cell Sensitivity to PGE2*
Fibroblast		-0.42		0.07
Myofibroblast	-0.07	-0.12	-0.09	
Epithelial Cell				

Table A.5E: Significant PRCC Values for Cell Number at Day 5 (p<0.01)

	TGF-β1 Activation	*TGF-β1 Receptor Dissociation*	*TGF-β1 Synthesis*	*PGE2 Binding Rate*	*Fibroblast Insensitivity to TGF-β1*	*TGF-β1 Proliferation Threshold*
Fibroblast				-0.16	0.13	-0.11
Myofibroblast	0.11		0.53		-0.13	
Epithelial Cell	-0.52	-0.088	-0.82	0.13	-0.16	
	PGE2 Proliferation Maximum	*αSMA Differentiation Maximum*	*TGF-β1 to PGE2 Differentiation Threshold*	*PGE2 Synthesis*	*Epithelial Cell TGF-β1 Binding Rate*	*Epithelial Cell Sensitivity to PGE2*
Fibroblast	0.18	0.085	0.19	-0.41		0.09
Myofibroblast			-0.26	-0.12	-0.10	
Epithelial Cell						

Table A.5F: Significant PRCC Values for Cell Number at Day 6 (p<0.01)

	TGF-β1 Activation	*TGF-β1 Receptor Dissociation*	*TGF-β1 Synthesis*	*PGE2 Binding Rate*	*Fibroblast Insensitivity to TGF-β1*	*TGF-β1 Proliferation Threshold*
Fibroblast			-0.08	-0.17	0.13	-0.11
Myofibroblast	0.11		0.54		-0.13	
Epithelial Cell	-0.49	-0.08	-0.81	0.13	-0.16	
	PGE2 Proliferation Maximum	*αSMA Differentiation Maximum*	*TGF-β1 to PGE2 Differentiation Threshold*	*PGE2 Synthesis*	*Epithelial Cell TGF-β1 Binding Rate*	*Epithelial Cell Sensitivity to PGE2*
Fibroblast	0.16	0.08	0.20	-0.41		0.08317
Myofibroblast			-0.26	-0.13	-0.09	
Epithelial Cell		-0.08				

Table A.5G: Significant PRCC Values for Cell Number at Day 7 (p<0.01)

	TGF-β1 Activation	*TGF-β1 Receptor Dissociation*	*TGF-β1 Synthesis*	*PGE2 Binding Rate*	*Fibroblast Sensitivity to PGE2*	*Fibroblast Insensitivity to TGF-β1*
Fibroblast			-0.11	-0.17	-0.12	0.12
Myofibroblast	0.10		0.54			-0.13
Epithelial Cell	-0.47	-0.10	-0.79	0.11		-0.14

	TGF-β1 Proliferation Threshold	*PGE2 Proliferation Maximum*	*Probability of Fibroblast Movement*	*αSMA Differentiation Maximum*	*TGF-β1 to PGE2 Differentiation Threshold*	*PGE2 Synthesis*
Fibroblast	-0.11	0.14	-0.08	0.07	0.19	-0.40
Myofibroblast					-0.26	-0.14
Epithelial Cell				-0.09		

	Epithelial Cell TGF-β1 Binding Rate	*Epithelial Cell Sensitivity to PGE2*
Fibroblast		0.07
Myofibroblast	-0.09	
Epithelial Cell		

A.4 Supplemental Figures

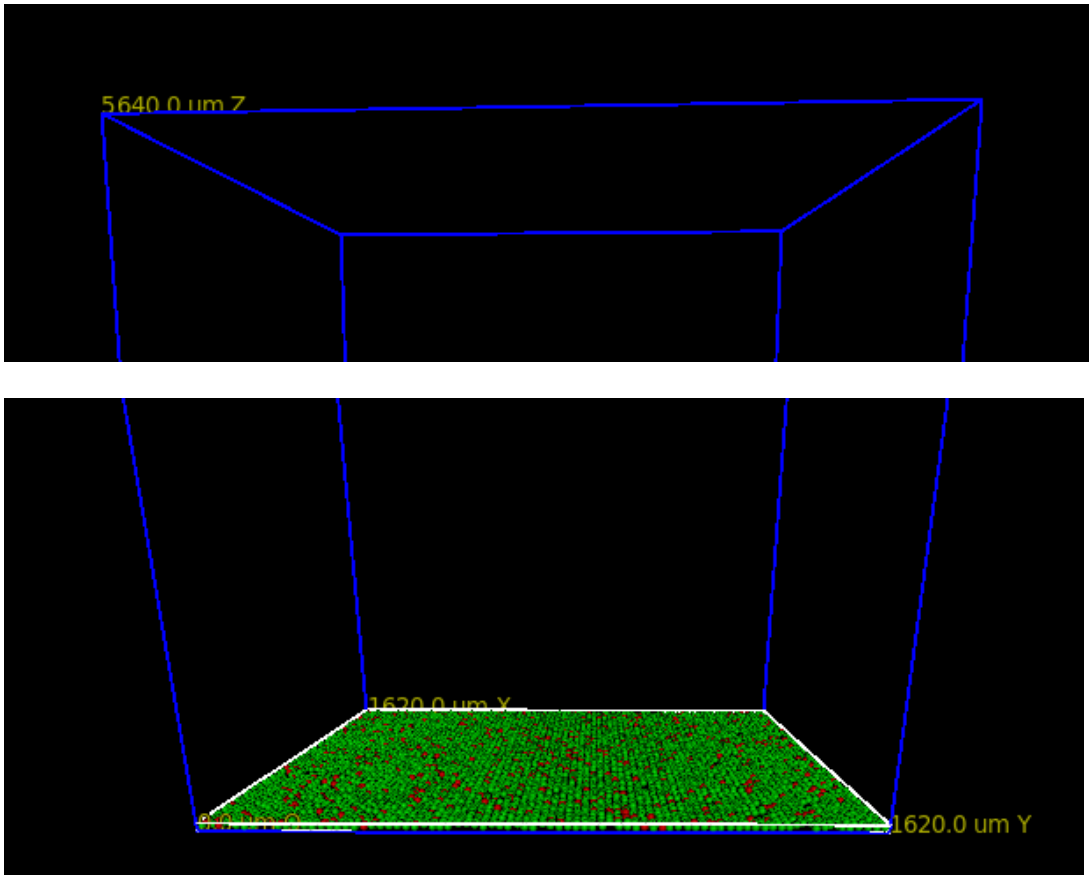

Figure A.1: Snapshot of the three-dimensional agent based model environment representing a virtual dish for the co-culture. Green spheres indicate epithelial cells while red spheres indicate fibroblasts. The blue lines indicated the edges of the boundaries of the ABM where media is present. Representative sections of top and bottom of the simulation environment are shown. The full simulation environment include 282 layers representing 6.17mm.The white lines indicate the edges of the boundaries of the cellular layer within the model (plastic bottom of well). Time lapse simulations of the model in 2D can be found at http://malthus.micro.med.umich.edu/lab/movies/Co-culture/.

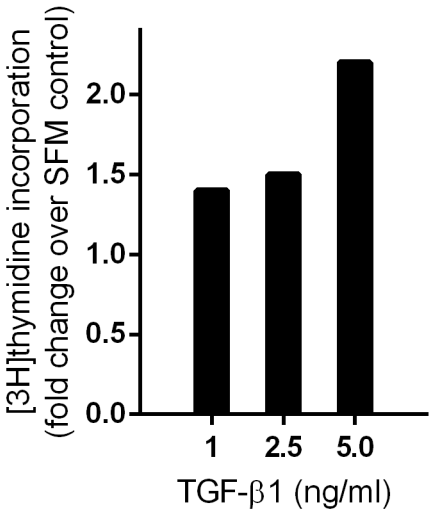

Figure A.2: **Data reproduced from Hetzel et al. 2005 showing TGF-β1 induce fibroblast proliferation** (70). Normal human lung fibroblasts were cultured in either serum free media (SFM), SFM + 1.0ng/ml TGF-β1, SFM + 2.5ng/ml TGF-β1, or SFM + 5.0ng/ml TGF-β1.

Appendix B

Supplementary Information for Chapter 4

Table B.1. Parameters and ranges used to generate baseline containment simulations

Parameter name	Value or range	Units
Mtb parameters		
Growth rate intracellular Mtb	1.003	cells
Growth rate extracellular Mtb	1.001	cells
Death rate of extracellular Mtb in caseum	1.5	cells
Core model parameters		
Diffusion time step	60	seconds
Molecular time step	6	seconds
Diffusion smoother time step	1.2	seconds
Number of smoother steps	0	n/a
Number of host cells causing caseation	10	n/a
Time to heal caseation	[1642, 2462]	days
Threshold for TNFα induced apoptosis	[1393, 2089]	molecules
Rate of TNFα induced apoptosis	[1.17e-6, 1.76e-6]	1/seconds
Minimum number of molecules allowing chemotaxis	[0.514, 0.77]	molecules
Maximum number of molecules allowing chemotaxis	[374, 562]	molecules
Diffusivity of TNFα	5.2e-8	cm^2/s
Diffusivity of IL10	5.2e-8	cm^2/s
Diffusivity of active TGF-β1	5.2e-8	cm^2/s
Diffusivity of chemokines	5.2e-8	cm^2/s
Degradation rate of TNFα	0.00158	molecules/molecular time step
Degradation rate of IL10	0.00048	molecules/molecular time step
Degradation rate of inactive TGF-β1	[9.28e-6, 1.39e-5]	molecules/molecular time step
Degradation rate of active TGF-β1	[8.0e-4, 0.0012]	molecules/molecular time step
Macrophage parameters		
Fraction of grid compartments with a macrophage	[0.024, 0.036]	n/a

Number of time steps before a resting macrophage can move	2	n/a
Number of time steps before an activated macrophage can move	16	n/a
Number of time steps before an infected macrophage can move	[112, 168]	n/a
Synthesis rate of TNFα ($MacTNF\alpha_{synth}$)	1.5	molecules/diffusion time step
Synthesis rate of CCL2	6	molecules/diffusion time step
Synthesis rate of CCL5	6	molecules/diffusion time step
Synthesis rate of CCL9	12	molecules/diffusion time step
Synthesis rate of IL10 by an activated macrophage	0.3	molecules/diffusion time step
Synthesis rate of IL10 by and infected macrophage	0.02	molecules/diffusion time step
Synthesis rate of Inactive TGF-β1 by macrophages	[1.4e-4, 2.12e-4]	molecules/diffusion time step
Number of bacteria a resting macrophage can phagocytose	1	n/a
Probability of resting macrophage killing bacteria ($MacKill_{baseline}$)	[0.23, 0.35]	n/a
Threshold for intracellular bacteria causing chronically infected macrophages	[8,12]	bacteria
Threshold for intracellular bacteria causing macrophage to burst	[13, 20]	bacteria
Number of bacteria an activated macrophage can phagocytose	[4, 6]	n/a
Fraction of inactive TGF-β1 activated by a mac ($Activation_{fraction}$)	[7e-5, 1e-4]	n/a
Amount of TGF-β1 that inhibits macrophages ($TGF\beta 1max_{Mac}$)	[0.01, 1]	molecules
Fraction of active TGF-β1 in a compartment bound by a mac	[1.1e-5, 1.7e-5]	n/a

Probability of an activated macrophage healing a caseated compartment in its Moore neighborhood	[0.0128, 0.0129]	n/a
T cell parameters		
Probability of a T cell moving to the same compartment as a macrophage	[0.05, 0.08]	n/a
Probability of a T cell moving to the same compartment as a T cell	0.08	n/a
Synthesis rate of TNFα by IFNγ-producing T-cell	0.15	molecules/diffusion time step
IFNγ-producing T-cell probability of inducing Fas/FasL mediated apoptosis	[0.0152, 0.0228]	n/a
Probability of IFNγ-producing T-cell to secrete TNFα	[0.048, 0.072]	n/a
Probability of IFNγ-producing T-cell to secrete TNFα	[0.288, 0.432]	n/a
Synthesis rate of TNFα by cytotoxic T-cell	0.015	molecules/diffusion time step
Probability of a cytotoxic T-cell killing a macrophage	[0.012, 0.18]	n/a
Probability of a cytotoxic T-cell killing a macrophage and all associated Mtb	[0.61, 0.91]	n/a
Probability of cytotoxic T-cell to secrete TNFα	[0.056, 0.084]	n/a
Synthesis rate of IL10 by regulatory T-cell	0.739	molecules/diffusion time step
Synthesis rate of TGF-β1 by regulatory T cell	[0.0067, 0.0101]	molecules/diffusion time step
Probability a regulatory T cell will deactivate an activated macrophage	[0.011, 0.016]	n/a
Amount of TGF-β1 that inhibits T cells ($TGF\beta 1max_{Tcell}$)	[0.01, 0.1]	molecules
Recruitment Parameters		
Maximum macrophage recruitment probability	[0.112, 0.168]	n/a

Maximum IFNγ-producing T cell recruitment probability	[0.112, 0.168]	n/a
Maximum cytotoxic T cell recruitment probability	[0.079, 0.12]	n/a
Maximum regulatory T cell recruitment probability	[0.0232, 0.0348]	n/a

* Indicates estimated parameters. All other parameters derived from prior work (193).

Table B.2: Significant PRCC values for TGF-β1 parameters introduced to this version of *GranSim* at day 30 PI. p > 0.001

Outputs \ Parameters	Degradation Rate of Active TGF-β1	Degradation Rate of Inactive TGF-β1	Synthesis of Inactive TGF-β1 by Macs	TGF-β1 Binding Rate by T cells	TGF-β1 Inhibition of Cytotoxic T cells	Synthesis of Inactive TGF-β1 by Regulatory T Cells
# Infected Macs		0.08			0.12	
# Chronically Infected Macs					0.08	
# Effector Cytotoxic T cells	0.09				0.08	
# Dead Regulatory T cells		0.08				
# Intracellular Mtb					0.13	
# Extracellular Mtb					0.13	
# Replicating Extracellular Mtb					0.12	
Total CFU					0.14	
Total CEQ					0.14	
# Mtb Killed by Apoptosis					0.14	
# Mtb Killed by Starvation					-0.13	
# Mtb Killed in Caseation					0.09	
Total TAG					0.13	
Total TNFα					0.14	
Total CCL2					0.13	
Total CCL5					0.13	
Total CXCL9					0.13	
Total Active TGF-β1	-0.34	-0.07	0.46			0.09
Total Inactive TGF-β1		-0.39	0.42			0.07

		Degradation Rate of Active TGF-β1	Degradation Rate of Inactive TGF-β1	Synthesis of Inactive TGF-β1 by Macs	TGF-β1 Binding Rate by T cells	TGF-β1 Inhibition of Cytotoxic T cells	Synthesis of Inactive TGF-β1 by Regulatory T Cells
Outputs	Total TNFα Induced Mac Apoptosis					0.13	
	TNFα Induced Resting Mac Apoptosis					0.10	
	TNFα Induced Infected Mac Apoptosis					0.12	
	TNFα Induced Chronically Infected Mac Apoptosis					0.16	
	TNFα Induced Activated Mac Apoptosis					0.07	
	Total Chronically Infected Mac Bursting				0.07	0.12	
	Total Resting Macs					0.10	
	Total Infected Macs					0.14	
	Total Chronically Infected Macs					0.14	
	Total Pet Hot					0.14	

The fraction of TGFB activated by macs, maximum TGFB bound by a macrophage, macrophage TGFB binding rate, and maximum TGFB bound by a T cell had no significant correlations at day 30 PI*

Table B.3: Significant PRCC values for TGF-β1 parameters introduced to this version of *GranSim* at day 200 PI. p > 0.001

Outputs \ Parameters	Degradation Rate of Active TGF-β1	Degradation Rate of Inactive TGF-β1	Synthesis of Inactive TGF-β1 by Macs	Fraction of TGF-β1 Activated by Macs	Macrophage TGF-β1 Binding Rate	Maximum TGF-β1 Bound by a T cell	TGF-β1 Inhibition of Cytotoxic T cells	Synthesis of Inactive TGF-β1 by Regulatory T Cells
# Total Macs							0.09	
# Resting Macs							0.08	
# Infected Macs		0.08					0.10	
# Chronically Infected Macs								
# Activated Macs		0.07					0.08	
# Dead Macs				-0.09				
# Total IFNg+ T cells							0.08	
# Active IFNg+ T cells							0.08	
# Down Regulated IFNg+ T cells								
# Dead IFNg+ T cells								
# Total Cytotoxic T cells							0.09	
# Effector Cytotoxic T cells		0.09						
# Total Regulatory T cells							0.07	
# Intracellular Mtb		0.08					0.09	
# Extracellular Mtb							0.09	
# Non-replicating Extracellular Mtb							0.09	
Total CFU		0.08					0.10	
Total CEQ		0.09					0.16	
# Mtb Killed by Apoptosis		0.09					0.17	
# Mtb Killed by Cytotoxicity		0.08					0.13	
# Mtb Killed by Fas/Fas-ligand		0.08					0.16	
# Mtb Killed by Macs		0.09					0.13	
# Mtb Killed in Caseation							0.14	
Total TAG		0.08					0.14	
Total TNF							0.08	
Total CCL2							0.08	
Total CCL5							0.10	
Total CXCL9							0.10	

		Degradation Rate of Active TGF-β1	Degradation Rate of Inactive TGF-β1	Synthesis of Inactive TGF-β1 by Macs	Fraction of TGF-β1 Activated by Macs	Macrophage TGF-β1 Binding Rate	Maximum TGF-β1 Bound by a T cell	TGF-β1 Inhibition of Cytotoxic T cells	Synthesis of Inactive TGF-β1 by Regulatory T Cells
Outputs	Total TAG							0.10	
	Total Active TGFB			0.07				0.09	
	Total Inactive TGFB		-0.28	0.23					0.15
	Total TNFα Induced Mac Apoptosis		0.08					0.13	
	TNFα Induced Resting Mac Apoptosis		0.07					0.11	
	TNFα Induced Infected Mac Apoptosis		0.09					0.14	
	Total Chronically Infected Mac Apoptosis							0.19	
	TNFα Induced Activated Mac Apoptosis		0.07					0.12	
	TNFα Induced T cell Apoptosis							0.11	
	Fas/FasL Killing		0.08					0.15	
	Cytotoxic Killing							0.12	
	Total Chronically Infected Mac Bursting		0.10					0.15	
	Total Pet Hot							0.08	

Macrophage TGFB binding rate, T cell TGFB binding rate had no significant correlations at day 200 PI*

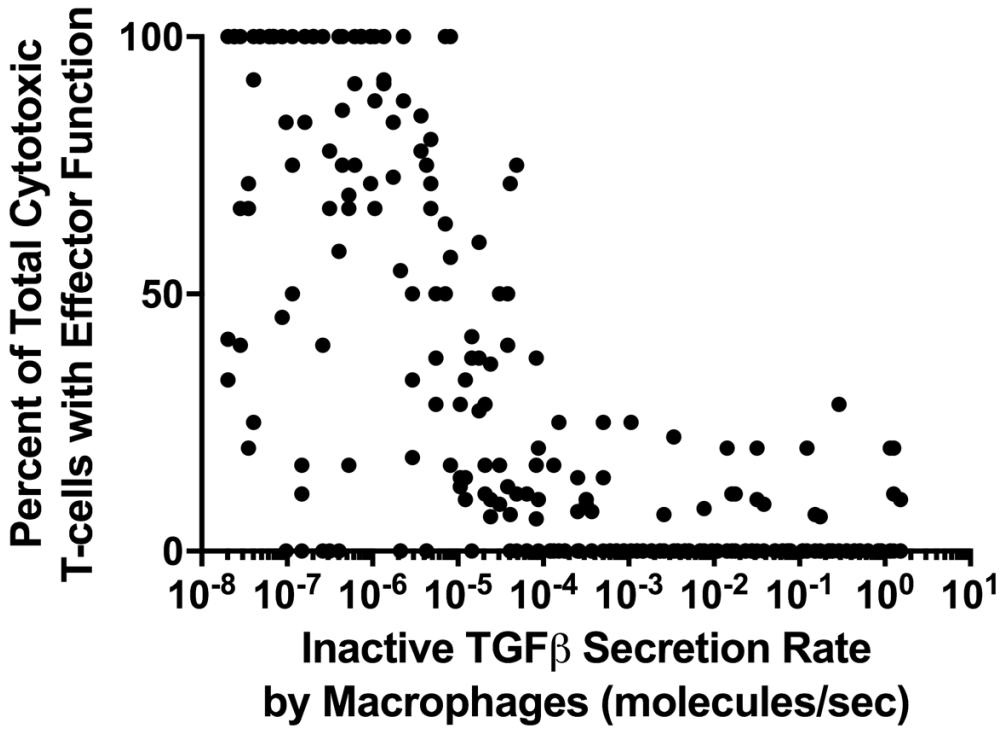

Figure B.1: Simulated decreased secretion of TGFβ by macrophages results in increasing percentage of effector cytotoxic T-cells at day 200. 300 granulomas were simulated for 200 days with differing rates of latent TGFβ secretion by macrophages. The rate of secretion by macrophages is plotted against percent of total cytotoxic T-cells that are effector cytotoxic T-cells at day 200.Effector cytotoxic T-cell activity shows sensitivity to different rates of TGF-β1 secretion.

Cytotoxic T-cell effector activity, and therefore bacterial killing efficiency, is inhibited by TGF-β1 signaling. In the absence of TGF-β1, effector cytotoxic T-cells in the granuloma are increased in number. Since macrophages are a major contributor to TGF-β1 levels in the granuloma, we compare how TGF-β1 secretion rates by macrophages affects the percent of effector cytotoxic T cells that are in granulomas (Figure. B.1). We predict there is a negative correlation between the secretion rate of TGF-β1 and the percent of effector cytotoxic T cells in the granuloma (Figure. B.1). In order to see a meaningful increase in the effector functions of cytotoxic T cells in our

simulations, the TGF-β1 secretion rate by macrophages required a decrease by several orders of magnitude (Figure. B.1).

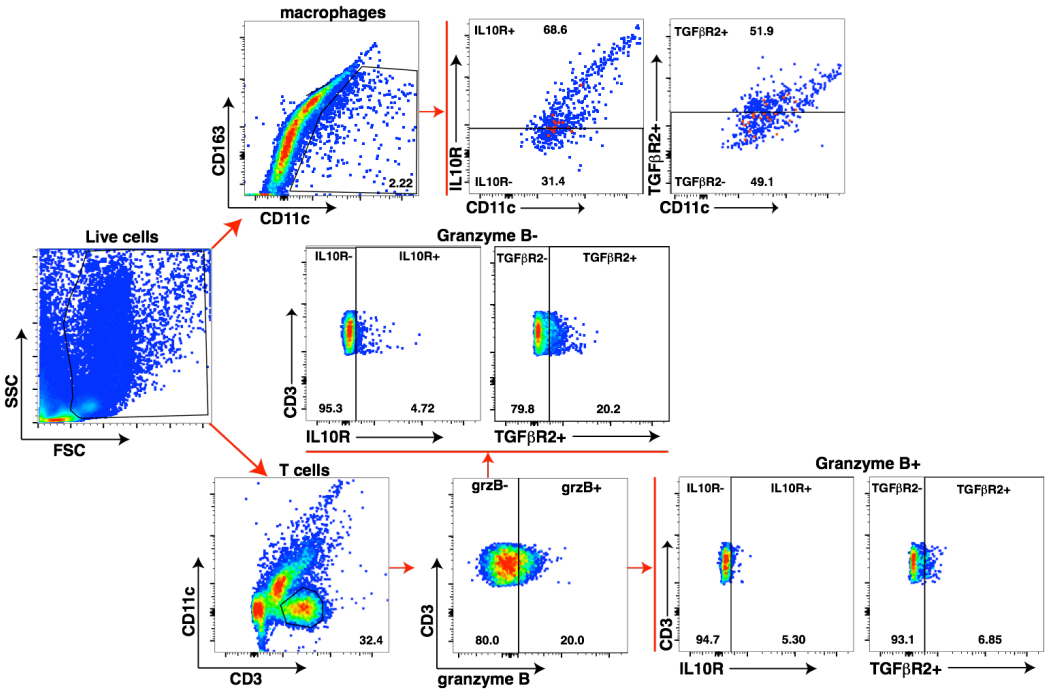

Figure B.2: Gating strategy for flow cytometry studies. Granulomas do not contain enough cells for gating controls, and so positive and negative gates were determined by gating on erythrocyte-lysed whole blood (not shown) and these gates were then applied to granuloma samples. Isolated granuloma cells were gated on viable cells to exclude small, low complexity objects that confound analysis and then macrophages and T cells were identified by surface marker expression. Epithelioid macrophages and T cells were identified as CD11c+CD163- and CD3+CD11c- cells, respectively. T cells underwent a second round of gating against granzyme B to differentiate cytotoxic (granzyme B+) and noncytotoxic (granzyme B-) T cells. Subsequent analysis was done by gating each population's primary surface marker (CD11c or CD3) against IL10R or TGFBR2 expression, and comparing the MFI of positive and negative populations.

Bibliography

1. Global Alliance against Chronic Respiratory Diseases. World Health Association; 2007.

2. Respiratory diseasesin the world: Realities of Today – Opportunities for Tomorrow. Sheffield, UK: Forum of International Respiratory Societies; 2013.

3. Walker CL, Rudan I, Liu L, Nair H, Theodoratou E, Bhutta ZA, et al. Global burden of childhood pneumonia and diarrhoea. Lancet. 2013;381(9875):1405-16.

4. Medical Expenditure Panel Survey Insurance Component Chartbook 2015. Rockville, MD: AHRQ; 2015.

5. Tilert T P-RR, Brody DJ. Lung obstruction among adults aged 40–79: United States, 2007–2012 [NCHS data brief]. Hyattsville, MD: National Center for Health Statistics; 2015 [no 180:[Available from: http://www.cdc.gov/nchs/products/databriefs/db180.htm.

6. Influenza. World Health Organization; March 2003.

7. Asthma Facts. United States Environmental Protection Agency; 2016.

8. Raghu G, Weycker D, Edelsberg J, Bradford WZ, Oster G. Incidence and prevalence of idiopathic pulmonary fibrosis. Am J Respir Crit Care Med. 2006;174(7):810-6.

9. Pulmonary Fibrosis Symptoms, Causes & Risk Factors: American Lung Association; 2016 [updated Oct. 13, 2016.

10. De Vries J, Kessels BL, Drent M. Quality of life of idiopathic pulmonary fibrosis patients. Eur Respir J. 2001;17(5):954-61.

11. Hodnett PA, Naidich DP. Fibrosing interstitial lung disease. A practical high-resolution computed tomography-based approach to diagnosis and management and a review of the literature. Am J Respir Crit Care Med. 2013;188(2):141-9.

12. Selman M, Thannickal VJ, Pardo A, Zisman DA, Martinez FJ, Lynch JP. Idiopathic Pulmonary Fibrosis: Pathogenesis and Therapeutic Approaches. Drugs. 2004;64(4):405-30.

13. Swigris JJ, Kuschner WG, Jacobs SS, Wilson SR, Gould MK. Health-related quality of life in patients with idiopathic pulmonary fibrosis: a systematic review. Thorax. 2005;60(7):588-94.

14. Patient Information Series: Idiopathic Pulmonary Fibrosis. In: Society AT, editor. 2011.

15. Pulmonary Fibrosis. 230 East Ohio Street, Suite 304, Chicago, Illinois 60611: Pulmonary Fibrosis GFoundation; 2016.

16. Daba MH, El-Tahir KE, Al-Arifi MN, Gubara OA. Drug-induced pulmonary fibrosis. Saudi Med J. 2004;25(6):700-6.

17. Maher TM, Wells AU, Laurent GJ. Idiopathic pulmonary fibrosis: multiple causes and multiple mechanisms? Eur Respir J. 2007;30(5):835-9.

18. Adamson IY. Drug-induced pulmonary fibrosis. Environ Health Perspect. 1984;55:25-36.

19. Baumgartner KB, Samet JM, Stidley CA, Colby TV, Waldron JA. Cigarette smoking: a risk factor for idiopathic pulmonary fibrosis. Am J Respir Crit Care Med. 1997;155(1):242-8.

20. Coomes SM, Farmen S, Wilke CA, Laouar Y, Moore BB. Severe gammaherpesvirus-induced pneumonitis and fibrosis in syngeneic bone marrow transplant mice is related to effects of transforming growth factor-beta. Am J Pathol. 2011;179(5):2382-96.

21. Cooper JA, Jr., White DA, Matthay RA. Drug-induced pulmonary disease. Part 1: Cytotoxic drugs. Am Rev Respir Dis. 1986;133(2):321-40.

22. Strieter RM. What differentiates normal lung repair and fibrosis? Inflammation, resolution of repair, and fibrosis. Proc Am Thorac Soc. 2008;5(3):305-10.

23. Wootton SC, Kim DS, Kondoh Y, Chen E, Lee JS, Song JW, et al. Viral infection in acute exacerbation of idiopathic pulmonary fibrosis. Am J Respir Crit Care Med. 2011;183(12):1698-702.

24. Buzan MT, Pop CM. State of the art in the diagnosis and management of interstitial lung disease. Clujul Med. 2015;88(2):116-23.

25. George G, Vaid U, Summer R. Therapeutic advances in Idiopathic Pulmonary Fibrosis. Clin Pharmacol Ther. 2015.

26. Loomis-King H, Flaherty KR, Moore BB. Pathogenesis, current treatments and future directions for idiopathic pulmonary fibrosis. Curr Opin Pharmacol. 2013;13(3):377-85.

27. Corte T, Bonella F, Crestani B, Demedts MG, Richeldi L, Coeck C, et al. Safety, tolerability and appropriate use of nintedanib in idiopathic pulmonary fibrosis. Respir Res. 2015;16(1):116.

28. Costabel U, Inoue Y, Richeldi L, Collard HR, Tschoepe I, Stowasser S, et al. Efficacy of Nintedanib in Idiopathic Pulmonary Fibrosis Across Pre-specified Subgroups in INPULSIS(R). Am J Respir Crit Care Med. 2015.

29. Dosanjh A, Ikonen T, Wan B, Morris RE. Pirfenidone: A novel anti-fibrotic agent and progressive chronic allograft rejection. Pulm Pharmacol Ther. 2002;15(5):433-7.

30. King TE, Jr., Bradford WZ, Castro-Bernardini S, Fagan EA, Glaspole I, Glassberg MK, et al. A phase 3 trial of pirfenidone in patients with idiopathic pulmonary fibrosis. N Engl J Med. 2014;370(22):2083-92.

31. Kreuter M. Pirfenidone: an update on clinical trial data and insights from everyday practice. Eur Respir Rev. 2014;23(131):111-7.

32. Roth GJ, Binder R, Colbatzky F, Dallinger C, Schlenker-Herceg R, Hilberg F, et al. Nintedanib: From Discovery to the Clinic. J Med Chem. 2014.

33. Xaubet A, Serrano-Mollar A, Ancochea J. Pirfenidone for the treatment of idiopathic pulmonary fibrosis. Expert Opin Pharmacother. 2014;15(2):275-81.

34. Koons C. Boehringer's New Lung Drug to Cost $96,000 a Year The Bloomberg Report: The Bloomberg Report; 2014 [Available from: http://www.bloomberg.com/news/articles/2014-10-20/boehringer-s-new-lung-drug-to-cost-96-000-a-year.

35. Ley B, Collard HR, King TE, Jr. Clinical course and prediction of survival in idiopathic pulmonary fibrosis. Am J Respir Crit Care Med. 2011;183(4):431-40.

36. Global tuberculosis report 2015. In: WHO, editor. 20th ed. Geneva: World Health Organization; 2015.

37. Flynn JL, Chan J. Tuberculosis: latency and reactivation. Infect Immun. 2001;69(7):4195-201.

38. Core Curriculum on Tuberculosis: What the Clinician Should Know. Sixth ed: Centers for Disease Control and Prevention; 2013 2013. 320 p.

39. Dorhoi A, Reece ST, Kaufmann SH. For better or for worse: the immune response against Mycobacterium tuberculosis balances pathology and protection. Immunol Rev. 2011;240(1):235-51.

40. Ramakrishnan L. Revisiting the role of the granuloma in tuberculosis. Nat Rev Immunol. 2012;12(5):352-66.

41. O'Garra A, Redford PS, McNab FW, Bloom CI, Wilkinson RJ, Berry MP. The immune response in tuberculosis. Annu Rev Immunol. 2013;31:475-527.

42. Lin PL, Coleman T, Carney JP, Lopresti BJ, Tomko J, Fillmore D, et al. Radiologic responses in cynomolgous macaques for assessing tuberculosis chemotherapy regimens. Antimicrob Agents Chemother. 2013.

43. Lin PL, Ford CB, Coleman MT, Myers AJ, Gawande R, Ioerger T, et al. Sterilization of granulomas is common in active and latent tuberculosis despite within-host variability in bacterial killing. Nat Med. 2014;20(1):75-9.

44. Cooper AM. Cell-mediated immune responses in tuberculosis. Annu Rev Immunol. 2009;27:393-422.

45. Silva Miranda M, Breiman A, Allain S, Deknuydt F, Altare F. The tuberculous granuloma: an unsuccessful host defence mechanism providing a safety shelter for the bacteria? Clin Dev Immunol. 2012;2012:139127.

46. Flynn JL, Chan J. Immunology of tuberculosis. Annu Rev Immunol. 2001;19:93-129.

47. Ehlers S, Schaible UE. The granuloma in tuberculosis: dynamics of a host-pathogen collusion. Front Immunol. 2012;3:411.

48. Davis JM, Ramakrishnan L. "The very pulse of the machine": the tuberculous granuloma in motion. Immunity. 2008;28(2):146-8.

49. DiFazio RM, Mattila JT, Klein EC, Cirrincione LR, Howard M, Wong EA, et al. Active transforming growth factor-beta is associated with phenotypic changes in granulomas after drug treatment in pulmonary tuberculosis. Fibrogenesis Tissue Repair. 2016;9:6.

50. Boe DM, Boule LA, Kovacs EJ. Innate immune responses in the ageing lung. Clin Exp Immunol. 2016.

51. Chiu C, Openshaw PJ. Antiviral B cell and T cell immunity in the lungs. Nat Immunol. 2015;16(1):18-26.

52. Whitsett JA, Alenghat T. Respiratory epithelial cells orchestrate pulmonary innate immunity. Nat Immunol. 2015;16(1):27-35.

53. Kopf M, Schneider C, Nobs SP. The development and function of lung-resident macrophages and dendritic cells. Nat Immunol. 2015;16(1):36-44.

54. Orme IM, Robinson RT, Cooper AM. The balance between protective and pathogenic immune responses in the TB-infected lung. Nat Immunol. 2015;16(1):57-63.

55. Lambrecht BN, Hammad H. The immunology of asthma. Nat Immunol. 2015;16(1):45-56.

56. Lin PL, Myers A, Smith L, Bigbee C, Bigbee M, Fuhrman C, et al. Tumor necrosis factor neutralization results in disseminated disease in acute and latent Mycobacterium tuberculosis infection with normal granuloma structure in a cynomolgus macaque model. Arthritis and Rheumatism. 2010;62(2):340-50.

57. Flynn JL, Gideon HP, Mattila JT, Lin PL. Immunology studies in non-human primate models of tuberculosis. Immunol Rev. 2015;264(1):60-73.

58. Mohan VP, Scanga CA, Yu K, Scott HM, Tanaka KE, Tsang E, et al. Effects of tumor necrosis factor alpha on host immune response in chronic persistent tuberculosis: possible role for limiting pathology. Infect Immun. 2001;69(3):1847-55.

59. Flynn JL, Chan J, Triebold KJ, Dalton DK, Stewart TA, Bloom BR. An essential role for interferon gamma in resistance to Mycobacterium tuberculosis infection. J Exp Med. 1993;178(6):2249-54.

60. Flynn JL, Chan J, Lin PL. Macrophages and control of granulomatous inflammation in tuberculosis. Mucosal Immunol. 2011;4(3):271-8.

61. Bergeron A, Soler P, Kambouchner M, Loiseau P, Milleron B, Valeyre D, et al. Cytokine profiles in idiopathic pulmonary fibrosis suggest an important role for TGF-beta and IL-10. Eur Respir J. 2003;22(1):69-76.

62. Broekelmann TJ, Limper AH, Colby TV, McDonald JA. Transforming growth factor beta 1 is present at sites of extracellular matrix gene expression in human pulmonary fibrosis. Proc Natl Acad Sci U S A. 1991;88(15):6642-6.

63. Brown BN, Price IM, Toapanta FR, DeAlmeida DR, Wiley CA, Ross TM, et al. An agent-based model of inflammation and fibrosis following particulate exposure in the lung. Math Biosci. 2011;231(2):186-96.

64. Denis M. Neutralization of transforming growth factor-beta 1 in a mouse model of immune-induced lung fibrosis. Immunology. 1994;82(4):584-90.

65. Di Guglielmo GM. TSP-1 in lung fibrosis. J Cell Commun Signal. 2010;4(4):185-6.

66. Epa AP, Thatcher TH, Pollock SJ, Wahl LA, Lyda E, Kottmann RM, et al. Normal Human Lung Epithelial Cells Inhibit Transforming Growth Factor-beta Induced Myofibroblast Differentiation via Prostaglandin E2. PLoS One. 2015;10(8):e0135266.

67. Hagimoto N, Kuwano K, Inoshima I, Yoshimi M, Nakamura N, Fujita M, et al. TGF-beta 1 as an enhancer of Fas-mediated apoptosis of lung epithelial cells. J Immunol. 2002;168(12):6470-8.

68. Hardie WD, Le Cras TD, Jiang K, Tichelaar JW, Azhar M, Korfhagen TR. Conditional expression of transforming growth factor-alpha in adult mouse lung causes pulmonary fibrosis. Am J Physiol Lung Cell Mol Physiol. 2004;286(4):L741-9.

69. Hernandez-Pando R, Orozco H, Arriaga K, Sampieri A, Larriva-Sahd J, Madrid-Marina V. Analysis of the local kinetics and localization of interleukin-1 alpha, tumour necrosis factor-alpha and transforming growth factor-beta, during the course of experimental pulmonary tuberculosis. Immunology. 1997;90(4):607-17.

70. Hetzel M, Bachem M, Anders D, Trischler G, Faehling M. Different effects of growth factors on proliferation and matrix production of normal and fibrotic human lung fibroblasts. Lung. 2005;183(4):225-37.

71. Jain R, Shaul PW, Borok Z, Willis BC. Endothelin-1 induces alveolar epithelial-mesenchymal transition through endothelin type A receptor-mediated production of TGF-beta1. Am J Respir Cell Mol Biol. 2007;37(1):38-47.

72. Kalter VG, Brody AR. Receptors for transforming growth factor-beta (TGF-beta) on rat lung fibroblasts have higher affinity for TGF-beta 1 than for TGF-beta 2. Journal Name: American Journal of Respiratory Cell and Molecular Biology; (USA); Journal Volume: 4:5. 1991:Medium: X; Size: Pages: 397-407.

73. Kapanci Y, Desmouliere A, Pache JC, Redard M, Gabbiani G. Cytoskeletal protein modulation in pulmonary alveolar myofibroblasts during idiopathic pulmonary fibrosis. Possible role of transforming growth factor beta and tumor necrosis factor alpha. Am J Respir Crit Care Med. 1995;152(6 Pt 1):2163-9.

74. Khalil N, Bereznay O, Sporn M, Greenberg AH. Macrophage production of transforming growth factor beta and fibroblast collagen synthesis in chronic pulmonary inflammation. J Exp Med. 1989;170(3):727-37.

75. Khalil N, O'Connor RN, Flanders KC, Unruh H. TGF-beta 1, but not TGF-beta 2 or TGF-beta 3, is differentially present in epithelial cells of advanced pulmonary fibrosis: an immunohistochemical study. Am J Respir Cell Mol Biol. 1996;14(2):131-8.

76. Khalil N, Parekh TV, O'Connor R, Antman N, Kepron W, Yehaulaeshet T, et al. Regulation of the effects of TGF-beta 1 by activation of latent TGF-beta 1 and

differential expression of TGF-beta receptors (T beta R-I and T beta R-II) in idiopathic pulmonary fibrosis. Thorax. 2001;56(12):907-15.

77. Koli K, Myllarniemi M, Keski-Oja J, Kinnula VL. Transforming growth factor-beta activation in the lung: focus on fibrosis and reactive oxygen species. Antioxid Redox Signal. 2008;10(2):333-42.

78. Lilja-Maula L, Syrja P, Laurila HP, Sutinen E, Ronty M, Koli K, et al. Comparative Study of Transforming Growth Factor-beta Signalling and Regulatory Molecules in Human and Canine Idiopathic Pulmonary Fibrosis. J Comp Pathol. 2014;150(4):399-407.

79. Nakagome K, Dohi M, Okunishi K, Tanaka R, Miyazaki J, Yamamoto K. In vivo IL-10 gene delivery attenuates bleomycin induced pulmonary fibrosis by inhibiting the production and activation of TGF-beta in the lung. Thorax. 2006;61(10):886-94.

80. Piguet PF, Collart MA, Grau GE, Sappino AP, Vassalli P. Requirement of tumour necrosis factor for development of silica-induced pulmonary fibrosis. Nature. 1990;344(6263):245-7.

81. Puthawala K, Hadjiangelis N, Jacoby SC, Bayongan E, Zhao Z, Yang Z, et al. Inhibition of integrin alpha(v)beta6, an activator of latent transforming growth factor-beta, prevents radiation-induced lung fibrosis. Am J Respir Crit Care Med. 2008;177(1):82-90.

82. Togo S, Liu X, Wang X, Sugiura H, Kamio K, Kawasaki S, et al. PDE4 inhibitors roflumilast and rolipram augment PGE2 inhibition of TGF-{beta}1-stimulated fibroblasts. Am J Physiol Lung Cell Mol Physiol. 2009;296(6):L959-69.

83. Warsinske HC, Wheaton AK, Kim KK, Linderman JJ, Moore BB, Kirschner DE. Computational Modeling Predicts Simultaneous Targeting of Fibroblasts and Epithelial Cells Is Necessary for Treatment of Pulmonary Fibrosis. Frontiers in Pharmacology. 2016;7(183).

84. Willis BC, Borok Z. TGF-beta-induced EMT: mechanisms and implications for fibrotic lung disease. Am J Physiol Lung Cell Mol Physiol. 2007;293(3):L525-34.

85. Bonecini-Almeida MG, Ho JL, Boechat N, Huard RC, Chitale S, Doo H, et al. Down-modulation of lung immune responses by interleukin-10 and transforming growth factor beta (TGF-beta) and analysis of TGF-beta receptors I and II in active tuberculosis. Infect Immun. 2004;72(5):2628-34.

86. Camoretti-Mercado B, Solway J. Transforming growth factor-beta1 and disorders of the lung. Cell Biochem Biophys. 2005;43(1):131-48.

87. Coomes SM, Wilke CA, Moore TA, Moore BB. Induction of TGF-beta 1, not regulatory T cells, impairs antiviral immunity in the lung following bone marrow transplant. J Immunol. 2010;184(9):5130-40.

88. Crosby LM, Waters CM. Epithelial repair mechanisms in the lung. American Journal of Physiology - Lung Cellular and Molecular Physiology. 2010;298(6):L715-L31.

89. Fine A, Goldstein RH. The effect of transforming growth factor-beta on cell proliferation and collagen formation by lung fibroblasts. J Biol Chem. 1987;262(8):3897-902.

90. Toossi Z, Gogate P, Shiratsuchi H, Young T, Ellner JJ. Enhanced production of TGF-beta by blood monocytes from patients with active tuberculosis and presence of TGF-beta in tuberculous granulomatous lung lesions. J Immunol. 1995;154(1):465-73.

91. Wheaton AK, Velikoff M, Agarwal M, Loo TT, Horowitz JC, Sisson TH, et al. The Vitronectin RGD motif regulates TGFbeta Induced Alveolar Epithelial Cell Apoptosis. Am J Physiol Lung Cell Mol Physiol. 2016:ajplung 00424 2015.

92. Bettinger DA, Yager DR, Diegelmann RF, Cohen IK. The effect of TGF-beta on keloid fibroblast proliferation and collagen synthesis. Plast Reconstr Surg. 1996;98(5):827-33.

93. de Caestecker M. The transforming growth factor-beta superfamily of receptors. Cytokine Growth Factor Rev. 2004;15(1):1-11.

94. Dexheimer V, Gabler J, Bomans K, Sims T, Omlor G, Richter W. Differential expression of TGF-beta superfamily members and role of Smad1/5/9-signalling in chondral versus endochondral chondrocyte differentiation. Sci Rep. 2016;6:36655.

95. Annes JP, Munger JS, Rifkin DB. Making sense of latent TGFbeta activation. J Cell Sci. 2003;116(Pt 2):217-24.

96. Assoian RK, Komoriya A, Meyers CA, Miller DM, Sporn MB. Transforming growth factor-beta in human platelets. Identification of a major storage site, purification, and characterization. J Biol Chem. 1983;258(11):7155-60.

97. Horiguchi M, Ota M, Rifkin DB. Matrix control of transforming growth factor-beta function. J Biochem. 2012;152(4):321-9.

98. Finnson KW, McLean S, Di Guglielmo GM, Philip A. Dynamics of Transforming Growth Factor Beta Signaling in Wound Healing and Scarring. Adv Wound Care (New Rochelle). 2013;2(5):195-214.

99. Rider CC, Mulloy B. Bone morphogenetic protein and growth differentiation factor cytokine families and their protein antagonists. Biochem J. 2010;429(1):1-12.

100. Thannickal VJ, Lee DY, White ES, Cui Z, Larios JM, Chacon R, et al. Myofibroblast differentiation by transforming growth factor-beta1 is dependent on cell adhesion and integrin signaling via focal adhesion kinase. J Biol Chem. 2003;278(14):12384-9.

101. Kubiczkova L, Sedlarikova L, Hajek R, Sevcikova S. TGF-beta - an excellent servant but a bad master. J Transl Med. 2012;10:183.

102. Cheifetz S, Like B, Massague J. Cellular distribution of type I and type II receptors for transforming growth factor-beta. J Biol Chem. 1986;261(21):9972-8.

103. Strutz F, Zeisberg M, Renziehausen A, Raschke B, Becker V, van Kooten C, et al. TGF-beta 1 induces proliferation in human renal fibroblasts via induction of basic fibroblast growth factor (FGF-2). Kidney Int. 2001;59(2):579-92.

104. Cordeiro MF, Bhattacharya SS, Schultz GS, Khaw PT. TGF-beta1, -beta2, and -beta3 in vitro: biphasic effects on Tenon's fibroblast contraction, proliferation, and migration. Invest Ophthalmol Vis Sci. 2000;41(3):756-63.

105. Desmouliere A, Geinoz A, Gabbiani F, Gabbiani G. Transforming growth factor-beta 1 induces alpha-smooth muscle actin expression in granulation tissue myofibroblasts and in quiescent and growing cultured fibroblasts. J Cell Biol. 1993;122(1):103-11.

106. Yanagisawa K, Osada H, Masuda A, Kondo M, Saito T, Yatabe Y, et al. Induction of apoptosis by Smad3 and down-regulation of Smad3 expression in response to TGF-beta in human normal lung epithelial cells. Oncogene. 1998;17(13):1743-7.

107. Kuwano K. Involvement of epithelial cell apoptosis in interstitial lung diseases. Intern Med. 2008;47(5):345-53.

108. Coffey RJ, Jr., Bascom CC, Sipes NJ, Graves-Deal R, Weissman BE, Moses HL. Selective inhibition of growth-related gene expression in murine keratinocytes by transforming growth factor beta. Mol Cell Biol. 1988;8(8):3088-93.

109. Pietenpol JA, Stein RW, Moran E, Yaciuk P, Schlegel R, Lyons RM, et al. TGF-beta 1 inhibition of c-myc transcription and growth in keratinocytes is abrogated by viral transforming proteins with pRB binding domains. Cell. 1990;61(5):777-85.

110. Ranges GE, Figari IS, Espevik T, Palladino MA, Jr. Inhibition of cytotoxic T cell development by transforming growth factor beta and reversal by recombinant tumor necrosis factor alpha. J Exp Med. 1987;166(4):991-8.

111. Li MO, Wan YY, Flavell RA. T cell-produced transforming growth factor-beta1 controls T cell tolerance and regulates Th1- and Th17-cell differentiation. Immunity. 2007;26(5):579-91.

112. Marie JC, Liggitt D, Rudensky AY. Cellular mechanisms of fatal early-onset autoimmunity in mice with the T cell-specific targeting of transforming growth factor-beta receptor. Immunity. 2006;25(3):441-54.

113. Leveen P, Carlsen M, Makowska A, Oddsson S, Larsson J, Goumans MJ, et al. TGF-beta type II receptor-deficient thymocytes develop normally but demonstrate increased CD8+ proliferation in vivo. Blood. 2005;106(13):4234-40.

114. Kronenberg M, Rudensky A. Regulation of immunity by self-reactive T cells. Nature. 2005;435(7042):598-604.

115. Liston A, Rudensky AY. Thymic development and peripheral homeostasis of regulatory T cells. Curr Opin Immunol. 2007;19(2):176-85.

116. Liu Y, Zhang P, Li J, Kulkarni AB, Perruche S, Chen W. A critical function for TGF-beta signaling in the development of natural CD4+CD25+Foxp3+ regulatory T cells. Nat Immunol. 2008;9(6):632-40.

117. Bendelac A, Rivera MN, Park SH, Roark JH. Mouse CD1-specific NK1 T cells: development, specificity, and function. Annu Rev Immunol. 1997;15:535-62.

118. Afzali B, Mitchell P, Lechler RI, John S, Lombardi G. Translational mini-review series on Th17 cells: induction of interleukin-17 production by regulatory T cells. Clin Exp Immunol. 2010;159(2):120-30.

119. Alleva DG, Burger CJ, Elgert KD. Tumor-induced regulation of suppressor macrophage nitric oxide and TNF-alpha production. Role of tumor-derived IL-10, TGF-beta, and prostaglandin E2. J Immunol. 1994;153(4):1674-86.

120. Champsi J, Young LS, Bermudez LE. Production of TNF-alpha, IL-6 and TGF-beta, and expression of receptors for TNF-alpha and IL-6, during murine Mycobacterium avium infection. Immunology. 1995;84(4):549-54.

121. Espevik T, Figari IS, Shalaby MR, Lackides GA, Lewis GD, Shepard HM, et al. Inhibition of cytokine production by cyclosporin A and transforming growth factor beta. J Exp Med. 1987;166(2):571-6.

122. Fine A, Poliks CF, Donahue LP, Smith BD, Goldstein RH. The differential effect of prostaglandin E2 on transforming growth factor-beta and insulin-induced collagen formation in lung fibroblasts. J Biol Chem. 1989;264(29):16988-91.

123. Huss DJ, Winger RC, Cox GM, Guerau-de-Arellano M, Yang Y, Racke MK, et al. TGF-beta signaling via Smad4 drives IL-10 production in effector Th1 cells and reduces T-cell trafficking in EAE. Eur J Immunol. 2011;41(10):2987-96.

124. Jarry A, Bossard C, Bou-Hanna C, Masson D, Espaze E, Denis MG, et al. Mucosal IL-10 and TGF-beta play crucial roles in preventing LPS-driven, IFN-gamma-mediated epithelial damage in human colon explants. J Clin Invest. 2008;118(3):1132-42.

125. Chen ML, Pittet MJ, Gorelik L, Flavell RA, Weissleder R, von Boehmer H, et al. Regulatory T cells suppress tumor-specific CD8 T cell cytotoxicity through TGF-beta signals in vivo. Proc Natl Acad Sci U S A. 2005;102(2):419-24.

126. Laiho M, DeCaprio JA, Ludlow JW, Livingston DM, Massague J. Growth inhibition by TGF-beta linked to suppression of retinoblastoma protein phosphorylation. Cell. 1990;62(1):175-85.

127. Nemeth K, Keane-Myers A, Brown JM, Metcalfe DD, Gorham JD, Bundoc VG, et al. Bone marrow stromal cells use TGF-beta to suppress allergic responses in a mouse model of ragweed-induced asthma. Proc Natl Acad Sci U S A. 2010;107(12):5652-7.

128. Vodovotz Y, Bogdan C, Paik J, Xie QW, Nathan C. Mechanisms of suppression of macrophage nitric oxide release by transforming growth factor beta. J Exp Med. 1993;178(2):605-13.

129. Ding A, Nathan CF, Graycar J, Derynck R, Stuehr DJ, Srimal S. Macrophage deactivating factor and transforming growth factors-beta 1 -beta 2 and -beta 3 inhibit induction of macrophage nitrogen oxide synthesis by IFN-gamma. J Immunol. 1990;145(3):940-4.

130. Gorelik L, Flavell RA. Abrogation of TGFbeta signaling in T cells leads to spontaneous T cell differentiation and autoimmune disease. Immunity. 2000;12(2):171-81.

131. Hirsch CS, Ellner JJ, Blinkhorn R, Toossi Z. In vitro restoration of T cell responses in tuberculosis and augmentation of monocyte effector function against Mycobacterium tuberculosis by natural inhibitors of transforming growth factor beta. Proc Natl Acad Sci U S A. 1997;94(8):3926-31.

132. Hirsch CS, Hussain R, Toossi Z, Dawood G, Shahid F, Ellner JJ. Cross-modulation by transforming growth factor beta in human tuberculosis: suppression of antigen-driven blastogenesis and interferon gamma production. Proc Natl Acad Sci U S A. 1996;93(8):3193-8.

133. Hirsch CS, Yoneda T, Averill L, Ellner JJ, Toossi Z. Enhancement of intracellular growth of Mycobacterium tuberculosis in human monocytes by transforming growth factor-beta 1. J Infect Dis. 1994;170(5):1229-37.

134. Kehrl JH, Wakefield LM, Roberts AB, Jakowlew S, Alvarez-Mon M, Derynck R, et al. Production of transforming growth factor beta by human T lymphocytes and its potential role in the regulation of T cell growth. J Exp Med. 1986;163(5):1037-50.

135. Langermans JA, Nibbering PH, Van Vuren-Van Der Hulst ME, Van Furth R. Transforming growth factor-beta suppresses interferon-gamma-induced toxoplasmastatic activity in murine macrophages by inhibition of tumour necrosis factor-alpha production. Parasite Immunol. 2001;23(4):169-75.

136. Laouar Y, Sutterwala FS, Gorelik L, Flavell RA. Transforming growth factor-beta controls T helper type 1 cell development through regulation of natural killer cell interferon-gamma. Nat Immunol. 2005;6(6):600-7.

137. Laouar Y, Town T, Jeng D, Tran E, Wan Y, Kuchroo VK, et al. TGF-beta signaling in dendritic cells is a prerequisite for the control of autoimmune encephalomyelitis. Proc Natl Acad Sci U S A. 2008;105(31):10865-70.

138. Lee YJ, Han Y, Lu HT, Nguyen V, Qin H, Howe PH, et al. TGF-beta suppresses IFN-gamma induction of class II MHC gene expression by inhibiting class II transactivator messenger RNA expression. J Immunol. 1997;158(5):2065-75.

139. Lucas PJ, Kim SJ, Melby SJ, Gress RE. Disruption of T cell homeostasis in mice expressing a T cell-specific dominant negative transforming growth factor beta II receptor. J Exp Med. 2000;191(7):1187-96.

140. Moses HL, Yang EY, Pietenpol JA. TGF-beta stimulation and inhibition of cell proliferation: new mechanistic insights. Cell. 1990;63(2):245-7.

141. Prud'homme GJ, Piccirillo CA. The inhibitory effects of transforming growth factor-beta-1 (TGF-beta1) in autoimmune diseases. J Autoimmun. 2000;14(1):23-42.

142. Reardon C, McKay DM. TGF-beta suppresses IFN-gamma-STAT1-dependent gene transcription by enhancing STAT1-PIAS1 interactions in epithelia but not monocytes/macrophages. J Immunol. 2007;178(7):4284-95.

143. Witte MB, Barbul A. General principles of wound healing. Surg Clin North Am. 1997;77(3):509-28.

144. Clark RA, Lanigan JM, DellaPelle P, Manseau E, Dvorak HF, Colvin RB. Fibronectin and fibrin provide a provisional matrix for epidermal cell migration during wound reepithelialization. J Invest Dermatol. 1982;79(5):264-9.

145. Dale PD, Sherratt JA, Maini PK. A mathematical model for collagen fibre formation during foetal and adult dermal wound healing. Proc Biol Sci. 1996;263(1370):653-60.

146. Dale PD, Sherratt JA, Maini PK. Role of fibroblast migration in collagen fiber formation during fetal and adult dermal wound healing. Bulletin of mathematical biology. 1997;59(6):1077-100.

147. Desmoulière A, Chaponnier C, Gabbiani G. Perspective Article: Tissue repair, contraction, and the myofibroblast. Wound Repair and Regeneration. 2005;13(1):7-12.

148. Diegelmann RF, Evans MC. Wound healing: an overview of acute, fibrotic and delayed healing. Front Biosci. 2004;9:283-9.

149. Goldman R. Growth factors and chronic wound healing: past, present, and future. Adv Skin Wound Care. 2004;17(1):24-35.

150. Guo S, Dipietro LA. Factors affecting wound healing. J Dent Res. 2010;89(3):219-29.

151. Lawrence DA. Transforming growth factor-beta: a general review. Eur Cytokine Netw. 1996;7(3):363-74.

152. Midwood KS, Williams LV, Schwarzbauer JE. Tissue repair and the dynamics of the extracellular matrix. Int J Biochem Cell Biol. 2004;36(6):1031-7.

153. Rivera AE, Spencer JM. Clinical aspects of full-thickness wound healing. Clin Dermatol. 2007;25(1):39-48.

154. Roberts AB, Frolik CA, Anzano MA, Sporn MB. Transforming growth factors from neoplastic and nonneoplastic tissues. Fed Proc. 1983;42(9):2621-6.

155. Robson MC, Steed DL, Franz MG. Wound healing: biologic features and approaches to maximize healing trajectories. Curr Probl Surg. 2001;38(2):72-140.

156. Velnar T, Bailey T, Smrkolj V. The wound healing process: an overview of the cellular and molecular mechanisms. J Int Med Res. 2009;37(5):1528-42.

157. Cilfone NA, Ford CB, Marino S, Mattila JT, Gideon HP, Flynn JL, et al. Computational modeling predicts IL-10 control of lesion sterilization by balancing early host immunity-mediated antimicrobial responses with caseation during mycobacterium tuberculosis infection. J Immunol. 2015;194(2):664-77.

158. Cilfone NA, Perry CR, Kirschner DE, Linderman JJ. Multi-scale modeling predicts a balance of tumor necrosis factor-alpha and interleukin-10 controls the

granuloma environment during Mycobacterium tuberculosis infection. PLoS One. 2013;8(7):e68680.

159. Fallahi-Sichani M, El-Kebir M, Marino S, Kirschner DE, Linderman JJ. Multiscale computational modeling reveals a critical role for TNF-alpha receptor 1 dynamics in tuberculosis granuloma formation. J Immunol. 2011;186(6):3472-83.

160. Fallahi-Sichani M, Flynn JL, Linderman JJ, Kirschner DE. Differential risk of tuberculosis reactivation among anti-TNF therapies is due to drug binding kinetics and permeability. J Immunol. 2012;188(7):3169-78.

161. Fallahi-Sichani M, Kirschner DE, Linderman JJ. NF-kappaB Signaling Dynamics Play a Key Role in Infection Control in Tuberculosis. Front Physiol. 2012;3:170.

162. Fallahi-Sichani M, Schaller MA, Kirschner DE, Kunkel SL, Linderman JJ. Identification of key processes that control tumor necrosis factor availability in a tuberculosis granuloma. PLoS Comput Biol. 2010;6(5):e1000778.

163. Gideon HP, Phuah J, Myers AJ, Bryson BD, Rodgers MA, Coleman MT, et al. Variability in tuberculosis granuloma T cell responses exists, but a balance of pro- and anti-inflammatory cytokines is associated with sterilization. PLoS Pathog. 2015;11(1):e1004603.

164. Marino S, Myers A, Flynn JL, Kirschner DE. TNF and IL-10 are major factors in modulation of the phagocytic cell environment in lung and lymph node in tuberculosis: a next-generation two-compartmental model. J Theor Biol. 2010;265(4):586-98.

165. Marino S, Sud D, Plessner H, Lin PL, Chan J, Flynn JL, et al. Differences in reactivation of tuberculosis induced from anti-TNF treatments are based on bioavailability in granulomatous tissue. PLoS Comput Biol. 2007;3(10):1909-24.

166. Moore AE, Greenhough A, Roberts HR, Hicks DJ, Patsos HA, Williams AC, et al. HGF/Met signalling promotes PGE(2) biogenesis via regulation of COX-2 and 15-PGDH expression in colorectal cancer cells. Carcinogenesis. 2009;30(10):1796-804.

167. Moore BB, Ballinger MN, White ES, Green ME, Herrygers AB, Wilke CA, et al. Bleomycin-induced E prostanoid receptor changes alter fibroblast responses to prostaglandin E2. J Immunol. 2005;174(9):5644-9.

168. Thomas PE, Peters-Golden M, White ES, Thannickal VJ, Moore BB. PGE(2) inhibition of TGF-beta1-induced myofibroblast differentiation is Smad-independent but involves cell shape and adhesion-dependent signaling. Am J Physiol Lung Cell Mol Physiol. 2007;293(2):L417-28.

169. Warsinske HC, Ashley SL, Linderman JJ, Moore BB, Kirschner DE. Identifying Mechanisms of Homeostatic Signaling in Fibroblast Differentiation. Bulletin of mathematical biology. 2015;77(8):1556-82.

170. Flynn JL, Goldstein MM, Chan J, Triebold KJ, Pfeffer K, Lowenstein CJ, et al. Tumor necrosis factor-alpha is required in the protective immune response against Mycobacterium tuberculosis in mice. Immunity. 1995;2(6):561-72.

171. Saunders BM, Briscoe H, Britton WJ. T cell-derived tumour necrosis factor is essential, but not sufficient, for protection against Mycobacterium tuberculosis infection. Clin Exp Immunol. 2004;137(2):279-87.

172. Couper KN, Blount DG, Riley EM. IL-10: the master regulator of immunity to infection. J Immunol. 2008;180(9):5771-7.

173. Redford PS, Boonstra A, Read S, Pitt J, Graham C, Stavropoulos E, et al. Enhanced protection to Mycobacterium tuberculosis infection in IL-10-deficient mice is accompanied by early and enhanced Th1 responses in the lung. Eur J Immunol. 2010;40(8):2200-10.

174. Redford PS, Murray PJ, O'Garra A. The role of IL-10 in immune regulation during M. tuberculosis infection. Mucosal Immunol. 2011;4(3):261-70.

175. Moore KW, de Waal Malefyt R, Coffman RL, O'Garra A. Interleukin-10 and the interleukin-10 receptor. Annu Rev Immunol. 2001;19:683-765.

176. Kamanaka M, Kim ST, Wan YY, Sutterwala FS, Lara-Tejero M, Galan JE, et al. Expression of interleukin-10 in intestinal lymphocytes detected by an interleukin-10 reporter knockin tiger mouse. Immunity. 2006;25(6):941-52.

177. Bhattacharyya S, Sen P, Wallet M, Long B, Baldwin AS, Jr., Tisch R. Immunoregulation of dendritic cells by IL-10 is mediated through suppression of the PI3K/Akt pathway and of IkappaB kinase activity. Blood. 2004;104(4):1100-9.

178. de Waal Malefyt R, Abrams J, Bennett B, Figdor CG, de Vries JE. Interleukin 10(IL-10) inhibits cytokine synthesis by human monocytes: an autoregulatory role of IL-10 produced by monocytes. J Exp Med. 1991;174(5):1209-20.

179. Higgins DM, Sanchez-Campillo J, Rosas-Taraco AG, Lee EJ, Orme IM, Gonzalez-Juarrero M. Lack of IL-10 alters inflammatory and immune responses during pulmonary Mycobacterium tuberculosis infection. Tuberculosis (Edinb). 2009;89(2):149-57.

180. Yamamoto T, Eckes B, Krieg T. Effect of interleukin-10 on the gene expression of type I collagen, fibronectin, and decorin in human skin fibroblasts: differential regulation by transforming growth factor-beta and monocyte chemoattractant protein-1. Biochem Biophys Res Commun. 2001;281(1):200-5.

181. Sziksz E, Pap D, Lippai R, Beres NJ, Fekete A, Szabo AJ, et al. Fibrosis Related Inflammatory Mediators: Role of the IL-10 Cytokine Family. Mediators Inflamm. 2015;2015:764641.

182. Liechty KW, Kim HB, Adzick NS, Crombleholme TM. Fetal wound repair results in scar formation in interleukin-10-deficient mice in a syngeneic murine model of scarless fetal wound repair. J Pediatr Surg. 2000;35(6):866-72; discussion 72-3.

183. Maeda H, Kuwahara H, Ichimura Y, Ohtsuki M, Kurakata S, Shiraishi A. TGF-beta enhances macrophage ability to produce IL-10 in normal and tumor-bearing mice. J Immunol. 1995;155(10):4926-32.

184. Sanjabi S, Zenewicz LA, Kamanaka M, Flavell RA. Anti-inflammatory and pro-inflammatory roles of TGF-beta, IL-10, and IL-22 in immunity and autoimmunity. Curr Opin Pharmacol. 2009;9(4):447-53.

185. Reinhold D, Bank U, Buhling F, Lendeckel U, Ansorge S. Transforming growth factor beta 1 inhibits interleukin-10 mRNA expression and production in pokeweed mitogen-stimulated peripheral blood mononuclear cells and T cells. J Interferon Cytokine Res. 1995;15(8):685-90.

186. Van Vlasselaer P, Borremans B, van Gorp U, Dasch JR, De Waal-Malefyt R. Interleukin 10 inhibits transforming growth factor-beta (TGF-beta) synthesis required for osteogenic commitment of mouse bone marrow cells. J Cell Biol. 1994;124(4):569-77.

187. Lama V, Moore BB, Christensen P, Toews GB, Peters-Golden M. Prostaglandin E2 synthesis and suppression of fibroblast proliferation by alveolar epithelial cells is cyclooxygenase-2-dependent. Am J Respir Cell Mol Biol. 2002;27(6):752-8.

188. Moore BB, Peters-Golden M, Christensen PJ, Lama V, Kuziel WA, Paine R, 3rd, et al. Alveolar epithelial cell inhibition of fibroblast proliferation is regulated by MCP-1/CCR2 and mediated by PGE2. Am J Physiol Lung Cell Mol Physiol. 2003;284(2):L342-9.

189. Hinz B, Celetta G, Tomasek JJ, Gabbiani G, Chaponnier C. Alpha-smooth muscle actin expression upregulates fibroblast contractile activity. Mol Biol Cell. 2001;12(9):2730-41.

190. Marino S, Gideon HP, Gong C, Mankad S, McCrone JT, Lin PL, et al. Computational and Empirical Studies Predict Mycobacterium tuberculosis-Specific T Cells as a Biomarker for Infection Outcome. PLoS Comput Biol. 2016;12(4):e1004804.

191. Mi Q, Riviere B, Clermont G, Steed DL, Vodovotz Y. Agent-based model of inflammation and wound healing: insights into diabetic foot ulcer pathology and the role of transforming growth factor-beta1. Wound Repair Regen. 2007;15(5):671-82.

192. Pienaar E, Dartois V, Linderman JJ, Kirschner DE. In silico evaluation and exploration of antibiotic tuberculosis treatment regimens. BMC Syst Biol. 2015;9:79.

193. Pienaar E, Matern WM, Linderman JJ, Bader JS, Kirschner DE. Multiscale Model of Mycobacterium tuberculosis Infection Maps Metabolite and Gene Perturbations to Granuloma Sterilization Predictions. Infect Immun. 2016;84(5):1650-69.

194. Price I, Ermentrout B, Zamora R, Wang B, Azhar N, Mi Q, et al. In vivo, in vitro, and in silico studies suggest a conserved immune module that regulates malaria parasite transmission from mammals to mosquitoes. J Theor Biol. 2013;334:173-86.

195. Stern JR, Christley S, Zaborina O, Alverdy JC, An G. Integration of TGF-beta- and EGFR-based signaling pathways using an agent-based model of epithelial restitution. Wound Repair Regen. 2012;20(6):862-71.

196. Walker DC, Hill G, Wood SM, Smallwood RH, Southgate J. Agent-based computational modeling of wounded epithelial cell monolayers. IEEE Trans Nanobioscience. 2004;3(3):153-63.

197. Zamora R, Azhar N, Namas R, Metukuri MR, Clermont T, Gladstone C, et al. Identification of a novel pathway of transforming growth factor-beta1 regulation by extracellular NAD+ in mouse macrophages: in vitro and in silico studies. J Biol Chem. 2012;287(37):31003-14.

198. Zhang L, Wang Z, Sagotsky JA, Deisboeck TS. Multiscale agent-based cancer modeling. J Math Biol. 2009;58(4-5):545-59.

199. Jordan DW, Smith P. Nonlinear ordinary differential equations: an introduction to dynamical systems: Oxford University Press, USA; 1999.

200. Railsback SF, Grimm V. Agent-based and individual-based modeling: a practical introduction: Princeton university press; 2011.

201. Cilfone NA, Pienaar E, Kirschner DE, Linderman JJ. Computational Modeling of Granuloma Formation in Tuberculosis Yields Insights into both Infection and Treatment. Biophys J. 2014;106(2):644a-a.

202. Cilfone NA, Pienaar E, Thurber GM, Kirschner DE, Linderman JJ. Systems Pharmacology Approach Toward the Design of Inhaled Formulations of Rifampicin and Isoniazid for Treatment of Tuberculosis. CPT Pharmacometrics Syst Pharmacol. 2015;4(3):e00022.

203. Hao W, Marsh C, Friedman A. A Mathematical Model of Idiopathic Pulmonary Fibrosis. PLoS One. 2015;10(9):e0135097.

204. Zi Z, Chapnick DA, Liu X. Dynamics of TGF-beta/Smad signaling. FEBS Lett. 2012;586(14):1921-8.

205. Zi Z, Feng Z, Chapnick DA, Dahl M, Deng D, Klipp E, et al. Quantitative analysis of transient and sustained transforming growth factor-beta signaling dynamics. Mol Syst Biol. 2011;7:492.

206. Zi Z, Klipp E. Constraint-based modeling and kinetic analysis of the Smad dependent TGF-beta signaling pathway. PLoS One. 2007;2(9):e936.

207. Vilar JM, Jansen R, Sander C. Signal processing in the TGF-beta superfamily ligand-receptor network. PLoS Comput Biol. 2006;2(1):e3.

208. Voit EO. Mesoscopic modeling as a starting point for computational analyses of cystic fibrosis as a systemic disease. Biochim Biophys Acta. 2014;1844(1 Pt B):258-70.

209. Marino S, Kirschner DE. The human immune response to Mycobacterium tuberculosis in lung and lymph node. J Theor Biol. 2004;227(4):463-86.

210. Marino S, Pawar S, Fuller CL, Reinhart TA, Flynn JL, Kirschner DE. Dendritic cell trafficking and antigen presentation in the human immune response to Mycobacterium tuberculosis. J Immunol. 2004;173(1):494-506.

211. Jung E, Lenhart S, Feng Z. Optimal control of treatments in a two-strain tuberculosis model. Discrete and Continuous Dynamical Systems Series B. 2002;2(4):473-82.

212. Wigginton JE, Kirschner D. A model to predict cell-mediated immune regulatory mechanisms during human infection with Mycobacterium tuberculosis. J Immunol. 2001;166(3):1951-67.

213. Sud D, Bigbee C, Flynn JL, Kirschner DE. Contribution of CD8+ T cells to control of Mycobacterium tuberculosis infection. J Immunol. 2006;176(7):4296-314.

214. Magombedze G, Mulder N. A mathematical representation of the development of Mycobacterium tuberculosis active, latent and dormant stages. J Theor Biol. 2012;292:44-59.

215. Oxman AD, Muir DC, Shannon HS, Stock SR, Hnizdo E, Lange HJ. Occupational dust exposure and chronic obstructive pulmonary disease. A systematic overview of the evidence. Am Rev Respir Dis. 1993;148(1):38-48.

216. An G. Introduction of an agent-based multi-scale modular architecture for dynamic knowledge representation of acute inflammation. Theor Biol Med Model. 2008;5:11.

217. Pollmacher J, Figge MT. Agent-based model of human alveoli predicts chemotactic signaling by epithelial cells during early Aspergillus fumigatus infection. PLoS One. 2014;9(10):e111630.

218. Cilfone NA, Kirschner DE, Linderman JJ. Strategies for efficient numerical implementation of hybrid multi-scale agent-based models to describe biological systems. Cell Mol Bioeng. 2015;8(1):119-36.

219. Marino S, El-Kebir M, Kirschner D. A hybrid multi-compartment model of granuloma formation and T cell priming in tuberculosis. J Theor Biol. 2011;280(1):50-62.

220. Segovia-Juarez JL, Ganguli S, Kirschner D. Identifying control mechanisms of granuloma formation during M. tuberculosis infection using an agent-based model. Journal of Theoretical Biology. 2004;231(3):357-76.

221. Ajelli M, Goncalves B, Balcan D, Colizza V, Hu H, Ramasco JJ, et al. Comparing large-scale computational approaches to epidemic modeling: agent-based versus structured metapopulation models. BMC Infect Dis. 2010;10:190.

222. Carpenter C, Sattenspiel L. The design and use of an agent-based model to simulate the 1918 influenza epidemic at Norway House, Manitoba. Am J Hum Biol. 2009;21(3):290-300.

223. Kasaie P, Andrews JR, Kelton WD, Dowdy DW. Timing of tuberculosis transmission and the impact of household contact tracing. An agent-based simulation model. Am J Respir Crit Care Med. 2014;189(7):845-52.

224. Kumar S, Grefenstette JJ, Galloway D, Albert SM, Burke DS. Policies to reduce influenza in the workplace: impact assessments using an agent-based model. Am J Public Health. 2013;103(8):1406-11.

225. Chang KC, Leung CC, Grosset J, Yew WW. Treatment of tuberculosis and optimal dosing schedules. Thorax. 2011;66(11):997-1007.

226. Marino S, Linderman JJ, Kirschner D. A Multi-Faceted Approach to Modeling the immune response in Tuberculosis (accepted with revision to WIRES Systems Biology 2010).

227. Ray JC, Flynn JL, Kirschner DE. Synergy between individual TNF-dependent functions determines granuloma performance for controlling Mycobacterium tuberculosis infection. J Immunol. 2009;182(6):3706-17.

228. Ray JC, Wang J, Chan J, Kirschner DE. The timing of TNF and IFN-gamma signaling affects macrophage activation strategies during Mycobacterium tuberculosis infection. J Theor Biol. 2008;252(1):24-38.

229. Marino S, Hogue IB, Ray CJ, Kirschner DE. A methodology for performing global uncertainty and sensitivity analysis in systems biology. Journal of Theoretical Biology. 2008;254(1):178-96.

230. Kirschner DE, Hunt CA, Marino S, Fallahi-Sichani M, Linderman JJ. Tuneable resolution as a systems biology approach for multi-scale, multi-compartment computational models. Wiley Interdiscip Rev Syst Biol Med. 2014;6(4):289-309.

231. Hinz B, Phan SH, Thannickal VJ, Prunotto M, Desmouliere A, Varga J, et al. Recent developments in myofibroblast biology: paradigms for connective tissue remodeling. Am J Pathol. 2012;180(4):1340-55.

232. Kim WJ, Gittes GK, Longaker MT. Signal transduction in wound pharmacology. Arch Pharm Res. 1998;21(5):487-95.

233. Clark RA. Fibrin and wound healing. Ann N Y Acad Sci. 2001;936:355-67.

234. Kolodsick JE, Peters-Golden M, Larios J, Toews GB, Thannickal VJ, Moore BB. Prostaglandin E2 inhibits fibroblast to myofibroblast transition via E. prostanoid receptor 2 signaling and cyclic adenosine monophosphate elevation. Am J Respir Cell Mol Biol. 2003;29(5):537-44.

235. Tobin SW, Douville K, Benbow U, Brinckerhoff CE, Memoli VA, Arrick BA. Consequences of altered TGF-beta expression and responsiveness in breast cancer: evidence for autocrine and paracrine effects. Oncogene. 2002;21(1):108-18.

236. Turley JM, Falk LA, Ruscetti FW, Kasper JJ, Francomano T, Fu T, et al. Transforming growth factor beta 1 functions in monocytic differentiation of hematopoietic cells through autocrine and paracrine mechanisms. Cell Growth Differ. 1996;7(11):1535-44.

237. Lehnert SA, Akhurst RJ. Embryonic expression pattern of TGF beta type-1 RNA suggests both paracrine and autocrine mechanisms of action. Development. 1988;104(2):263-73.

238. Peyton SR, Kim PD, Ghajar CM, Seliktar D, Putnam AJ. The effects of matrix stiffness and RhoA on the phenotypic plasticity of smooth muscle cells in a 3-D biosynthetic hydrogel system. Biomaterials. 2008;29(17):2597-607.

239. Ramasastry SS. Acute wounds. Clin Plast Surg. 2005;32(2):195-208.

240. Ibrahim MM, Chen L, Bond JE, Medina MA, Ren L, Kokosis G, et al. Myofibroblasts contribute to but are not necessary for wound contraction. Lab Invest. 2015;95(12):1429-38.

241. Camelo A, Dunmore R, Sleeman MA, Clarke DL. The epithelium in idiopathic pulmonary fibrosis: breaking the barrier. Front Pharmacol. 2014;4:173.

242. Mayer AK, Dalpke AH. Regulation of local immunity by airway epithelial cells. Arch Immunol Ther Exp (Warsz). 2007;55(6):353-62.

243. Holtzman MJ, Byers DE, Alexander-Brett J, Wang X. The role of airway epithelial cells and innate immune cells in chronic respiratory disease. Nat Rev Immunol. 2014;14(10):686-98.

244. Crystal RG, Randell SH, Engelhardt JF, Voynow J, Sunday ME. Airway epithelial cells: current concepts and challenges. Proc Am Thorac Soc. 2008;5(7):772-7.

245. Prasad S, Hogaboam CM, Jarai G. Deficient repair response of IPF fibroblasts in a co-culture model of epithelial injury and repair. Fibrogenesis Tissue Repair. 2014;7:7.

246. Jastrzebski D, Kozielski J, Banas A, Cebula T, Gumola A, Ziora D, et al. Quality of life during one-year observation of patients with idiopathic pulmonary fibrosis awaiting lung transplantation. J Physiol Pharmacol. 2005;56 Suppl 4:99-105.

247. Maher TM, Evans IC, Bottoms SE, Mercer PF, Thorley AJ, Nicholson AG, et al. Diminished prostaglandin E2 contributes to the apoptosis paradox in idiopathic pulmonary fibrosis. Am J Respir Crit Care Med. 2010;182(1):73-82.

248. Adamson IY, Bowden DH. The pathogenesis of bloemycin-induced pulmonary fibrosis in mice. Am J Pathol. 1974;77(2):185-97.

249. Krieg T, Abraham D, Lafyatis R. Fibrosis in connective tissue disease: the role of the myofibroblast and fibroblast-epithelial cell interactions. Arthritis Res Ther. 2007;9 Suppl 2:S4.

250. Wang J, Yang Y, Xu J, Lin X, Wu K, Yu M. Pirfenidone inhibits migration, differentiation, and proliferation of human retinal pigment epithelial cells in vitro. Mol Vis. 2013;19:2626-35.

251. Justus CR, Leffler N, Ruiz-Echevarria M, Yang LV. In vitro cell migration and invasion assays. J Vis Exp. 2014(88).

252. Liang CC, Park AY, Guan JL. In vitro scratch assay: a convenient and inexpensive method for analysis of cell migration in vitro. Nat Protoc. 2007;2(2):329-33.

253. Jonkman JE, Cathcart JA, Xu F, Bartolini ME, Amon JE, Stevens KM, et al. An introduction to the wound healing assay using live-cell microscopy. Cell Adh Migr. 2014;8(5):440-51.

254. Della Latta V, Cecchettini A, Del Ry S, Morales MA. Bleomycin in the setting of lung fibrosis induction: From biological mechanisms to counteractions. Pharmacol Res. 2015;97:122-30.

255. Izbicki G, Or R, Christensen TG, Segel MJ, Fine A, Goldstein RH, et al. Bleomycin-induced lung fibrosis in IL-4-overexpressing and knockout mice. Am J Physiol Lung Cell Mol Physiol. 2002;283(5):L1110-6.

256. Moeller A, Ask K, Warburton D, Gauldie J, Kolb M. The bleomycin animal model: A useful tool to investigate treatment options for idiopathic pulmonary fibrosis? The International Journal of Biochemistry & Cell Biology. 2008;40(3):362-82.

257. Christensen PJ, Goodman RE, Pastoriza L, Moore B, Toews GB. Induction of lung fibrosis in the mouse by intratracheal instillation of fluorescein isothiocyanate is not T-cell-dependent. Am J Pathol. 1999;155(5):1773-9.

258. Kolodsick JE, Toews GB, Jakubzick C, Hogaboam C, Moore TA, McKenzie A, et al. Protection from fluorescein isothiocyanate-induced fibrosis in IL-13-deficient, but not IL-4-deficient, mice results from impaired collagen synthesis by fibroblasts. J Immunol. 2004;172(7):4068-76.

259. Adam J. A simplified model of wound healing (with particular reference to the critical size defect). Mathematical and computer modelling. 1999;30(5):23-32.

260. Arnold J, Adam J. A simplified model of wound healing II: The critical size defect in two dimensions. Mathematical and computer modelling. 1999;30(11):47-60.

261. Sherratt JA, Murray JD. Epidermal wound healing: the clinical implications of a simple mathematical model. Cell Transplant. 1992;1(5):365-71.

262. Christley S, Lee B, Dai X, Nie Q. Integrative multicellular biological modeling: a case study of 3D epidermal development using GPU algorithms. BMC Syst Biol. 2010;4:107.

263. Cobbold CA, Sherratt JA. Mathematical modelling of nitric oxide activity in wound healing can explain keloid and hypertrophic scarring. J Theor Biol. 2000;204(2):257-88.

264. Cumming BD, McElwain DL, Upton Z. A mathematical model of wound healing and subsequent scarring. J R Soc Interface. 2010;7(42):19-34.

265. Adra S, Sun T, MacNeil S, Holcombe M, Smallwood R. Development of a three dimensional multiscale computational model of the human epidermis. PLoS One. 2010;5(1):e8511.

266. Buganza Tepole A, Kuhl E. Systems-based approaches toward wound healing. Pediatr Res. 2013;73(4 Pt 2):553-63.

267. Efficacy and Safety of Nintedanib in Idiopathic Pulmonary Fibrosis. N Engl J Med. 2015;373(8):782.

268. Adams DH, Hathaway M, Shaw J, Burnett D, Elias E, Strain AJ. Transforming growth factor-beta induces human T lymphocyte migration in vitro. J Immunol. 1991;147(2):609-12.

269. Geris L, Gerisch A, Schugart RC. Mathematical modeling in wound healing, bone regeneration and tissue engineering. Acta Biotheor. 2010;58(4):355-67.

270. Murphy KE, Hall CL, McCue SW, Sean McElwain DL. A two-compartment mechanochemical model of the roles of transforming growth factor beta and tissue tension in dermal wound healing. J Theor Biol. 2011;272(1):145-59.

271. Reinstein DZ, Archer TJ, Randleman JB. Mathematical model to compare the relative tensile strength of the cornea after PRK, LASIK, and small incision lenticule extraction. J Refract Surg. 2013;29(7):454-60.

272. Sinha Roy A, Dupps WJ, Jr., Roberts CJ. Comparison of biomechanical effects of small-incision lenticule extraction and laser in situ keratomileusis: finite-element analysis. J Cataract Refract Surg. 2014;40(6):971-80.

273. Maini PK, McElwain DL, Leavesley DI. Traveling wave model to interpret a wound-healing cell migration assay for human peritoneal mesothelial cells. Tissue Eng. 2004;10(3-4):475-82.

274. Ruberti JW, Roy AS, Roberts CJ. Corneal biomechanics and biomaterials. Annu Rev Biomed Eng. 2011;13:269-95.

275. Ziraldo C, Mi Q, An G, Vodovotz Y. Computational Modeling of Inflammation and Wound Healing. Adv Wound Care (New Rochelle). 2013;2(9):527-37.

276. Solovyev A, Mi Q, Tzen YT, Brienza D, Vodovotz Y. Hybrid equation/agent-based model of ischemia-induced hyperemia and pressure ulcer formation predicts greater propensity to ulcerate in subjects with spinal cord injury. PLoS Comput Biol. 2013;9(5):e1003070.

277. Bailon-Plaza A, van der Meulen MC. A mathematical framework to study the effects of growth factor influences on fracture healing. J Theor Biol. 2001;212(2):191-209.

278. Yang L, Witten TM, Pidaparti RM. A biomechanical model of wound contraction and scar formation. J Theor Biol. 2013;332:228-48.

279. Ben Amar M, Bianca C. Towards a unified approach in the modeling of fibrosis: A review with research perspectives. Phys Life Rev. 2016.

280. Carloni A, Poletti V, Fermo L, Bellomo N, Chilosi M. Heterogeneous distribution of mechanical stress in human lung: A mathematical approach to evaluate abnormal remodeling in IPF. J Theor Biol. 2013;332:136-40.

281. Garikipati K. The kinematics of biological growth. Applied Mechanics Reviews. 2009;62(3):030801.

282. Garikipati K, Arruda E, Grosh K, Narayanan H, Calve S. Erratum:"A continuum treatment of growth in biological tissue: the coupling of mass transport and mechanics"[Journal of Mechanics and Physics of Solids 52 (2004) 1595]. Journal of the Mechanics and Physics of Solids. 2004;52(12):2909-10.

283. Kuhl E, Garikipati K, Arruda EM, Grosh K. Remodeling of biological tissue: mechanically induced reorientation of a transversely isotropic chain network. Journal of the Mechanics and Physics of Solids. 2005;53(7):1552-73.

284. Kendall RT, Feghali-Bostwick CA. Fibroblasts in fibrosis: novel roles and mediators. Front Pharmacol. 2014;5:123.

285. Flynn JL. Lessons from experimental Mycobacterium tuberculosis infections. Microbes Infect. 2006;8(4):1179-88.

286. Grosset J. Mycobacterium tuberculosis in the extracellular compartment: an underestimated adversary. Antimicrob Agents Chemother. 2003;47(3):833-6.

287. Ito T, Connett JM, Kunkel SL, Matsukawa A. The linkage of innate and adaptive immune response during granulomatous development. Front Immunol. 2013;4:10.

288. Gengenbacher M, Kaufmann SH. Mycobacterium tuberculosis: success through dormancy. FEMS Microbiol Rev. 2012;36(3):514-32.

289. Kaufmann SH. How can immunology contribute to the control of tuberculosis? Nat Rev Immunol. 2001;1(1):20-30.

290. Oddo M, Renno T, Attinger A, Bakker T, MacDonald HR, Meylan PR. Fas ligand-induced apoptosis of infected human macrophages reduces the viability of intracellular Mycobacterium tuberculosis. J Immunol. 1998;160(11):5448-54.

291. Algood HM, Lin PL, Yankura D, Jones A, Chan J, Flynn JL. TNF influences chemokine expression of macrophages in vitro and that of CD11b+ cells in vivo during Mycobacterium tuberculosis infection. J Immunol. 2004;172(11):6846-57.

292. Barry CE, 3rd, Boshoff HI, Dartois V, Dick T, Ehrt S, Flynn J, et al. The spectrum of latent tuberculosis: rethinking the biology and intervention strategies. Nat Rev Microbiol. 2009;7(12):845-55.

293. Lin PL, Dartois V, Johnston PJ, Janssen C, Via L, Goodwin MB, et al. Metronidazole prevents reactivation of latent Mycobacterium tuberculosis infection in macaques. Proc Natl Acad Sci U S A. 2012;109(35):14188-93.

294. Lin PL, Rodgers M, Smith L, Bigbee M, Myers A, Bigbee C, et al. Quantitative comparison of active and latent tuberculosis in the cynomolgus macaque model. Infect Immun. 2009;77(10):4631-42.

295. Mattila JT, Ojo OO, Kepka-Lenhart D, Marino S, Kim JH, Eum SY, et al. Microenvironments in tuberculous granulomas are delineated by distinct populations of macrophage subsets and expression of nitric oxide synthase and arginase isoforms. J Immunol. 2013;191(2):773-84.

296. Kesavan AK, Brooks M, Tufariello J, Chan J, Manabe YC. Tuberculosis genes expressed during persistence and reactivation in the resistant rabbit model. Tuberculosis (Edinb). 2009;89(1):17-21.

297. Kjellsson MC, Via LE, Goh A, Weiner D, Low KM, Kern S, et al. Pharmacokinetic evaluation of the penetration of antituberculosis agents in rabbit pulmonary lesions. Antimicrob Agents Chemother. 2012;56(1):446-57.

298. Manabe YC, Dannenberg AM, Jr., Tyagi SK, Hatem CL, Yoder M, Woolwine SC, et al. Different strains of Mycobacterium tuberculosis cause various spectrums of disease in the rabbit model of tuberculosis. Infect Immun. 2003;71(10):6004-11.

299. Manabe YC, Kesavan AK, Lopez-Molina J, Hatem CL, Brooks M, Fujiwara R, et al. The aerosol rabbit model of TB latency, reactivation and immune reconstitution inflammatory syndrome. Tuberculosis (Edinb). 2008;88(3):187-96.

300. Prideaux B, Dartois V, Staab D, Weiner DM, Goh A, Via LE, et al. High-sensitivity MALDI-MRM-MS imaging of moxifloxacin distribution in tuberculosis-infected rabbit lungs and granulomatous lesions. Anal Chem. 2011;83(6):2112-8.

301. Subbian S, O'Brien P, Kushner NL, Yang G, Tsenova L, Peixoto B, et al. Molecular immunologic correlates of spontaneous latency in a rabbit model of pulmonary tuberculosis. Cell Commun Signal. 2013;11(1):16.

302. Subbian S, Tsenova L, O'Brien P, Yang G, Koo MS, Peixoto B, et al. Phosphodiesterase-4 inhibition alters gene expression and improves isoniazid-

mediated clearance of Mycobacterium tuberculosis in rabbit lungs. PLoS Pathog. 2011;7(9):e1002262.

303. Subbian S, Tsenova L, O'Brien P, Yang G, Kushner NL, Parsons S, et al. Spontaneous latency in a rabbit model of pulmonary tuberculosis. Am J Pathol. 2012;181(5):1711-24.

304. Via LE, Schimel D, Weiner DM, Dartois V, Dayao E, Cai Y, et al. Infection dynamics and response to chemotherapy in a rabbit model of tuberculosis using [(1)(8)F]2-fluoro-deoxy-D-glucose positron emission tomography and computed tomography. Antimicrob Agents Chemother. 2012;56(8):4391-402.

305. Keane J, Shurtleff B, Kornfeld H. TNF-dependent BALB/c murine macrophage apoptosis following Mycobacterium tuberculosis infection inhibits bacillary growth in an IFN-gamma independent manner. Tuberculosis (Edinb). 2002;82(2-3):55-61.

306. Goutelle S, Bourguignon L, Maire PH, Van Guilder M, Conte JE, Jr., Jelliffe RW. Population modeling and Monte Carlo simulation study of the pharmacokinetics and antituberculosis pharmacodynamics of rifampin in lungs. Antimicrob Agents Chemother. 2009;53(7):2974-81.

307. Wilkins JJ, Savic RM, Karlsson MO, Langdon G, McIlleron H, Pillai G, et al. Population pharmacokinetics of rifampin in pulmonary tuberculosis patients, including a semimechanistic model to describe variable absorption. Antimicrob Agents Chemother. 2008;52(6):2138-48.

308. Escude M, Rigozzi MK, Terentjev EM. How cells feel: stochastic model for a molecular mechanosensor. Biophys J. 2014;106(1):124-33.

309. Ankomah P, Levin BR. Two-drug antimicrobial chemotherapy: a mathematical model and experiments with Mycobacterium marinum. PLoS Pathog. 2012;8(1):e1002487.

310. Dong ZX, Tai WL, Lei W, Wang Y, Li ZK, Zhang T. [Effects of interleukin 27 and its receptor on TGFbetainduced murine pulmonary fibroblast proliferation and transformation]. Nan Fang Yi Ke Da Xue Xue Bao. 2015;35(10):1411-6.

311. Stratton R, Rajkumar V, Ponticos M, Nichols B, Shiwen X, Black CM, et al. Prostacyclin derivatives prevent the fibrotic response to TGF-beta by inhibiting the Ras/MEK/ERK pathway. FASEB J. 2002;16(14):1949-51.

312. Tomioka H, Imanaka K, Hashimoto K, Iwasaki H. Health-related quality of life in patients with idiopathic pulmonary fibrosis--cross-sectional and longitudinal study. Intern Med. 2007;46(18):1533-42.

313. Taniguchi H, Kondoh Y, Ebina M, Azuma A, Ogura T, Taguchi Y, et al. The clinical significance of 5% change in vital capacity in patients with idiopathic

pulmonary fibrosis: extended analysis of the pirfenidone trial. Respir Res. 2011;12:93.

314. Richeldi L, du Bois RM, Raghu G, Azuma A, Brown KK, Costabel U, et al. Efficacy and safety of nintedanib in idiopathic pulmonary fibrosis. N Engl J Med. 2014;370(22):2071-82.

315. Vizan P, Miller DSJ, Gori I, Das D, Schmierer B, Hill CS. Controlling Long-Term Signaling: Receptor Dynamics Determine Attenuation and Refractory Behavior of the TGF-{beta} Pathway. Sci Signal. 2013;6(305):ra106-.

316. Liu F, Mih JD, Shea BS, Kho AT, Sharif AS, Tager AM, et al. Feedback amplification of fibrosis through matrix stiffening and COX-2 suppression. J Cell Biol. 2010;190(4):693-706.

317. Huang X, Yang N, Fiore VF, Barker TH, Sun Y, Morris SW, et al. Matrix stiffness-induced myofibroblast differentiation is mediated by intrinsic mechanotransduction. Am J Respir Cell Mol Biol. 2012;47(3):340-8.

318. Tamada M, Sheetz MP, Sawada Y. Activation of a signaling cascade by cytoskeleton stretch. Dev Cell. 2004;7(5):709-18.

319. Sawada Y, Tamada M, Dubin-Thaler BJ, Cherniavskaya O, Sakai R, Tanaka S, et al. Force sensing by mechanical extension of the Src family kinase substrate p130Cas. Cell. 2006;127(5):1015-26.

320. Ulrich TA, de Juan Pardo EM, Kumar S. The mechanical rigidity of the extracellular matrix regulates the structure, motility, and proliferation of glioma cells. Cancer Res. 2009;69(10):4167-74.

321. Giannone G, Sheetz MP. Substrate rigidity and force define form through tyrosine phosphatase and kinase pathways. Trends Cell Biol. 2006;16(4):213-23.

322. Tian M, Schiemann WP. PGE2 receptor EP2 mediates the antagonistic effect of COX-2 on TGF-beta signaling during mammary tumorigenesis. FASEB J. 2010;24(4):1105-16.

323. Huang SK, White ES, Wettlaufer SH, Grifka H, Hogaboam CM, Thannickal VJ, et al. Prostaglandin E(2) induces fibroblast apoptosis by modulating multiple survival pathways. FASEB J. 2009;23(12):4317-26.

324. Saltzman LE, Moss J, Berg RA, Hom B, Crystal RG. Modulation of collagen production by fibroblasts. Effects of chronic exposure to agonists that increase intracellular cyclic AMP. Biochem J. 1982;204(1):25-30.

325. Sugimoto Y, Narumiya S. Prostaglandin E receptors. J Biol Chem. 2007;282(16):11613-7.

326. Wakefield LM, Winokur TS, Hollands RS, Christopherson K, Levinson AD, Sporn MB. Recombinant latent transforming growth factor beta 1 has a longer plasma half-life in rats than active transforming growth factor beta 1, and a different tissue distribution. J Clin Invest. 1990;86(6):1976-84.

327. Di Guglielmo GM, Le Roy C, Goodfellow AF, Wrana JL. Distinct endocytic pathways regulate TGF-beta receptor signalling and turnover. Nat Cell Biol. 2003;5(5):410-21.

328. Lin LL, Lin AY, DeWitt DL. Interleukin-1 alpha induces the accumulation of cytosolic phospholipase A2 and the release of prostaglandin E2 in human fibroblasts. J Biol Chem. 1992;267(33):23451-4.

329. Ishihara O, Sullivan MH, Elder MG. Differences of metabolism of prostaglandin E2 and F2 alpha by decidual stromal cells and macrophages in culture. Eicosanoids. 1991;4(4):203-7.

330. Zimmermann CS, Carvalho CR, Silveira KR, Yamaguti WP, Moderno EV, Salge JM, et al. Comparison of two questionnaires which measure the health-related quality of life of idiopathic pulmonary fibrosis patients. Braz J Med Biol Res. 2007;40(2):179-87.

331. Lauffenburger DA, Linderman JJ. Receptors : models for binding, trafficking, and signaling. New York: Oxford University Press; 1993. x, 365 p. p.

332. Derynck R, Zhang YE. Smad-dependent and Smad-independent pathways in TGF-beta family signalling. Nature. 2003;425(6958):577-84.

333. Discher DE, Janmey P, Wang YL. Tissue cells feel and respond to the stiffness of their substrate. Science. 2005;310(5751):1139-43.

334. Levental KR, Yu H, Kass L, Lakins JN, Egeblad M, Erler JT, et al. Matrix crosslinking forces tumor progression by enhancing integrin signaling. Cell. 2009;139(5):891-906.

335. Penheiter SG, Mitchell H, Garamszegi N, Edens M, Dore JJ, Jr., Leof EB. Internalization-dependent and -independent requirements for transforming growth factor beta receptor signaling via the Smad pathway. Mol Cell Biol. 2002;22(13):4750-9.

336. Vanhee D, Gosset P, Wallaert B, Voisin C, Tonnel AB. Mechanisms of fibrosis in coal workers' pneumoconiosis. Increased production of platelet-derived growth factor, insulin-like growth factor type I, and transforming growth factor beta and relationship to disease severity. Am J Respir Crit Care Med. 1994;150(4):1049-55.

337. Zhou X, Loomis-King H, Gurczynski SJ, Wilke CA, Konopka KE, Ptaschinski C, et al. Bone marrow transplantation alters lung antigen-presenting cells to promote

T17 response and the development of pneumonitis and fibrosis following gammaherpesvirus infection. Mucosal Immunol. 2015.

338. Tzanakis N, Samiou M, Lambiri I, Antoniou K, Siafakas N, Bouros D. Evaluation of health-related quality-of-life and dyspnea scales in patients with idiopathic pulmonary fibrosis. Correlation with pulmonary function tests. Eur J Intern Med. 2005;16(2):105-12.

339. Verma G, Marras T, Chowdhury N, Singer L. Health-related quality of life and 6 min walk distance in patients with idiopathic pulmonary fibrosis. Can Respir J. 2011;18(5):283-7.

340. Raghu G, King TE, Jr., Behr J, Brown KK, du Bois RM, Leconte I, et al. Quality of life and dyspnoea in patients treated with bosentan for idiopathic pulmonary fibrosis (BUILD-1). Eur Respir J. 2010;35(1):118-23.

341. Nishiyama O, Taniguchi H, Kondoh Y, Kimura T, Ogawa T, Watanabe F, et al. Health-related quality of life in patients with idiopathic pulmonary fibrosis. What is the main contributing factor? Respir Med. 2005;99(4):408-14.

342. Sanders YY, Cui Z, Le Saux CJ, Horowitz JC, Rangarajan S, Kurundkar A, et al. SMAD-independent down-regulation of caveolin-1 by TGF-beta: effects on proliferation and survival of myofibroblasts. PLoS One. 2015;10(2):e0116995.

343. Thannickal VJ, Horowitz JC. Evolving concepts of apoptosis in idiopathic pulmonary fibrosis. Proc Am Thorac Soc. 2006;3(4):350-6.

344. Warsinske HC, Ashley SL, Linderman JJ, Moore BB, Kirschner DE. Identifying Mechanisms of Homeostatic Signaling in Fibroblast Differentiation. Bull Math Biol. 2015.

345. Saha D, Datta PK, Sheng H, Morrow JD, Wada M, Moses HL, et al. Synergistic induction of cyclooxygenase-2 by transforming growth factor-beta1 and epidermal growth factor inhibits apoptosis in epithelial cells. Neoplasia. 1999;1(6):508-17.

346. Myllarniemi M, Kaarteenaho R. Pharmacological treatment of idiopathic pulmonary fibrosis - preclinical and clinical studies of pirfenidone, nintedanib, and N-acetylcysteine. Eur Clin Respir J. 2015;2.

347. Lederer DJ, Bradford WZ, Fagan EA, Glaspole I, Glassberg MK, Glasscock KF, et al. Sensitivity Analyses of the Change in FVC in a Phase 3 Trial of Pirfenidone for Idiopathic Pulmonary Fibrosis. Chest. 2015;148(1):196-201.

348. Thorne BC, Bailey AM, Peirce SM. Combining experiments with multi-cell agent-based modeling to study biological tissue patterning. Brief Bioinform. 2007;8(4):245-57.

349. Mansury Y, Kimura M, Lobo J, Deisboeck TS. Emerging patterns in tumor systems: simulating the dynamics of multicellular clusters with an agent-based spatial agglomeration model. J Theor Biol. 2002;219(3):343-70.

350. An G, Mi Q, Dutta-Moscato J, Vodovotz Y. Agent-based models in translational systems biology. Wiley Interdiscip Rev Syst Biol Med. 2009;1(2):159-71.

351. Salkind N, Abdi H. The Bonferonni and Sidak Corrections for Multiple Comparisons. Encyclopedia of Measurement and Statistics. 2007.

352. Hinz B, Phan SH, Thannickal VJ, Galli A, Bochaton-Piallat ML, Gabbiani G. The myofibroblast: one function, multiple origins. Am J Pathol. 2007;170(6):1807-16.

353. Crosas-Molist E, Fabregat I. Role of NADPH oxidases in the redox biology of liver fibrosis. Redox Biol. 2015;6:106-11.

354. Bohm M, Dosoki H, Kerkhoff C. Is Nox4 a key regulator of the activated state of fibroblasts in systemic sclerosis? Exp Dermatol. 2014;23(9):679-81.

355. Budihardjo I, Oliver H, Lutter M, Luo X, Wang X. Biochemical pathways of caspase activation during apoptosis. Annu Rev Cell Dev Biol. 1999;15:269-90.

356. Muraoka RS, Dumont N, Ritter CA, Dugger TC, Brantley DM, Chen J, et al. Blockade of TGF-beta inhibits mammary tumor cell viability, migration, and metastases. J Clin Invest. 2002;109(12):1551-9.

357. Chen DB, Yang ZM, Hilsenrath R, Le SP, Harper MJ. Stimulation of prostaglandin (PG) F2 alpha and PGE2 release by tumour necrosis factor-alpha and interleukin-1 alpha in cultured human luteal phase endometrial cells. Hum Reprod. 1995;10(10):2773-80.

358. Hashimoto S, Gon Y, Takeshita I, Maruoka S, Horie T. IL-4 and IL-13 induce myofibroblastic phenotype of human lung fibroblasts through c-Jun NH2-terminal kinase-dependent pathway. J Allergy Clin Immunol. 2001;107(6):1001-8.

359. Kraft M, Lewis C, Pham D, Chu HW. IL-4, IL-13, and dexamethasone augment fibroblast proliferation in asthma. J Allergy Clin Immunol. 2001;107(4):602-6.

360. Saito A, Okazaki H, Sugawara I, Yamamoto K, Takizawa H. Potential action of IL-4 and IL-13 as fibrogenic factors on lung fibroblasts in vitro. Int Arch Allergy Immunol. 2003;132(2):168-76.

361. Letterio JJ, Roberts AB. Regulation of immune responses by TGF-beta. Annu Rev Immunol. 1998;16:137-61.

362. Paralkar VM, Borovecki F, Ke HZ, Cameron KO, Lefker B, Grasser WA, et al. An EP2 receptor-selective prostaglandin E2 agonist induces bone healing. Proc Natl Acad Sci U S A. 2003;100(11):6736-40.

363. Audoly LP, Tilley SL, Goulet J, Key M, Nguyen M, Stock JL, et al. Identification of specific EP receptors responsible for the hemodynamic effects of PGE2. Am J Physiol. 1999;277(3 Pt 2):H924-30.

364. Huang SK, Fisher AS, Scruggs AM, White ES, Hogaboam CM, Richardson BC, et al. Hypermethylation of PTGER2 confers prostaglandin E2 resistance in fibrotic fibroblasts from humans and mice. Am J Pathol. 2010;177(5):2245-55.

365. Corti M, Brody AR, Harrison JH. Isolation and primary culture of murine alveolar type II cells. Am J Respir Cell Mol Biol. 1996;14(4):309-15.

366. Segovia-Juarez JL, Ganguli S, Kirschner D. Identifying control mechanisms of granuloma formation during M. tuberculosis infection using an agent-based model. J Theor Biol. 2004;231(3):357-76.

367. Chang SL, Cavnar SP, Takayama S, Luker GD, Linderman JJ. Cell, isoform, and environment factors shape gradients and modulate chemotaxis. PLoS One. 2015;10(4):e0123450.

368. Shi F, Harman J, Fujiwara K, Sottile J. Collagen I matrix turnover is regulated by fibronectin polymerization. Am J Physiol Cell Physiol. 2010;298(5):C1265-75.

369. WHO. Global Tuberculosis Report 2016. Geneva, Switzerland World Health Organization; 2016.

370. Marakalala MJ, Raju RM, Sharma K, Zhang YJ, Eugenin EA, Prideaux B, et al. Inflammatory signaling in human tuberculosis granulomas is spatially organized. Nat Med. 2016;22(5):531-8.

371. Prideaux B, Via LE, Zimmerman MD, Eum S, Sarathy J, O'Brien P, et al. The association between sterilizing activity and drug distribution into tuberculosis lesions. Nat Med. 2015;21(10):1223-7.

372. Mohammad Fallahi-Sichani SM, JoAnne L. Flynn, Jennifer J. Linderman, Denise E. Kirschner Chapter 7: A Systems Biology Approach for Understanding Granuloma Formation and Function in Tuberculosis In: Johnjoe McFadden DB, Andrzej Kierzek, editor. Systems Biology of Tuberculosis. NY: Springer; 2013.

373. Mosser DM, Edwards JP. Exploring the full spectrum of macrophage activation. Nat Rev Immunol. 2008;8(12):958-69.

374. Harris J, Hope JC, Keane J. Tumor necrosis factor blockers influence macrophage responses to Mycobacterium tuberculosis. J Infect Dis. 2008;198(12):1842-50.

375. Abnaof K, Mallela N, Walenda G, Meurer SK, Sere K, Lin Q, et al. TGF-beta stimulation in human and murine cells reveals commonly affected biological processes and pathways at transcription level. BMC Syst Biol. 2014;8:55.

376. Corradin SB, Buchmuller-Rouiller Y, Smith J, Suardet L, Mauel J. Transforming growth factor beta 1 regulation of macrophage activation depends on the triggering stimulus. J Leukoc Biol. 1993;54(5):423-9.

377. Vodovotz Y, Bogdan C. Control of nitric oxide synthase expression by transforming growth factor-beta: implications for homeostasis. Prog Growth Factor Res. 1994;5(4):341-51.

378. Sime PJ, Marr RA, Gauldie D, Xing Z, Hewlett BR, Graham FL, et al. Transfer of tumor necrosis factor-alpha to rat lung induces severe pulmonary inflammation and patchy interstitial fibrogenesis with induction of transforming growth factor-beta1 and myofibroblasts. Am J Pathol. 1998;153(3):825-32.

379. Thomas DA, Massague J. TGF-beta directly targets cytotoxic T cell functions during tumor evasion of immune surveillance. Cancer Cell. 2005;8(5):369-80.

380. Mempel TR, Pittet MJ, Khazaie K, Weninger W, Weissleder R, von Boehmer H, et al. Regulatory T cells reversibly suppress cytotoxic T cell function independent of effector differentiation. Immunity. 2006;25(1):129-41.

381. Lin JT, Martin SL, Xia L, Gorham JD. TGF-beta 1 uses distinct mechanisms to inhibit IFN-gamma expression in CD4+ T cells at priming and at recall: differential involvement of Stat4 and T-bet. J Immunol. 2005;174(10):5950-8.

382. Toossi Z, Young TG, Averill LE, Hamilton BD, Shiratsuchi H, Ellner JJ. Induction of transforming growth factor beta 1 by purified protein derivative of Mycobacterium tuberculosis. Infect Immun. 1995;63(1):224-8.

383. Ordway D, Henao-Tamayo M, Harton M, Palanisamy G, Troudt J, Shanley C, et al. The hypervirulent Mycobacterium tuberculosis strain HN878 induces a potent TH1 response followed by rapid down-regulation. J Immunol. 2007;179(1):522-31.

384. Newton SM, Smith RJ, Wilkinson KA, Nicol MP, Garton NJ, Staples KJ, et al. A deletion defining a common Asian lineage of Mycobacterium tuberculosis associates with immune subversion. Proc Natl Acad Sci U S A. 2006;103(42):15594-8.

385. Marshall BG, Wangoo A, Cook HT, Shaw RJ. Increased inflammatory cytokines and new collagen formation in cutaneous tuberculosis and sarcoidosis. Thorax. 1996;51(12):1253-61.

386. Toossi Z, Ellner JJ. The role of TGF beta in the pathogenesis of human tuberculosis. Clin Immunol Immunopathol. 1998;87(2):107-14.

387. Wu M, Aung H, Hirsch CS, Toossi Z. Inhibition of Mycobacterium tuberculosis-induced signalling by transforming growth factor-beta in human mononuclear phagocytes. Scand J Immunol. 2012;75(3):301-4.

388. Marcoe JP, Lim JR, Schaubert KL, Fodil-Cornu N, Matka M, McCubbrey AL, et al. TGF-beta is responsible for NK cell immaturity during ontogeny and increased susceptibility to infection during mouse infancy. Nat Immunol. 2012;13(9):843-50.

389. Gammack D, Ganguli S, Marino S, Segovia-Juarez J, Kirschner DE. Understanding the immune response in tuberculosis using different mathematical models and biological scales. Multiscale Model Sim. 2005;3(2):312-45.

390. Ouyang W, Rutz S, Crellin NK, Valdez PA, Hymowitz SG. Regulation and functions of the IL-10 family of cytokines in inflammation and disease. Annu Rev Immunol. 2011;29:71-109.

391. Speck S, Lim J, Shelake S, Matka M, Stoddard J, Farr A, et al. TGF-beta signaling initiated in dendritic cells instructs suppressive effects on Th17 differentiation at the site of neuroinflammation. PLoS One. 2014;9(7):e102390.

392. Robinson SC, Scott KA, Balkwill FR. Chemokine stimulation of monocyte matrix metalloproteinase-9 requires endogenous TNF-alpha. Eur J Immunol. 2002;32(2):404-12.

393. Ben David D, Reznick AZ, Srouji S, Livne E. Exposure to pro-inflammatory cytokines upregulates MMP-9 synthesis by mesenchymal stem cells-derived osteoprogenitors. Histochem Cell Biol. 2008;129(5):589-97.

394. Vaday GG, Schor H, Rahat MA, Lahat N, Lider O. Transforming growth factor-beta suppresses tumor necrosis factor alpha-induced matrix metalloproteinase-9 expression in monocytes. J Leukoc Biol. 2001;69(4):613-21.

395. Dheda K, Booth H, Huggett JF, Johnson MA, Zumla A, Rook GA. Lung remodeling in pulmonary tuberculosis. J Infect Dis. 2005;192(7):1201-9.

396. TB Elimination Extensively Drug-Resistant Tuberculosis (XDR TB). In: National Center for HIV/AIDS VH, STD, and TB Prevention editor. Atlanta: Center for Disease Control; 2015.

397. Emile JF, Patey N, Altare F, Lamhamedi S, Jouanguy E, Boman F, et al. Correlation of granuloma structure with clinical outcome defines two types of idiopathic disseminated BCG infection. J Pathol. 1997;181(1):25-30.

398. Gil O, Diaz I, Vilaplana C, Tapia G, Diaz J, Fort M, et al. Granuloma encapsulation is a key factor for containing tuberculosis infection in minipigs. PLoS One. 2010;5(4):e10030.

399. Hunter RL. Pathology of post primary tuberculosis of the lung: an illustrated critical review. Tuberculosis (Edinb). 2011;91(6):497-509.

400. Klein E. Personal communication regarding formation of fibrotic TB granulomas. In: Warsinske H, editor. 2016.

401. Hinz B. The myofibroblast: paradigm for a mechanically active cell. J Biomech. 2010;43(1):146-55.

402. Aung H, Toossi Z, McKenna SM, Gogate P, Sierra J, Sada E, et al. Expression of transforming growth factor-beta but not tumor necrosis factor-alpha, interferon-gamma, and interleukin-4 in granulomatous lung lesions in tuberculosis. Tuber Lung Dis. 2000;80(2):61-7.

403. Hernandez-Pando R, Aguilar D, Hernandez ML, Orozco H, Rook G. Pulmonary tuberculosis in BALB/c mice with non-functional IL-4 genes: changes in the inflammatory effects of TNF-alpha and in the regulation of fibrosis. Eur J Immunol. 2004;34(1):174-83.

404. Scotton CJ, Chambers RC. Molecular targets in pulmonary fibrosis: the myofibroblast in focus. Chest. 2007;132(4):1311-21.

405. Barbarin V, Xing Z, Delos M, Lison D, Huaux F. Pulmonary overexpression of IL-10 augments lung fibrosis and Th2 responses induced by silica particles. Am J Physiol Lung Cell Mol Physiol. 2005;288(5):L841-8.

406. Shi J-H, Guan H, Shi S, Cai W-X, Bai X-Z, Hu X-L, et al. Protection against TGF-β1-induced fibrosis effects of IL-10 on dermal fibroblasts and its potential therapeutics for the reduction of skin scarring. Archives of Dermatological Research. 2013;305(4):341-52.

407. Bottner M, Krieglstein K, Unsicker K. The transforming growth factor-betas: structure, signaling, and roles in nervous system development and functions. J Neurochem. 2000;75(6):2227-40.

408. Massague J, Chen YG. Controlling TGF-beta signaling. Genes Dev. 2000;14(6):627-44.

409. Narayan S, Thangasamy T, Balusu R. Transforming growth factor -beta receptor signaling in cancer. Front Biosci. 2005;10:1135-45.

410. Shi M, Zhu J, Wang R, Chen X, Mi L, Walz T, et al. Latent TGF-beta structure and activation. Nature. 2011;474(7351):343-9.

411. Shi Y. Structural insights on Smad function in TGFbeta signaling. Bioessays. 2001;23(3):223-32.

412. Leask A, Abraham DJ. TGF-beta signaling and the fibrotic response. FASEB J. 2004;18(7):816-27.

413. Arnold J. A simplified model of wound healing III—the critical size defect in three dimensions. Mathematical and computer modelling. 2001;34(3):385-92.

414. Safferling K, Sutterlin T, Westphal K, Ernst C, Breuhahn K, James M, et al. Wound healing revised: a novel reepithelialization mechanism revealed by in vitro and in silico models. J Cell Biol. 2013;203(4):691-709.

415. Feghali CA, Bost KL, Boulware DW, Levy LS. Control of Il-6 Expression and Response in Fibroblasts from Patients with Systemic-Sclerosis. Autoimmunity. 1994;17(4):309-18.

416. Feghali CA, Bost KL, Boulware DW, Levy LS. Mechanisms of Pathogenesis in Scleroderma .1. Overproduction of Interleukin-6 by Fibroblasts Cultured from Affected Skin Sites of Patients with Scleroderma. J Rheumatol. 1992;19(8):1207-11.

417. Feghali CA, Boulware DW, Ferriss JA, Levy LS. Expression of C-Myc, C-Myb, and C-Sis in Fibroblasts from Affected and Unaffected Skin of Patients with Systemic-Sclerosis. Autoimmunity. 1993;16(3):167-71.

418. Kawakami T, Ihn H, Xu W, Smith E, LeRoy C, Trojanowska M. Increased expression of TGF-beta receptors by scleroderma fibroblasts: evidence for contribution of autocrine TGF-beta signaling to scleroderma phenotype. J Invest Dermatol. 1998;110(1):47-51.

419. Leask A. Potential Therapeutic Targets for Cardiac Fibrosis: TGF β , Angiotensin, Endothelin, CCN2, and PDGF, Partners in Fibroblast Activation. Circulation Research. 2010;106(11):1675-80.

420. Sullivan DE, Ferris M, Nguyen H, Abboud E, Brody AR. TNF-alpha induces TGF-beta1 expression in lung fibroblasts at the transcriptional level via AP-1 activation. J Cell Mol Med. 2009;13(8B):1866-76.

421. Tredget EE, Wang R, Shen Q, Scott PG, Ghahary A. Transforming growth factor-beta mRNA and protein in hypertrophic scar tissues and fibroblasts: antagonism by IFN-alpha and IFN-gamma in vitro and in vivo. J Interferon Cytokine Res. 2000;20(2):143-51.

422. Jester JV, Barry-Lane PA, Petroll WM, Olsen DR, Cavanagh HD. Inhibition of corneal fibrosis by topical application of blocking antibodies to TGF beta in the rabbit. Cornea. 1997;16(2):177-87.

423. Guo Y, Xiao L, Sun L, Liu F. Wnt/beta-catenin signaling: a promising new target for fibrosis diseases. Physiol Res. 2012;61(4):337-46.

424. Kim TH, Kim SH, Seo JY, Chung H, Kwak HJ, Lee SK, et al. Blockade of the Wnt/beta-catenin pathway attenuates bleomycin-induced pulmonary fibrosis. Tohoku J Exp Med. 2011;223(1):45-54.

425. Lam AP, Gottardi CJ. beta-catenin signaling: a novel mediator of fibrosis and potential therapeutic target. Curr Opin Rheumatol. 2011;23(6):562-7.

426. Piersma B, Bank RA, Boersema M. Signaling in Fibrosis: TGF-beta, WNT, and YAP/TAZ Converge. Front Med (Lausanne). 2015;2:59.

427. Warner DR, Greene RM, Pisano MM. Cross-talk between the TGFbeta and Wnt signaling pathways in murine embryonic maxillary mesenchymal cells. FEBS Lett. 2005;579(17):3539-46.

428. Park JY, Pillinger MH, Abramson SB. Prostaglandin E2 synthesis and secretion: the role of PGE2 synthases. Clin Immunol. 2006;119(3):229-40.

429. Liu Y-C, Zou X-B, Chai Y-F, Yao Y-M. Macrophage polarization in inflammatory diseases. Int J Biol Sci. 2014;10(5):520-9.

430. Oishi Y, Manabe I. Macrophages in age-related chronic inflammatory diseases. npj Aging and Mechanisms of Disease. 2016;2:16018.

431. Wu CY, Roybal KT, Puchner EM, Onuffer J, Lim WA. Remote control of therapeutic T cells through a small molecule-gated chimeric receptor. Science. 2015;350(6258):aab4077.

432. Even-Ram S, Yamada KM. Cell migration in 3D matrix. Current opinion in cell biology. 2005;17(5):524-32.

433. Shapiro BL, Feigal RJ, Laible NJ, Biros MH, Warwick WJ. Doubling time alpha-aminoisobutyrate transport and calcium exchange in cultured fibroblasts from cystic fibrosis and control subjects. Clin Chim Acta. 1978;82(1-2):125-31.

434. Wieser RJ, Heck R, Oesch F. Involvement of plasma membrane glycoproteins in the contact-dependent inhibition of growth of human fibroblasts. Exp Cell Res. 1985;158(2):493-9.

435. Wieser RJ, Janik-Schmitt B, Renauer D, Schafer A, Heck R, Oesch F. Contact-dependent inhibition of growth of normal diploid human fibroblasts by plasma membrane glycoproteins. Biochimie. 1988;70(11):1661-71.

436. Duhamel P, Vetterli M. Fast Fourier-Transforms - a Tutorial Review and a State-of-the-Art. Signal Process. 1990;19(4):259-99.

437. Hayley C. Warsinske SLA, Jennifer J. Linderman, Bethany B. Moore, Denise E. Kirschner. Identifying Mechanisms of Homeostatic Signaling in Fibroblast Differentiation. Bulletin of mathematical biology. 2015(11538):27.

438. Jin J, Zhang T. Effects of glucose restriction on replicative senescence of human diploid fibroblasts IMR-90. Cell Physiol Biochem. 2013;31(4-5):718-27.